Technische Universität München

Fakultät für Chemie

Professur für Molekulare Katalyse

Inorganic and Organometallic Compounds and their Application in Medicinal Chemistry

Elisabeth Beatrice Bauer

Vollständiger Abdruck der von der Fakultät für Chemie der Technischen Universität München zur Erlangung des akademischen Grades eines

Doktors der Naturwissenschaften (Dr. rer. nat.)

genehmigten Dissertation.

Vorsitzender:	Prof. Dr. Matthias Feige
Prüfer der Dissertation:	1. Prof. Dr. Fritz E. Kühn
	2. Prof. Dr. Klaus Köhler

Die Dissertation wurde am 21.11.2019 bei der Technischen Universität München eingereicht und durch die Fakultät für Chemie am 12.12.2019 angenommen.

Die vorliegende Arbeit wurde im Zeitraum von Juli 2016 bis November 2019 im Fachgebiet Molekulare Katalyse der Technischen Universität München angefertigt.

Mein ganz besonderer Dank gilt meinem Doktorvater

Herrn Prof. Dr. Fritz E. Kühn

für die Aufnahme in seinen Arbeitskreis, das entgegengebrachte Vertrauen und die damit verbundene finanzielle und wissenschaftliche Freiheit bei der Erforschung und Entdeckung des äußerst spannenden Themenbereichs. Vielen Dank für Ihre Unterstützung und die spannende und lehrreiche Zeit unter anderem auch durch die Ermöglichung internationaler Kooperationen.

DANKSAGUNG

First, I like to thank Professor Debbie C. Crans, also known in our group as Gerri's Mom. It was a great pleasure and a fruitful and informative experience to work with you and Allison. Thank you for your support in numerous skype meetings by successfully submitting, revising and publishing my first publication. At this point, also thanks to Gerri for the great time, we had together and that you introduced your mom to our group.

Moreover, I want to thank Dr. Rianne Lord for sharing her valuable experiences in cell culture work and the evaluation of the results. Your support made it finally possible to publish my latest experimental results. I also really enjoyed the time working with you in the lab and getting insights into new methods and techniques.

Ein großer Dank geht ebenfalls an Frau Hifinger, die stets freundlich und geduldig die Überwindung bürokratischer Hürden ermöglicht und der gesamten Gruppe immer unterstützend zur Seite steht.

Danke auch an Frau Dr. Oksana Storcheva, unter deren Leitung ich gerne das AC I Praktikum betreut habe. Danke auch für die netten, spontanen Gespräche auf dem Gang oder in der U-Bahn. Ich habe mich immer gefreut, dich zu sehen. Zudem möchte ich dir bei der wertvollen Unterstützung meiner EPR Messungen danken.

Danke auch an Maria, die die unzähligen paramagnetischen VT NMR Messungen möglich gemacht hat und aus diesen Spektren das Beste herausgeholt hat. Vielen Dank auch an Ulrike Ammari und Bircan Dilki für die Durchführung der Elementaranalysen und der Hilfsbereitschaft und stets freundlichen Begrüßung in ihrem Labor.

Weiterer Dank geht an Christian Jakob für das Messen unzähliger ESIs zu jeder Uhrzeit, aber auch danke, dass du ein so entspannter und unkomplizierter Labornachbar warst und dich nie über mein kleines Chaos beschwert hast, das schon mal entstanden ist, wenn es hektisch wurde.

Danken möchte ich auch Herrn Dr. Markus Anneser. Ich habe es dir immer wieder persönlich gesagt, möchte es aber hier nochmal erwähnen. Von dir kann man immer etwas lernen, wenn man sich mit dir unterhält. In diesem Sinne bin ich dir sehr dankbar für alles, was ich von dir lernen durfte und auch für deine tollen und hilfreichen Ideen, die meistens dann auch noch so funktioniert haben, wie du es gesagt hast und mich stets weitergebracht haben.

Jemand, dem ich ebenfalls sehr dankbar bin, ist Herr Dr. Robert Reich. Du warst immer eine wertvolle Unterstützung, sowohl wissenschaftlich als auch privat. Nicht umsonst steht dein Name mit auf meinen Publikationen. Auch danke für das Korrekturlesen meiner Arbeiten. Du warst immer und zu jederzeit erreichbar, egal um welches Problem es ging. Danke dafür! Ohne dich würde dieser Arbeitskreis nicht

so gut funktionieren. Du bist eine sehr wichtige Person für den Zusammenhalt, die Organisation und die Wissenschaft in unserer Gruppe und dafür danke ich dir.

Bedanken möchte ich mich auch bei dir, Ben Hofmann. Du bist und warst von Anfang an im Studium sowie in der Promotion ein treuer Begleiter und Weggefährte, von dem ich auch immer sehr viel lernen durfte und konnte. Es waren einige unvergessliche Momente auf unserem Weg, wie beispielsweise die Fahrt nach Ingolstadt oder der erste Tag unserer Promotion, der eine freudige Überraschung war. Bei dir weiß ich, dass keine Frage zu blöd ist, sie zu stellen, und ich immer eine hilfreiche und gute Antwort erhalten habe. Auch danke für die Unterstützung bei jeglichen IT-Problemen und bei der Auswertung der EPR Messungen.

Eine weitere langjährige Weggefährtin des Studiums und der Promotion ist und war Frau Dr. Pauline Fischer. Danke für die guten, aufmunternden, lieben und interessanten Gespräche auch außerhalb der Wissenschaft. Vor allem danke ich dir auch für die unfassbare Motivation, die ich alleine durch deine Anwesenheit bekommen habe. Ohne dich hätte ich wahrscheinlich nicht mal halb so viel Sport gemacht, wäre wohl doppelt so faul gewesen und mir hätte dieser wertvolle Ausgleich zur Arbeit gefehlt. Nochmal herzlichen Glückwunsch an dich und den Julius, ich freu mich ;) Danke an dieser Stelle an Julius für das Korrekturlesen und die hilfreiche Kritik und die guten Anmerkungen zu dieser Arbeit.

Bruno Dominelli, an dich geht ein besonderer Dank. Danke für die unzähligen lustigen und unterhaltsamen U-Bahn-Fahrten und Gespräche, die wertvollen wissenschaftlichen Diskussionen, den Aufbau des Zelllabors, das angenehme gemeinsame Durchführen der Zelltests und und und… Einfach danke für alles ☺

Mein Dank geht auch an Jens Oberkofler, der den Platz von Dr. Florian Groche sehr gut füllen konnte und immer ein guter und aufgeschlossener Sitz- und Labornachbar war. Dir konnte/kann ich einfach alles sagen, was mich gerade beschäftigt und du hörst immer zu ☺ Danke auch an dich und Annika, die mich vor allem gegen Ende der Promotion beim Verfassen meiner Dissertation stets mit Bananen abends vor dem ‚verhungern' gerettet haben.

Ebenfalls danken möchte ich Marco Bernd. Möglicherweise anfangs nicht ganz so absehbar, haben wir doch gemeinsam sehr gut und erfolgreich zusammenarbeiten können. Deine Art ist einfach einmalig, ich denke, das weißt du auch, und es war eine lustige und gute Zeit mit dir.

Dann danke ich noch Dr. Lorenz Pardatscher, Dr. Sebastian Hölzl und Andreas Hinterberger für ihr stets offenes Ohr und die guten Gespräche, sowohl wissenschaftlich als auch die Jobsuche betreffend oder außerhalb derartiger Arbeitsthemen.

Danke an den gesamten AK Kühn für die unkomplizierte Aufnahme in den Arbeitskreis, den guten und lustigen Mittags- und Kaffeepausen und der Anerkennung meiner Führungsposition, was das Beenden

der Pausen betrifft ;) Auch danke für die Grillabende, Partys und Feierabend-Biere, bei denen auch der AK Fischer nicht unerwähnt bleiben soll. Danke an Julius, Konsn, Christian, und allen anderen für die gute Zeit.

Dabei möchte ich besonders Max Schütz danken, der mit seiner Masterarbeit einen sehr wertvollen und guten Beitrag zu meiner Forschung beigetragen hat und mit dem ich sehr gerne zusammengearbeitet habe.

Mein Dank geht auch an die ‚ehemaligen' Dr. Anja Lindhorst, Dr. Florian Groche, Dr. Özden Karaca und Dr. Felix Kaiser und noch viele andere, die natürlich vor allem am Anfang meiner Promotion eine wertvolle Unterstützung waren.

Ein großer Dank geht auch an die Studierenden Ben, Enrica, Jonas, Daniel, Yogi, Matthias, Elena und Anna, die mich auf dem Weg meiner Promotion wissenschaftlich unterstützt und begleitet haben und mit ihrer Arbeit einen wertvollen Beitrag geleistet haben.

Danken möchte ich noch dem AK Buchner und vor allem Dr. Martin Haslbeck für die Bereitstellung des Zelllabors sowie einiger Zelllinien, ohne die diese Arbeit so nicht möglich gewesen wäre. Genauso danke ich dem AK Wester für die bereitwillige Überlassung einiger Vials PC3 Zellen.

Generell bedanke ich mich bei all den lieben und netten Menschen, die ich hier an der Uni kennenlernen durfte und die mich auf diesem Weg belgeitet haben.

Michi, auch dir danke ich hier sehr. Du hast mich ebenfalls das ganze Chemiestudium bis hin zur Promotion begleitet und warst immer eine wertvolle Stütze an meiner Seite. Du hast mich geduldig und ausdauernd in diesem wichtigen Lebensabschnitt begleitet und hast all meine Launen und meine Müdigkeit ohne Meckern ertragen und tust das hoffentlich auch in Zukunft ;) Es ist wunderbar, zu wissen, dass du mich immer unterstützt und hinter mir stehst und dafür bin ich dir sehr dankbar.

Meiner Familie mit Helga bin ich von ganzem Herzen dankbar für die Bereitschaft, immer und jeder Zeit für mich da zu sein, wenn ich sie brauche. Es gab doch ein paar Momente, auch während meiner Promotion, die ich ohne eure Unterstützung und Hilfe nicht so leicht überwunden hätte. Ihr seid die beste und wichtigste Unterstützung, die ich mir vorstellen kann. Und Bella, du bist sowieso einer der wichtigsten Menschen in meinem Leben und ich denke, das weißt du auch. An dieser Stelle danke ich dir deshalb vor allem für deinen hilfreichen Input zu den Problemen bei den Zelltests, die ich mir deiner Hilfe lösen konnte.

KURZZUSAMMENFASSUNG

Unzählige biologische Studien beschäftigen sich mit der Behandlung von Krebs und der Verbesserung des Therapieergebnisses. Dabei ist eine der größten Herausforderungen die Ähnlichkeit der Krebszellen zu gesunden Zellen, was mit schweren Nebenwirkungen einhergehen kann. Zudem sind Krebszellen in der Lage, sich ihrer Umgebung anzupassen und bei längerer Behandlung beispielsweise mit Cisplatin, Resistenzen zu entwickeln.

Die vorliegende Arbeit geht diese beiden Probleme in unterschiedlicher Weise an. Palladium-basierte supramolekulare Koordinationsverbindungen (SCCs) wurden in kürzlich erschienen biologischen Studien getestet und zeigten eine Erhöhung der Selektivität für Krebszellen, wenn Cisplatin in derartige SCCs eingeschlossen wird. Daher besteht die Möglichkeit, dass mit dieser Methode Nebenwirkungen zu reduzieren. Die Stabilität sowie der Einschluss solcher Wirkstoffe hängt jedoch sehr von Parametern, wie die verwendeten Liganden oder dem Lösungsmittel ab. Die Liganden sind starre, bifunktionelle organische Liganden, die über eine Pyridin-Einheit an das Metall koordinieren und so eine dreidimensionale Käfigstruktur bilden. Im Kontext dieser Arbeit wurden Studien zum Austausch dieses Metalls durch Molybdän, Chrom und Gold durchgeführt. Für den verwendeten Dimolybdän-Baustein konzentrierten sich die Ansätze auf die Synthese homoleptischer Pyridin-Komplexe, da derartige Verbindungen in der Literatur noch nicht zu finden sind. Diese Studien wurden jedoch durch die inhärente Reaktivität und Instabilität der Mo-Mo-Vierfachbindung erschwert. Einige der Versuche, die im Fall von Chrom durchgeführt wurden, waren vielversprechend, konnten jedoch nicht vollständig charakterisiert werden. Starke Hinweise für eine erfolgreiche Synthese von Au(III)-Käfigen wurden erhalten, wobei der endgültige Nachweis der Art und Weise der Koordination noch ausstehend ist.

Eine Möglichkeit, Platinresistenzen, die für platinbasierte Wirkstoffe wie Cisplatin bekannt sind, zu umgehen, ist die Anwendung anderer Metallzentren. Aufgrund der Vielseitigkeit von *N*-heterozyklischen Carbenen (NHCs) und ihrer Fähigkeit, mit einer Vielzahl von Übergangsmetallen in unterschiedlichen Oxidationsstufen stabile Komplexe zu bilden, wurde die Synthese potentiell biologisch aktiver NHC Komplexe basierend auf Chrom, Vanadium und Gold untersucht. Die Ansätze, die im Fall von Chrom und Vanadium durchgeführt wurden, stellten eine Herausforderung dar, was die Isolation und Charakterisierung der Produkte betrifft. Nichtsdestotrotz gelang die Synthese und Charakterisierung eines neuartigen makrozyklischen Au(III)-NHC-Komplexes sowie eines neuen Benzimidazol-Liganden und entsprechender Ag(I)- und Au(I)-Komplexe. Zusammen mit weiteren bereits publizierten Au(I)-NHC Komplexen wurden diese in ersten biologischen Studien getestet. Diese zeigten für einen der Komplexe eine selektive Zytotoxizität in A2780cisR und MCF-7 Krebszellen.

ABSTRACT

Innumerable biological studies focus on the treatment of cancer and the improvement of the therapeutic outcome. One major challenge is the high similarity of cancer cells to healthy cells, which leads to severe side effects of cancer treatment. Furthermore, such malignant cells are able to adapt to their environment and thus are capable of developing resistances upon prolonged treatment e.g. with cisplatin.

In this thesis, these two issues were addressed in two different ways. Palladium-based supramolecular coordination compounds (SCCs) have been evaluated in recent biological studies showing an enhanced selectivity for cancer cells of cisplatin upon encapsulation in these SCCs and thus might be able to reduce side effects. However, the stability of the investigated palladium-based SCCs as well as encapsulation of small drugs was shown to depend highly on various parameters such as the ligand structure or the solvent. The ligands are rigid, organic bifunctional ligands coordinating *via* pyridyl moieties to the metal creating three dimensional cage structures. In this thesis, studies for the exchange of the metal center were performed. These metals are molybdenum, chromium and gold. For the applied dimolybdenum core, the approaches focused on the synthesis of homoleptic pyridine complexes, which are none, reported in literature so far. The studies were impeded by the inherent reactivity and instability of the Mo-Mo quadruple bond. Some of the approaches using chromium seemed promising, however, lack of full characterization. Strong hints for the successful synthesis of Au(III) cages were achieved, however, a final proof for the coordination mode is still required.

One method to overcome platinum resistance reported for platinum-based drugs like cisplatin is the application of other metal centers. Due to the versatility of *N*-heterocyclic carbenes (NHCs) and the ability to form stable complexes with a wide range of transition metals in different oxidation states, the synthesis of potentially biologically active NHC complexes based on chromium, vanadium and gold was studied. The approaches performed for chromium and vanadium complexes appeared to be challenging in terms of product isolation and characterization. Nevertheless, synthesis and characterization of a novel macrocyclic Au(III)-NHC-complex as well as a new benzimidazole ligand and the respective Ag(I)- and Au(I)-complexes was achieved. In combination with further previously published Au(I)-NHC-complexes, initial biological studies were performed showing that one complex exhibits a selective cytotoxicity for A2780cisR and MCF-7 cancer cells.

List of Abbreviations

Å	angstrom
acac	acetyl acetone
BEOV	bis(ethylmaltolato)oxovanadium(IV)
BMOV	bis(maltolato)oxovanadium(IV)
BODIPY	boron dipyrromethene
COSY	correlation spectroscopy
CV	cyclic voltammetry
DLT	dose-limiting toxicity
DMF	*N*,*N*-dimethylformamide
DMSO	dimethyl sulfoxide
DNA	deoxyribonucleic acid
EPR	electron paramagnetic resonance
EPR effect	enhanced permeability and retention effect
equiv.	equivalent
ESI	electrospray ionization
Et al.	*et alia* (latin: and others)
FCS	fetal calf serum
FDA	Food and Drug Administration
g	gram
GR	Glutathione reductase
GSH	Glutathione
h	hour
HSA	human serum albumin
Hz	hertz
IC_{50}	half-maximal inhibition concentration
KHMDS	potassium hexamethyldiasilazide
LCAO	linear combination of atomic orbitals
LIFDI MS	liquid injection field desorption ionization mass spectrometry
M	molar (mol/liter)
m/z	mass to charge ratio
mg	milligram
MHz	mega hertz

min	minute
mL	milliliter
mM	millimolar
MO	molecular orbital
MOF	metal-organic framework
MS	mass spectrometry
MTT	3-(4,5-dimethylthiazol-2-yl)-2,5-diphenyltetrazoliumbromide)
NHC	*N*-heterocyclic carbene
NMR	nuclear magnetic resonance
Oda	oxadiacetate
PBS	phosphate buffered saline
ppm	parts per million
Py	pyridine
ROS	reactive oxygen species
rt	room temperature
SCC	supramolecular coordination compound
SC-XRD	single-crystal X-ray diffraction
thf	tetrahydrofuran
tht	tetrahydrothiophene
Tmeda	tetramethylethylenediamine
Trx	Thioredoxin
TrxR	Thioredoxin reductase

TABLE OF CONTENTS

Danksagung II

Kurzzusammenfassung V

Abstract VI

List of Abbreviations VII

Table Of Contents IX

1 Introduction 1

1.1 Cancer – Evolution and Hallmarks 1

1.2 Cancer treatment 2

1.2.1 Inorganic supramolecular coordination compounds (SCCs) 5

1.2.2 Metalorganic *N*-heterocyclic carbene (NHC) complexes 10

1.3 Early transition metals in medicinal chemistry 16

1.3.1 Molybdenum in biology 16

1.3.2 Chromium in biology 19

1.3.3 Vanadium in biology 20

2 Objective 23

3 Discussion of Results 24

3.1 Supramolecular coordination compounds 24

3.1.1 Molybdenum 25

3.1.2 Chromium 33

3.1.3 Gold 38

3.1.4 Ligand modifications 49

3.1.5 Summary of studies towards new supramolecular coordination compounds 53

3.2 *N*-heterocyclic carbene complexes 55

3.2.1 Chromium 55

3.2.2 Vanadium 65

3.2.3 Gold 76

3.2.4 Summary of studies towards new *N*-heterocyclic carbene complexes 92

4 Conclusion and Outlook 94
5 Experimental Section 96
5.1 General remarks 96
5.2 X-ray crystallographic measurements 96
5.3 Stability studies 97
5.4 MTT assays 97
5.5 Electrochemical studies 98
5.6 Synthetic procedures 99
5.6.1 $[Mo_2(OAc)_2(bipy)_2](OTf)_2$ (**19**) 99
5.6.2 $[Cr(MeCN)_2](OTf)_2$ (**25**) 99
5.6.3 1,3-bis(pyridin-3-ylethynyl)benzene iodine(III) benzene bistriflate (**34**) 100
5.6.4 3,3'-(1,3-phenylenebis(ethyne-2,1-diyl))diisonicotinaldehyde (**36**) 101
5.6.5 1,3-bis((4-(hept-1-en-1-yl)pyridin-3-yl)ethynyl)benzene (**37**) 102
5.6.6 Hexyltriphenylphosphonium bromide (**42**) 103
5.6.7 Calix[4]benzimidazolium trifluoromethanesulfonate (**49**) 104
5.6.8 Calix[4]imidazolyl-Au(III) hexafluorophosphate (**51**) 105
5.6.9 Calix[4]benzimidazolyl-Ag(I) trifluoromethanesulfonate (**52**) 106
5.6.10 Calix[4]benzimidazolyl-Au(I) trifluoromethanesulfonate (**53**) 107
6 Supplementary Data 108
6.1 Crystallographic data 108
6.2 NMR and ESI-MS data 110
6.3 MTT assays 142
6.3.1 HeLa cells 142
6.3.2 MCF-7 cells 144
6.3.3 PC3 cells 145
6.3.4 A2780cisR cells 146
7 Reprint Permissions 148
7.1 Royal Society of Chemistry 148

7.2 Royal Society of Chemistry 151

8 References 152

1 INTRODUCTION

1.1 Cancer – Evolution and Hallmarks

The latest cancer statistics for the United States of America show, that the cancer death rate decreased by 27 % from 1991 to 2016. However, with a number of 1 762 450 newly diagnosed cancer incidents and 606 880 cancer deaths in 2019 in the US, it is still one of the leading causes for death worldwide.[1] The cancer's ability to develop resistances, its high complexity, diversity and the similarity to normal healthy cells are still the main challenges for today's cancer treatment. Although cancer research identified a multitude of biological processes and characteristics related to cancer so far, a complete recovery from cancer is not assured. The following paragraph gives a brief overview of today's understanding of cancer with some hallmarks identified over the last decades of cancer research together with some details about one of the most prominent inorganic anti-cancer drugs.

The evolution of human cancer can be termed a Darwinian type of evolution. Multistep genetic alterations eventually lead to conversion of normal cells to malignant, fast dividing cells. Thereby, each small change contributes to different types of growth improvements and selective advantages. This finally results in almost limitless proliferating cells dominating the local cellular environment. According to Hanahan and Weinberg, there are two main characteristics leading to the evolution of cancer.[2] First, a certain instability of the genome is present causing genetic diversity and thus genetic mutations, which is true for all human beings and second, the adaptation of the cancer cells to the body's immune response.[2, 3] In fact, inflammation was found to promote tumorigenesis by producing supportive molecules such as growth and proangiogenic factors or matrix-modifying enzymes, which assist in invasion and angiogenesis. These characteristics lead to the ten hallmarks found for most of the human cancers and are listed below.[3]

(1) Genetic mutations and genomic instability
(2) Self-dependence of growth signals
(3) Resistance to growth-inhibitory signals
(4) Circumvention of programmed cell death (apoptosis)
(5) Replicative immortality
(6) Maintained angiogenesis
(7) Metastasis and tissue invasion
(8) Carcinogenic inflammation
(9) Reprogramming cellular energy metabolism
(10) Evasion of immune response

The underlying details and mechanisms of each of these hallmarks are very complex and are out of the scope of this work. However, these hallmarks present a valuable basis for understanding the fundamental principles of the biology of cancer. In addition, these hallmarks highlight the most common differences between cancerous and normal tissue and thus provide some basic targeting concepts for cancer treatment. Nevertheless, the tumor tissue does not only consist of accumulated primary cancer cells, as these rather represent the basis of a tumor. The tumor itself consists of a set of different cell types forming and promoting the tumors' microenvironment. In brief, this malignant microenvironment of solid tumors contains primary cancer cells, invasive cancer cells, cancer stem cells, immune and inflammatory cells, cancer-associated fibroblasts, pericytes and endothelial cells.[3] In addition, the different tumor cells were discovered to exist in different variants of subpopulations. The rarely existing populations of cancer stem cells were attributed to have self-renewable abilities, are therapy resistant and potentially lead to recurrence of cancer.[4] Accordingly, tumors reflect a dynamic, heterogeneous tissue and therefore, researchers of the past decades have become increasingly aware of recognizing tumors as organs. In fact, its complexity is equal to or even exceeds that of normal tissues underlining the challenges of cancer treatment.[3]

1.2 Cancer treatment

The approach for treatment of malignancies is mainly influenced by type, stage and location of the tumor. If possible, all malignant cells are surgically removed followed by chemotherapeutic or hormonal treatment.[5] Another method is the application of radiotherapeutic agents.[5] The term 'chemotherapy' was invented by Paul Ehrlich at the end of the 19th century.[6] Paul Ehrlich was also the first proposing a connection of chemistry and biology and postulated the possibility of targeting biological receptors with distinct chemical structures. Basis for this assumption have been his observations that different types of dyes used for histological staining showed different affinities and local accumulation on different cell lines. Thus, the correlation between chemistry and biology and his pioneering research have been paving the way for modern medicine.[6] A major breakthrough in treatment of solid tumors (cancerous tissue without liquid areas or cysts) was the discovery of the antiproliferative properties of cisplatin (*cis*-diamminedichloridoplatinum(II); see Figure **1**) by Rosenberg *et al.* in 1965.[7] In 1978, the Food and Drug Administration (FDA) approved cisplatin for treatment of ovarian and testicular cancer.[8] Until today, cisplatin and its derivatives carboplatin and oxaliplatin (approval in 1989 and 2002, respectively) are the most widely applied inorganic chemotherapeutic drugs against solid tumors like testicular, ovarian, colorectal, bladder or lung cancer.[9] Nevertheless, these drugs face two main drawbacks namely the severe side effects and the development of resistances. These days, both events can be explained by the mechanism of action of these platinum-based drugs.

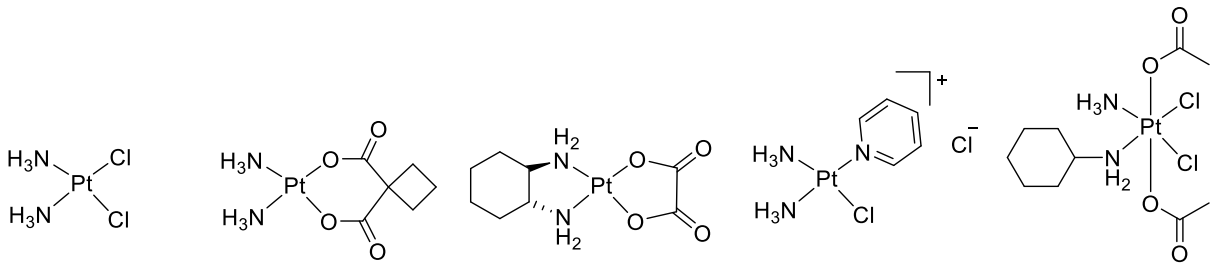

Figure **1**: Structures of the chemotherapeutic platinum-based drugs cisplatin, carboplatin, oxaliplatin, cDPCP (*cis*-diammine(pyridine)chloroplatinum(II) chloride and satraplatin.[10]

For decades, interdisciplinary investigations have been carried out to identify their mechanism of action and thus, establish solutions for these problems. At first, the structural features of the complexes needed to be assessed. Accordingly, the square planar coordination geometry of the platinum(II) compounds displays two *cis*-standing amine-based ligands ('nonleaving group') and two *cis*-standing 'leaving' ligands (see Fig. **1**), which are replaced as initiation of the drugs' mode of action. When the drug is administered by intravenous injection, a chloride concentration of about 100 mM sustains the composition of the drug. For the non-chloride platinum drugs, a replacement of the 'leaving ligands' by chloride is assumed. Subsequently, the agent enters the cell either *via* passive diffusion and/or *via* active transport by membrane proteins.[11] In the cytoplasm, where a decreased chloride concentration of $[Cl^-] \approx 4$ - 10 mM is present, *cis*-$[Pt(NR_3)_2Cl(H_2O)]^+$ and/or *cis*-$[Pt(NR_3)_2(H_2O)_2]^{2+}$ forms with a half-life of approximately 2 h.[11] When applying chelating ligands opposite to the amine ligands (like carboplatin and oxaliplatin, see Fig. **1**), the stability of the drug in aqueous solution is increased to periods of a week up to months. The thus formed positively charged aquated platinum drug enters the cell nucleus and a heterocyclic DNA base subsequently replaces the weakly bound water molecules. The most nucleophilic nucleotides are guanine and adenine and thus these are readily platinated. Following, cross-links between either the same (intrastrand cross-links) or another DNA strand (interstrand cross-link) are generated (see Fig. **2**). The same process occurs upon treatment with carboplatin or oxaliplatin, however, the ratio of the coordinated base pairs differs.[11] Platination of the DNA leads to unwinding and bending and therefore damage of the DNA. This causes an inhibition of DNA transcription and replication and thus, cell death is initiated.[12] However, this process is highly unselective because the platinum-based drugs are not able to distinguish between healthy and cancerous tissue thus leading to severe side effects, which are similar for the three drugs. The major differences in their effects is the dose-limiting toxicity (DLT), which is defined as a severe effect of the drug that prevents a dose increase or even a stop of this level of treatment.[12] In the case of cisplatin, the DLT is nephrotoxicity (damage of the kidneys). Carboplatin causes myelotoxicity and oxaliplatin can be severely neurotoxic. Additionally, for the three platinum drugs, more than 40 particular side effects are known, which can be categorized

in seven groups: nephrotoxicity, neurotoxicity, ototoxicity, cardiotoxicity, hepatotoxicity, hematological toxicity and gastrointestinal toxicity highlighting the need for new, similar effective but less toxic chemotherapeutic drugs.[12]

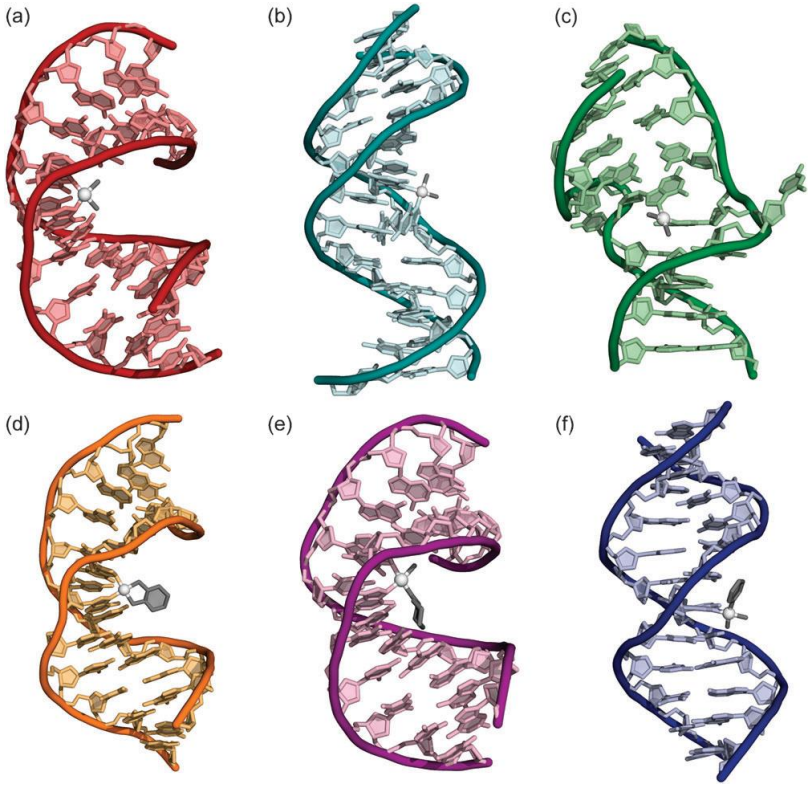

Figure **2**: Schemes of double stranded DNA – platinum adducts of different platinum-based anti-cancer agents obtained by X-Ray crystallography and NMR studies. (a) cisplatin intrastrand cross-link; (b) cisplatin intrastrand cross-link; (c) cisplatin interstrand cross-link; (d) oxaliplatin intrastrand cross-link; (e) satraplatin intrastrand cross-link; (f) cDPCP monofuntional adduct. [10] Reprinted from Ref. [10] by permission of The Royal Society of Chemistry.

Despite the serious side effects, another major limitation for the clinical application of platinum-based chemotherapeutics is the development of resistances leading to therapeutic failure. These chemoresistances are often developed during a prolonged treatment. Accordingly, for example, cisplatin-treatment of ovarian cancer with an original response of about 70 % may lead to a patient survival rate of 15 – 20 % in five years mainly due to the development of cisplatin-resistance. In addition, these cisplatin-resistant cancers are completely crossresistant to carboplatin indicating a similar mechanism of resistance for both drugs.[13] During the years of intensive research on platinum-resistance, the identified pathways can be categorized into four groups. First, the pre-target resistance, where changes lead to quenching of platinum-drugs prior to DNA binding. Second, the on-target resistance concerning resistances related to DNA-platinum adducts. Third, the post-target resistance correlated with the signaling pathways initiated by the DNA-platinum adducts. And fourth, the off-target resistance, which is not clearly linked with the platinum drug, however, is platinum-mediated.[9]

Several different approaches were evaluated for their ability to circumvent the side effects of cisplatin treatment and/or cisplatin-resistance. For instance, these are addressing two different anti-cancer mechanisms by combining cisplatin with other anti-cancer agents, the further modifications of platinum-based compounds, a change of metal, the application of platinum(IV) prodrugs, or the use of drug-delivery systems like micelles, nanoparticles, polymers, proteins or supramolecular coordination compounds (SCCs).[11, 14]

1.2.1 Inorganic supramolecular coordination compounds (SCCs)

SCCs are three-dimensional (3D) inorganic entities providing cavities for the encapsulation of guest molecules. In contrast to the polymeric metal-organic frameworks (MOFs), SCCs are distinct inorganic compounds forming 2D and 3D capsules, which are synthesized *via* coordination-driven self-assembly. Suitable ligand systems provide at least two binding sites for different metals forming molecular assemblies with an M_xL_y composition (M = metal ion, L = ligand). Size and shape of the SCCs can be influenced by the metal-to-ligand ratio, the coordination geometry of the applied metal and by the ligand's shape and denticity. Accordingly, several different geometries like cyclic, polyhedral, cubic or prismatic are reported.[15, 16] These supramolecular compounds were evaluated for their applications e.g. as molecular sensors, probes, catalysts or in host-guest chemistry. In host-guest chemistry, these cage-like structures with internal cavities were used to encapsulate different molecules by specific as well as nonspecific host-guest interactions like Coulomb, van-der-Waals and steric interactions. In addition, also hydrogen bonding, ion-association forces and a supportive combination of charge, shape, size and solvation was found to enhance encapsulation. This molecular recognition was exploited in host-guest chemistry for different applications such as nanoreactors or as drug delivery system.[15] A successful example for a drug delivery system is based on metals displaying four accessible coordination sites and a rigid, organic ditopic ligand. In most cases, Pd(II) or Pt(II) were applied. A general structure of this system is given in Figure **3**.[15, 17-22] Initial studies on the host-guest-chemistry of Pd(II) supramolecular structures with simple hydrocarbons such as toluene or naphthalene did not show any encapsulation. However, 1,4-dicyanobenzene was successfully incorporated into the cavity. Studies to understand this selectivity were performed and some basic features of encapsulation of neutral molecules were found. First, a suitable shape and size of the guest molecule is required. Second, the guest has to have at least one appropriate donor-group for interactions with the host. One main opponent for encapsulation was found to be solvent molecules, however, also the counterion was already observed inside the cavity.[23] Encapsulation studies with cisplatin proved the inclusion of two cisplatin molecules inside the cavity of **1**. Interestingly, no encapsulation was observed for **2** highlighting the importance of internal interactions between host and guest. For [**1**(cisplatin)$_2$](BF$_4$)$_4$, hydrogen-bonding interactions of the amine ligands and the central pyridine unit and the chloride ligands and the internal CH moieties of the coordinated

pyridine were observed. Moreover, Crowley *et al.* performed reversible dis- and re-assembly studies of cisplatin-SCC adducts confirming a potential release of cisplatin.[24] This opens perspectives for drug delivery with controlled drug release in cancer cells.[24] *Endo*- and *exo*-functionalization was shown to tailor the properties of the cages for specific applications. In terms of drug delivery, the space inside the cavity needs to be maintained for drug encapsulation and thus, research mainly focuses on *exo*-functionalization. This includes the variation of the counterion influencing the solubility of the cages.[23] One approach to versatile functionalized cages was invented by Crowley *et al.* They modified the cages with azide-moieties which enables the introduction of several functionalities *via* click-chemistry.[25] Thus, important properties like solubility, biological targeting or photophysical and electrochemical activity can be tuned.

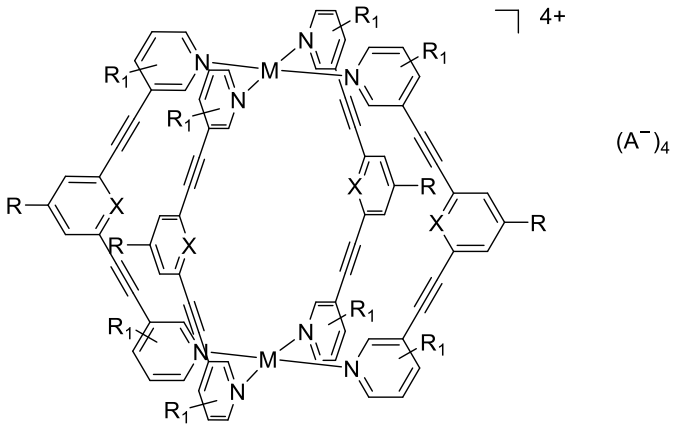

1 M = Pd, X = N R_1 = H, A^- = BF_4^-, R = H
2 M = Pd, X = CH, R_1 = H, A^- = BF_4^-, R = H
3 M = Pd, X = CH, R_1 = H, A^- = BF_4^-, R = CH_2OH
4 M = Pd, X = CH, R_1 = H, A^- = BF_4^-, R = COOH
5 M = Pd, X = CH, R_1 = *m*-OMe, A^- = BF_4^-, R = NH_2
6 M = Pd, X = N, R_1 = *m*-OMe, A^- = BF_4^-, R = H
7 M = Pd, X = CH, R_1 = H, A^- = OTf^-, R = OMe
8 M = Pt, X = CH, R_1 = H, A^- = OTf^-, R = OMe
9 M = Pd, X = CH, R_1 = H, A^- = BF_4^-, R = NH_2

Figure **3**: General structure of M_2L_4 SCCs evaluated for cisplatin encapsulation and biological activity.[24, 25]

In first biological studies, the cages without encapsulated cisplatin were observed to be moderately cytotoxic in cancer cells.[19, 22, 26] Encapsulated cisplatin displayed a slightly increased antiproliferative effect compared to free cisplatin. However, this effect strongly depends on the applied cage-system and the cancer cell line (see Table **1**) and only little data is published. In general, a quantitative comparison of these results is difficult since a uniform investigation of all cage-cisplatin systems is lacking. However, qualitative conclusions can be drawn. For example, cisplatin encapsulated in cage **6**, even exhibits a higher IC_{50} value in HepG2 cells compared to cisplatin alone.[19]

Table **1**: IC_{50} values [µM] determined for different M_2L_4 cages, cisplatin and encapsulated cisplatin in different cancer cell lines.

Compound	Cancer cell line	Compound	Cancer cell line	Cancer cell line
	SKOV-3		A549	HepG2
3	11.6 ± 1.7[22] (72 h, MTT)	**5**	> 100[19] (48 h, MTT)	> 100[19] (48 h, MTT)
[(cisplatin)$_2$ ⊂ 3]	1.9 ± 0.5[22] (72 h, MTT)	**[(cisplatin)$_2$ ⊂ 5]**	11.0 ± 1.3[19] (48 h, MTT)	5.2 ± 0.3[19] (48 h, MTT)
4	94.4 ± 7.9[20] (72 h, MTT)	**6**	> 100[19] (48 h, MTT)	96.1 ± 1.4[19] (48 h, MTT)
[(cisplatin)$_2$ ⊂ 4]	12.8 ± 1.2[20] (72 h, MTT)	**[(cisplatin)$_2$ ⊂ 6]**	6.6 ± 1.0[19] (48 h, MTT)	13.4 ± 3.0[19] (48 h, MTT)
Cisplatin	15.4 ± 2.2[22] (72 h, MTT)	**Cisplatin**	16.8 ± 0.7[19] (48 h, MTT)	6.7 ± 0.9[19] (48 h, MTT)

An interesting encapsulation behavior was observed for cages **7** and **8** by Amouri *et al.*[17] The square planar Au(III) thiolate compound [*n*-Bu_4N][$Au(bdt)_2$] (bdt = benzene-1,2-dithiolate) was chosen as guest molecule for simulating competitive coordination environment. It provides strongly coordinating sulfur ligands and as well as challenging magnetic and redox properties. Encapsulation studies with Pd-based cage **7** revealed decomposition of the cage instead of guest incorporation. In contrast, the analogous Pt-based cage **8** readily encapsulated the guest molecule without signs of decomposition. Along with DFT calculations, this shows a higher stability for the Pt-based cage compared to **7** and thus, **8** provides a different host-guest chemistry.[17]

A further example for self-assembled M_2L_4 capsules evaluated in host-guest chemistry and anti-cancer studies is given in Figure **4**. Structurally, the metal centers of these SCCs are connected *via* fluorescent anthracene-based ligands, which might be useful for imaging purposes either for visualization of the localization of the drug or for identification of cancerous cells.

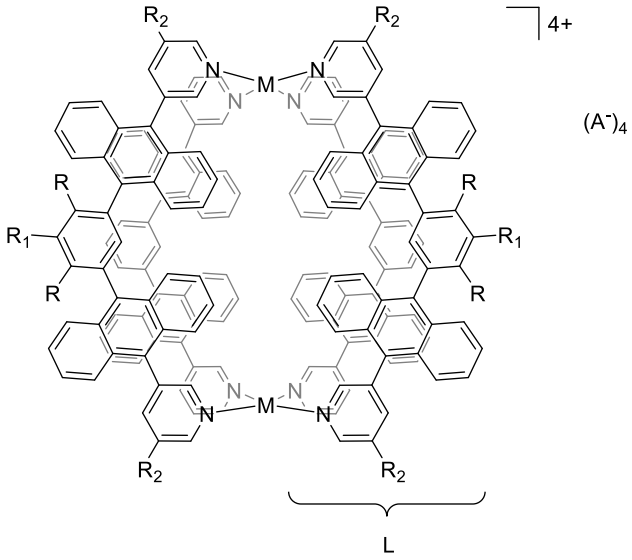

M = Mn^{2+}, Co^{2+}, Ni^{2+}, Cu^{2+}, Zn^{2+}, Pd^{2+}, Pt^{2+}
L_1: R = R_1 = $OCH_2CH_2OCH_3$, R_2 = H
L_2: R = $OCH_2CH_2OCH_3$; R_1 = H, R_2 = H
L_3: R = $OCH_2CH_2OCH_3$; R_1 = H, R_2 = OCH_3
A^- = NO_3^-, OTf^-, ClO_4^-

Figure **4**: General structure of anthracene-based self-assembled SCCs.

The ligand system was shown to stabilize a variety of different transition metals, each altering the fluorescent properties of the resulting cage.[27] The ligand itself has a quantum yield of ϕ = 0.79. The respective Cu^{2+}, Co^{2+}, Pd^{2+} or Pt^{2+} capsules were shown to be non-emissive due to heavy metal quenching. Ni^{2+} and Mn^{2+} based capsules were found to be weakly emissive and the highest quantum yield was determined for Zn^{2+}-based cages with ϕ = 0.81 with a strong blue fluorescence at λ = 438 nm.[27] In X-Ray single crystal analysis, the central cavity was determined to exhibit a volume of about 600 $Å^3$ for the Pd^{2+} species. Together with the shell-like character of the anthracene ligands isolating the cavity from the outside, these capsules represent interesting transport system or molecular flask.[27] Thus, the Pd- and Pt-based anthracene capsules were evaluated for the encapsulation of different guest molecules showing to incorporate a great number of planar small molecules like cyclophane, pyrene or triphenylene.[28] Preliminary biological studies in cancer and healthy cell lines showed a good selectivity to leukemia cells over non-malignant kidney cells. In addition, in particular the Pd-based capsule maintained a low IC_{50} value (1.9 ± 0.2 µM) in cisplatin-resistant HL-60 cells thus lacking cross-resistance.[29]

An important issue of *in vivo* studies of cancer drugs is the determination of their distribution in different tissues and within different cell compartments. Fluorescence microscopy has been established as a broadly available tool to study the spatial distribution of labeled molecules in living systems. As shown for inherently fluorescent ligand systems upon coordination and cage formation with heavy metals like

Pd and Pt, the fluorescence significantly decreases. Therefore, labeling of cage systems via *exo*-functionalization with fluorescent dies was investigated making advantage of applicable methods as e.g. click chemistry. Further functionalization include fluorophore-coupling. A successful example is presented in figure **5**.[20, 21, 30] Thus, cage **4** was successfully modified by coupling with naphthalene or anthracene moieties.[20] However, the determined quantum yields were too low for fluorescence microscopy (< 1 % or no fluorescence at all). Even the quantum yields of the barely functionalized ligands of **4** and **9** were higher (8 % and 52 %, respectively). The reason for the poor photophysical properties of the naphthalene and anthracene functionalized ligands and cages was found to be the torsion of the amide bond, which was determined using DFT calculations.[20] Superior imaging properties were expected for heteronuclear Pd/Ru-based cage **10**, where a greater separation of the fluorophore and the fluorescence-quenching Pd^{2+} was implemented. In contrast to that, cage **11** was lacking that linker between the rigid cage-forming moiety and the Ru-tripyridyl tag (see Figure **5**).[21] Thus, the ligand of **10** was highly fluorescent with quantum yield of 88 % and the corresponding Pd cage was determined to have a quantum yield of 66 % at λ = 640 nm. However, the excitation wavelength was in the UV region, which is not optimal for fluorescence microscopy since the high energy radiation was shown to cause severe damages to cells.[21] Hence, another fluorescent label, namely boron dipyrromethene (BODIPY), was evaluated as potential fluorophore for these SCCs by Casini *et al.* (see Figure **5**, cages **12**, **13** and **14**).[30] Evaluation of the cages in A375 cancer cells showed no toxicity of the complexes, which makes them useful candidates for imaging purposes. In addition, determination of the quantum yield performed with an excitation wavelength of λ = 540 nm in the visible region resulted in a yield of 50 – 70 % rendering these cages as promising alternatives for fluorescence imaging in cells. Initial imaging experiments indicate that the cellular uptake proceeds *via* active endocytosis.[30]

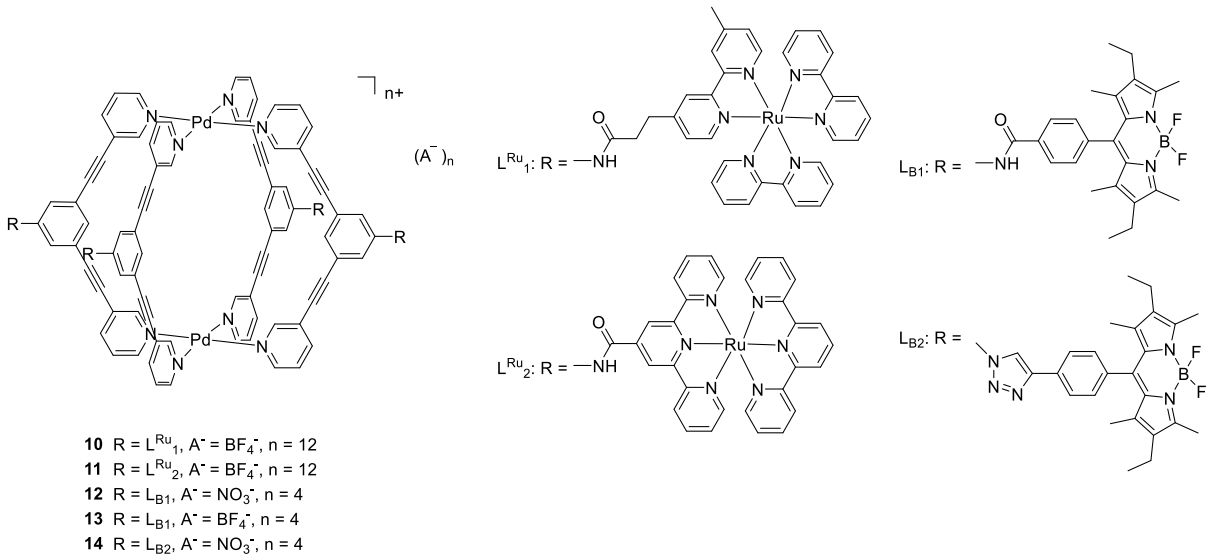

Figure **5**: Structures of fluorophore-tagged SCCs.[21, 30]

However, tumor-targeting exploiting the 'enhanced permeability and retention' (EPR) effect is not likely to be effective for such M_2L_4 metallacages, because they are too small.[31] Thus, investigations in modifying the cages with peptides targeting specific tumor receptors like integrins showed the first promising results in reducing platinum accumulation in non-target tissues.[32] Nevertheless, before these and similar systems may be applied for enhancing chemotherapeutic treatments or as imaging agents, they first need to enter clinical trials and proof their applicability.[33]

1.2.2 Metalorganic *N*-heterocyclic carbene (NHC) complexes

A further method to overcome cisplatin-resistance is the change of the metal center and the ligand system used for such small molecules. During the past decades, the versatile chemistry of *N*-heterocyclic carbenes (NHCs) is increasingly studied in experimental as well as theoretical investigations. The keyword '*N*-heterocyclic carbene' is part of numerous publications each year exceeding even a thousand the last two years (see Figure **6**, left). Nevertheless, it appears that a particular plateau is reached for the number of published studies. The studies focus for example on the rich coordination chemistry of NHCs, which were found to be suitable ligands for transition metals but also main group and f-block metals.[34-37] These metalorganic complexes are applied in many different fields like catalysis[38-42] or medicinal chemistry[43-47]. In terms of medicinal chemistry, a search for '*N*-heterocyclic carbene anti-cancer' proves the increasing interest in that topic (see figure **6**, right).

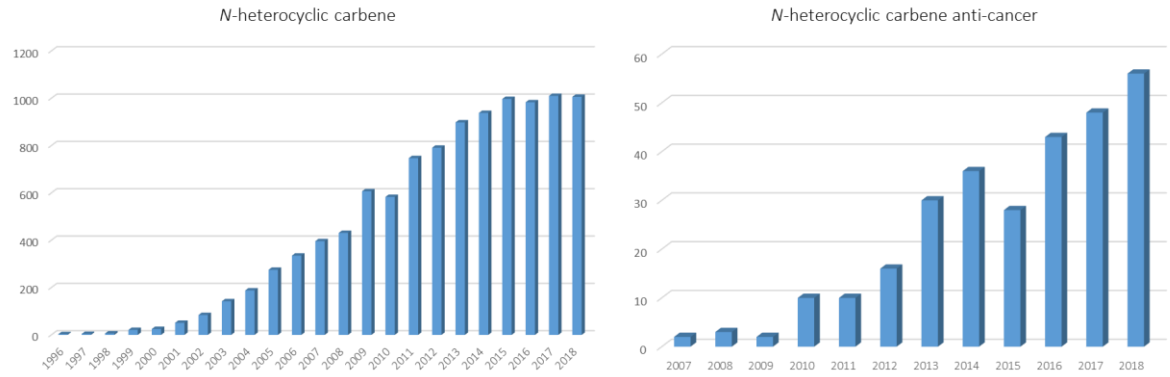

Figure **6**: Numbers of publications with the keyword '*N*-heterocyclic carbene' (left) and '*N*-heterocyclic carbene anti-cancer' (right) searching in *Web of Science*.

Historically, in 1964, Ernst Otto Fischer published the first metal carbene complex with an electronegative singlet carbene coordinated to tungsten(0).[48] Thus, 'Fischer-type carbenes' were described as electrophilic carbenes with a singlet ground state stabilizing late transition metals in low oxidation states. Contradictory, 'Schrock carbenes' first reported by Schrock *et al.* were described as nucleophilic triplet carbenes stabilizing early transition metals in high oxidation states.[49] The third type of carbenes, the nitrogen containing singlet-carbene-containing *N*-heterocyclic carbene compounds, were simultaneously discovered by Öfele and Wanzlick in 1968.[50, 51] Together, these pioneers formed a

valuable basis for the upcoming carbene chemistry and the discovery of the first stable, isolated free NHC published in 1991 by Arduengo *et al.*[52, 53] A structural overview of these historic milestones is given in Figure **7**.

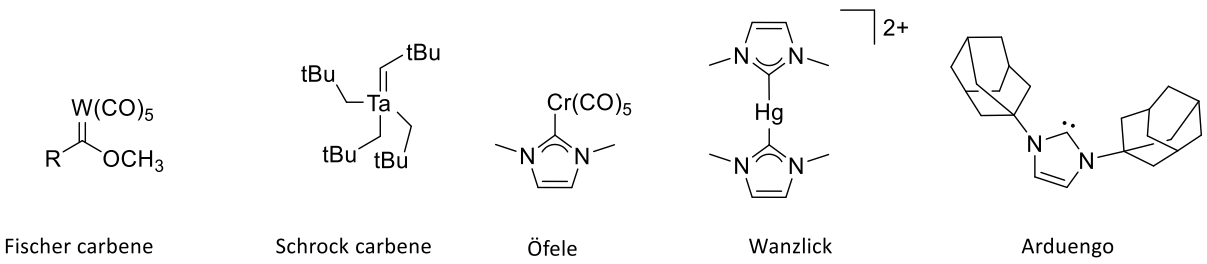

Figure **7**: Structures of historically important carbenes and carbene complexes.

By definition, carbenes are neutral compounds exhibiting a divalent carbon atom displaying six rather than eight valence electrons.[34] As consequence from this unsaturated nature, two different electronic configurations of the carbene carbon atom are possible. The first is a triplet configuration with two singly occupied sp^3 hybrid orbitals. The second possible configuration is a singlet state with both electrons located in one sp^2 hybrid orbital accompanied by one unoccupied p_z orbital. For NHCs, the carbene is present in a singlet configuration due to the electron withdrawing (-I-effect) nature and the mesomeric effect (+M-effect) pushing electron density to the unoccupied p_z orbital of the neighboring nitrogen atoms (see Figure **8**).[34] Upon coordination to a metal center, the sp^2 hybrid orbital interacts with the empty d orbital of the metal atom, which is the most important contribution to the metal-NHC bond. Additionally, π*-backdonation of the metal's d orbital to the unoccupied NHC p_z orbital and π-donation from the carbene to the metal d-orbital contributes to the bonding as depicted in Figure **8**.

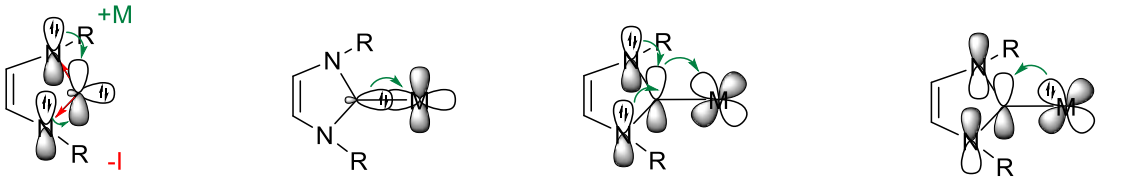

Figure **8**: General electronic structure of a free NHC (left) and the three bonding contributions of a metal-NHC bond.[54]

Despite this theoretical description, the metal-NHC bond is most commonly drawn as a single bond because this best describes the experimentally observed rotation of the metal-NHC bond and further enables a discrimination between NHCs and the Fischer- and Schrock-carbenes. The double bond character is drawn as a bent line between the heteroatoms representing the delocalization of the π-electrons.[34]

After the spectroscopic characterization of the first stable NHCs, the similarity to phosphanes was rapidly recognized. Both are strong σ-donor and weaker π-acceptor ligands. However, NHCs display stronger electron-donating properties than phosphanes, which leads to an enhanced thermodynamic stability of the metal-NHC bond. Thus, a shorter metal-NHC bond and a greater bond dissociation energy is generally observed compared to analogous phosphane complexes.[34] Consequently, NHC-metal complexes are thermally and oxidative more stable. Another advantage of NHCs compared to phosphanes are their easily tunable steric and electronic properties. Accordingly, modification of phosphane-based ligands is not trivial but NHCs can be modified relatively simple in terms of their nitrogen substituents ('wingtips'), the backbone functionalities and the type of heterocycle. However, the most widely used skeletal structures for NHCs are imidazoles.[34] The structural versatility is exploited for different applications of NHC-metal compounds. One very prominent example is the catalytic application of NHC complexes, where again NHCs outperform phosphanes.[38] One of the first synthetic routes to a simple Pd-*bis*-NHC-complex along with its advantages over phosphanes and its relevance for catalysis was reported in 1995 by Herrmann *et al*.[55] Since then, numerous reactions were found to be catalyzed by NHC compounds, such as C-H activation, C-C, C-H, C-O, C-N bond formation, reduction reactions like hydrosilylations or transfer hydrogenation, cyclization reactions and polymerizations.[39, 56]

Another application of increasing interest is the use of NHC complexes, and especially gold-NHC-complexes, in medicinal chemistry (see figure 6). Since 2004, when Berners-Price *et al*. reported studies on the antimitochondrial properties of various Au(I) NHC-based compounds (see Figure 9), numerous biological studies of gold-based NHC compounds are published each year.[57-70] However, none of these versatile NHC complexes reached clinical trials yet. Thus, in terms of medical applications, the Au(I) phosphane complex 1-thio-β-D-glucopyranosatotiethylphosphine gold(I)-2,3,4,6-tetraacetate, named auranofin (see Figure 9), is superior to NHC-based gold compounds. Sutton *et al.* developed auranofin in 1972 along with biological studies showing auranofin's antiarthritic properties.[71] In 1985, it was approved by the FDA for the treatment of rheumatoid arthritis.[72] Moreover, auranofin has been evaluated for its therapeutic effects on many different human diseases such as cancer, neurodegenerative disorder and parasitic and bacterial infections and is still part of clinical trials up to phase II. In fact, a strong anti-cancer activity against various cancer types *in vitro* as well as *in vivo* is reported for auranofin. Due to its versatile medicinal effects, many studies to evaluate the mechanism of action were performed, however, the mechanism is not fully elucidated yet. Nevertheless, some biological targets were identified for auranofin. These targets were also identified for other gold-based anti-cancer agents and thus are briefly discussed using the example of auranofin. At cytotoxic concentrations, a dose-dependent inhibition of DNA, RNA and protein synthesis was observed for auranofin.[72] However, the DNA-interaction and the inhibition of DNA replication is found to be not

responsible for the cytotoxic effects.[44] Apoptosis was observed to be induced in several cancer cell lines by an increase of reactive oxygen species (ROS) and a change of the intracellular redox state. In addition, the gold drug was found to strongly inhibit Thioredoxin reductases (TrxRs), which is related to that change of redox state of the cell causing severe oxidative stress.[72]

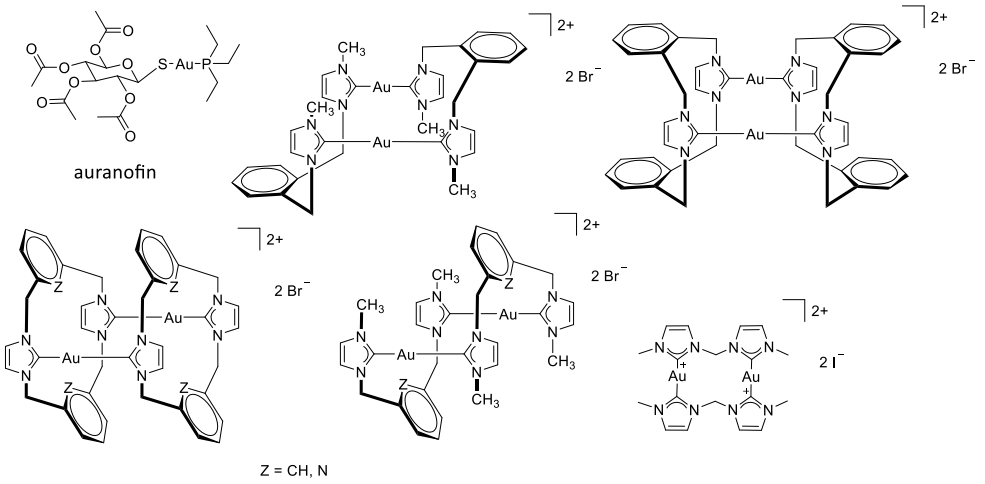

Figure 9: Structures of auranofin and some exemplary Au(I)-NHC-complexes studied by Berners-Price *et al*.[59, 72]

The inhibition of TrxR was found for numerous antitumor gold compounds thus presenting a relevant target for gold complexes in general.[61, 65, 73-77] The high affinity of gold-based compounds for TrxR originates from the high affinity of gold for selenium and the fact that TrxR displays selenocysteine moieties. The selenoenzyme is expressed in different cellular compartments, such as in the cytosol (TrxR1) and the mitochondria (TrxR2).[72, 78] Thioredoxin (Trx) and its reductase contribute to many different biological processes like redox homeostasis, antioxidative effects, regulation of transcription factors, and cell proliferation and replication. In addition, the Trx system is involved in diverse physiologic and pathogenic pathways in cancer, parasitic infections and neurodegenerative disorders. Moreover, high expression rates of Trx and TrxR in cancer cells are directly related to difficult-to-treat carcinomas of e.g. lung, ovarian and breast. Investigations showed that in particular TrxR1 plays a crucial role in cancer cell proliferation and the development of metastases. This key role is highlighted by analysis of the expression level of TrxR1 and drug-effectiveness. For instance, in highly expressing TrxR1 cancer cells, the cytotoxic effect of cisplatin is increased compared to cells with low TrxR1 expression levels.[72]

Another similar redox relevant protein is glutathione (GSH). The GSH system consisting of GSH and glutathione reductase (GR) is closely related to the Trx system; however, GSH does not feature seleno-groups but thiol-entities. Consequently, gold complexes preferably interact with TrxR over GSH.[61] Nevertheless, GSH is the most abundant thiol-containing protein in cells with a concentration of 0.5 – 10 mM and thus represent an important target for gold-based compounds as well.[67] Most commonly,

compounds display gold in oxidation states +3, +1 and 0. However, in the presence of these intracellular thiols, Au(III) is readily reduced to Au(I)/(0) which is accompanied by ligand exchange due to a change in coordination geometry. While Au(III) complexes display a planar, four-fold coordination geometry, Au(I)/(0) are most commonly linearly coordinated by two ligands.[67] Depending on the applied ligand system, the ligand exchange can increase or decrease the cytotoxic properties of such compounds. Nevertheless, the reactivity of Au(III)/(I)/(0) can be influenced by the selection of ligand and its degree of chelation.[67] For example, the thiol reactivity of the gold center, e.g. towards GSH is strongly influenced by the wingtip substituents of the NHC ligands. Accordingly, the application of methyl wingtips will lead to the most reactive compounds and the use of bulkier substituents such as mesityl will offer protection of the Au-center. Additionally, the nature of the ligand in trans-position also influences ligand exchange reactions. Nevertheless, a certain stability of the gold complex is needed to prevent off-target binding.[79]

Another described mechanism of such anti-cancer complexes is based on intercalation, thus the non-covalent stacking of planar (heterocyclic) aromatic entities with DNA base pairs. This intercalation influences the conformation of the DNA double helix and may lead to lengthening, stiffing, and unwinding. The resulting effect is the same as for covalent DNA interactions leading to inhibition of replication and transcription.[80] One important therapeutic anti-cancer agent displaying intercalation properties is the widely applied organic drug doxorubicin (see Figure 10). Another widely applied organic intercalator is ethidium bromide (Figure 10), which is used to stain DNA in cellular studies. Moreover, transition metal based compounds like a Pt(II) terpyridine entity shown in Figure 10 was observed to be an effective DNA intercalator. In addition, the incorporation of metal centers opens perspectives for introducing further properties like luminescence as observed for Ru(II) polypyridine compounds, or photoinduced DNA cleavage. Moreover, in such systems, the use of further ligands for specific targeting is possible.[81]

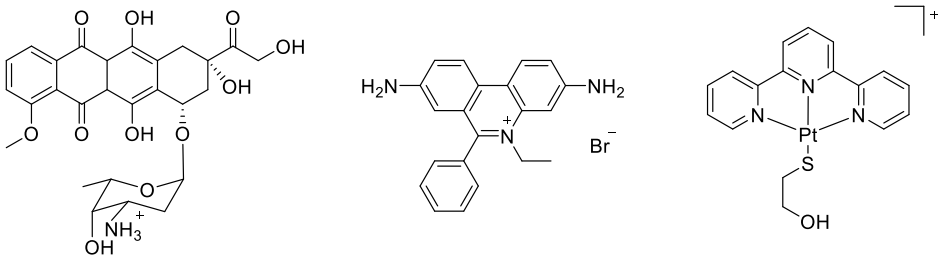

Figure 10: Structures of known DNA intercalators.[81]

Furthermore, a number of gold-based NHC complexes was designed to specifically intercalate to distinct parts of the DNA, namely the G-quadruplexes.[82] These quadruplex DNA structures are formed in guanine-rich sequences, were four guanine bases form the square planar 'guanine tetrad' *via* Hoogsten

hydrogen bonding. Two or more of these tetrads build up the G-quadruplex by stacking on top of each other. Enhanced physiological stability is provided by cations in the center of these oligonucleotides.[83] Specifically the 3'-ends of human chromosomes, the telomeres, consist of aggregated d(TTAGGG) motifs building such G-quadruplexes. During each cell division, the telomeres are shortened. To tackle this, specific enzymes, the telomerases, are present in cells for retaining the lengths of the telomeres and thus protection of the chromosomes.[84] Interestingly, it was observed that the telomerases are inactivated when the telomeric G-quadruplexes are stabilized by such intercalating drugs.[85] Consequently, stabilizing or enhancing the formation of G-quadruplexes by specific small molecules decreases cell proliferation and potentially lead to cell death. Thus, intercalation offers potential for the development of novel effective anti-cancer agents.[82] The majority of such stabilizing compounds consist of planar organic heteroaromatic systems as shown in Figure 10. Moreover, some general features as basic requirements for G-quadruplex DNA intercalation have been evaluated. First, the ligand/compound needs to be planar. Second, a positive charge is beneficial for interaction with the negatively charged DNA. And third, the compound is, at least partly, aromatic for π-stacking interactions with the guanine moieties.[82] In Figure 11, some of these G-quadruplex intercalating systems based on Au(I)/(III) are presented.

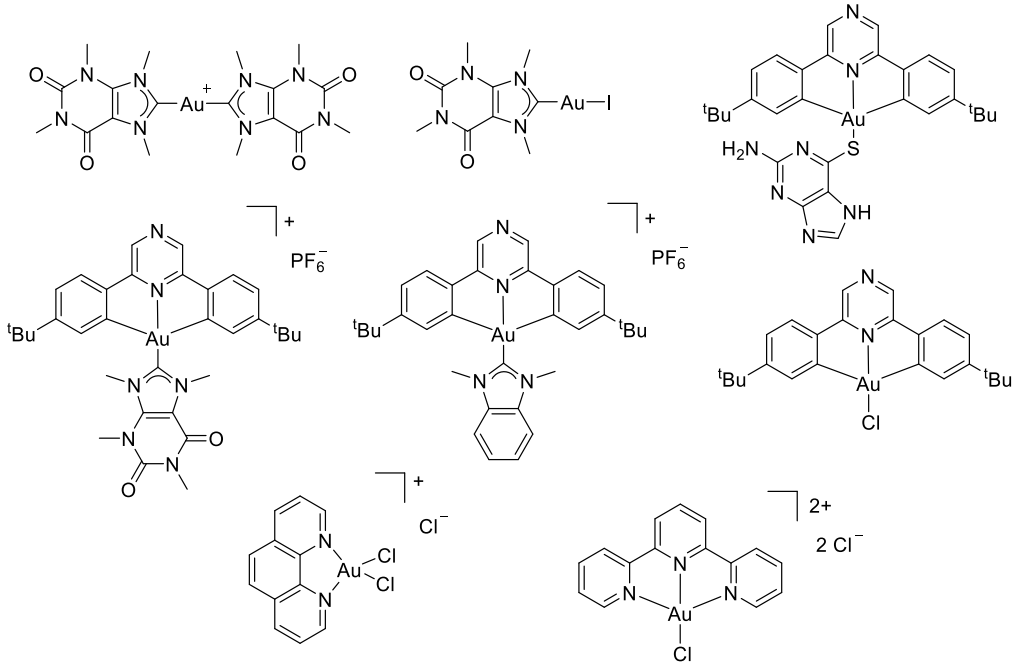

Figure 11: Structures of G-quadruplex-intercalating Au(I) and Au(III) based complexes.[70, 82, 86, 87]

This special combination of Au and NHC allows the synthesis of a wide variety of Au-NHC-complexes, which are sufficiently stable for potential applications.

In summary, the special combination of the versatile chemistry of NHC ligands and Au allows the synthesis of a wide variety of Au-NHC-complexes, which are sufficiently stable for the development of potent anti-cancer agents. Some general trends for the rational design of such compounds were discovered. One important feature for anti-cancer activity is the balance between hydrophilicity and lipophilicity. Numerous studies draw the same conclusion that an increase in lipophilicity results in an increased anti-cancer activity. However, when a certain limit is exceeded, the beneficial influence of the gold atom is diminished and the ligand itself has the greatest influence on the cytotoxicity. Moreover, increasing anti-cancer effects can be observed for multidentate ligands compared to monodentate ligands.[58] In addition, multinuclear Au compounds also seem to exhibit beneficial effects on the cytotoxicity. However, this increase is not proportional to the number of gold atoms. No difference in anti-cancer activity was observed for neutral and cationic compounds. Finally yet also important, a synergistic effect is observed for heterometallic complexes leading to increased cytotoxicity and lower resistance effects due to addressing different anti-cancer mechanisms.[58]

1.3 Early transition metals in medicinal chemistry

Despite the above-discussed manifold medicinal applications of palladium, platinum and gold compounds, also early transition metal complexes were evaluated in biological studies. The following paragraphs will focus on molybdenum-, chromium- and vanadium-containing compounds and their biological relevance.

1.3.1 Molybdenum in biology

Molybdenum was mistaken for graphite by early chemists until 1778, when Carl Scheele was able to identify the element.[88] Naturally, it only exists in association with other elements, especially oxygen. In dilute solutions like soil and natural water, the predominant form is the molybdate anion MoO_4^{2-}. In higher concentrations, polymerization takes place leading to divers structures including polyoxomolybdates.[89] The most stable oxidation states, generally ranging from 2-6, are 4 and 6. Metallic molybdenum is obtained from primary mining processes and as byproduct of copper mining from ores like molybdenite(MoS_2) and ferrimolydenite ($Fe_2[MoO_4]_3$). It is used in steel alloys for e.g. power generation in gas and steam turbines, in missiles, and airplanes or as catalyst. Molybdenum acetyl acetonate for instance, is applied as catalyst in ethylene polymerization and in the production of polyurethane foams.[89]

Overall, molybdenum is an essential element for the human body. Molybdenum-containing enzymes catalyze important steps in basic metabolic processes like the carbon, sulfur, and nitrogen cycles. Nevertheless, little is reported about the toxicity of molybdenum.[89] Medicinally, the most prominent

example is tetrathiomolybdate, which is currently in phase II clinical trials for treatment of the Wilson's disease as well as different malignancies like breast cancer. Wilson's disease is a genetic mutation that leads to toxic copper accumulation in the body, which is successfully treated with tetrathiomolybdate. The mechanism of action is based on tetrathiomolybdate's ability to form a complex in association with copper and human serum albumin (HSA), which is subsequently excreted from the body and thus copper reabsorption is prevented. The same mechanism is beneficial for cancer treatment, because copper is required in angiogenetic processes. There, it is supposed, that a certain copper deficiency leads to inhibition of angiogenesis while other copper-mediated cellular processes are maintained.[90]

In general, compared to anti-cancer compounds based on gold, molybdenum-based complexes are little present in anti-cancer-studies. Searching for the terms 'gold anti-cancer' in *Web of Science* led to 2828 publications with 478 published in 2018. Searching for 'molybdenum anti-cancer' only resulted in 61 publications with nine in 2018. However, a slight increase of the number of publications might be identified.

Besides this unique anticopper mechanism of tetrathiomolybdate, a relevant biological target for molybdenum-based anti-cancer compounds was found to be the DNA. The identified mechanism includes intercalation like discussed for Au-NHC-complexes earlier, or DNA cleavage upon photoactivation. The structures of these compounds are given in Figure **12**.[91]

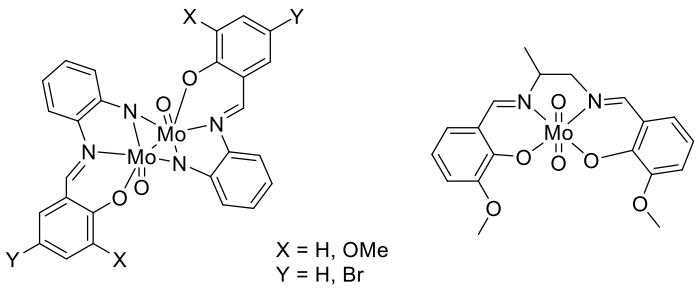

Figure **12:** DNA-targeting anti-cancer complexes based on molybdenum.[91]

One outstanding property of molybdenum is the ability to form a Mo_2^{4+} unit with a metal-metal quadruple bond. Historically, the first report of a quadruple bond was published in 1965 for $Re_2Cl_8^{2-}$. Theoretically, the bonding between elements is described with linear combination of atomic orbitals (LCAO) and molecular orbital (MO) theory. These calculations describe a single bond as an overlap of two s, two p or in this case two dz^2 orbitals from each of the two involved atoms and thus forming the σ molecular orbital. A double bond is formed by the overlap of the p or $d_{xz,yz}$ orbitals creating the π molecular orbital. An additional overlap of the d_{xy} orbitals form a δ molecular orbital resulting in a

quadruple bond.[92] In Figure **13**, the MO diagram of a D_{4h} symmetric compound with a metal-metal bond like $Re_2Cl_8^{2-}$ is presented.[93]

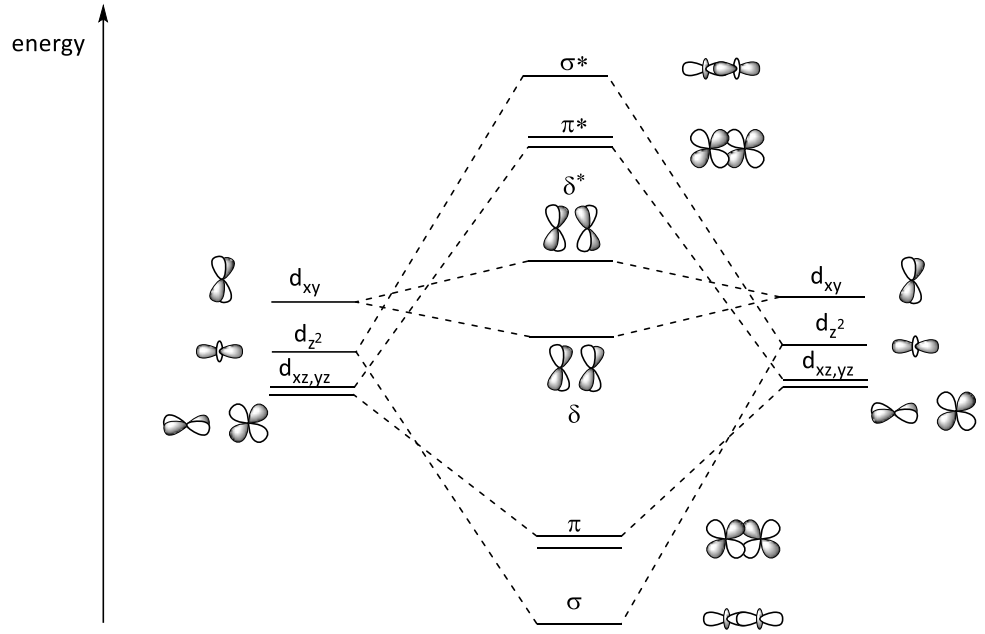

Figure **13**: Schematic representation of the MO diagram of a D_{4h} symmetric metal-metal compound such as $Re_2Cl_8^{2-}$.[93]

Such compounds featuring M-M multiple bonds are inherently rather unstable, reactive and non-water-soluble compounds. This drawback however provides also advantage in cancer treatment like antiradical and antioxidant properties if the molecule is appropriately stabilized. Therefore, different approaches were investigated to stabilize or protect such compounds, e.g. encapsulation in liposomes.[94] A very successful example are the dirhenium(III) complexes depicted in Figure **14**, which were encapsulated in liposomes and evaluated for their anti-cancer activity *in vitro* as well as *in vivo*. In general, the complexes were found to be non-toxic in cells. However, synergistic effects were observed when co-encapsulated in such liposomes with cisplatin, which is generally very toxic in dividing cells.[94]

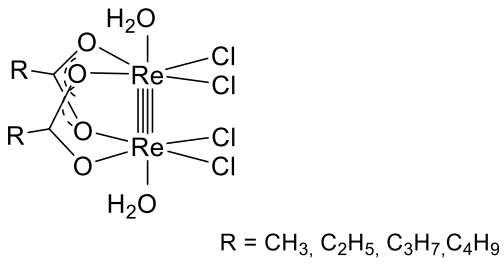

Figure **14**: Liposomal encapsulated dirhenium complex featuring a Re-Re quadruple bond evaluated in biological studies.[5, 94]

Co-encapsulated of the dirhenium compound with cisplatin in a ratio of 1:4, the dirhenium-platinum liposome exhibits remarkable anti-cancer activity exceeding that of cisplatin and the liposomal rhenium cluster. *In vivo*, this encapsulated rhenium-platinum compound shows a strong anti-cancer effect by

reducing the determined tumor volume in mice from about 60 – 100 mm^3 to 0 – 2 mm^3.[94] The strongest effect was observed for methyl-substituted dicarboxylates compared to ethyl, propyl or butyl. In addition to that, no toxicity for the hepatobiliary system was observed.[5]

1.3.2 Chromium in biology

In 1761, Johann Gottlob Lehmann, a German mineralogist, discovered an orange-red mineral in the Ural Mountains, which he misidentified as red lead mineral. 1797, Louis-Nicolas Vauquelin, who was the first able to isolate Cr_2O_3 from Crocoit, later recognized this compound as PbCrO4. The name 'chromium' derives from Greek words meaning 'color' which is chosen for chromium due its colorful compounds.[95] Industrially, metallic chromium is used in various applications such as dyes and pigments, metallurgy, catalysis or tanning.[95] In terms of its biological role, chromium is one of the most debated metals. The discussion focusses on different oxidation states of chromium, and predominantly on Cr(III) and Cr(VI). Cr(VI) based compounds are classified as class I human carcinogens. Models explaining this genotoxicity have identified different processes. At first, the Cr(VI) transport into cells is performed either actively *via* anion channels or passively by phagocytosis. It is assumed that this process is followed by reduction of the metal leading to Cr(V/IV) DNA-damaging intermediates and organic radicals. Additionally, kinetically inert DNA-Cr(III)-protein and DNA-Cr(III)-DNA crosslinks causing severe DNA damage.[96] In contrast to that, nutritionists claim that Cr(III) picolinate has anti-diabetic properties and thus is an essential nutrient. However, no distinct mechanism of action or proof for this statement could be identified yet. In addition to that, a study showing that Cr picolinate is mutagenic *in vitro* and thus even exhibits an adverse effect. Furthermore, this study has shown that equal doses of free picolinate were more toxic compared to Cr(III) picolinate, however, non-mutagenic in cells. The simple compound $Cr(III)Cl_3$, which does not display any organic ligands, was found to be non-toxic and non-mutagenic. Therefore, the majority of the toxicity is assumed to be caused by the picolinate ligand. A study funded by the manufacturing company, applied the same assay proofing that Cr(III)picolinate was non-mutagenic, however within a shorter exposure period. In fact, studies are not able to unambiguously show that Cr(III) is both toxic and mutagentic or beneficial for the human body. Moreover, the effect was observed to be highly dependent on the coordinating environment of Cr(III). In addition to that, its effect also depends on the applied *in vitro* and *in vivo* model.[97] Furthermore, the media that are used in cell culture studies need to be taken into account, because the formation of Cr(III) protein and amino acid complexes was observed at 37°C. These ligand exchange reactions increase the ability of physiological processes and oxidants like H_2O_2 to oxidize Cr(III). In such media, $Cr(VI)O_4^{2-}$ formed predominantly, which can readily enter the cells *via* anion channels. Subsequent reduction may produce stable and highly genotoxic Cr(IV/V) species.[98] In contrast, some studies argue that the anti-diabetic effect of Cr(III) compounds is based on the formation of Cr(VI), which is assumed to act as phosphatase

inhibitor and thus insulin mimic like the isoelectronic vanadium(V). [96, 98] Even the solvents, the Cr(III) compound is dissolved in prior to such experiments was shown to influence the biological results. Thus, in general, compounds dissolved in DMSO are less toxic due to its radical scavenging properties.[97, 99] In summary, a biological application of chromium compounds is a challenge due to its different adverse biological effects as well as its diverse reactivity and redox activity.

In terms of anti-cancer studies, a search on *Web of Science* for 'chromium anti-cancer' resulted in 53 results since 1945. However, most studies focus on other aspects and the chromium compounds are mentioned in a different context, as represented by the most recent publications of Pumera *et al.*[100], Kheiri *et al*.[101] and Koley *et al*.[102] Nevertheless, a few studies are reported evaluating chromium-based compounds in cellular anti-cancer studies. For example, Cr(III) clusters $[Cr_2(B\text{-}\beta\text{-}XW_8O_{31})_2]^{14-}$ (X = Si, Ge) were studied against different cancer cell lines resulting in low IC_{50} values in the same range as the respective reference drug.[103] In contrast, a tris-(*N*,*N*-diethyldithiocarbamato)-Cr(III) complex published by Sedlacek *et al.* was shown to be non-toxic in the studied cancer cell lines.[104]

1.3.3 Vanadium in biology

Vanadium was discovered twice in history. Its first discovery dates back to 1801, when the mineralogist Andres Manuel del Rio from Mexico identified a new metal, which he named erythronium. This metal was found to have similarities to chromium and uranium and thus, in later studies, he withdrew his statement. The mineral is known as vanadinite, $PbCl_2{\cdot}3Pb_3(VO_4)_2$ nowadays. 30 years later, in 1831, the Swedish professor Nils Gabriel Sefström unambiguously identified a new metal, which he entitled 'vanadium'. Moreover, it was proven that this metal was identical to erythronium. The first investigations showed, that the studied vanadium species were all associated with oxygen or nitrogen. In 1867, the first reports about the similarities of vanadium compounds and phosphates were published. There, Henry Roscoe identified different vanadium compounds and compared their structural features to the corresponding phosphorous species, like V_2O_5 and P_2O_5, $VOCl_3$ and $POCl_3$.[105] This similarity is still part of today's research on vanadium and its potential in biological applications. Both are tetrahedral anions (see Figure 15) with an analogous structure and almost the same size with a difference of 23 $Å^3$. Thus, vanadate was studied as a potential surrogate for phosphate for example in enzymes like phosphatases and kinases. Such studies do not only highlight the similarities but also the differences. One important difference is the comparably high stability of penta-coordinated vanadate species, which are metastable in case of phosphate ions.[106] This results in inhibition of different phosphate-involved biological processes like phosphorylations.[107] One prominent example is the inhibition of the enzyme Na^+,K^+-ATPase by vanadate, which led to studies about the 'insulin-like' properties of vanadate. Another difference is the redox behavior and the protonation states at neutral pH. Thus, at pH 7, phosphate is

present in a mixture of mono- and diprotonated phosphate species, whereas vanadate is predominantly present as dihydrogen vanadate (as shown in Figure **15**). Additionally, vanadate(V) is prone to reduction to $V(IV)O^{2+}$ and vanadium(III) species. Accordingly, the biologically most stable oxidation states of vanadium are +5, +4 and +3 allowing a vast redox chemistry under physiological conditions.[106]

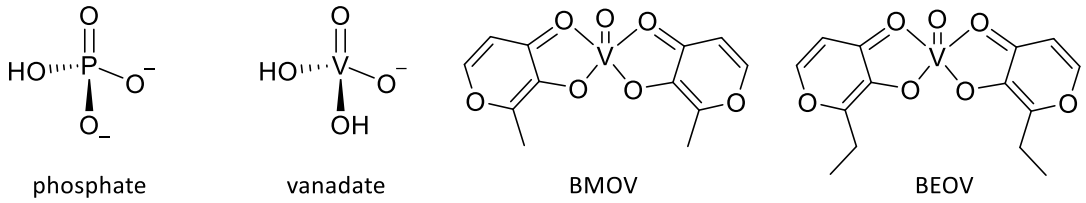

Figure **15**: Structure of phosphate and vanadate in their predominant protonation state at neutral pH.[106] Additionally, the structures of anti-diabetic compounds BMOV and BEOV are given.[107]

In 1899, the first report about vanadium salts and their anti-diabetic effects in human was published.[108] Some further symptoms of diabetes were observed to be reduced like an increased lipid level and secondary consequences such as heart diseases, cataracts and kidney diseases. In comparison to inorganic vanadium compounds evaluated for diabetes treatment, vanadium-based compounds with organic ligands were shown to exceed these effects. In particular, bis(maltolato)oxovanadium(IV) (BMOV) and its ethyl analogue bis(ethylmaltolato)oxovanadium(IV) (BEOV) were evaluated to act as successful prodrugs (see Figure **15**). Thus, a phase I clinical trial comprising BEOV treatment was completed in 2003. The study showed, that BEOV has a faster and more efficient uptake and thus beneficial bioavailability versus $VOSO_4$. Moreover, no side effects were reported.[108, 109] This was followed by a phase II study. The patent protection for BEOV expired in 2011 but since then, no further clinical evaluation was reported. Nevertheless, it is still accessible to the public as nutritional additive.[110]

As one of the few agents being potent in treatment of more than one diseases, in addition to its anti-diabetic effects, vanadium also shows anti-cancer properties. Most commonly, it is assumed that the inhibition of phosphatases is involved in the mechanism of action. Additionally, vanadium compounds were shown to interact strongly with different biological targets like transferrin or other proteins by the loss of the organic ligand at low concentrations. Other studies showed that a change of the cellular redox state or the formation of reactive oxygen species is involved. Thus, the versatile biological effects of vanadium include (1) different stable oxidation states in aqueous solution, (2) the similarity of vanadate to phosphate, (3) the capacity to form peroxo- and polyoxovanadates, (4) the interaction and binding to biologically important molecules such as ATP and glutathione and in general molecules providing coordinating entities with nitrogen, oxygen or sulfur, and (5) the ability to adopt different coordination geometries by binding of various substrates.[111]

One of the first classes of vanadium-based complexes studied for their anti-cancer properties are the vanadocenes. For example, the simplest and most effective derivative is bis(cyclopentadienyl)dichloro-vanadium(IV) (Figure **16**), which was extensively studied *in vitro* in cancer cell lines as well as *in vivo* in animals. Bis(cyclopentadienyl)dichlorovanadium (figure **16**) was shown to be more active compared to its titanium-analogue. In these studies, it was observed that the cyclopentadienyl vanadium moiety remains unchanged in cells and biofluids. It was also observed to cause cellular oxidative stress resulting in promising anti-cancer activity, where a cisplatin-like mode of action is suggested. A further class studied are the vanadium(IV/V) oxido compounds. These compounds contained a VO^{2+} or VO_2^+ center coordinated by organic ligands. For instance, V(oda)(phen) (oda = oxadiacetate, phen = phenanthroline) was observed to exhibit strong antiproliferative activity, which was mainly based on DNA intercalation.[107, 111] Moreover, bis(peroxo) vanadium(V) complexes were discovered to exhibit antitumor activity in cell culture studies. These compounds form a unique vanadium structure with a three-membered ring depicted in Figure **16**, which supports the reactivity of such compounds. The compounds were involved in the formation of cellular reactive oxygen species and other radicals and thus are part of cellular metabolic processes. However, due to their reactive nature, the peroxo compounds possess only limited stability. Nevertheless, since they were observed to highly activate insulin receptors and far exceed the anti-diabetic effects of the studied vanadium salts at least 10-fold, these compounds were also evaluated for their anti-cancer effects.[107] This phenanthroline coordinated vanadium peroxo complex shown in Figure **16**.[110]

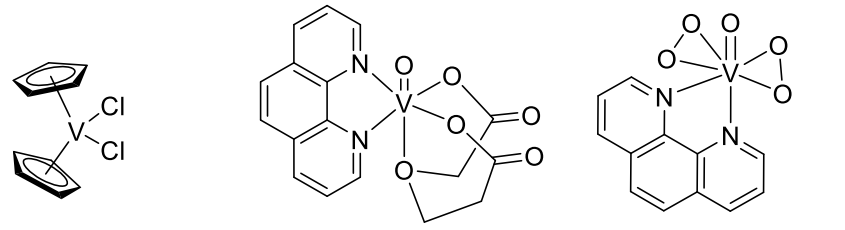

bis(cyclopentadienyl)dichloro-vanadium(IV) | bis(oxadiacetate)vanadium phenanthrolin | bis(peroxo)vanadium(V) phenanthrolin

Figure **16**: Structures of vanadium-based complexes studied for their anti-cancer properties.[107, 110]

As previously discussed for gold-based compounds, also vanadium compounds showed strong interaction with thiols like cysteine and glutathione in biological environment. Thus, vandate(V) compounds were found to be fully reduced to oxo-vanadium(IV).[112] Taken together, the versatile chemical profile of vanadium opens many possibilities for biological applications. Although some possible biological targets are already identified, many processes are still unknown and need to be investigated.

2 OBJECTIVE

Although it is part of uncountable studies and intensive research, treatment of cancer is still a challenge. One major obstacle in the battle against cancerous cells is the high similarity to normal cells. Severe side effects are caused by chemotherapeutic treatments because the anti-cancer compounds also attack healthy cells. The performance of cisplatin, one of the most commonly applied inorganic anti-cancer drugs until today, is diminished by severe side effects.

One method to overcome this issue is the application of inorganic supramolecular coordination compounds (SCCs), which are reported to encapsulate small molecules like cisplatin. In first *in vitro* studies of these host-guest systems, SCCs were found to be suitable for drug delivery. The SCC-cisplatin adduct displayed a lower toxicity in healthy cells and an increased toxicity in cancerous cells compared to non-encapsulated cisplatin or the SCC itself. These SCCs have a composition of M_2L_4 (M = metal, L = ligand) with palladium or platinum as metal center. However, these complexes have to be sufficiently stable under physiological conditions as well as soluble in water. Both properties can be tuned e.g. by functionalization of the ligand, which is part of some recent studies. In this thesis, the change of the metal center is evaluated and investigated for its influence on properties like stability. Moreover, the applied metal may also influence the pore size and thus the size of the compound that can be encapsulated. Accordingly, the drug may easily enter a bigger pore, but may also be encapsulated more efficiently in smaller pores. Therefore, one goal of this thesis was to synthesize new SCCs based on molybdenum, chromium or gold and potentially to evaluate the new properties provided by these metals. Furthermore, molybdenum and chromium are much cheaper than palladium, but also gold displays a lower price, which may be beneficial for potential clinical applications.

Additionally, the second part of the thesis deals with studies on the synthesis and characterization of organometallic *N*-heterocyclic carbene (NHC) complexes of chromium, vanadium and gold. In particular, vanadium and gold NHCs are interesting for biological applications since numerous studies investigate the biological effects of compounds of these metals and show some promising results. Accordingly, these compounds will be evaluated for their potential in cancer cells.

3 Discussion of Results

3.1 Supramolecular coordination compounds

The encapsulation of known anti-cancer drugs like cisplatin within the voids of supramolecular coordination compounds is a promising approach to raise their activity and selectivity for cancer cells in cancer therapy. The enhancing effects are based on the protection of the encapsulated drug from the biological environment as well as an improved targeting of the cancer cells by either the EPR effect or the coupling of the cage with biomolecules. The addition of different functionalities by exo or endo functionalization was also shown to result in varying biological activity with improved cytotoxicity e.g. for a CH_2OH functionalization. Moreover, some of these cages themselves have been found to be cytotoxic.[22,18, 31-33, 73, 113, 114] One major drawback of these approaches is their dependability on platinum or palladium compounds which has however been shown to result in the development of platinum (cross)resistances in certain tumors.[13] Therefore, the aim of this study is to identify promising non-platinum-based alternatives for SCCs as well as organometallic complexes. Thus, SCCs based on Au, Cr and Mo shall be studied. SCCs are based on a rigid organic ligand backbone featuring coordinating groups and a central transition metal ion. Due to the bidentate nature of the ligand, together with appropriate transition metal ions, they can form hollow three-dimensional structures, which allow the incorporation of small compounds. In scheme **1**, the general synthesis of the bispyridyl ligand system, which will be mainly studied in this thesis, is presented. The ligand can be synthesized in a single step *via Sonogashira* coupling and subsequent cage formation can be achieved via reaction with the appropriate transition metal ion.[15, 18, 20-22] One requisite for the formation of SCCs starting with this bispyridyl ligand system is the usage of transition metal ion that allow a square planar coordination geometry.

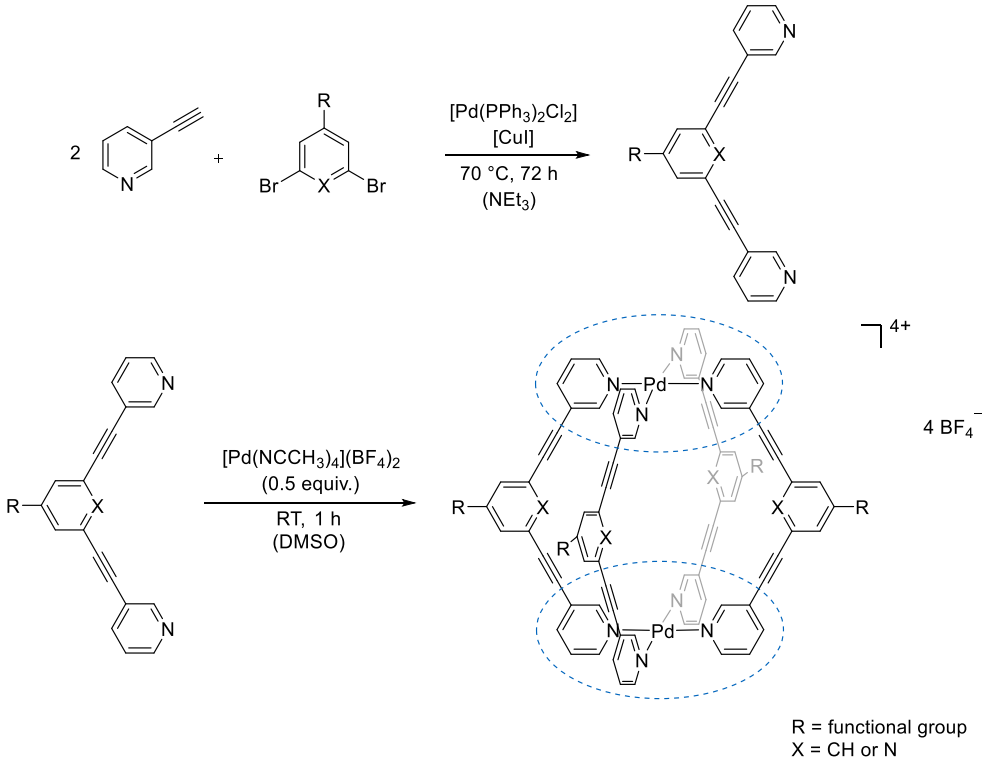

Scheme **1**: *Sonogashira* coupling of 3-ethynylpyridine and the potentially functionalized bibromobenzene or dibromopyridine yielding the ligand system used the self-assembly of Pd-based three-dimensional cage structures. Blue highlights: terminal pyridyl moieties relevant for metal coordination.

As highlighted in blue in scheme **1**, metal coordination takes place *via* the terminal pyridyl units of the bifunctional ligand. Accordingly, the investigations on the feasibility to exchange the palladium/platinum metal center by molybdenum, chromium or gold starts with the search for corresponding square planar coordinated compounds with special emphasis on their pyridine complexes.

3.1.1 Molybdenum

For the dimolybdenum Mo_2^{4+} center, which was intended to be evaluated for the ability to form a cage structure, no homoleptic pyridine-coordinated complexes can be found in literature. Thus, attempts to synthesize a dimolybdenum pyridine complex are presented in this paragraph. As metal precursor, the respective acetonitrile complex **16** was chosen. First, because a palladium acetonitrile complex is commonly applied for the synthesis of the SCCs (see scheme **1**) and thus is an applicable metal source. Second, because such nitrile-solvent coordination complexes are generally suitable precursors because they are sufficiently stable to be synthesized, however, very reactive. The synthesis of $[Mo_2(MeCN)_{10}](BF_4)_4$ was performed according to a process published by Kühn *et al.* in 1999 and is presented in scheme **2**.[115]

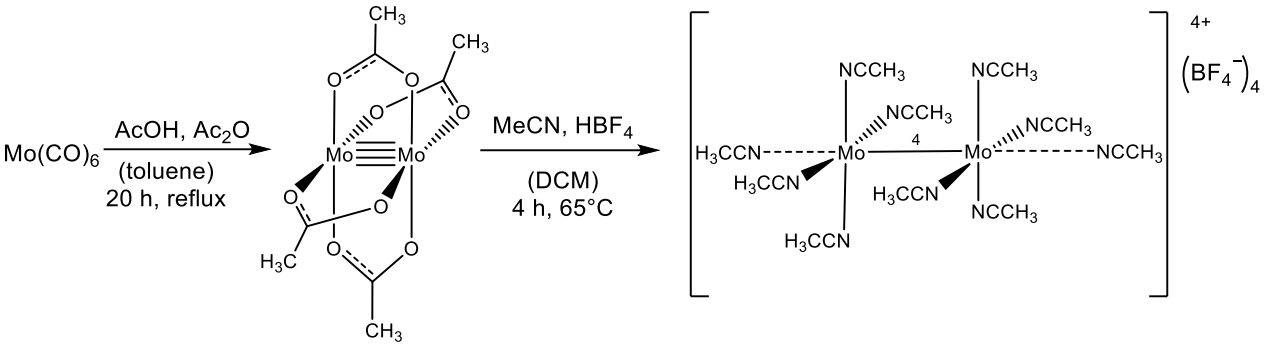

15 **16**

Scheme **2**: Schematic representation of the synthesis of $[Mo_2(MeCN)_{8\text{-}10}](BF_4)_4$ **16** starting from $Mo(CO)_6$.

The acetate complex **15**, which is a bright yellow powder, was readily obtained by conversion of $Mo(CO)_6$ in concentrated acetic acid and acetic anhydride. The deep blue acetonitrile complex **16** was synthesized by conversion of **15** with HBF_4 in a mixture of dry and degassed DCM and acetonitrile. After 4 hours of reaction time, the blue product precipitated and was obtained by filtration.[115] Using acetonitrile complex **16**, different experimental conditions were tested for the synthesis of a respective pyridine complex. Therefore, various reaction parameters were evaluated, like temperature, solvents, time and applied equivalents. Due to the reactive nature of **16** and its rapid decomposition, the reactions were generally conducted under argon atmosphere and in dry solvents using either Schlenk techniques or a glovebox. The reactions were predominantly analyzed by ^{1}H NMR. For most of the attempts, no distinct product formation was observed. For these reactions, only numerous signals in the NMR spectra were obtained, which could not be assigned and therefore, these attempts are not further discussed. Nevertheless, some crystallization experiments were performed. One of these attempts, where an excess of pyridine was added to an NMR sample of **16**, yielded red crystals from a green solution, which were analyzed by X-ray diffraction analysis. This analysis showed that two different compounds co-crystallized, namely **17** and **18**. The ORTEP style representation as well as the drawing of complex **17** is shown in figure **17**. For this complex, a Mo-Mo bond distance of about 2.12 Å was found, which is only slightly longer than the Mo-Mo distances in **15** (2.0924(8) Å) and slightly shorter than in **16** (2.187(1) Å).[116]

In case of **17**, two chelating acetamide ligands were found. Since no further compounds were added to the solution except for **16** and pyridine in acetonitrile, acetamide has to be formed from these compounds. In fact, the same observation was discussed by Cotton in 1998, were he discovered, that an end-on coordination of acetonitrile to a Mo_2^{4+} species in the presence of small amounts of water leads to the formation of acetamide.[117] The mechanism of the formation is presented in scheme **3**. Therefore, the structure proves insufficient drying of the applied solvents and apparatus. Nevertheless, it also shows a four-fold almost square planar coordination of pyridine to the dimolybdenum entity and

the maintenance of the quadruple bond. The Mo–$N_{pyridine}$ distances were found to be 2.223(3) and 2.215(2) Å, which is longer than found for the acetamide Mo–N distance (2.124(2) Å) and longer than for other pyridyl-based ligands coordinating to a dimolybdenum core.[116, 118-120] Nevertheless, comparable Mo–$N_{pyridine}$ bond lengths (2.197 – 2.220 Å) were observed for another pyridine coordinated Mo_2(O-*i*-Pr)$(py)_4$ complex. In comparison to **16** (2.113(1) – 2.141(9) Å), the Mo–$N_{pyridine}$ distances are rather long indicating a certain lability and thus reactivity of such dimolybdenum-pyridine adducts.[121]

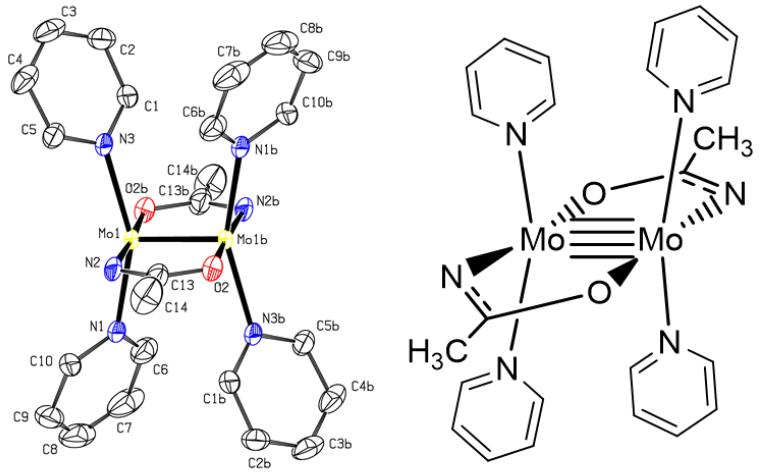

17

Figure **17**: ORTEP style representation of complex **17** with ellipsoids shown at a 50% probability level. Hydrogen atoms and tetrafluoroborate counterions are omitted for clarity. Selected bond lengths [Å]: Mo1–Mo1b 2.1151(7), Mo1–N1 2.223(3), Mo1–N2 2.124(2), Mo1–N3 2.215(2), Mo1–O2 2.098(2).

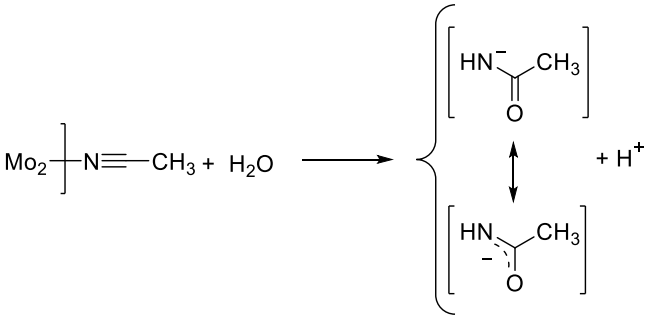

Scheme **3**: Schematic presentation of the mechanism of the formation of acetamide from end-on coordination of acetonitrile to a dimolybdenum unit in presence of water.[117]

For co-crystallized complex **18**, a metal-metal distance of 2.5257(8) Å was determined, which is in the range of a single Mo-Mo bond.[116] The ORTEP style presentation and the structural drawing is presented in figure **18**. This structure revealed some interesting features. First, oxygen is coordinated in a bridging coordination mode between the two molybdenum centers, which represents the reactivity of this complex with oxygen. Furthermore, four coordinated fluorine atoms were found in the structure, which are likely to be generated upon decomposition of the tetrafluoroborate counterions. Nevertheless, also

four pyridine molecules were observed to coordinate, with an even longer Mo–$N_{pyridine}$ bond (2.274(2) and 2.285(2) Å) than determined for **17**. Consequently, the exchange of the acetonitrile ligands by pyridine is possible; however, no homolopetic pyridine complex was obtained. By interpretation of the formation of structures **17** and **18**, the formation of chelating acetamide ligands, decomposition of the counterion and change in the bond order rather than saturation of the coordination sites by pyridine occurred.

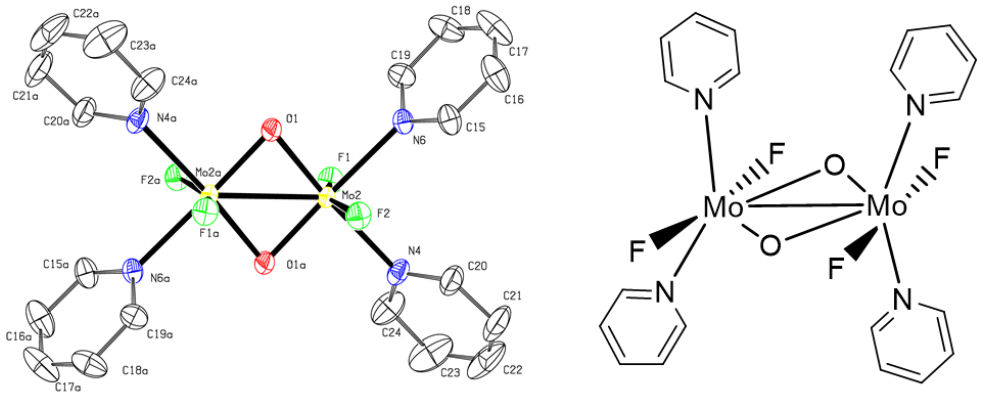

18

Figure **18**: ORTEP style representation of complex **18** with ellipsoids shown at a 50% probability level. Hydrogen atoms and tetrafluoroborate counterions are omitted for clarity. Selected bond lengths [Å]: Mo2–Mo2a 2.5257(8), Mo2–N4 2.274(2), Mo2–F2 1.8534(17), Mo2–O1 1.9147(19), Mo2–N6 2.285(2), Mo2–F1 1.8434(17).

One of the most promising approaches according to ^{1}H NMR studies was performed by stepwise addition of 2 eqiuv. of pyridine every 45 minutes to an acetonitrile solution of **16** until a total amount of 10 equiv. was added at room temperature. The ^{1}H NMR of the isolated precipitate in comparison with free pyridine is shown in figure **19**. There, one can see that the protons next to the nitrogen atom of pyridine are slightly shifted down field, which is an indication for coordination.[22] However, this result could not be reproduced and thus could not be further analyzed.

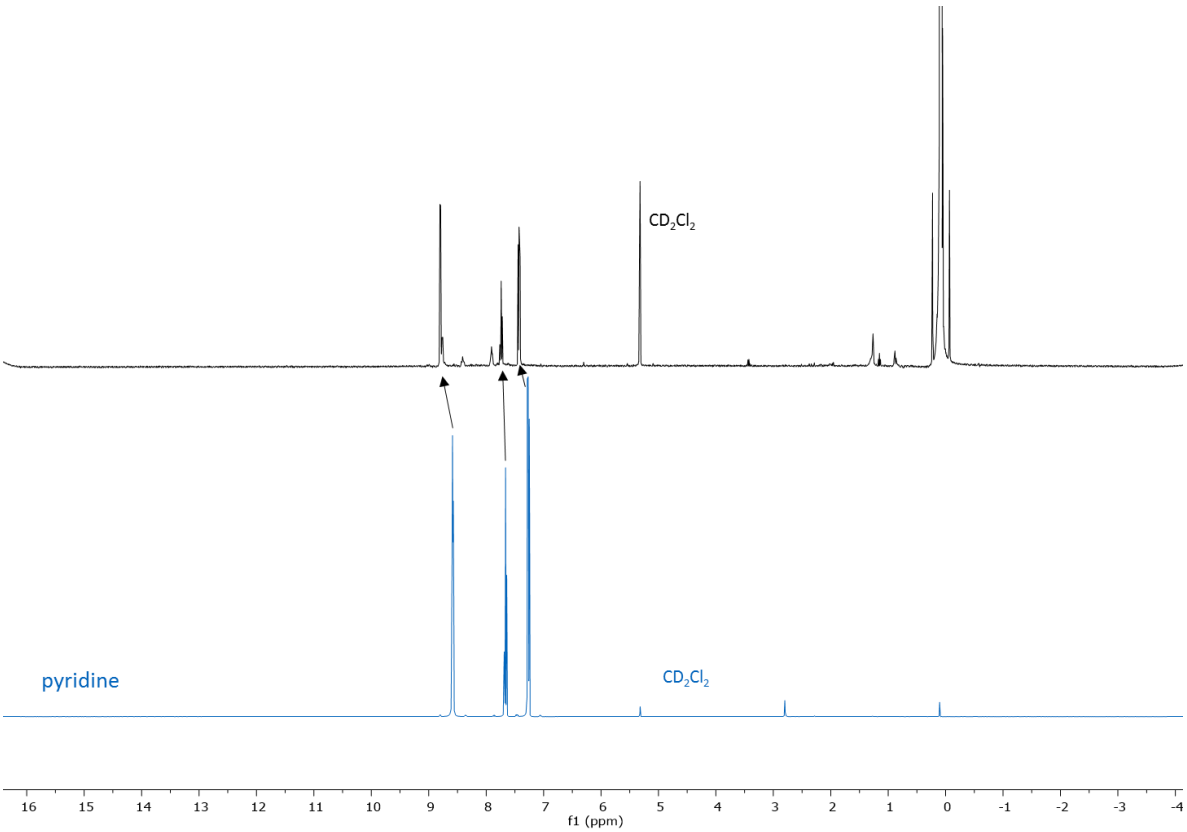

Figure **19**: NMR spectra of free pyridine (blue) and the most promising approach (black) for the synthesis of a homoleptic dimolybdenum-pyridine complex.

Consequently, according to the observations and results obtained from the crystal structures of **17** and **18**, a change of the counterion was investigated. $[Mo_2(MeCN)_{10}](OTf^-)_4$ was synthesized and used as a starting material for the synthetic attempts towards the respective pyridine complex.[115] To obtain such pyridine complexes, different conditions and solvents were tested. All syntheses were conducted at room temperature, with a solvent mixture of MeCN and different equivalents of pyridine. Subsequently, different additional solvents for precipitating a potential product were tested. In all cases, one particular product was isolated according to ^{1}H NMR studies, where also a down field shift of the NMR signals was observed. In addition, the ratio of the integrals are the same as observed for free pyridine. However, a new signal at 13.46 ppm was observed with an integral relative to the other pyridine-based signals of 1. In ^{19}F NMR, no decomposition of the triflate anion could be observed as well as the same green color as found for the pyridine-containing approaches with tetrafluoroborate. This product could be successfully crystalized. Unfortunately, it was found to be protonated pyridine. Accordingly, the ^{1}H NMR signals observed in these attempts were now unambiguously assigned to protonated pyridine with triflate as anion. The fate of the molybdenum atoms remains unknown. Because these approaches using $[Mo_2(MeCN)_{10}](OTf^-)_4$ as precursor always yielded the same signals in the ^{1}H NMR, namely the protonated pyridine, this approach was no longer followed.

Thus, further anion exchange to BPh_4^- and PF_6^- was studied. However, this is not as straight forward as in case of triflate. Synthesis of **16** and its triflate analogue were performed with the respective acid of the counterion, HBF_4 and HOTf, respectively. In doing so, acetic acid was formed from the acetate ligands, which were replaced by acetonitrile. For BPh_4^- and PF_6^-, only the inorganic salts or the acids in aqueous solutions are available. However, due to the air- and moisture-sensitivity of the acetonitrile complex, the aqueous solutions cannot be applied and thus, the inorganic salts were applied. $NaBPh_4$ and $[(^tBu)_4N]PF_6$ were considered the most promising candidates due to their solubility in dry acetonitrile. All other salts lack solubility in organic solvents. For both, $NaBPh_4$ and $[(^tBu)_4N]PF_6$, two different methods were tested. First, using $Mo_2(OAc)_4$ as precursor and synthesize the acetonitrile complex as it works in case of tetrafluoroborate and triflate or, direct exchange of the counterion of either $[Mo_2(MeCN)_{10}](BF_4)_4$ or the triflate analogue by either BPh_4^- or PF_6^-. In brief, straightforward exchange of the counterion of the acetonitrile complex was not possible. Only dry, organic solvents can be applied and thus, the difference in solubility is not significantly different for isolating any products, as it is done for example in salt metathesis in water. According to ^{19}F NMR, either a mixture of anions or the original one was present. Nevertheless, using $Mo_2(OAc)_4$ and $NaBPh_4$, the ^1H NMR was very promising. There, the acetate precursor as well as the counterion can easily be monitored. For at least two approaches, the formation of $[Mo_2(MeCN)_{8\text{-}10}](BPh_4)_4$ can be assumed. There, the signal originating from $Mo_2(OAc)_4$ decreased significantly, a shifted acetonitrile signal can be observed as well as a slight shift of the BPh_4 protons (see figure **20**).

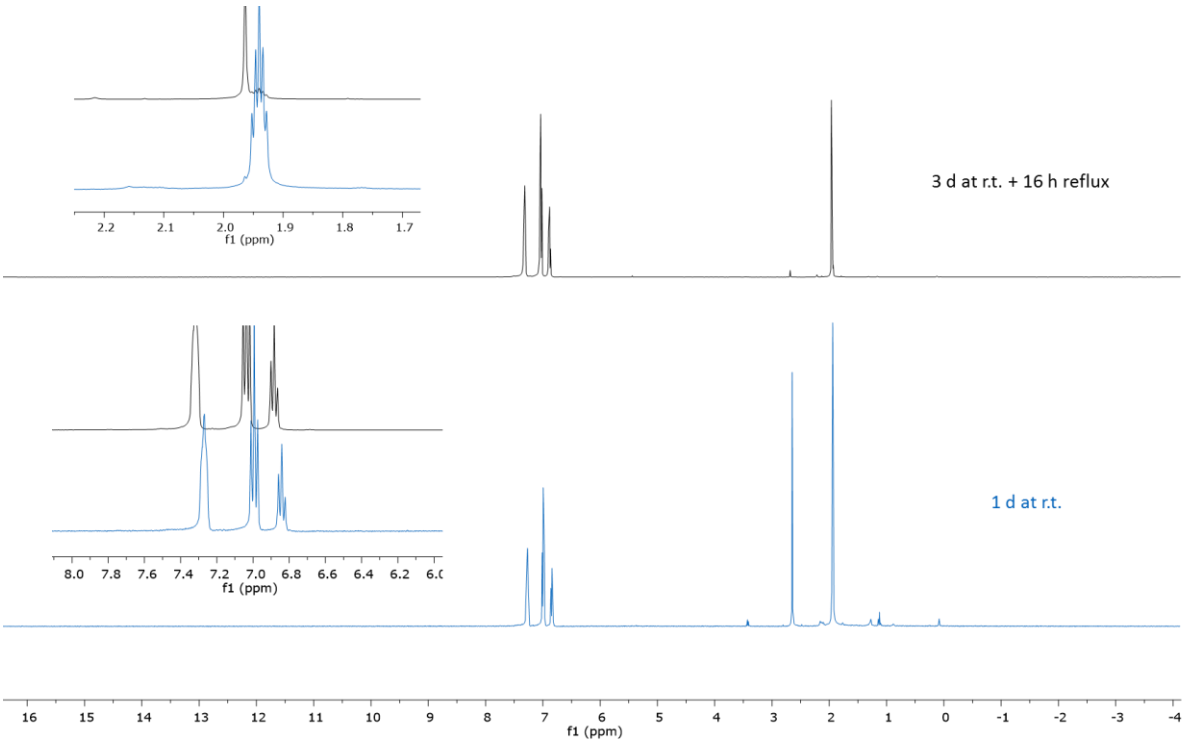

Figure 20: Full ^{1}H NMR spectrum of the most promising synthesis of a $[Mo_2(MeCN)_{10}](BPh_4)_4$ complex. For the most relevant areas, a detailed cutout of the ^{1}H NMR is added.

This promising NMR was taken from the bulk reaction mixture and could be reproduced, however, all attempts to isolate a product, failed. There, no tested solvent mixture was found to precipitate the desired product even at -20 °C. Most of the time, the acetate precursor was recovered indicating a very low stability of the previously observed BPh_4-complex. Further attempts like removing the solvents under reduced pressure always resulted in decomposition.

In summary, the main issues in synthesizing a homoleptic pyridine coordinated dimolybdenum complex have been the high reactivity of the dimolybdenum core accompanied by immediate addition and/ or reactivity with oxygen or water or its counterion resulting in unreproducible results and non-isolable products.

Consequently, the focus was shifted to mixed-ligand complexes with stabilizing acetate ligands in combination with pyridine. Therefore, $[Mo_2(OAc)_2(MeCN)_6](OTf)_2$ was synthesized according to previously published procedures.[115] This complex was used as precursor for the respective $[Mo_2(OAc)_2(py)_6](OTf)_2$ complex. Some similar complexes have been published[120, 122, 123], however, all these pyridyl ligands used in these publications were chelating ligands, which enhances the overall stability of such complexes. Still, some reactions were performed to test the feasibility to synthesize a complex with the composition of $[Mo_2(OAc)_2(py)_6](OTf)_2$. Therefore, $[Mo_2(OAc)_2(MeCN)_6](OTf)_2$ was dissolved in acetonitrile together with 15 equivalents of pyridine and stirred at room temperature for 2 days. The resulting ^{1}H NMR shows two main sets of signals in the aromatic region as well as for the

acetate signals. Nevertheless, the integral ratios of acetate to pyridine cannot be assigned to any reasonable product. Additionally, proton signals of the protonated pyridine and as well as further signals were visible. The NMR spectrum is given in the supplementary in figure **S1**.

According to the NMR analysis, this approach appeared to be promising, however, also here, reproducibility as well as isolation and characterization of any reasonable product was not possible. Additionally, the suggested products could not unambiguously be assigned. Thus, further attempts were performed using bipyridine instead of pyridine.

At first, $[Mo_2(MeCN)_{10}](BF_4)_4$ was reacted with four equivalents of bipyridine, because a similar ligand to metal ratio as found for $Mo_2(OAc)_4$ was assumed. However, the resulting ^1H NMR showed numerous signals in the range of -2 ppm to 14 ppm. This showed that although applying a chelating pyridine ligand, no reasonable product was formed. Next, the reaction of $[Mo_2(OAc)_2(MeCN)_6](OTf)_2$ with two equivalents of bipyridine was evaluated. Right after the addition of bipyridine, the degassed and dry solution turned purple. After stirring for one hour at room temperature, the reaction was evaluated by ^1H NMR. The NMR showed the formation of one particular product which can be assigned to $[Mo_2(OAc)_2(bipy)_2](OTf)_2$ (**19**). In addition, the product could be crystallized from the MeCN solution by slow diffusion of diethyl ether. The crystal structure of **19** is shown in figure **21**. The Mo-Mo bond distance was determined to be 2.1576(10) Å and thus is in the same range as other Mo-Mo quadruple bonds.[116] The observed Mo–N bond distances are slightly shorter than the ones determined for **17** and **18**.

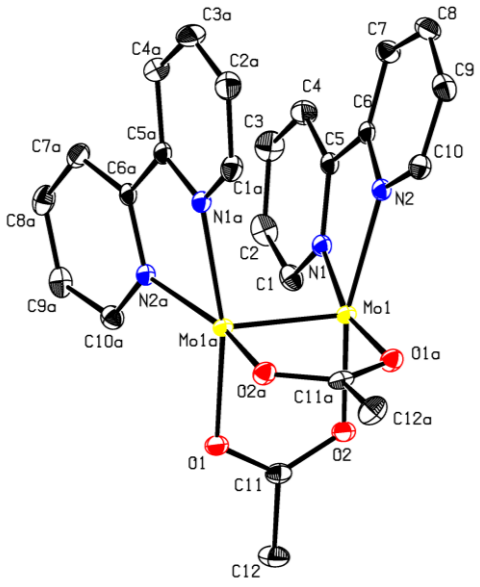

Figure **21**: ORTEP style representation of complex **19** with ellipsoids shown at a 50% probability level. Hydrogen atoms and trifluoromethanesulfonate counterions are omitted for clarity. Selected bond lengths [Å]: Mo1–Mo1a 2.1576(10), Mo1–O1a 2.1057(16), Mo1–O2 2.0977(15), Mo1–N1 2.1864(19), Mo1–N2 2.1783(18).

The successful synthesis of complex **19** led to the perspective to synthesize a cage-like structure with a dimolybdenum core from $[Mo_2(OAc)_2(MeCN)_6](OTf)_2$ with a chelating bipyridine-based ligand as shown in scheme **4**. A potential synthesis route for the ligand is presented in scheme **4**.

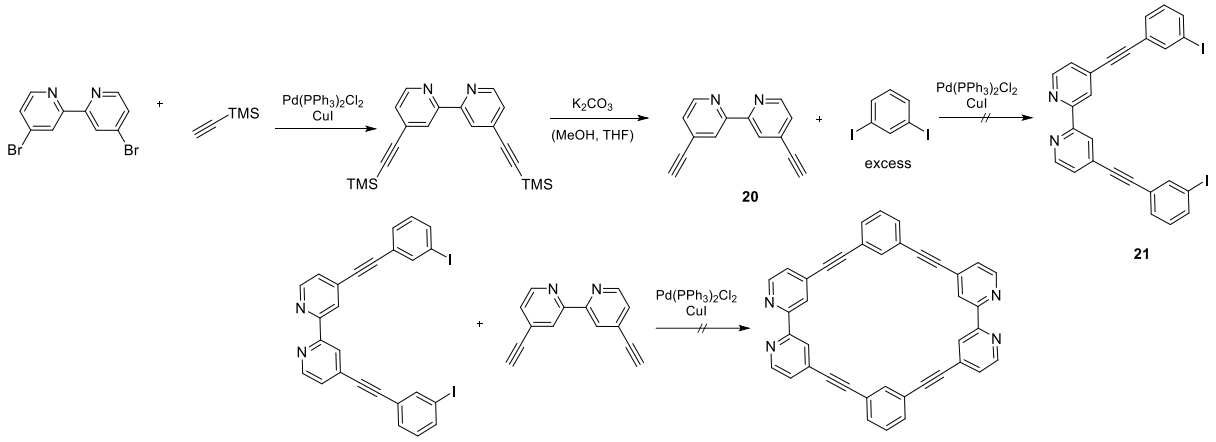

Scheme **4**: Scheme of the potential synthesis route for a new bipyridine based ligand potentially suitable for Mo_2^{4+} cage formation.

Synthesis of compound **20** was readily achieved according to the synthetic procedures published by Ziessel *et al.* and Armaroli *et al.*[124, 125] However, unfortunately, synthesis of compound **21** was not achieved in this work and thus the new chelating ligand could not be synthesized. Accordingly, it does not seem very likely that the desired cage structure will be obtained for a dinuclear molybdenum center. Still, the application of a mononuclear molybdenum center would be a suitable approach for future investigations.

3.1.2 Chromium

In contrast to molybdenum, a homoleptic mononuclear pyridine-coordinated chromium(II) complex **24** (not considering the interactions with the counterions) is known in literature.[126] The complex is obtained by conversion of the Cr(II) acetonitrile complex **23** or **25** with pyridine in DCM, as shown in scheme **5**.[126]

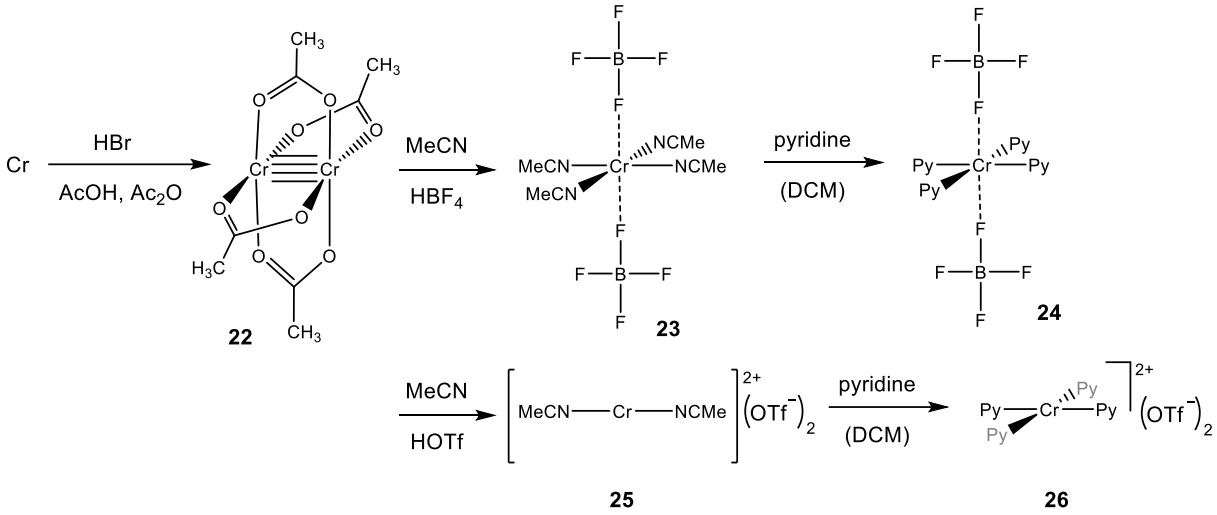

Scheme **5**: Schematic representation of the synthesis of $[Cr(py)_4](BF_4)_2/(OTf)_2$ (**24** and **26**).[126, 127]

The synthesis of **23** and **25** was very similar to the synthesis of dimolybdenum acetonitrile complex **16**. Accordingly, also the dimetal acetate is used as precursor, which was synthesized with small modifications compared to $Mo_2(OAc)_4$.[127] Strikingly, the synthesis does not require the exclusion of water and the compound can be handled on air in the solid state for a short period without decomposition. Synthesis of air and moisture sensitive acetonitrile complexes **23** and **25** was performed according to previously published methods.[126] The fact, that in course of this reaction the Cr-Cr quadruple bond brakes leading to a single-chromium containing complex, highlights the decreased stability of the dichromium quadruple bond compared to the dimolybdeum quadruple bond, which might be beneficial for the approaches towards 3D cages.[126] Nevertheless, only the synthesis of **22** is described by Romao *et al.*, however, due to the similarity to the synthesis of the respective molybdenum complexes, **25** was synthesized in the same manner. Interestingly, for **25**, a composition of $[Cr(MeCN)_2](OTf)_2$ was found by analysis of the solid powder by elemental analysis. Unfortunately, attempts to crystallize the complex were not successful and the recorded NMR spectra could not be assigned due to the strong paramagnetic properties. In the same manner as found in complexes **23** and **24**, an interaction with the counterion can be assumed. Nevertheless, pyridine complexes **24** and **26** were successfully synthesized for proof of concept with minor modifications according to Romao *et al.*[126] Though, for complex **26**, no analysis despite paramagnetic ^{1}H NMR was possible due to the high instability of the complex. Thus, the following studies focused on previously characterized complex **24**.

To continue the discussion, a short excursion to the interpretation of paramagnetic NMR spectra is given. Paramagnetic compounds are compounds with unpaired electrons. These compounds may be radicals, but also transition metal complexes, where the metal displays unpaired electrons. This has a strong influence on the magnetic properties of the resulting complexes leading to paramagnetic NMR spectra. Many different theoretical and experimental parameters need to be considered for such

systems.[128, 129] Some relevant effects for the interpretation of paramagnetic ^{1}H NMR spectra are mentioned in this short insertion. In general, a paramagnetic signal may appear outside the 'normal' diamagnetic region (-3 ppm to 16 ppm). In the following, the range from about -3 ppm to 16 ppm in ^{1}H NMR spectra is termed 'diamagnetic region' and all other scanned regions are termed 'paramagnetic regions'. For predicting the signal shift, theoretical calculations are necessary, which are out of the scope of this work. Nevertheless, a scan of a wide range of ppm in search of signals was performed. In addition, paramagnetic signals are more sensitive to temperature changes compared to diamagnetic signals. Therefore, a significant signal shift can be observed by ^{1}H NMR measurements at variable temperatures enabling to distinguish between diamagnetic and paramagnetic signals. In general, the signal is moved towards the region it would appear in case of an analogous diamagnetic compound with increasing temperature. Moreover, paramagnetic signals can be very broad and sometimes may be hard to distinguish from the baseline. By increasing the temperature, such broad signals sharpen and thus, they may be only detected at higher temperatures. Additionally, the concentration of the sample is also important because the higher the concentration the better the resolution of a paramagnetic ^{1}H NMR. Therefore, many challenges were faced by interpretation of paramagnetic ^{1}H NMR studies. Nevertheless, it is a fast and easy-to-perform method without destruction of the sample and without the need to purify the compound.[129]

Due to solubility reasons, the amine-functionalized ligand shown in scheme **6** was chosen for the first attempts to synthesize a chromium-based SCC. The synthesis was performed under inert atmosphere with **23** advanced in acetonitrile and followed by addition of 2 equiv. of the ligand (see scheme **6**). After stirring for one day at room temperature, a precipitate formed from the brown-reddish mixture. After filtering the solution, diethyl ether was added to precipitate a potential product. The thus obtained fractions were attempted to be analyzed by ^{1}H NMR. However, due to the low solubility in acetonitrile and the paramagnetism of chromium, no predictions about a formation of a cage could be made from any fraction. Thus, the precipitated solid was tried to be analyzed by ESI-MS and elemental analysis.

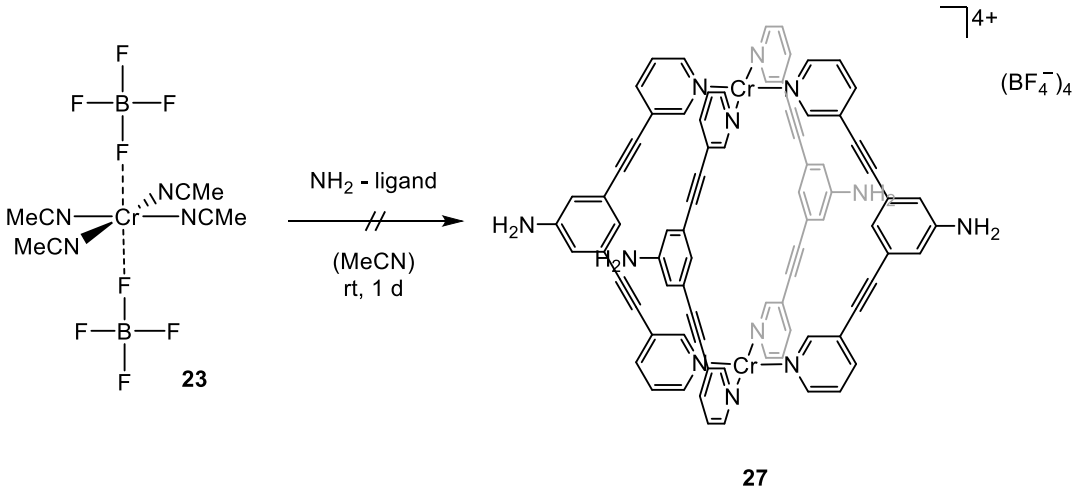

Scheme **6**: Schematic representation of the synthetic approach for **27**.

The result of the elemental analysis was promising (deviations from calculated mass percentages for the intended cage to measured mass percentages: ΔC -1.36 %, ΔH +0.43 %, ΔN +0.40 %); however, further analytics is needed to obtain more details about the formed product. Thus, ESI-MS was performed in aqueous and aerated environment. Further mass spectrometric methods under inert atmosphere were tested, however, due to restrictions concerning the applicable solvents, no signals were observed. Thus, ESI-MS was performed and the resulting spectrum is given in figure **22**.

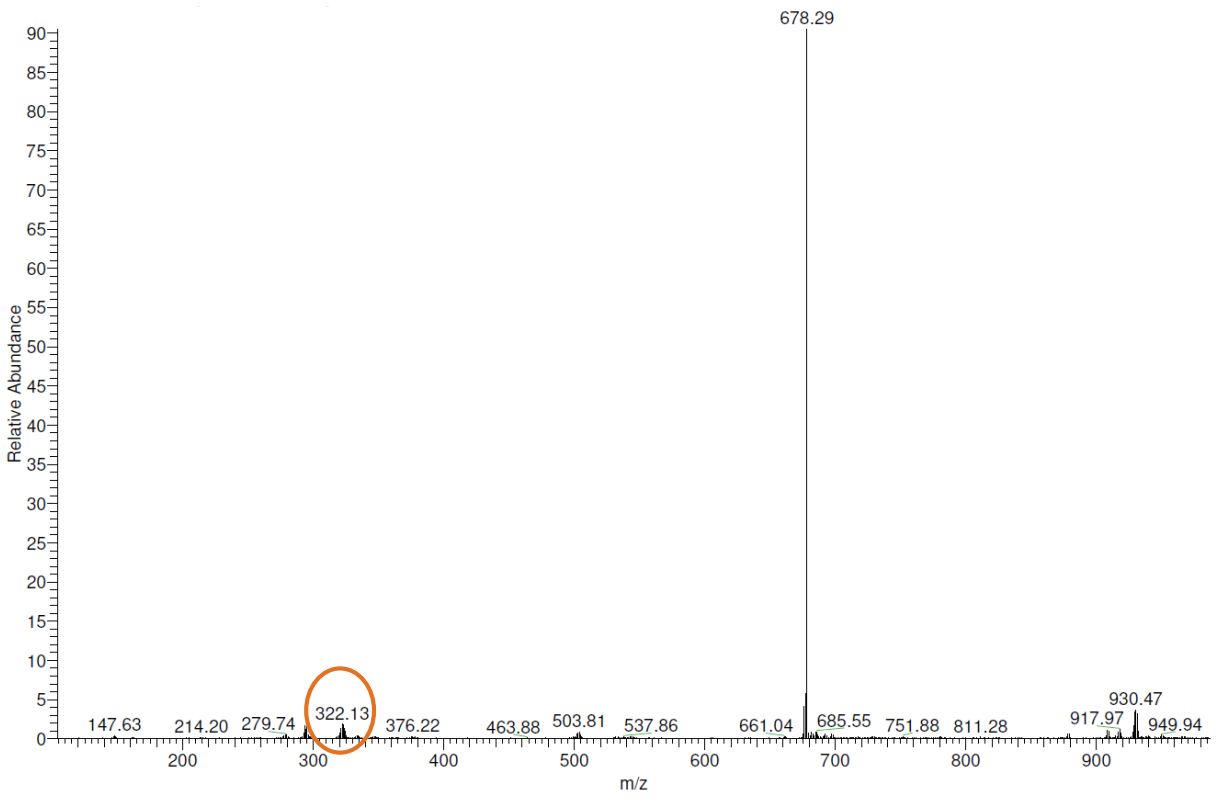

Figure **22**: ESI-MS spectrum of the reaction mixture of **27**.

The ESI-MS spectrum showed a main signal at 678.49 m/z, however, this signal could not be assigned. Nevertheless, a signal at 322.13 can be assigned for a $[Cr_2(ligand)_4]^{4+}$ fragment. The 4+ charge of the fragment is somewhat surprising because the solution was exposed to air and thus, Cr(II) is very likely to be oxidized to Cr(III). The further signals at 293 m/z and 930 m/z could not be assigned as well. Nevertheless, no distinct statement about the composition of the product is possible and thus, crystallization of the product was tested. Therefore, DMSO was added to the product mixture to ensure a complete dissolution and thus beneficial conditions for growth of single crystals by diffusion of diethyl ether. Unfortunately, the blue crystals obtained after a few weeks were analyzed to be $[Cr(DMSO)_6](BF_4)_3$, indicating that even if such Cr cages are accessible, they are highly instable and can easily be destroyed by competing ligands. Öhrström *et al.* have published the corresponding crystal structure in 2000.[130] Therefore, this promising approach was repeated avoiding DMSO. The elemental analysis determined for this second approach showed the following deviations from the mass percentages calculated for the desired cage structure to measured mass percentages: ΔC -2.27 %, ΔH +0.19 %, ΔN +0.39 %. This is in the same range as determined for the first approach. Additionally, more detailed ^{1}H NMR analyses were performed. At first, a range from -60 to +120 ppm was screened in order to miss no signals. ^{1}H NMR at different temperatures (rt. and 60°C) followed this. Because the shift of a paramagnetic signal is highly dependent on the temperature, paramagnetic signals can be assigned quite easy using variable temperatures NMR studies. Nevertheless, an increase in temperature may cause a reaction and thus, the NMR sample also needs to be monitored after heating if a significant change is observed after increasing the temperature. Accordingly, in figure 23 the zoom of the significant part of the ^{1}H NMR spectra at room temperature, 60 °C and again at room temperature are displayed.

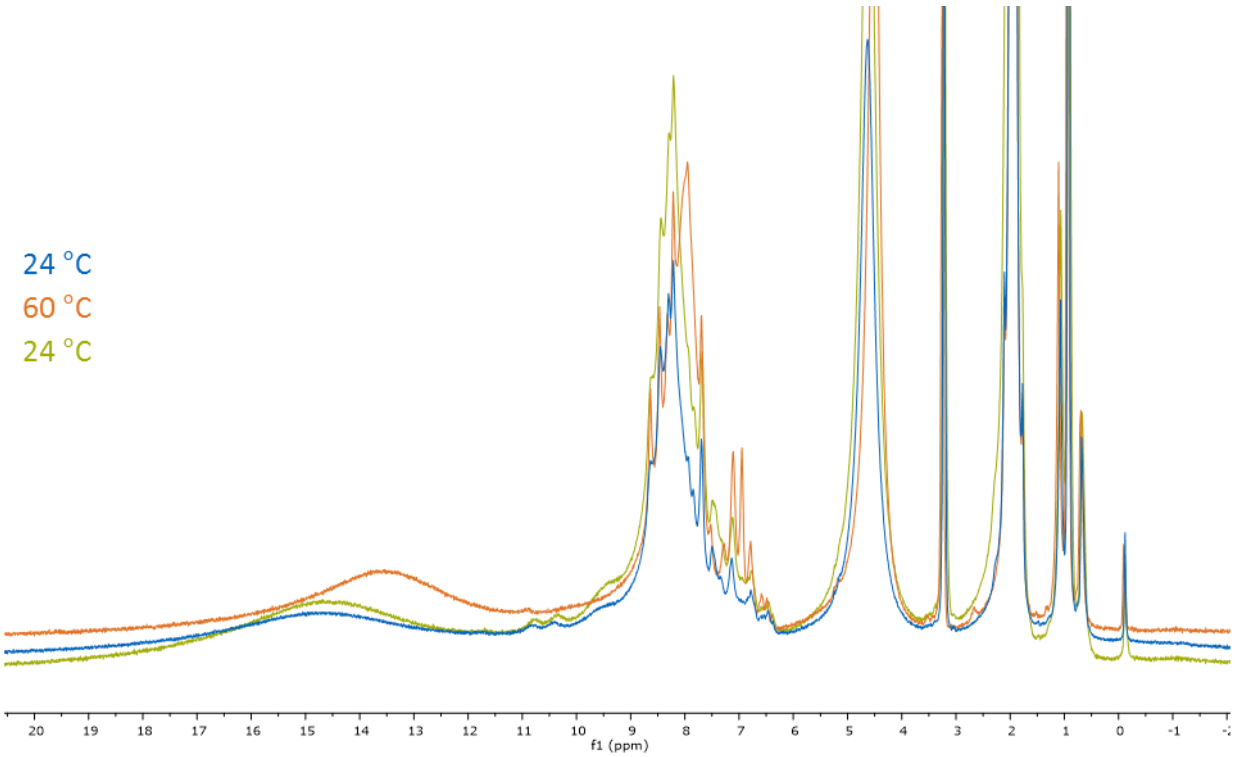

Figure **23**: Significant part of a paramagnetic ^{1}H NMR at indicated temperatures determined of a potential chromium-based cage structure **27**.

This NMR showed a shift of the signal at about 15 ppm towards the diamagnetic region by increasing the temperature. In addition, a huge accumulation of signals was observed at 8.5 ppm, which prevents any assignments or interpretation. Nevertheless, the compound appeared to be stable at 60°C because the NMR spectrum measured after cooling down to room temperature did not show any changes compared to the first room temperature spectrum. Crystallization attempts with DMF instead of DMSO were performed. However, no crystal growth was achieved. Further attempts applying ligands with other or no functional groups (shown in figure **3** in the introduction) and further solvents like acetone, toluol, DMF and THF were also evaluated. However, no reasonable products could be obtained and thus, these approaches are not further discussed.

3.1.3 Gold

In 2016, Dutton *et al.* published the synthesis of homoleptic pyridine-based complexes of Au(I) and Au(III), which represents a valuable basis for the following studies.[131] The first synthetic approach for these Au(I) as well as Au(III) complexes is shown in scheme **7**.

Approach 1

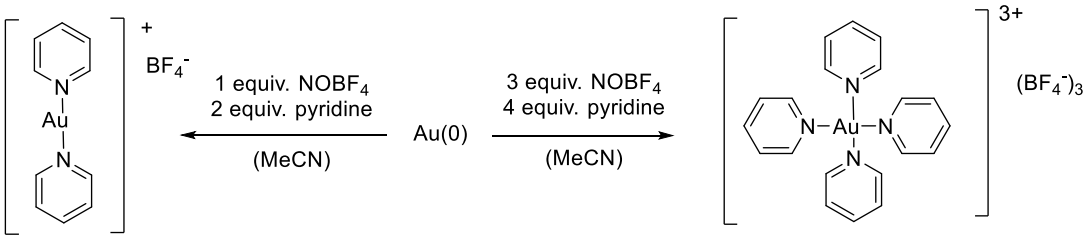

Scheme **7**: Synthetic procedure for the synthesis of pyridine-coordinated Au(I) and Au(III) complexes according to *Dutton et al.*[131]

In contrast to the statement in the publication, that all Au(III) complexes were found to be moisture-sensitive, stability studies performed with $[Au(py)_4](BF_4)_3$ showed, that the complex was stable for weeks even in the presence of water and oxygen according to ^1H NMR studies. This is very promising for being able to access a stable Au(III) based SCC. Additionally, Dutton *et al.* presented a further three-step procedure for heteroleptic/pseudo-homoleptic pyridine-derived Au(III) complexes, which is shown in scheme **8**.[132]

Approach 2

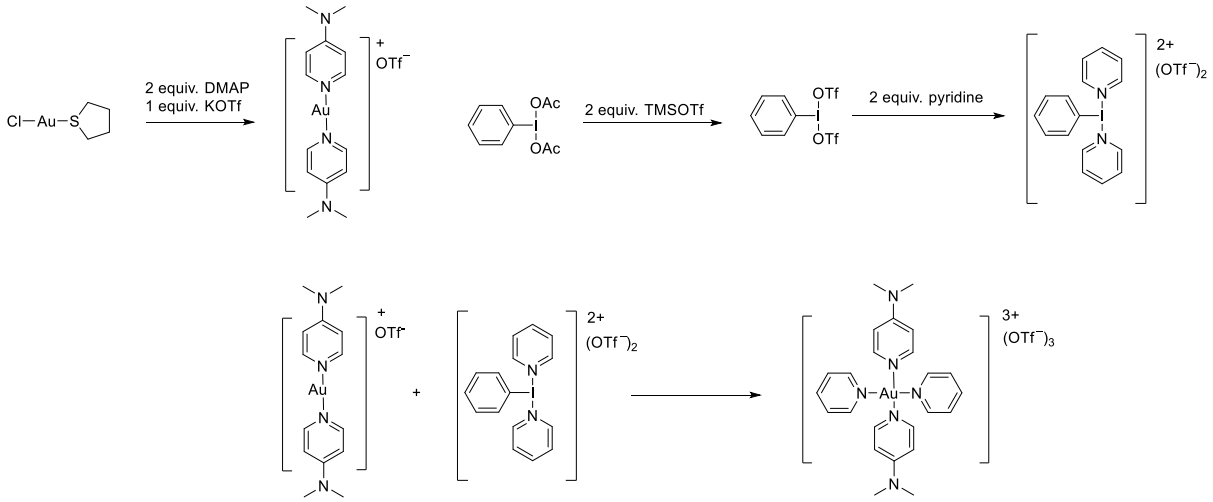

Scheme **8**: Schematic representation of the synthesis of a heteroleptic/pseudo-homoleptic pyridine-based Au(III) complex by oxidation with a I(III) complex.[132]

It is worth mentioning, that according to Dutton *et al.* the homoleptic $[Au(py)_4]^{3+}$ complex was not accessible applying the synthetic conditions of approach 2 presented in scheme **8**.[131]

Both procedures were evaluated for their suitability to adapt the conditions for the synthesis of an Au based SCC. As previously mentioned in the introduction, in general, Au(I) forms twofold linear coordinated complexes and Au(III) complexes are usually fourfold coordinated with a square planar geometry. Accordingly, in case of Au(I), rather metallacycles than cages may be obtained.

STUDIES FOR THE SYNTHESIS OF AU(I) METALLACYCLES

A brief schematic overview of the attempts to synthesize such Au(I) metallacycles according to approach 2 (scheme **8**) is presented in scheme **9**.

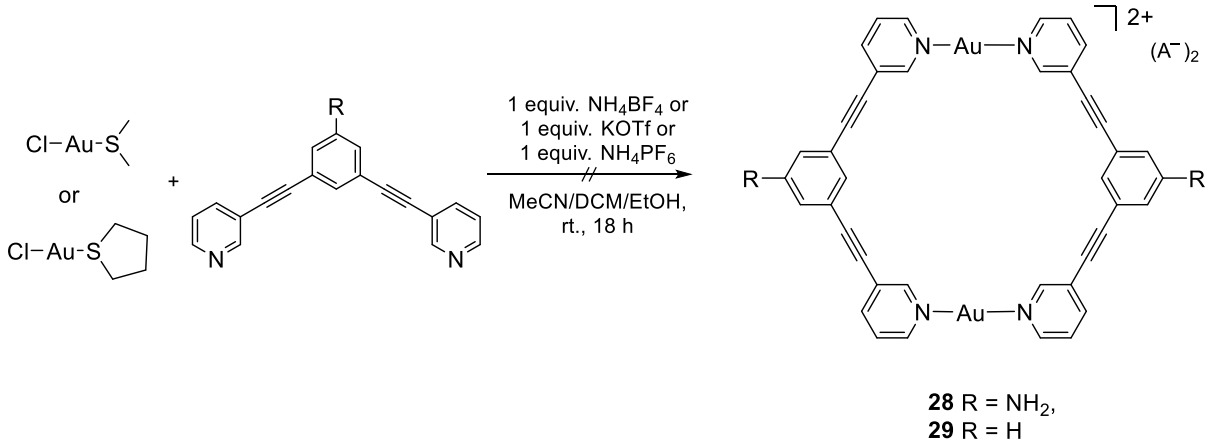

Scheme **9**: Overview of the synthetic approaches performed for the synthesis of an Au(I) metallacycle.

Performing the synthesis for the intended product **28** according to scheme **9** yielded two sets of signals in the ^{1}H NMR. One set was assigned to the free ligand. The other one was shifted downfield compared to the free ligand and thus, to some extent, formation of a metallacycle was assumed. The obtained ratios were about 1:2.5 and 1:5 (free ligand:metallacycle) for KOTf and NH_4BF_4, respectively. The corresponding NMR spectra are given in figure **24**.

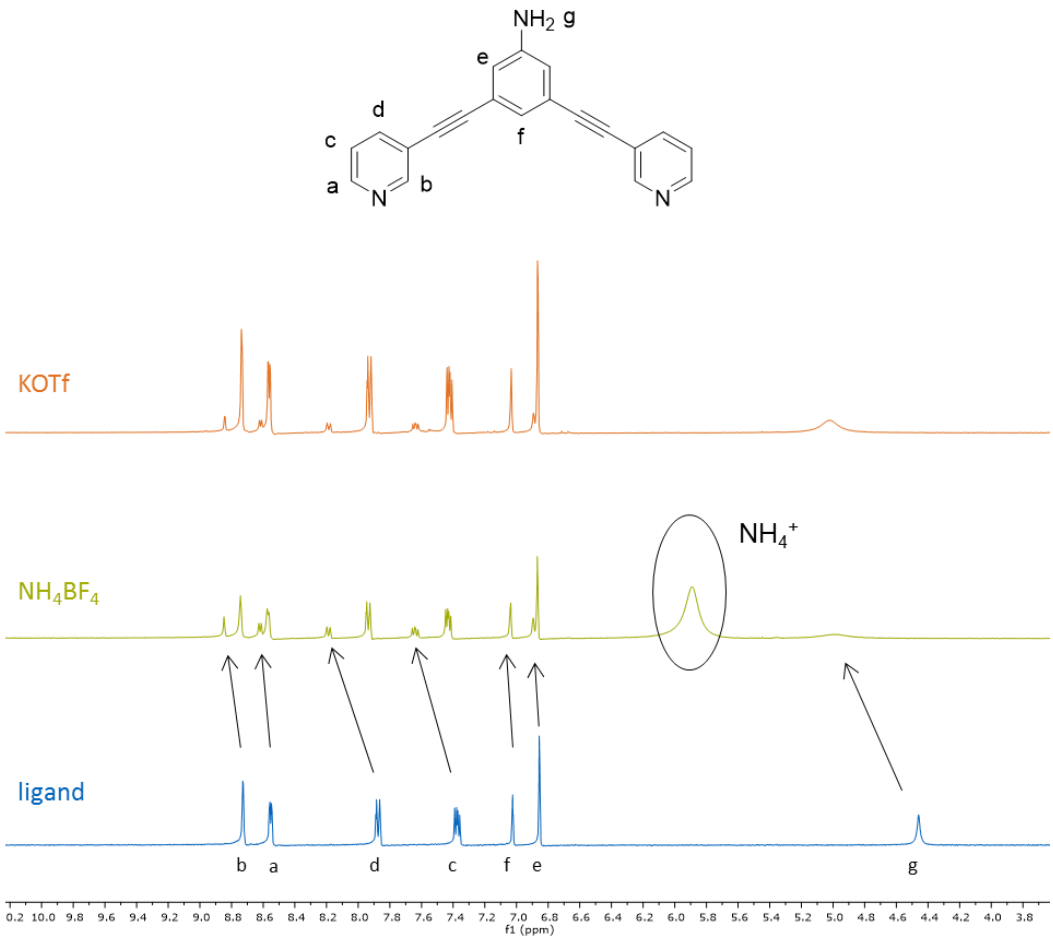

Figure **24**: ^{1}H NMR spectra in MeCN-d_3 of the free ligand (blue) and the attempts to synthesize Au(I) metallacycle **28** using NH_4BF_4 (green) or KOTf (orange).

To rule out, whether chloride extraction from Au(I) precursor was a limiting factor on conversion to the metallacycle **28**, $AgBF_4$ and AgOTf, respectively, were added to the NMR samples. However, this resulted in formation of a precipitate and the disappearance of the signals in the ^{1}H NMR spectra. Thus, the formation of insoluble coordination polymers was assumed. Schröder *et al.* reported a systematic evaluation of the dynamic equilibria of coordination polymers and showed the dependence of the solubility on different solvents as well as anions.[133] Accordingly, the reaction product was observed to be significantly influenced by the addition of such silver salts. To analyze the solutions of **28** further, ESI-MS spectra were recorded. However, these showed only signals of the ligand in association with one additional proton and no signals could be assigned to a metallacycle or any gold-coordination. In addition, due to the shift of the amine protons (signal g, figure **24**), some kind of interactions with the amine functionality are likely to occur. Thus, the non-functionalized ligand intended to yield metallacycle **29** was tested. Despite the observation that all signals were shifted downfield compared to the free ligand, a new signal at 13.3 ppm arose, which strongly indicates the protonation of the terminal pyridine moiety of the ligand. In addition to these observations, also a different shift of the signals was found for different solvents, highlighting the dynamic coordination mode of the formed product.

Therefore, no product could be isolated and thus, approach 1 as depicted in scheme **7** was applied to evaluate the synthesis of metallacycles **28** and **29**. The reaction scheme is shown in scheme **10**.

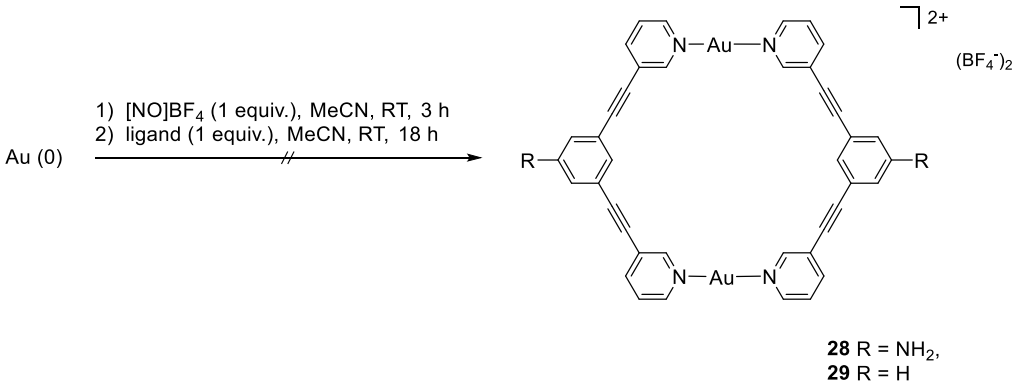

Scheme **10**: Scheme of the synthetic procedure for Au(I) metallacycles **28** and **29** according to approach 1.

The resulting ^{1}H NMR spectrum of **28** (see supplementary section figure **S2**) showed that mainly protons c and d (notation according to figure **24**) were shifted downfield and a broad signal at 8.3 ppm developed resulting from the amine protons g. According to these observations, it was assumed that a coordination or at least interaction with gold takes place at the terminal pyridine as well as at the amine group. However, the structure cannot be predicted according to that analysis. Noticeable, the signals slightly changed upon prolonged standing, leading to the assumption that for Au(I) cages, a dynamic coordination takes place in solution. For **29**, the interpretation was challenging. A downfield shift as well as a broadening of the signals was observed. In addition, some new signals were generated, assuming that decomposition of the ligand takes place. In conclusion, one can assume that an Au(I) metallacycle was accessible from both approaches. Yet, isolation and crystallization was prevented due to the observed instability and dynamics of the formed products. Nevertheless, the results show that these Au(I) metallacycles are labile, however accessible and thus are promising with respect to *in situ* oxidation to a corresponding Au(III) complex.

Studies for the Synthesis of Au(III) cage structures

At first, the oxidation starting from Au(0) *via in situ* formed Au(I) metallacycle to Au(III) cage applying $[NO]BF_4$ was tested using different ligands (approach 1). A summary of the conditions of the reaction and the applied ligands is presented in scheme **11**.

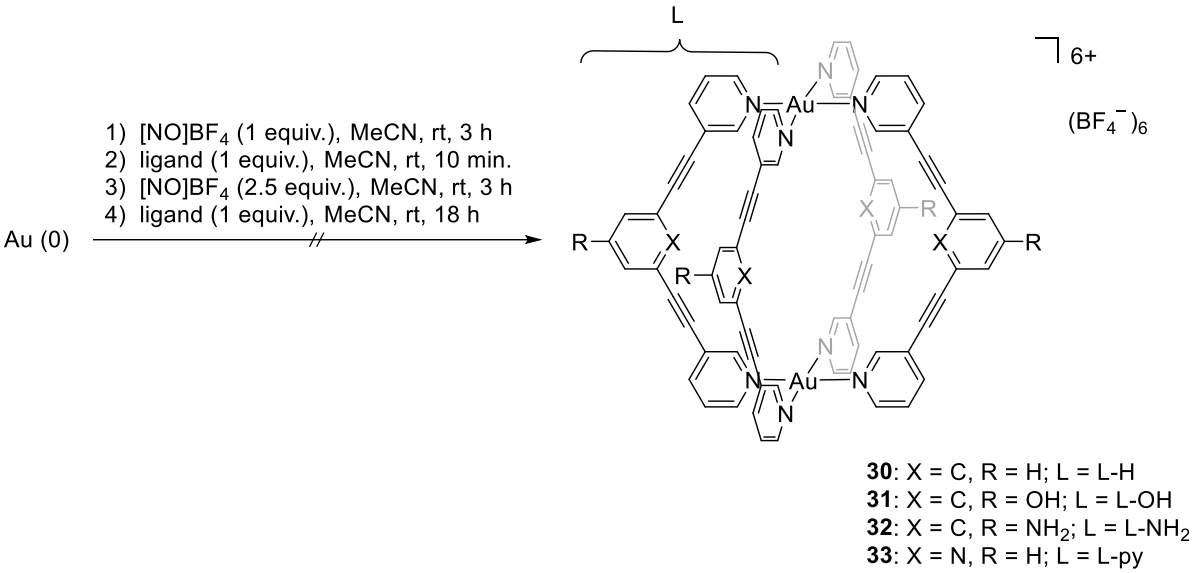

Scheme **11**: Reaction scheme of the synthetic condition applied for the oxidation of Au(0) to Au(III) SCCs.

The ligand with a central benzene moiety is applied in the first reaction intended to yield **30**. The resulting ^{1}H NMR compared to the free ligand is displayed in figure **25**.

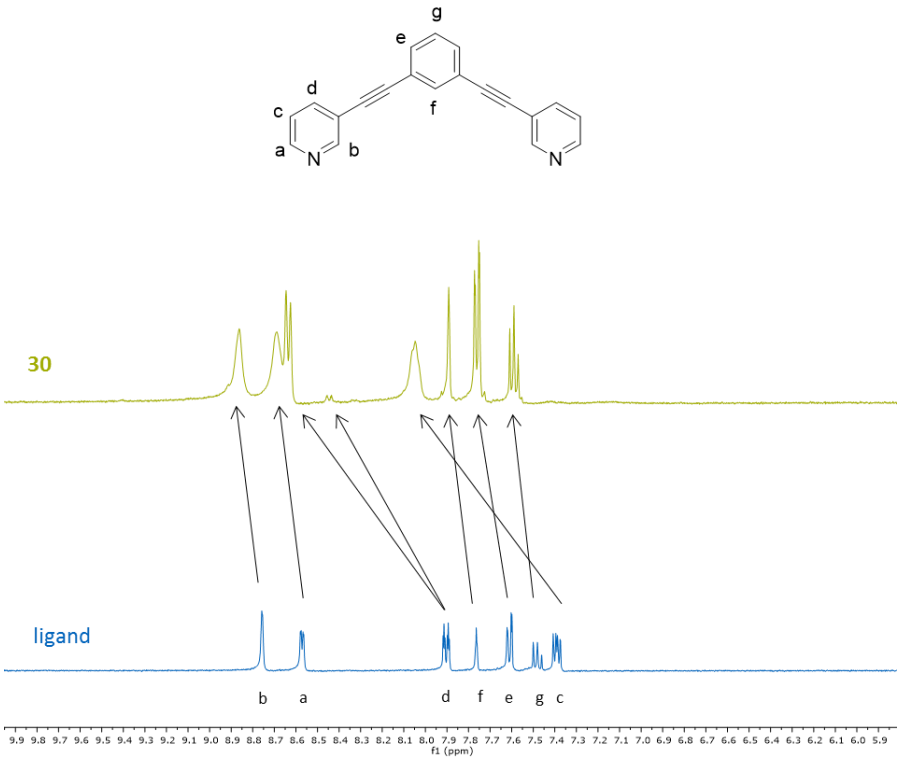

Figure **25**: Cutout from the ^{1}H NMR in MeCN-d_3 of **30** in comparison to the corresponding free ligand.

The ^{1}H NMR signals of **30** were assigned applying a 2D COSY NMR experiment (figure **S3**, supplementary section). Thus, the signal splitting of the proton d was identified. In figure **25**, only a cutout of the most significant part of the NMR of **30** is presented. However, a broad signal at 13.2 ppm was also observed indicating protonation of the terminal pyridine. Nevertheless, all signals were downfield shifted. To

obtain further insight into the composition of the product, elemental analysis was performed. The result showed the following deviations from calculated for the desired cage to measured mass percentages: ΔC +2.41 %, ΔH +0.62 %, ΔN +0.50 %, ΔAu -13.55 %. Strikingly, the solid contained too small amounts of gold and thus, the signal shifts were assumed to mainly originate from pyridine protonation. In fact, crystallization of the product confirms this assumption. Unfortunately, for **31**, the same proton signal at 13.1 ppm was observed showing that also in case of the phenol-functionalized ligand protonation of the terminal pyridine occurs.

Nevertheless, the results of the synthesis **32** were much more promising, since no pyridine-protonation occurred according to ^{1}H NMR analysis. Also for this approach, a downfield shift of the signals compared to the free ligand was found which is displayed in figure **26**.

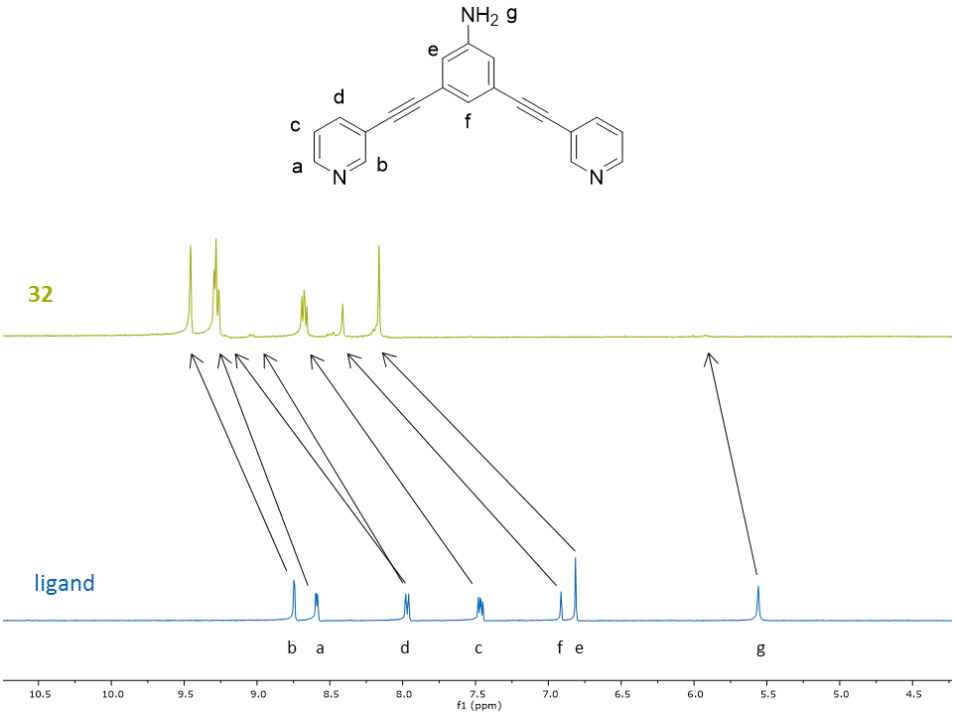

Figure **26**: Cutout from the ^{1}H NMR in DMSO-d_6 of **32** with respect to the corresponding free ligand.

Additionally, an ^{11}B NMR of **32** was recorded, which showed two signals at -0.46 and -1.28 ppm (see supplementary **S4**). In comparison to $AgBF_4$, where one signal at -1.30 ppm was found, this result might indicate partial encapsulation of BF_4 into a potentially formed cage. This would result in shielding and thus a shift of the signal due to weak intermolecular interactions like it is observed for encapsulated cisplatin.[22] Further analysis of the sample was performed using ESI-MS and elemental analysis. The ESI-MS in acetonitrile on air and moisture showed two fragments which were assigned for $[Au(L\text{-}NH_2)_3+BF_4+H]^{3+}$ and $[Au(MeCN)_2+3H]^{+}$ as well as further signals which were not assignable (m/z = 401.79, 602.19). Still, the ESI-MS indicates presence and coordination of gold. The performed elemental analysis

of **31** showed the following deviations from calculated (for the desired $[Au_2(L\text{-}NH_2)_4](BF_4)_4$ cage compound) to measured mass percentages: ΔC -4.56 %, ΔH -0.13 %, ΔN +0.26 %, ΔAu -3.59 %. This result was very promising because the gold content was found to be in the expected range and the Au:ligand ratio was calculated from these values to be 2:1, which is in accordance with a formed Au(III) cage. Due to the red color of **31**, which might also be caused by the formation of gold nanoparticles, a sample dissolved in acetonitrile was treated with elemental Hg. The solution should maintain its red color, if no Au nanoparticles are present. In contrast, if such nanoparticles would be present, the solution will lose its color and turn blueish due to amalgam formation.[134] The Hg-treated solution, however, maintained its color and therefore, does not contain Au nanoparticles. Moreover, red-colored Au(III) complexes with pyridine and bipyridine based ligands are reported in literature.[131, 132] The color is caused by a π-σ* transition of the Au-ligand bond due to the d^8 electronic configuration of Au(III). Therefore, UV-vis spectra of the ligand as well as **31** were recorded. Both spectra are presented in figure **27**. The sample of **32** was determined in a sealed vial under inert atmosphere and in a high concentration. As the resulting spectrum shows, the concentration was too high for a good resolution of the ligand-based transitions. Nevertheless, a further transition at 515 nm was observed, which was not visible in the spectrum of the ligand.

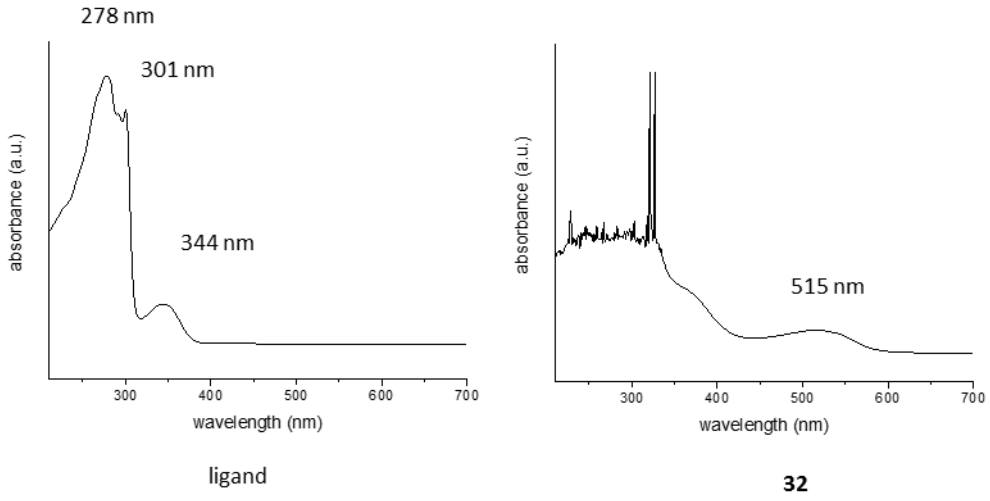

Figure **27**: UV-vis spectra recorded of acetonitrile solutions of ligand $L\text{-}NH_2$ and the reaction product **32**, respectively.

The wavelength of this transition is comparable to other gold-pyridine-based complexes such as $[Au(DMAP)_2(CN\text{-}py)_2](OTf)_3$ at 461 nm and $[Au(DMAP)_2(py)_2](OTf)_3$ at 427 nm.[132]

However, the final proof for the desired **32** is still missing. All attempts to grow crystals of the product by diffusion of either diethyl ether or methylene chloride into an acetonitrile or acetone solution resulted in amorphous material. Furthermore, stability of the product using ^1H NMR indicates that the product was air- and moisture-sensitive.

Finally yet importantly, the synthesis of **33** with a central pyridine was tested. Also for this reaction, the determined ^{1}H NMR showed a downfield shift of all signals. For this approach, however, the greatest shift was observed for protons d and e (see figure **28**), both next to the alkyne bond.[135, 136] Accordingly, this suggests an interaction of gold with the alkyne entity. Additionally, a very broad but not intense signal at 13.35 ppm again points to the formation of a protonated ligand.

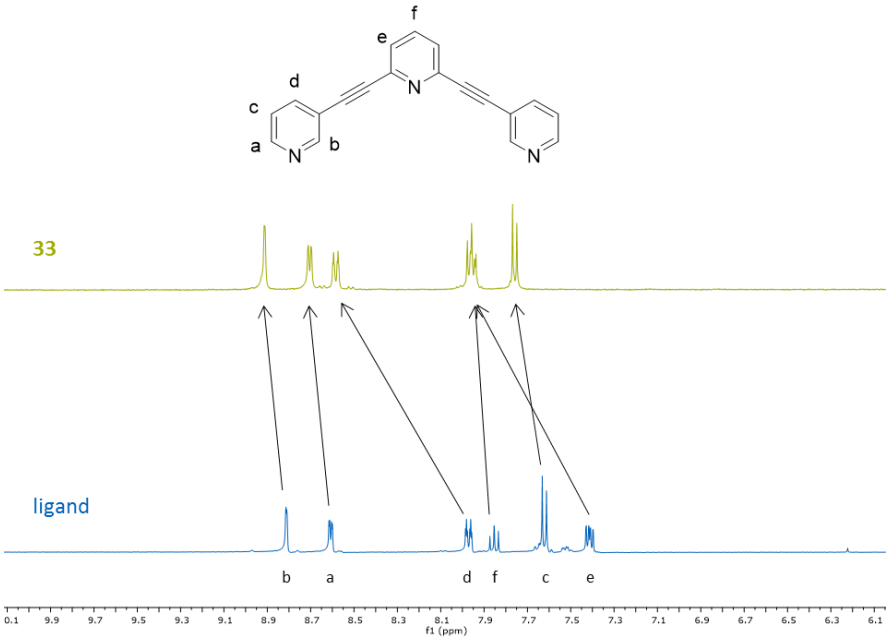

Figure **28**: ^{1}H NMR spectra recorded in MeCN-d_3 of a sample of **33** in comparison to the free ligand.

Nevertheless, the elemental analysis showed good conformity with the intended composition. The following deviations from calculated to measured mass percentages: ΔC -0.85 %, ΔH +0.72 %, ΔN -0.4 %, ΔAu +3.29 % were determined. The higher gold content might be caused by accumulated colloidal gold, which might be formed upon decomposition. In contrast to decomposition of organic compounds, where the majority of such impurities can be removed by washing the sample, colloidal gold can be accumulated. Additionally, determined ESI-MS showed fragments which could be assigned to the free ligand and a $[Au_2(L)_4]^{3+}$. These results represent strong hints for the formation of a gold cage, however, a strong involvement of the central pyridine can be suggested according to the obtained NMR spectra by proton e. This huge shift was not observed for the corresponding palladium cage reported by Crowley *et al.*[24] Accordingly, a crystal structure is needed to elucidate the coordination mode of this product and to further understand the analytical results. When exposed to air, an upfield shift of proton d is observed. Exposition to water resulted in a further upfield shift together with a splitting of the signal assigned for protons e and f. This observation underlines again the assumption that some sort of interaction with the alkyne bond occurs, which seems to be changed upon addition of water and

exposure to air. Strikingly, the signals of the free ligand were not observed after introduction of air and water. The corresponding NMR spectra are given in the supplementary section in figure **S5**.

Additionally, the synthesis for potential Au(III) cage **30** according to the procedure shown in scheme **11** was tested replacing $[NO]BF_4$ by $[NO]PF_6$. The stacked ^1H NMR spectra in comparison to the ligand are given in figure **29**.

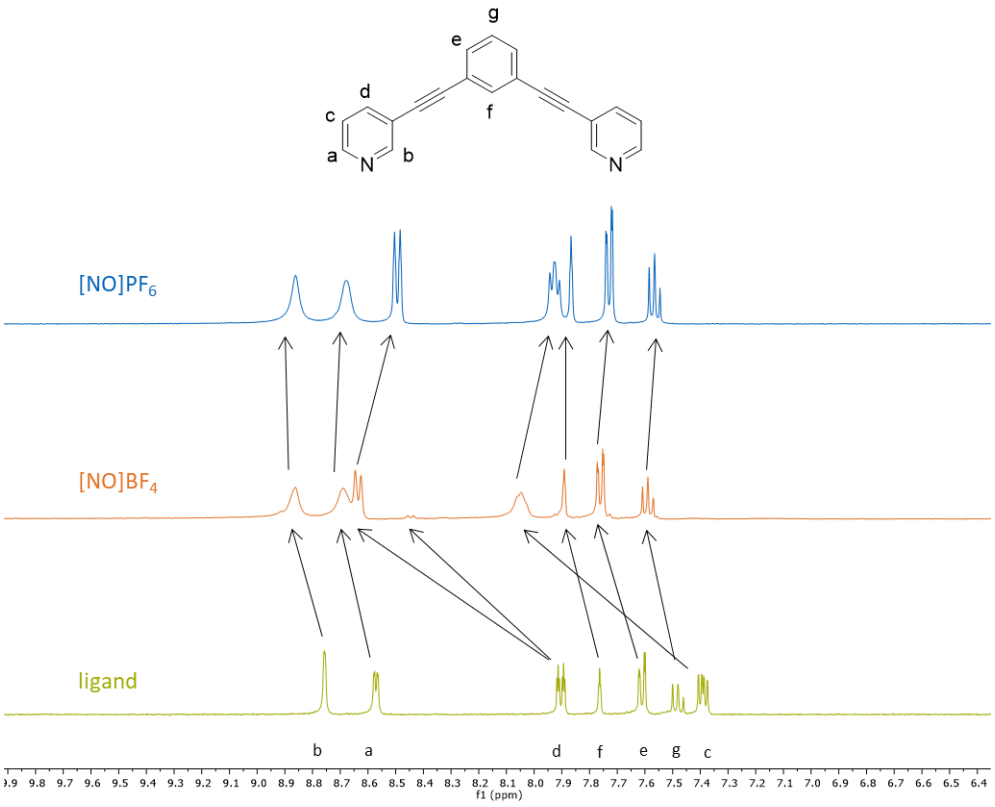

Figure **29**: Comparison of ^1H NMR spectra determined for the syntheses of **30** synthesized with $[NO]PF_6$ or $[NO]BF_4$ according to the procedure presented in scheme **11**.

By comparing the ^1H NMR spectra obtained from synthesis of **30** with using either $[NO]BF_4$ or $[NO]PF_6$, only a slight difference of the shift of the signals were observed. The most significant difference was the upfield shift of proton d and the upfield shift of a (see figure **29**). This might be explained by a change of the electronic interactions with either BF_4^- or PF_6^- with these particular protons. Even if these anions are considered as 'non-coordinating' anions, crystal structures revealing coordinating interactions were reported.[126, 137] Furthermore, a small signal at about 14 ppm was visible indicating again the formation of a protonated pyridine moiety. Nevertheless, these studies encourage blocking these positions showing such strong interactions with the counterions or Au atoms to possibly enhance cage formation. Therefore, studies involving modifications of the ligand structure are discussed in section 3.1.4.

Furthermore, also approach 2, where oxidation of Au(I) was realized by applying a hypervalent iodine species was tested for the feasibility to synthesize an Au(III) cage structure. A scheme of the conducted synthesis is presented in scheme **12.**

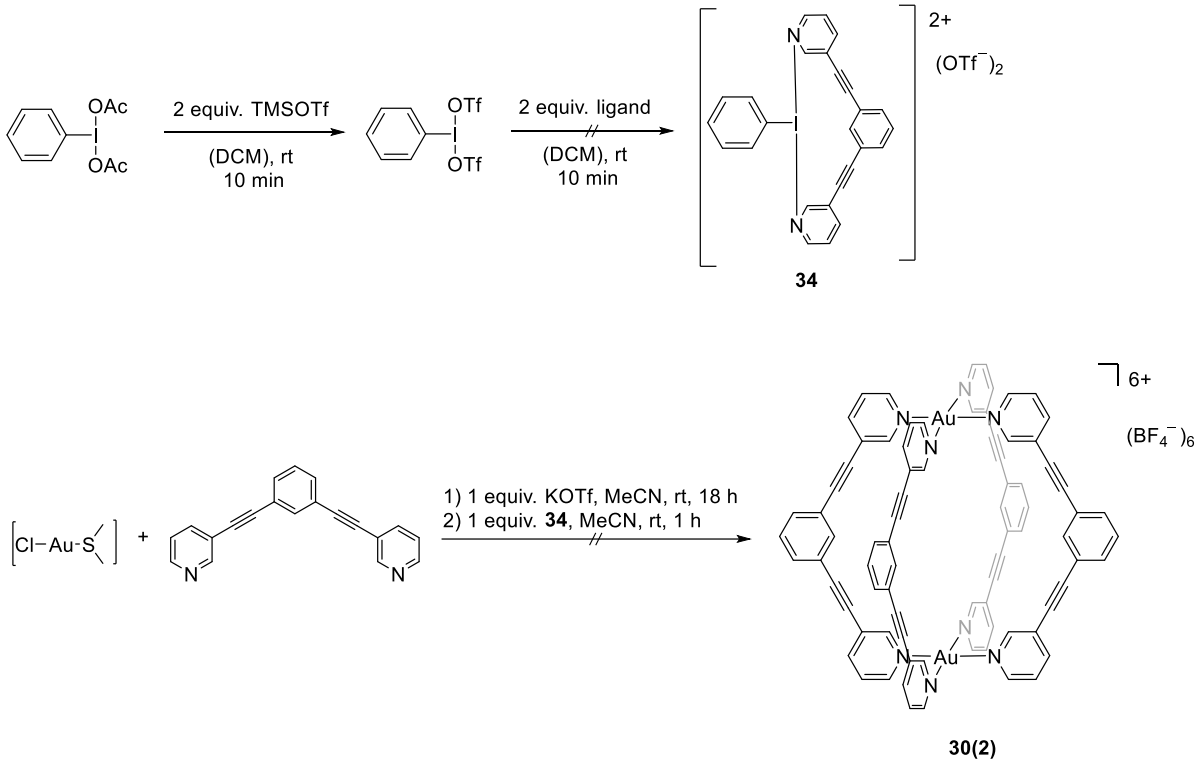

Scheme **12**: Schematic representation of the synthetic procedures performed according to approach 2.[132]

Based on NMR spectroscopic findings in ^{1}H and ^{13}C NMR as well as 2D COSY NMR, the proposed structure of **34** is depicted in scheme **12**. The NMR spectra are given in the supplementary section in figures **S6**, **S7** and **S8**, showing a highly symmetric product. However, a signal at 13.77 ppm appeared which in theory will indicate protonation of the terminal pyridine moieties. Nevertheless, the 2D COSY NMR did not show any correlations of the ligand protons to that signal, so it might derive from some impurity. Still, the assumed chelation of the iodine I^{2+} is surprising given that Pd^{2+} is even smaller and for which no chelation was observed.[15, 18-21] However, the structure can only be assumed, because no crystals suitable for X-ray diffraction were obtained.

Nevertheless, synthesis of **30(2)** was attempted according to the indicated conditions in scheme **12** yielding a white solid. Analysis was performed using NMR as well as ESI-MS. The ^{1}H NMR spectra is given in the supplementary section in figure **S9**. The ^{1}H NMR indicated complete consumption of **34** because no signals originating from iodobenzene were observed. Additionally, all signals were downfield shifted compared to the free ligand. Interestingly, the NMR was mainly consistent with the results obtained for the corresponding Au(I) metallacycle synthesized from (tht)AuCl with KOTf. Thus, it is assumed that an Au(I) metallacycle might be formed rather than **30**. The ESI-MS showed various signals where only one

could unambiguously be assigned to the protonated ligand. No further attempts with other ligands were performed in this work, because much more investigations are needed which are out of the scope of this work. The attempt requires a full characterization of **34**, because without knowing the distinct composition and structural features, the stoichiometry for the following reaction cannot be calculated. Nevertheless, it still seems to be a rather promising approach.

3.1.4 Ligand modifications

In particular, the previously discussed studies for the synthesis of gold cages show that the presence of a functional group was beneficial for the formation of such SCCs. Moreover, it was also shown, that unspecific interactions with different parts of the ligands take place instead of coordination of the metal atoms and that the applied solvents strongly influence such interactions and the potential cage formation. Moreover, especially in case of gold, an interaction with the bridging alkyne was assumed. Consequently, also attempts to modify the ligands slightly were performed. In doing so, also the applicable solvents vary, which might enhance the formation of SCCs.

Thus, the first study was intended to make use of already published results for preventing interactions of the applied metal with the alkyne bond. Accordingly, the most obvious solution was replacing the alkyne bond as it was realized with the anthracene-containing ligands published by Yoshizawa *et al.*[27, 28] There, the ligands were already shown to form 3D capsules with different metals like Cu^{2+}, Co^{2+}, Pd^{2+} or Pt^{2+}. In brief, the synthesis of such ligands already failed in the first steps. The reason for this failure was not elucidated, still, the idea seemed promising.

Thus, modifications of the original ligands were tested. Therefore, the position *para* to the nitrogen of the terminal pyridine was chosen to be varied as shown in scheme **13**. There, the methyl-modified ligand **35** was chosen representing minor modifications. Nevertheless, enhancing the lipophilicity of a complex is known to enhance its cytotoxicity and cellular uptake as shown for comparable bistriazole based Pd_2L_4 cage.[138] In addition, for that cage, a shielding of the metal center seems possible by the long alkane chains blocking certain decomposition mechanisms, because it was found to be extraordinary stable against biological nucleophiles.[138] Thus, heptenyl-modified ligand **37** was developed. Ligand **36** is an intermediate structure towards **37**.

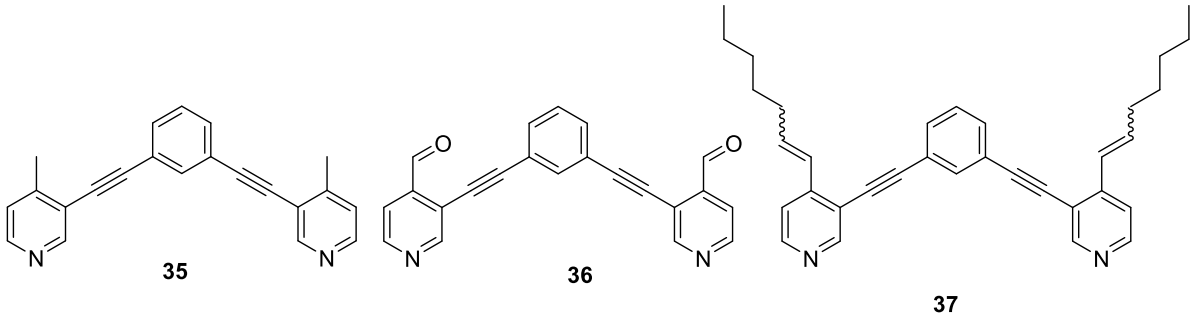

Scheme **13**: Modifications of the ligands in *para*-position to the pyridyl-nitrogen.

For the synthesis of **35**, 3-bromo-4-methylpyridine was used as starting material for a *Sonogashira* coupling with trimethylsilylacetylene according to scheme **14**. A yield of 51 % of product **38** was achieved. However, the following deprotection, namely removal of the trimethylsilyl group, was not successful. All attempts resulted in either complete decomposition or a mixture of products and side products. Although performing the synthesis under inert atmosphere, already during *Sonogashira* coupling yielding **38**, decomposition of the starting materials was observed which made the purification of **38** challenging. Additionally, *in situ* deprotection of **38** did not yield **39**. Noticeable, a synthetic process for a compound very similar to **39** was only found to be part of a patent[139] and not of any paper which is surprising taking the simple structure of this compound into account.

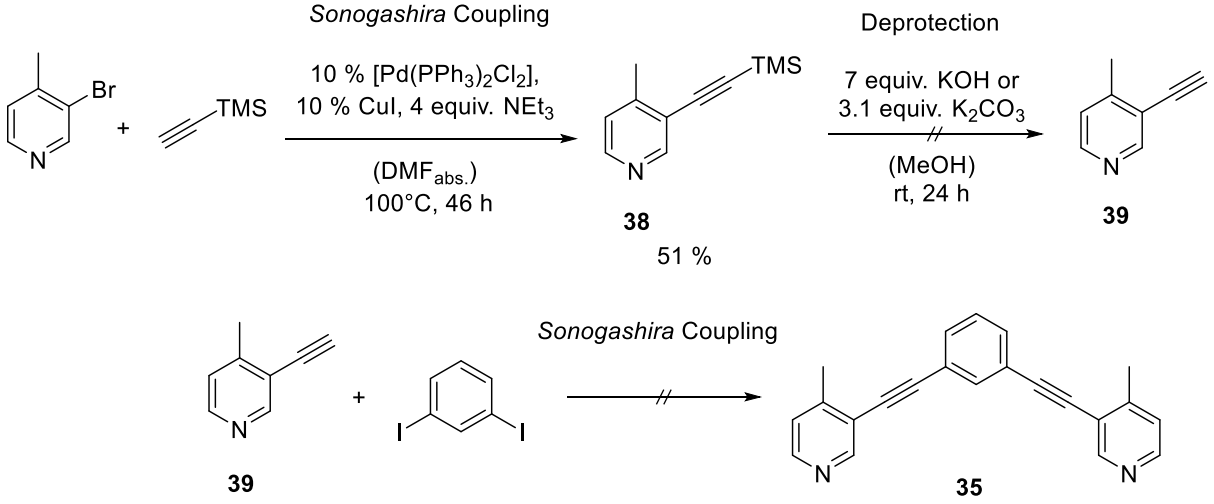

Scheme **14**: Synthetic approach for the synthesis of **35**. However, already purification of **39** was not successful.

Consequently, this synthesis was not further pursued. Instead, synthesis of **36** and **37** was tested. Thus, the synthesis of **36** was conducted as shown in scheme **15**. The first step was a *Sonogashira* coupling of 3-bromo-isonicotinaldeyde and trimethylsilylacetylene yielding **40**.[140] Without purifying the compound, it was deprotected *in situ* resulting in a yield of 47 % for **41**. Subsequently, **41** and 1,3-diiodobenzene were coupled by another *Sonogashira* reaction resulting in ligand **35** with a yield of 68 % after purification using column chromatography.

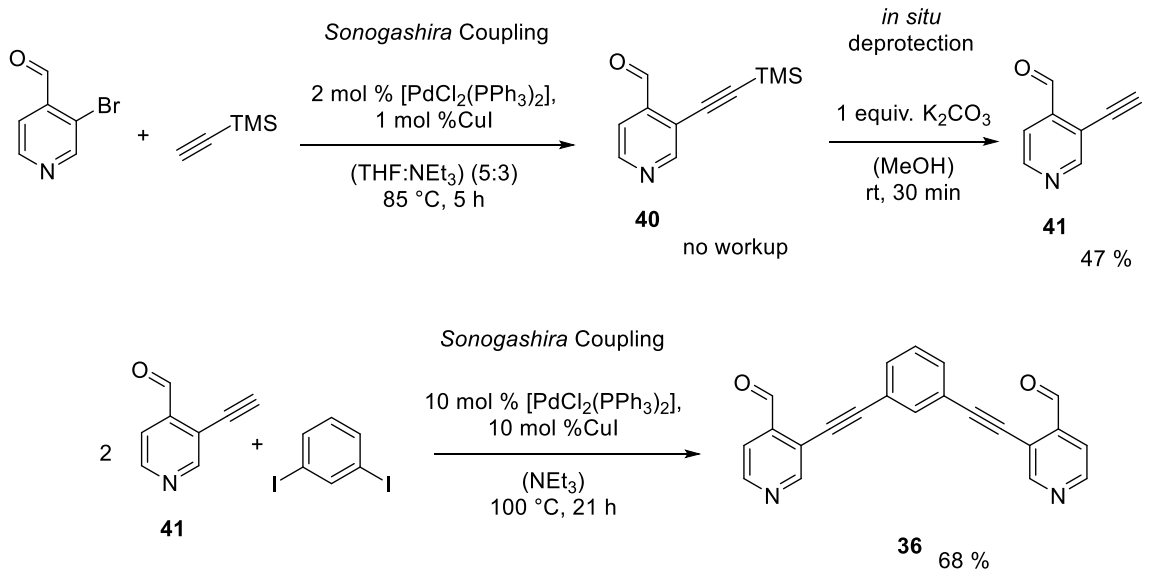

Scheme **15**: Schematic representation of the synthetic procedures for the synthesis of ligand **36**.

^{1}H and ^{13}C NMR as well as ESI-MS were used to characterized ligand **36**. Both NMR spectra are given in the supplementary section in figures **S10** and **S11**, respectively. These spectra still shows aliphatic impurities however indicate ligand formation. The ESI-MS showed two fragments, [**36**+H]$^{+}$ and [**36**+MeCN+H]$^{+}$, underlining the formation of the ligand.

Synthesis of **37** was developed according to the *Wittig* reaction published by Yikang *et al.*[141] Therefore, the phosphonium bromide salt **42** was synthesized in about 5 % yield. This was followed by preparation of the respective ylide applying *n*-butyl lithium. *In situ* reaction with **36** afforded the desired heptentyl-modified ligand **37**. The successful synthesis was proven by ESI-MS analysis showing the fragments [**37**+H]$^{+}$ and [**37**+MeCN+H]$^{+}$. From the complex mixture of **37**, which contains different isomer (ZZ, EZ, EE), triphenylphosphane oxide, unreacted **36** as well as other impurities, the product was purified by column chromatography. Using ethyl acetate: pentane in a ratio of 1:2, some impurities were eluted first, accompanied by the ZZ, the EZ and the EE isomers. The final fractions contained phosphane oxide and **36**. However, a complete separation of the EE isomer, phosphane oxide and **36** was not achieved.

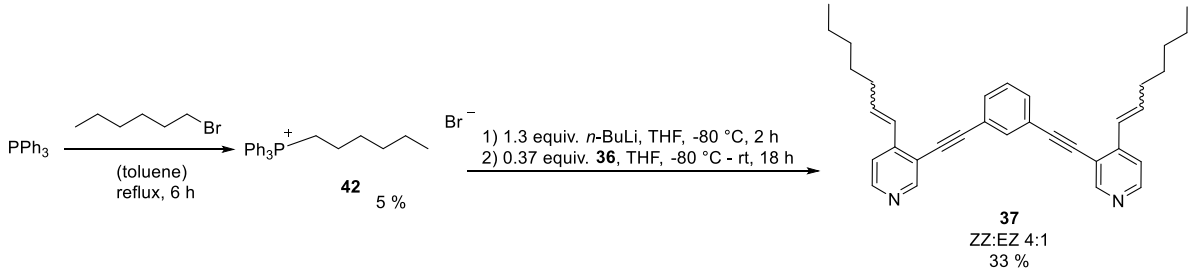

Scheme **16**: Synthesis of the phosphonium salt yielding ligand **37** in a subsequent *Wittig* reaction.

A discrimination between the single isomers was made by the coupling constants and the chemical shifts observed in the ^{1}H NMR spectra.[142] In general, the E isomers have higher coupling constants (about 16 Hz) compared to the Z isomers (10 – 12 Hz).[142] The corresponding NMR spectra with the assignments for the isomers and the isomeric mixtures obtained for ligand **37** are given in the supplementary section in figure **S12**. Additionally, 500 MHz cryo NMR was conducted for further characterization. Noticeable, in the ^{1}H NMR, a splitting of the signals in the aromatic region is shown (supplementary section figure **S13**), indicating that the fraction consists of a mixture of the EZ and the ZZ isomer in a ratio of 1:4. The assignments were made according to a cryo 2D COSY NMR (see supplementary section figure **S14** (aliphatic region) and **S15** (aromatic region)). Nevertheless, some aliphatic impurities hampered a proper assignment of all signals. Still, the synthetic conditions are suitable for the synthesis of **37**, however, purification needs to be optimized for separation of the isomers. Therefore, a purification using HPLC seems reasonable, however, was out of the scope of this work.

Nevertheless, having this ligand mixture, a first trial for the formation of the corresponding Pd^{2+} cage was tested. The synthetic conditions are depicted in scheme **17**. The reaction was monitored by ^{1}H NMR spectroscopy. A cutout of the aromatic region of the resulting NMR is shown in figure **30**.

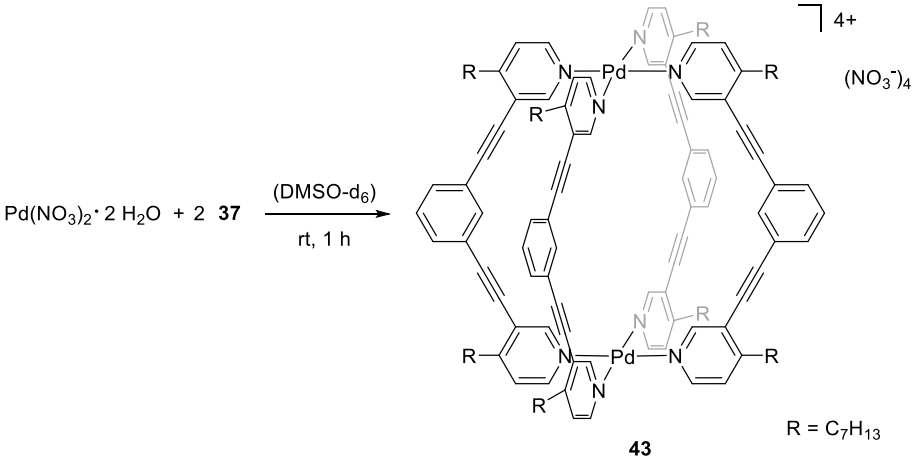

Scheme **17**: Formation of Pd-based cage **43** applying the indicated conditions.

A comparison of the ^{1}H NMR shifts of the ligand **37** to the respective cage **43** showed a significant downfield shift of the aromatic protons, which strongly indicates cages formation (see figure **30**). This assumption was supported by ESI-MS analysis showing signals of [**43**-3NO_3^-]$^+$ and [**43**-3NO_3-**37**+DMSO]$^+$. Because of the small sample available, no isolation of the cage was attempted, however, growth of single crystals was attempted. Unfortunately, no single crystals suitable for X-ray diffraction were obtained. Nevertheless, this ligand and the corresponding cage are interesting for future investigations.

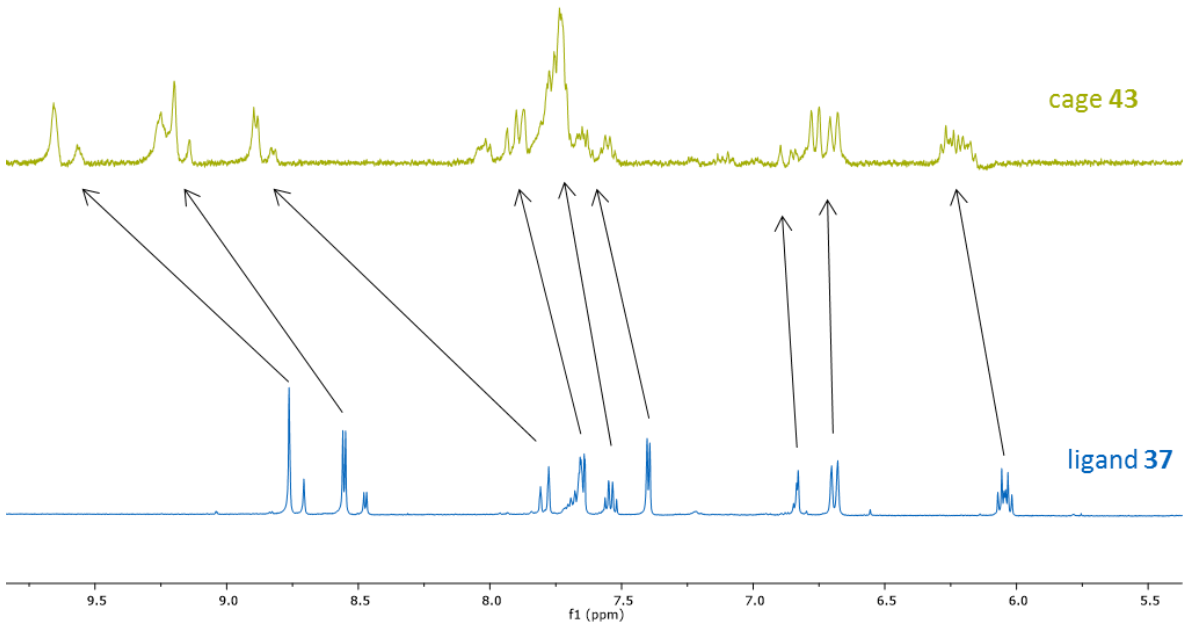

Figure **30**: ^{1}H NMR shifts of ligand **37** (2:1 ZZ:EZ, cryo NMR) compared to the signals of the synthesis of the respective palladium cage measured in DMSO-d_6.

3.1.5 Summary of studies towards new supramolecular coordination compounds

In summary, the previously discussed studies show, that these 3D molecular cage-structures based on palladium are easily accessible and that a change of the metal is rather challenging. In case of molybdenum, it does not seem likely that a 3D structure of any kind will from applying the given ligands. The dimolybdenum core was found to be too reactive and not appropriately stabilized by non-chelating pyridine ligands. It rather requires ligands with O-donor-atoms and ideally chelating ligands as previously published studies on the synthesis of Mo_2^{4+}-containing supramolecular entities show.[123, 143-149] Additionally, the demand for chelating ligands was in particular represented by the attempts to synthesize $[Mo_2(OAc)_2(py)_6](OTf)_2$, where no reasonable product was obtained. The analysis showed a mixture of many different products, which could not be assigned. In addition, reproduction of any somewhat promising approaches was not possible. In contrast, applying bipyridine instead of pyridine, two different conformers of $[Mo_2(OAc)_2(bipy)_2](OTf)_2$ were obtained and characterized. However, even if a cage structure will form, it is not likely that it will be sufficiently stable for any biological purpose. One method to stabilize a quadruple bond for biological applications is the encapsulation of such compounds in liposomes, which is successfully evaluated for dirhenium complexes, as already mentioned in the introduction.[94] Moreover, the application of mononuclear compounds and thus different Mo-precursor might be more promising for the synthesis of such cage structures.

For chromium, the biggest drawback was the analysis of the products. The general analysis was based on NMR spectroscopy, which is however a challenge for the paramagnetic Cr-based substances. In

combination with hardly crystallizable structures like such supramolecular coordination compounds, the analysis of such compounds was difficult. The only crystal structure determined was determined to be $[Cr(DMSO)_6]^{3+}$ indicating that Cr is prone to coordinate to DMSO rather than the pyridyl-ligands. Nevertheless, some of the approaches seemed to be promising. However, despite the analytical challenges, also reproduction of some of the results was not possible. Having in mind that chromium is a widely discussed metal in terms of its biological impact, further research and investigations concerning chromium-based cages does not seem very promising for any biological application. Nevertheless, for both metals, chromium as well as molybdenum, such cages might be interesting for catalytic purposes.

Of the three evaluated metals, gold represents the most promising one for biological use. First, because gold is part of numerous biological studies as it has promising anti-cancer properties. Second, because the performed studies, at least for cages **32** and **33** have been very promising. For some further tested ligands, rather protonation of the terminal pyridine moiety occurred than cage formation. The first studies for the synthesis of Au(I) metallacycles already showed, that even if not isolable, the complexes were formed and were used for *in situ* conversion to Au(III) cages. There, cages **32** and **33** were very promising according to NMR spectroscopy, ESI-MS and elemental analysis. However, a crystal structure for final prove is still missing. In addition, another approach exploiting a hypervalent iodine species was tested. It also revealed some promising analytical data; however, the synthesis consists of multiple steps, which first required complete characterization of the intermediates. Still, the synthesis of such supramolecular entities by self-assembly is a very sensitive reaction and product formation highly depends on weak interactions like hydrogen bonding and π-π interactions.[150, 151] In particular the applied ligands containing aromatic rings connected with alkyne spacers display a large polarizability and are thus capable of forming such interactions.[151] However, the formation of cages not only depends on the ligand structure. Despite the desired molecular, dimeric structures, also coordination polymers can be formed depending on the reaction conditions like temperature and applied solvent, as well as solution behavior and counterions. An interesting study addressing these issues is reported by Lee *et al.*[151] There, a silver(I) complex with similar ligands was shown to form dimeric metallacycles or polymeric zigzag chains, dependent on the applied solvent and counterion.[151] Consequently, also the functional groups of the ligands play an important role and influence the reaction outcome, as the previous paragraphs demonstrated. Therefore, the outcomes of such reactions can hardly be predicted due to manifold influencing parameters, however, the first steps towards a potential replacement of palladium by other metals were made opening new perspectives for the biological applications of such 3D supramolecules. Still, a lot needs to be investigated in this wide research area.

3.2 *N*-heterocyclic carbene complexes

3.2.1 Chromium

The calix[4]imidazolylidene ligand **44** (figure **31**) was widely studied in our group and has shown to stabilize different transition metals in different oxidation states such as Ag(I), Au(I),Cu(I), Pd(II), Pt(II), Ni(II), Fe(II), Fe(III).[152-157] In particular the Fe(II) and Fe(III) complexes, which are shown in figure **31** were studied for their properties of oxygen-binding[155] or catalytic properties in homogeneous epoxidation with H_2O_2 [154] and aldehyde olefination[153].

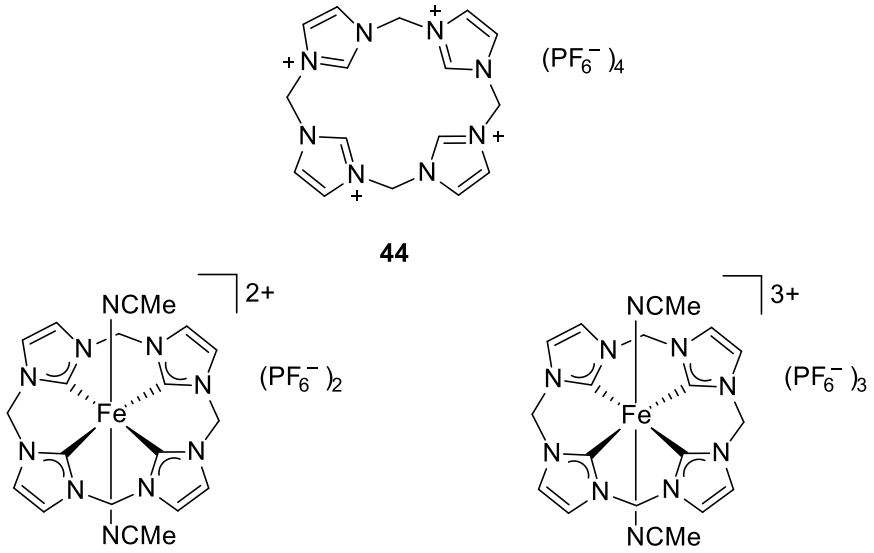

Figure **31**: Structures of macrocyclic calix[4]imidazolylidene ligand **44** and the corresponding catalytically active Fe(II)/(III) complexes.[153, 154, 157]

Jenkins *et al.* published similar versatile macrocyclic imidazolylidene ligands in 2010 and 2013, respectively.[158, 159] Comparably to **44**, these ligands were reported to stabilize different transition metals in different oxidations states like Ag(I), Au(III), Co(II), Ru(II), Ni(II), Pt(II), Pd(II), Cr(II) and Cr(III).[158-161] In particular, the Cr(II) and Cr(III) based complexes were studied for their catalytic properties. Thus, the Cr(II) complex was evaluated to be a successful catalyst for oxidative group transfer reaction and the Cr(III) NHC compound was found to be catalytically applicable for aziridination reactions.[161, 162] The structures of the two Cr-based NHC complexes are shown in figure **32**.

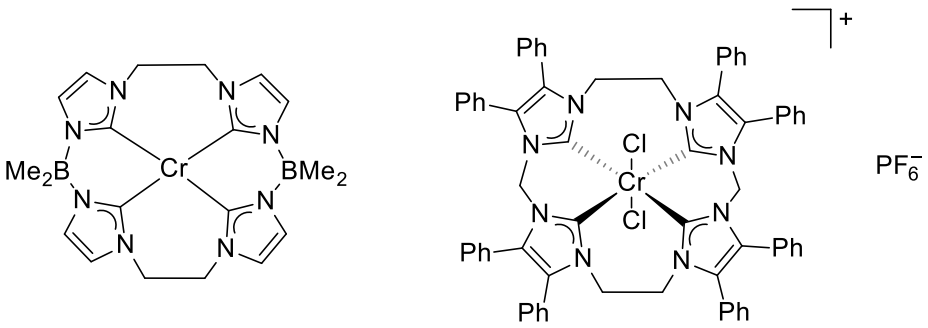

Figure **32**: Structures of catalytically active Cr(II)- and Cr(III)-NHC-complexes published by Jenkins *et al.*[161, 162]

Both synthetic approaches performed by Jenkins *et al.* involve $CrCl_2$ as a chromium source. The Cr(II)-NHC-complex was obtained by deprotonation of the ligand with *n*-BuLi and in situ metalation using $CrCl_2$.[161] The Cr(III) complex was synthesized *via* transmetalation from the respective Ag(I) complex. There, the reason for the oxidation of Cr(II) to Cr(III) was not elucidated, however, redox reactions involving the reduction of Ag(I) to Ag(0) were likely to occur.[160]

Encouraged by these two macrocyclic Cr(II/III)-NHC-complexes and the similarity to **44**, studies for the synthesis of chromium complexes of **44** were performed. Following the approaches performed by Jenkins *et al.*, the studies can be split into two approaches, namely direct metalation on the one hand and transmetalation applying the respective Ag(I) precursor on the other hand. In doing so, also the *tetra*-NHC Ag(I) complex **45** as well as *bis*-imidazolylidene ligand **46** and the respective Ag(I) complex **47** (structures given in figure **33**) were included in these studies. For complex **45** and also the respective Au(I) complex, the metal ions were coordinated between two ligands forming a box-type structure.[157] This structure was generated because Ag(I) and Au(I) form linearly coordinated NHC complexes in contrast to Pd or Pt, for instance, which prefer a square planar coordination mode.[157, 160] For Cr(II/III), a square planar geometry is expected as it was found for the *tetra*-NHC Cr complexes by Jenkins *et al.*

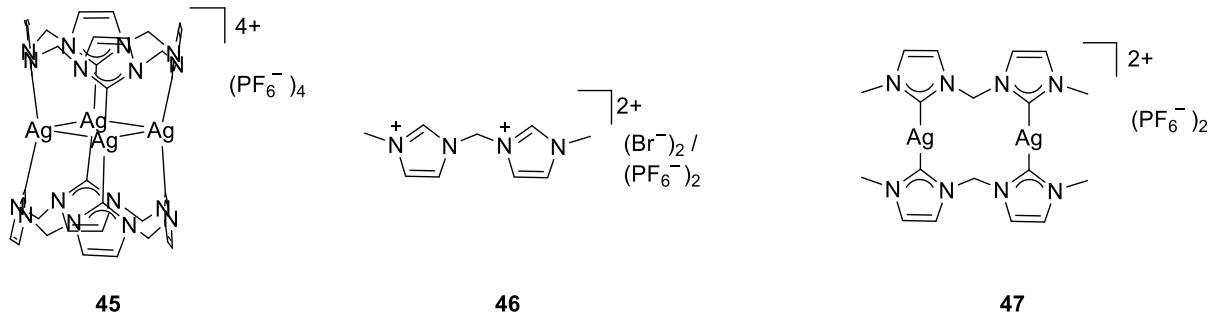

45 **46** **47**

Figure **33**: Structures of Ag(I)-NHC-complexes **45** and **47** and ligand **46**.

Having the previously mentioned complexes **22** ($Cr_2(OAc)_4$) and **23** ($[Cr(MeCN)_4](BF_4)_2$) by hand, these were also evaluated for the suitability as precursors, besides the previously applied $CrCl_2$ for the synthesis of Cr-NHC-complexes. Table **2** presents an overview of the majority of the reactions performed

for the synthesis of Cr-NHC-complexes together with the conditions and stoichiometry. The listed reactions are separated in two parts according to the principle of the reaction, namely either direct metalation or transmetalation. The table is followed by a more detailed discussion of the reactions and their outcome.

Table **2**: Conditions tested for the synthesis of chromium-NHC-complexes.

Method: direct metalation							
Entry	Cr precursor (equiv.)	ligand counterion (equiv.)	base (equiv.)	temperature	solvent	time	atmosphere
1	**22** (1)	**44** PF_6^- (1)		rt	MeCN-d_3	2 h	inert gas
2	**22** (1)	**44** PF_6^- (2)	Cs_2CO_3 (4)	rt	MeCN-d_3	2 h	inert gas
3	**23** (1)	**44** PF_6^- (1)	Cs_2CO_3 (4)	rt	MeCN-d_3	2 h	inert gas
4	**22** (1)	**44** PF_6^- (2)	NBu_4OAc (6)	rt	MeCN-d_3	2 h	inert gas
5	**23** (1)	**44** PF_6^- (1)	NBu_4OAc (4)	rt	MeCN-d_3	2 h	inert gas
6	$CrCl_2$ (1)	**44** Otf^- (1)	BuLi (4)	- 80 °C - rt	THF	overnight	inert gas
7	$CrCl_2$ (1)	**44** PF_6^- (1)	BuLi (4)	- 80 °C - rt	THF	overnight	inert gas
8	$CrCl_2$ (1)	**44** Otf^- (1)	NBu_4OAc (4)	rt	water	overnight	ambient
9	$CrCl_2$ (5)	**44** Otf^- (1)	NBu_4OAc (4)	rt	water	overnight	ambient
10	$CrCl_2$ (1)	**44** PF_6^- (1)	NBu_4OAc (4)	rt	MeCN-d_3	overnight	inert gas
11	$CrCl_2$ (5)	**44** PF_6^- (1)	NBu_4OAc (4)	rt	MeCN-d_3	overnight	inert gas
12	$CrCl_2$ (1)	**46** Br^- (2)	Cs_2CO_3 (4)	rt	THF	overnight	ambient
13	$CrCl_2$ (1)	**46** Cl^- (2)	Cs_2CO_3 (4)	rt	THF	overnight	ambient
14	$CrCl_2$ (1)	**46** Cl^- (2)	KO^tBu (4)	rt	THF	overnight	ambient
15	$CrCl_2$ (1)	**46** Br^- (2)	Cs_2CO_3 (4)	rt	water	overnight	ambient
Method: transmetalation							
Entry	Cr precursor (equiv.)	Ag complex counterion (equiv.)		temperature	solvent	time	atmosphere
16	$CrCl_2$ (5)	**45** PF_6^- (1)		rt	THF/DCM 1/1	26 h	inert gas
17	$CrCl_2$ (5)	**47** PF_6^- (1)		rt	THF	overnight	ambient
18	$CrCl_2$ (10)	**47** PF_6^- (1)		rt	THF	overnight	ambient
19	$CrCl_2$ (5)	**47** PF_6^- (1)		rt	THF/MeCN 1/1	overnight	ambient

Direct Metalation approaches

For the synthesis of Cr-NHC-complexes by direct metalation, the imidazolylidene ligands require deprotonation. This can be realized by either applying metal precursor coordinated by ligands that can act as weak bases like acetate or acetyl acetonate and thus such precursors are so-called internal

bases.[163] Alternatively, an external base is added to the ligand followed by the metal precursor. Accordingly, one approach (entry 1) was made using $Cr_2(OAc)_4$ **22** and ligand **44** without the addition of base. It was shown in previous studies with other metals, that **44** can be successfully deprotonated and converted to the respective metal NHC complexes applying acetate as internal base.[156] However, this approach was not successful applying **22**, possibly due to solubility issues. Therefore, Cs_2CO_3 was added in a further approach (entry 2). Both approaches were performed using dry and degassed acetontonitirle-d_3 at room temperature, because the ligand as well as most of the respective metal complexes are soluble in acetonitrile. Still, **22** as well as Cs_2CO_3 are not soluble. The resulting paramagnetic ^{1}H NMR determined of the filtered acetonitrile solution at variable temperatures revealed two paramagnetic signals along with not identified diamagnetic signals. Extrapolated, paramagnetic signals can be shifted to their diamagnetic position by the highest concentration and the highest temperature. Thus, NMR samples are prepared in high concentrations and determined at increasing temperatures for identifying the nature of the NMR signals. In figure **34**, one can see that the two paramagnetic signals (cutouts on the left) are shifted upfield with increasing temperature. All spectra were referenced to the residual signal of MeCN-d_3. All other signals stayed in place. According to other square planar complexes of ligand **44**, two signals are expected for these complexes.[157] However, the signal at about 2.8 ppm (- 40°C) can possibly originate from coordinated acetate and not from any formed NHC complex. Still, the signal at about 45 ppm (- 40 °C) is very promising. However, this approach lacks further analysis and no single crystals could be grown.

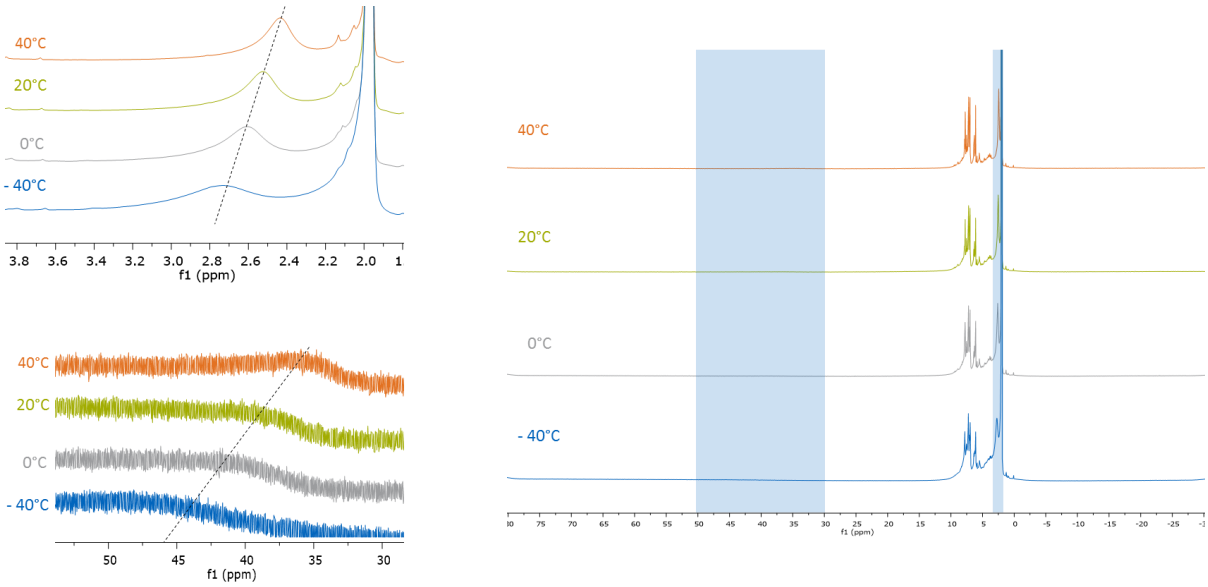

Figure **34**: Comparison of the shifts observed in paramagnetic ^{1}H NMR spectra measured in MeCN-d_3 at different temperatures (- 40°C, 0 °C, 20 °C and 40°C) of the reaction with entry number 2 (left: cutouts from 1.9 – 3.8 ppm and 25 – 55 ppm with lines highlighting the signal shifts).

Besides, the same conditions were evaluated using acetonitrile complex **23** (entry 3). There, only one paramagnetic signal could be identified. This is in the range of 2.5 ppm to 2.1 ppm (see figure **35**).

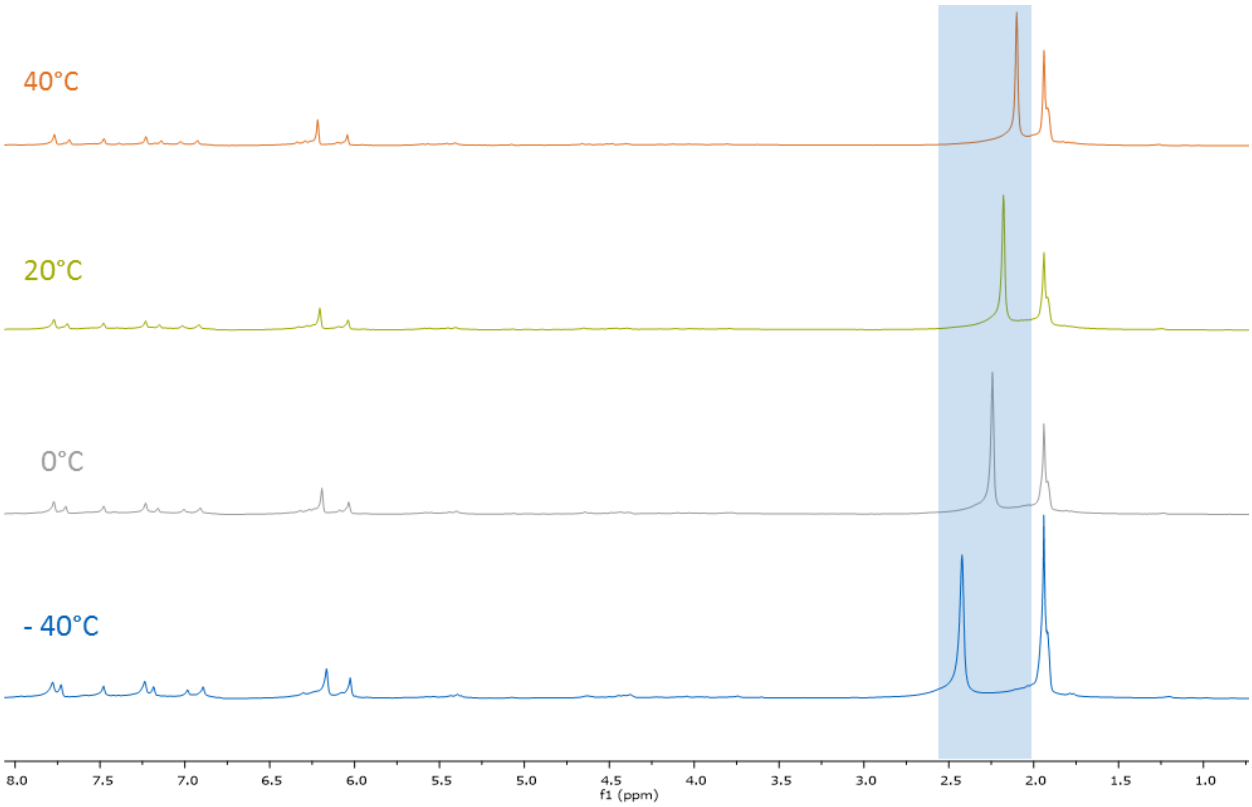

Figure **35**: Cutout of the paramagnetic ^{1}H NMR of the reaction with entry number 3 (blue highlight: paramagnetic signal).

A subsequent comparison of the signal located in the same region found for entry 2 indicates that these are not the same signals, although the rest of the signals of the diamagnetic region are comparable (see figure **35**). Therefore, it can be suggested that these signals originate from coordinated acetate and acetonitrile, respectively. Because no crystals suitable for single crystal X-ray diffraction could be grown, the reaction products could not be identified.

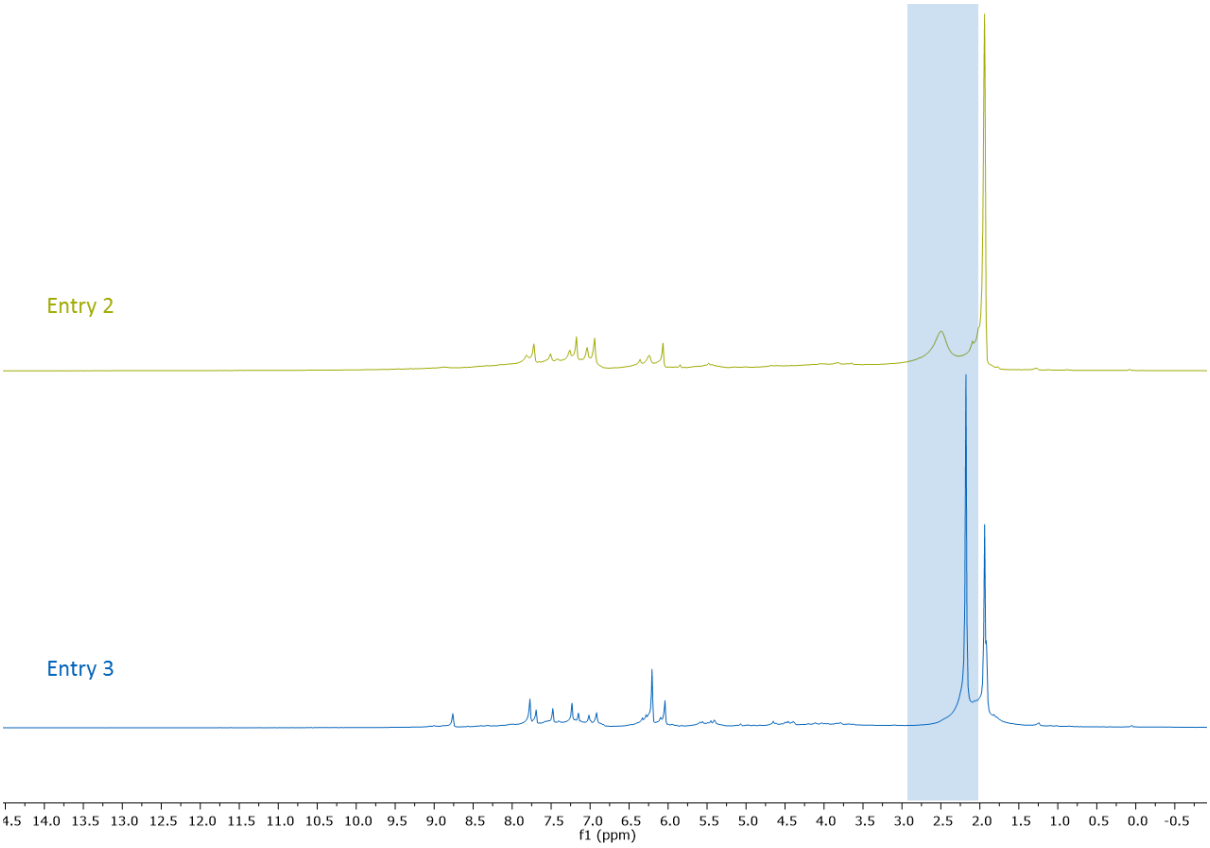

Figure **36**: Comparison of the paramagnetic ^{1}H NMR spectra in MeCN-d_3 of entries 2 and 3. Highlighted in blue: paramagnetic signal potentially generated by coordinated acetate and acetonitrile, respectively.

For further investigation of the suitability of **22** and **23** as potential precursors for the synthesis of a Cr complex of ligand **44**, NBu_4OAc instead of Cs_2CO_3 was tested. Previously, NBu_4OAc was found to be a suitable base for ligand **44**.[156] As a start, **22** was tested as Cr source, however, the resulting ^{1}H NMR did not show any paramagnetic signals (entry 4). Nevertheless, applying **23** as precursor was more promising (entry 5). The full range of the paramagnetic ^{1}H NMR spectra determined at different temperatures (20 °C, 40 °C, and 60 °C) as well as cutouts of the of the two regions showing paramagnetic signals are shown in figure **37**.

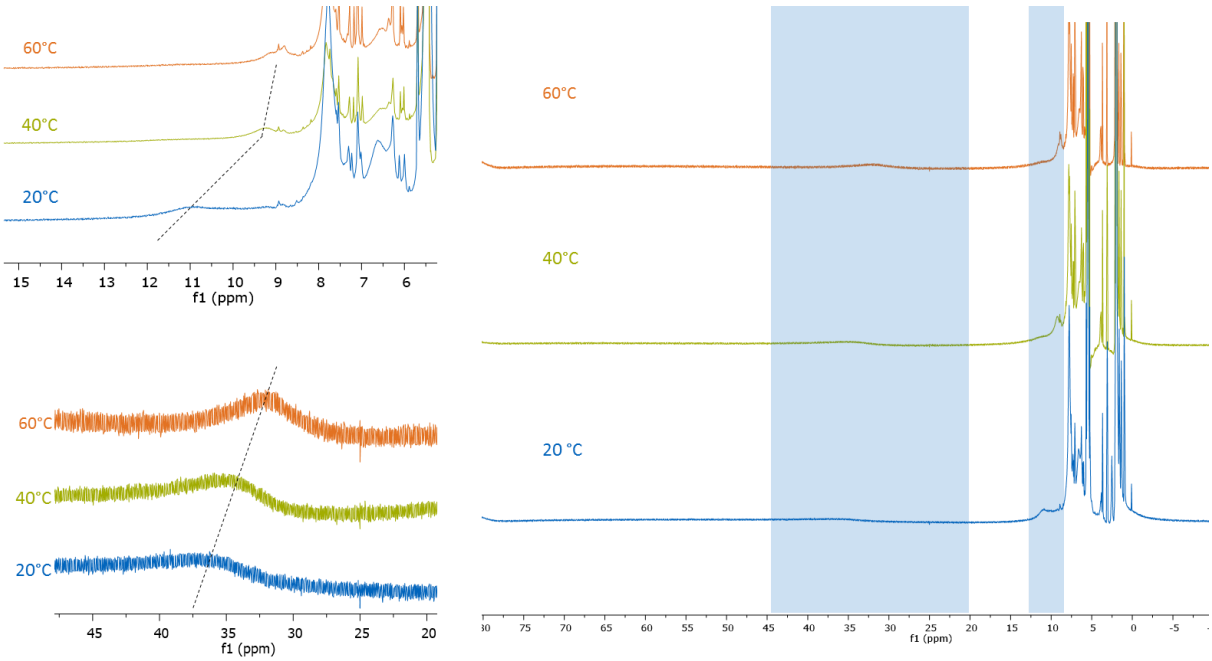

Figure 37: Paramagnetic ^{1}H NMR of the reaction with entry number 5. Blue highlights: paramagnetic signals and the corresponding temperature-dependent shift.

The signal at 11 ppm (20 °C) shows a significant temperature-dependent shift indicating its paramagnetic origin. This signal was not observed for the other approaches. Nevertheless, another signal at about 37 ppm (20°C) with significant movement with increasing temperature is observed and compared to the signal obtained for entry 2 (see figure 38). The comparison shows, that these signals have the same shift and thus may originate from the same paramagnetic compound. Since in both approaches, 2 and 5, the same ligand was applied and a signal with the same shift can be observed (see figure 38), one can assume that the signals is generated by the desired Cr-NHC-complex.

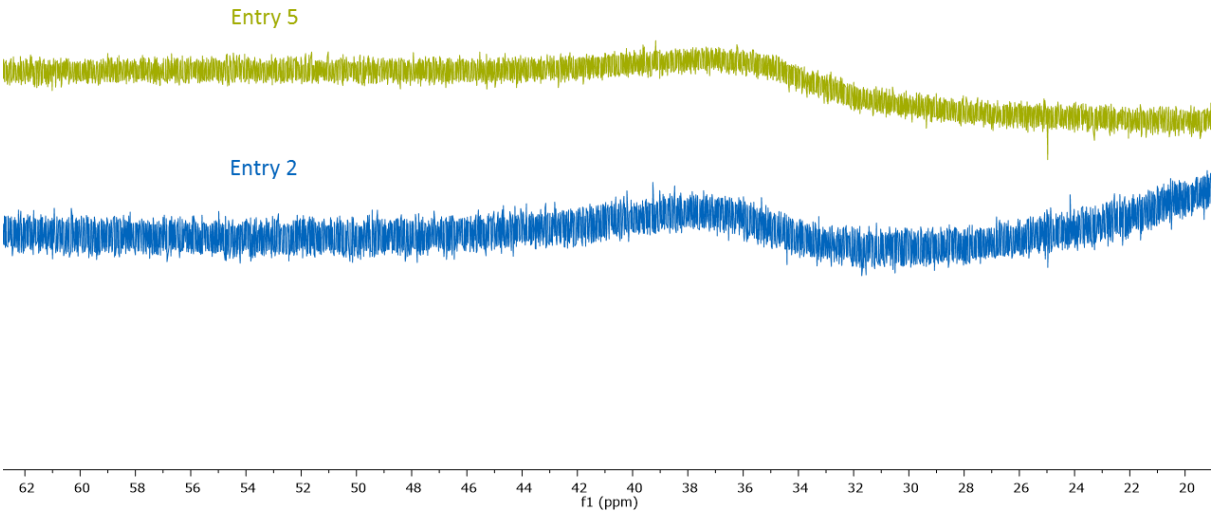

Figure 38: Comparison of the shift of the signal at about 38 ppm at room temperature observed for the reactions of entries 2 and 5.

The measurement of a ^{19}F NMR of reaction entry 5 showed that BF_4^- as well as PF_6^- are present without any signs of decomposition or coordination of fluoride. In addition, for this approach, the growth of single crystals was attempted, however, not successful.

Further approaches applying ligand **44** were conducted with the reaction conditions in entries 8 and 9 using $CrCl_2$ as precursor (1 equiv. and 5 equiv., respectively) and NBu_4OAc as base in water. Both approaches however, did not show any conversion of the ligand resulting in ^1H NMR spectra showing the signals of the ligand as well as NBu_4OAc. Similar, entries 10 and 11 were not successful. Here, a major obstacle might be the varying solubility of the applied compounds. $CrCl_2$ is hardly soluble in organic solvents and **44** is only moderately soluble in water when applying OTf^- as counterion. The PF_6^- analogue displays no solubility in water. Thus, different solvents were tested as reaction media as well as for purification and separation of potentially formed products, however, no successful combination of the reaction conditions were found for ligand **44**. Additionally, to possibly overcome this issue, attempts to synthesize **44** with either bromide or chloride counterions were conducted according to published methods.[164] In general, these halide counterions leads to water-solubility of such imidazolium salts. However, the obtained products were not sufficiently pure for further use in complex synthesis.

Because *bis*-imidazolylidene ligand **46** was successfully synthesized with different counterions (Cl^-, Br^-, PF_6^-), further attempts were made using this ligand. The first attempts with Cs_2CO_3 as base (entries 12 and 13) did not yield any assignable signals in the paramagnetic ^1H NMR spectra. Moreover, ESI-MS analysis was performed, but only the signal generated by the free imidazolylidene ligand was observed together with not assignable signals. For the reaction with entry number 14, the ^1H NMR only showed unassignable, diamagnetic signals which might be formed upon decomposition of the ligand. For reaction 15, all reaction components were dissolved in water and stirred overnight at room temperature. Subsequently, a precipitation of the potentially formed product was intended by using NH_4PF_6. But the thus formed turquoise solid was insoluble in any tested solvent (water, DMSO, acetone, acetonitrile, ethyl acetate, THF, diethyl ether, methylene chloride, benzene, methanol, chloroform, fluorobenzene as well as DMF were tested) and consequently, could not be further characterized. Here, it is assumed that the formed product has a mixture of different counterions leading to this insolubility. Next, the focus will therefore be on transmetalation reactions.

Transmetalation approaches

Starting with entry 16 applying Ag(I) complex **45** as precursor and a slight excess of $CrCl_2$, the resulting AgCl was filtered off and the solution was dried under reduced pressure. The thus obtained grayish solid was redissolved in MeCN-d_3 and used for ^{1}H and ^{19}F NMR analysis. However, no analyzable signals were observed besides MeCN-d_3 and residual THF. Some small signals were found in the diamagnetic region. The ^{19}F NMR revealed two small signals besides the signals generated by PF_6^- indicating a certain involvement of PF_6^- in this reaction, which suggests either decomposition or at least formation of unintended products.

Entry 17 applying Ag(I) *bis*-NHC complex **47** was analyzed *via* ^{1}H NMR and powder XRD. Powder XRD analysis was determined of the precipitate formed in course of the reaction to evaluate, whether this solid consists of AgCl. The generation of AgCl is a driving force of this reaction and needs to be formed upon transmetalation. Actually, the formation of AgCl could be verified using powder XRD. The paramagnetic ^{1}H NMR spectra determined at different temperatures (-40 °C, 23 °C, 40 °C) are given in Figure **39**.

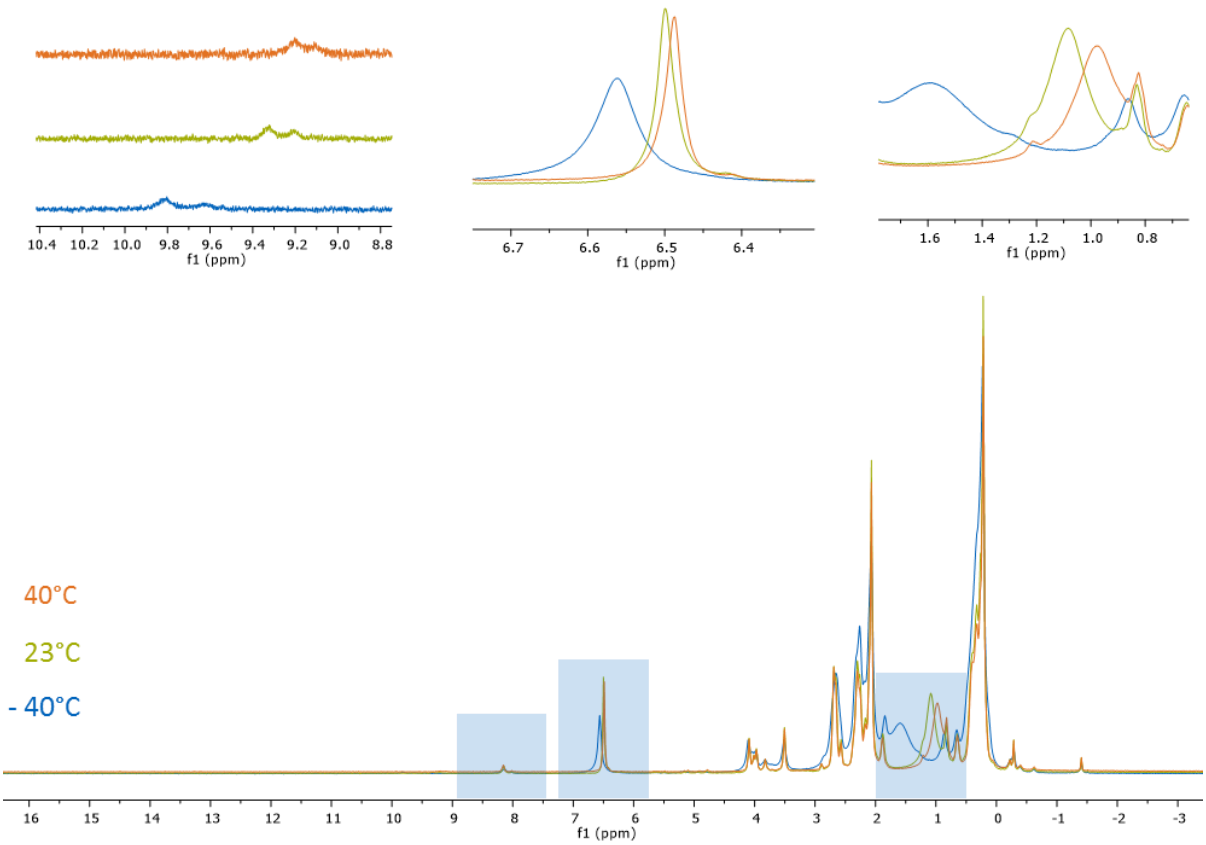

Figure **39**: Comparison of ^{1}H NMR spectra performed at indicated temperatures of reaction entry 17 in THF-d_8. The observed paramagnetic signals are highlighted in blue and given more detailed in the above-posted cutouts.

There, three paramagnetic signals are highlighted and shown in more detail. Interestingly, these signals are all located in the diamagnetic region. In fact, 4 to 5 signals are expected to be observed for a Cr complex. For **47**, 5 signals can be found in a ^{1}H NMR spectrum measured in DMSO-d_6. Nevertheless, the signal originating from the methyl-bridge are very weak and split into two signals, which is due to interactions with the solvents and the silver ions. When measured in MeCN-d_3, these two signals coincide in one signal. Due to the relative low intensity of this signal, it can be assumed that it will not be detected in a paramagnetic spectrum. Furthermore, it is also possible that a symmetric, square planar complex is formed with a composition of two ligands and one chromium center. In this case, three signals are expected. Thus, the analysis of this approach strongly supports the possibility of the formation of a chromium-NHC-complex. Still, a method for purification needs to be investigated. Additionally, further analysis is needed to confirm the assumptions. Attempts for crystallization were performed to determine the formation and coordination of such a chromium-NHC-complex unambiguously. A repetition of this approach increasing the amount of $CrCl_2$ to 10 equivalents showed the same signal pattern in the ^{1}H NMR (approach 18); however, a purification as well as growing single crystals was not possible. A third approach (entry 19) was performed changing the solvents from THF to a THF/MeCN mixture with a ratio of 1:1. Surprisingly, this resulted in a completely different ^{1}H NMR spectrum. An additionally performed ESI-MS measurement showed two distinct signals with m/z = 322.89 and 790.80. Unfortunately, an assignment was not possible. In summary, similarly to the studies for the synthesis of a chromium-based cage structure, the synthesis of a chromium-based NHC complex was rather challenging. Nevertheless, for chromium NHCs, transmetalation seems to be the most promising method at least for the *bis*-NHC ligands. Nevertheless, no crystals suitable for X-ray diffraction could be obtained and thus, a prediction of the synthesized products can hardly be made. Still, a chromium complex of ligand **44** would be interesting to test in biological studies as well as for catalytic comparison to the Cr-NHC catalysts reported by *Jenkins et al.*[160, 161]

3.2.2 Vanadium

Vanadium-NHC-complexes are not widespread in research. Nevertheless, some examples are discussed in the following and, when given, the potential application. Abernethy *et al.* reported one of the first V(V) NHC-containing complexes in 2003.[165] The complex was synthesized from $VOCl_3$ and the free carbene. The high stability, the crystal structure as well as DFT calculations, which agree with the experimentally observed structural features, were discussed.[165] The structure is given in figure **40**. Additionally, examples of V(II)- and V(III)-NHC-complexes were published by Lorber *et al.* The complexes were synthesized from different vanadium precursor including $VCl_3(THF)_3$, $VCl_2(py)_4$ and $V(NMe_2)_4$ and characterized by X-ray crystallography.[166] The structures are also given in figure **40**.

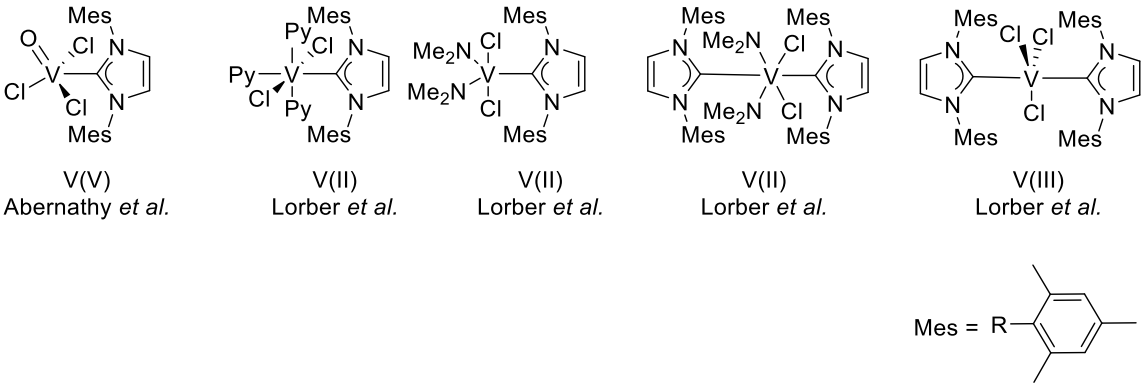

Figure **40**: Vanadium-NHC-complexes with vanadium in different oxidation states given below the compounds found in literature.[165, 166]

Further 'pincer' type vanadium complexes were published in 2005 coordinating vanadium in different oxidation states (II), (III) and (IV). These complexes were synthesized from VCl_2(tmeda) (tmeda = tetramethylethylenediamine) and characterized by X-ray diffraction. Additionally, the V(III) complex was shown to be sufficiently stable to be oxidized to the respective V(IV) complex using 4-methylmorpholine *N*-oxide.[167]

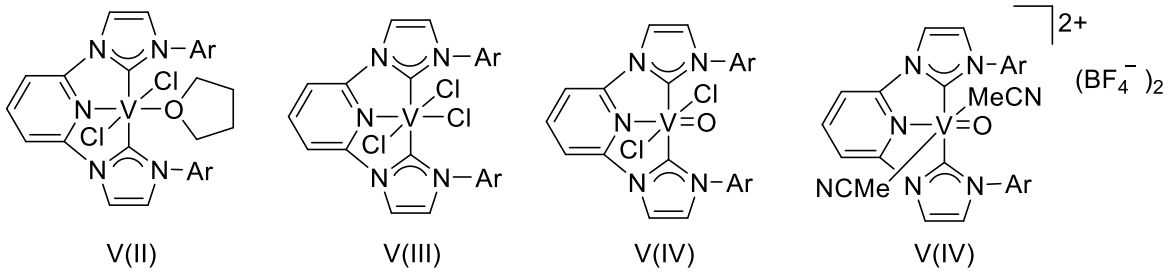

Figure **41**: Vanadium(II), -(III) and -(IV) complexes with 'pincer' type NHC ligands.[167]

Further similar vanadium-NHC-complexes were evaluated for their use as catalyst precursors for ethylene/propylene copolymerization after activation with $Et_3Al_2Cl_3$. The structures are given in figure **42**. The obtained results show, that these complexes are similar or less active compared to the commercially applied vanadium-based pre-catalysts and thus, further development is needed. The synthesis of these vanadium-NHC-complexes was performed using the respective free carbene ligand and $VOCl_3$.[168]

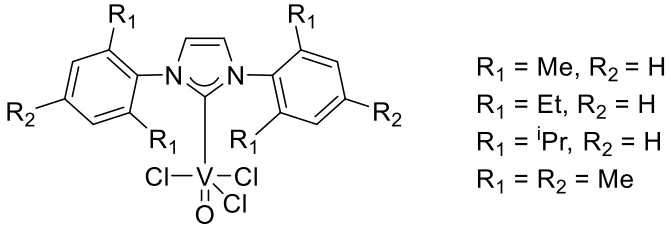

Figure **42**: Vanadium-NHC-complexes evaluated for their application as pre-catalysts for the synthesis of ethylene/propylene polymers.[168]

Furthermore, Arnold *et al.* published studies for the destruction of simulants of chemical warfare agents applying different transition metal NHC complexes including vanadium-NHCs.[169] Selected moisture and air stable vanadium-NHC-complexes reported by Abernathy *et al.* (presented in figure **40**) and by Zhang and Wu *et al.* (presented in figure **42**) were tested showing to destroy 2-chloroethyl ethyl sulphide, a simulant for sulfur mustard successfully. The study revealed a complete destruction of different simulants within 5 h in presence of artificial sunlight either *via* cleavage of a P-OAr bond or by reduction of vanadium and the formation of disulfide species.[169] Looking for homoleptic vanadium-NHC-complexes, only one example was found in literature. Siebert *et al.* present the synthesis of air and moisture sensitive V(III) complex shown in scheme **18** using $VCl_3(thf)_3$ as precursor and the free anionic NHC.[170] The paramagnetic complex crystallized in a distorted tetrahedral geometry with two smaller (about 94 °) and two larger (about 118 °) C-V-C angles. The C-V bond lengths are very similar varying in the range of 2.119 – 2.132 Å.

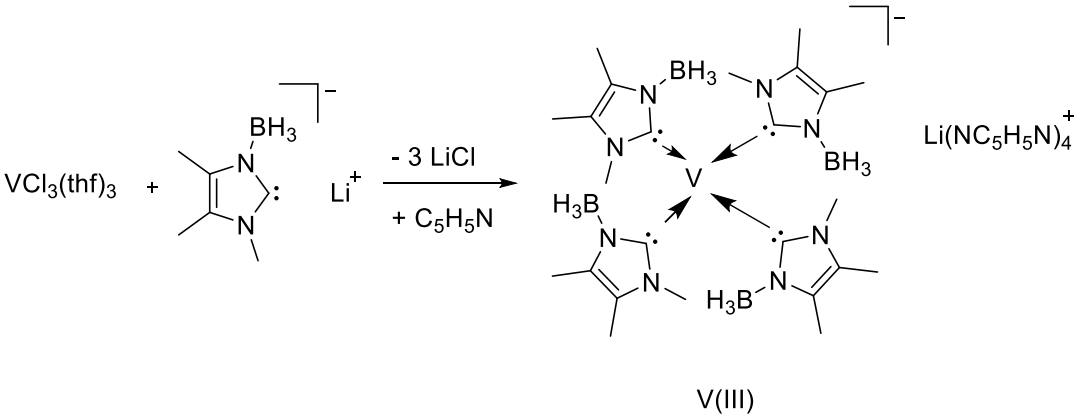

Scheme **18**: Scheme of the synthesis of a homoleptic V(III)-NHC-complex using $VCl_3(thf)_3$.[170]

However, none of the studies addresses biological applications, which might be mainly due to air and moisture sensitivity of the majority of the complexes. In addition, vanadium is prone to form very stable complexes in association with biological nucleophiles providing O-, S- or N-donors such as cysteine, histidine or citrate.[171] Moreover, in aqueous environment, a versatile coordination chemistry with varying oxidation states depending on the pH of the solution is observed.[171] Nevertheless, cyclopentadienyl complexes were found to be very stable under physiological conditions and exhibit strong anti-cancer activity, as already stated in the introduction. In theory, although vanadium-NHC-complexes are rare, it should be possible to stabilize a vanadium core using ligand **44**. In general, many different oxidation states with different coordination geometries and coordination numbers are possible for vanadium complexes and thus, no particular oxidation state will be addressed. Searching literature for macrocyclic vanadium-based complexes, vanadium-porphyrin-complexes were found. In general, vanadium as well as other transition metal porphyrin complexes are readily synthesized

reacting the metal salt with the porphyrin in DMF.[172] Thus, V(II)-,-(III)- and -(IV)-porphyrin complexes are reported in literature and some structures are presented in figure **43**. Different functionalized vanadium(IV)-porphyrin-complexes were synthesized from the free porphyrin ligand together with $VO(acac)_2$ as vanadium source. These air and moisture stable complexes were also found to be stable in the presence of glutathione and were evaluated for their anti-HIV properties showing inhibition of HIV-1 replication.[173] Also, V(III) was observed to be stabilized by porphyrin ligands by Woo *et al*.[174] For the synthesis, the lithium salt of the ligand was applied in combination with $VCl_3(thf)_3$.[174] Furthermore, V(II) complexes were obtained by reduction of the respective V(IV) porphyrin complex using zinc almalgam.[175]

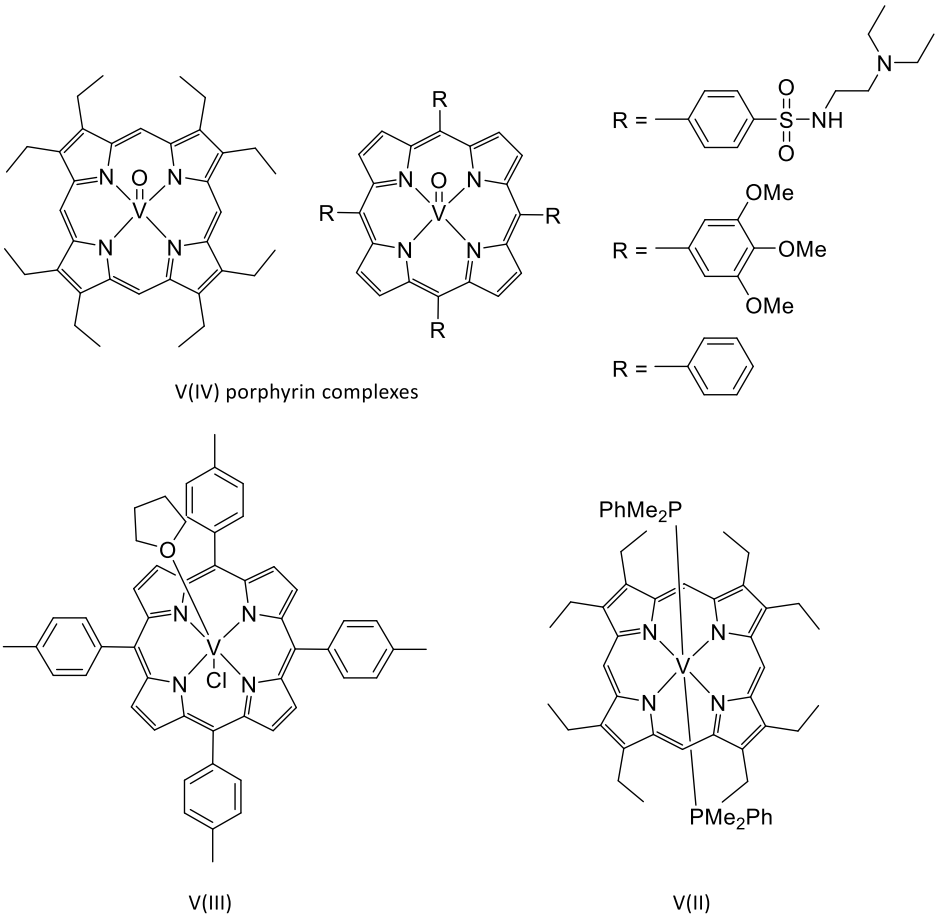

Figure **43**: Structures of different vanadium-based porphyrin complexes with vanadium in oxidation states (IV), (III) and (II).[173-175]

Considering the coordination geometry and the oxidation states found for the porphyrin complexes, V(II), -(III) and -(IV) are considered being suitable for the synthesis of a vanadium-NHC-complex of ligand **44**. The conditions, reaction stoichiometry and the different applied vanadium precursor applied are listed in table **3**. As precursor for reaction 1 (table **3**), $[V(MeCN)_6](BPh_4)_2$ was synthesized according to literature.[176] The turquoise suspension of reaction 1 was analyzed by ^1H NMR showing decomposition signals of the ligand as well as the proton signals of BPh_4^- and NBu_4OAc.

Table **3**: Conditions tested for the synthesis of vanadium-NHC-complexes.

Method: direct metalation							
Entry	V precursor (equiv.)	ligand counterion (equiv.)	base (equiv.)	temperature	solvent	time	atmosphere
1	$V(MeCN)_6(BPh_4)_2$ (1)	**44** Otf^- (1)	NBu_4OAc (4)	rt	MeCN-d_3	overnight	inert gas
2	$VCl_3(thf)_3$ (1)	**44** Otf^- (1)	BuLi (4)	- 80 °C - rt	THF	overnight	inert gas
3	$VO(acac)_2$ (1)	**44** PF_6^- (1)	NBu_4OAc (2)	rt	MeCN-d_3	overnight	ambient
4	$VO(acac)_2$ (1)	**44** PF_6^- (2)	NBu_4OAc (4)	rt	MeCN-d_3	overnight	ambient
5	$VO(acac)_2$ (1)	**44** PF_6^- (1)	Cs_2CO_3 (4.3)	rt	MeCN-d_3	overnight	ambient
6	$VO(acac)_2$ (1)	**44** PF_6^- (1)	$CaCO_3$ (4.3)	rt	MeCN-d_3	overnight	ambient
7	$VO(acac)_2$ (1)	**44** PF_6^- (1)	Cs_2CO_3 (4.3)	rt	MeCN-d_3	overnight	inert gas
8	$V(acac)_3$ (1)	**44** PF_6^- (1)	NBu_4OAc (4)	rt	MeCN-d_3	20 min	inert gas
9	$V(acac)_3$ (1)	**44** PF_6^- (1)	Cs_2CO_3 (4.3)	rt	MeCN-d_3	overnight	inert gas
10	$VO(acac)_2$ (1)	**48** PF_6^- (1)	Cs_2CO_3 (2)	rt	MeCN-d_3	3 d	ambient
11	$VO(acac)_2$ (1)	**48** PF_6^- (1)	Cs_2CO_3 (2)	rt	MeCN-d_3	3 d	inert gas
12	$VO(acac)_2$ (1)	**48** PF_6^- (1)	KOtBu (2)	rt	MeCN-d_3	overnight	inert gas
13	$VO(acac)_2$ (1)	**48** PF_6^- (1)	KHMDS (2)	rt	MeCN-d_3	overnight	inert gas
14	$V(acac)_3$ (1)	**48** PF_6^- (1)	KOtBu (2)	rt	MeCN-d_3	overnight	inert gas
15	$V(acac)_3$ (1)	**48** PF_6^- (1)	KHMDS (2)	rt	MeCN-d_3	overnight	inert gas
16	$VO(acac)_2$ (1)	**44** PF_6^- (1)	KOtBu (4)	rt	MeCN-d_3	overnight	inert gas
17	$VO(acac)_2$ (1)	**44** PF_6^- (1)	KHMDS (4)	rt	MeCN-d_3	overnight	inert gas
Method: transmetalation							
Entry	V precursor (equiv.)	Ag complex counterion (equiv.)		temperature	solvent	time	atmosphere

18	VCl_4 (1)	**45** PF_6^- (1)	rt	DMSO/ DCM 1/0.5	3 d	inert gas
19	VCl_4 (1)	**45** PF_6^- (2)	rt	DMSO/ DCM 1/1	3 d	inert gas

Because no literature was found applying this V(II) precursor for the synthesis of a vanadium-NHC-complex and it did not seem to form a complex using the indicated conditions, this approach is not pursued further. Thus, $VCl_3(thf)_3$ was synthesized according to a reported procedure and used as precursor for reaction 2 in table **3**.[177] For that approach, the ligand was suspended in dry and degassed THF at -80 °C. After adding *n*-BuLi, the reaction was stirred for about ten minutes before $VCl_3(thf)_3$ was added. Thus, the reaction mixture turned orange, and then red and finally a brown precipitate formed. Different solvents were tested to dissolve the isolated solid. Using MeCN-d_3, the solution turned brownish yellow and thus, this fraction was analyzed by ^{1}H NMR. This NMR, however, only showed signals of THF and acetonitrile. Washing the precipitate with DMF, a purple solution was obtained, which was used to grow single crystals by slow diffusion of diethyl ether. However, no single crystals were obtained for this approach. Reaction 3 (table **3**) was at first attempted without base. Therefore, the ligand and $VO(acac)_2$ were dissolved in acetonitrile resulting in a clear, turquoise solution. After stirring the reaction mixture for 2 h, the mixture still looked the same and thus, the solution was heated to 60 °C for 2 h. However, still no change could be observed and thus, two equivalents of NBu_4OAc were added to the solution whereupon the solution color changed to a light green. However, for proof of principle, a solution of only $VO(acac)_2$ and NBu_4OAc in acetonitrile was prepared without addition of ligand observing the same color. Nevertheless, reaction 3 was analyzed using ^{1}H NMR and ESI-MS. The ^{1}H NMR, however, was difficult to assign despite NBu_4OAc. The ESI-MS showed two signals (m/z = 242.24 and 628.74). The smaller signal could be assigned to either NBu_4^+ or $[(Hacac)_2(MeCN)+H]^+$. The higher signal can be assigned for $[VO(\mathbf{44})(acac)_2+MeCN]^{2+}$, which is, however, very unlikely to form. Still, the difference of the both signals refer to $[VO(\mathbf{44})]^+$ which is very promising, although the assignments for both signals may be not correct. Reaction with entry number 4 was subsequently conducted, where in total four equivalent of base were added to the reaction right after mixing ligand and $VO(acac)_2$. The ESI-MS determined from this approach only showed one signal, m/z = 242.24, which could not be assigned for any vanadium-containing species. Thus, approach 5 was tested. Right after preparation, the reaction mixture turned green, similar to approach 4. After stirring the mixture over night, the solution turned yellow. Having the remaining solids, mainly insoluble Cs_2CO_3, filtered off and evaporated the solvent, a paramagnetic ^{1}H NMR as well as ESI-MS was used to analyze the reaction products. The determined NMR showed numerous signals in the diamagnetic region and two paramagnetic signals at

15.92 and 17.02 ppm, which is promising. The ESI-MS spectrum (see supplementary data figure **S16**) shows numerous signals as well. Some can be assigned as follows: $[V(\mathbf{44})(PF_6)_2]^{2+}$ (m/z = 331.00), $[V(\mathbf{44})]^{+}$ (m/z = 371.06), $[V(\mathbf{44})(PF_6)]^{3+}$ + MeCN (m/z = 557.05), $[V(\mathbf{44})(acac)]^{2+}$ + MeCN (m/z = 610.19). Surprisingly, these assigned complexes do not contain a VO^{2+} unit. Replacing the base by $CaCO_3$ (entry 6) no reaction was observed. Thus, reaction 5 was repeated but under inert atmosphere (see entry 7). This time, less diamagnetic signals were obtained together with the two paramagnetic signals at 15.92 and 17.02 ppm. Interestingly, three new paramagnetic signals at 41.39, 46.80 and 48.86 ppm were also displayed with the first two being assigned to $V(III)(acac)_3$. The spectrum is given in the supplementary data in figure **S17**. If the assignment to $V(acac)_3$ is correct, a disproportionation of V(IV) to V(III) and V(V) might occur. Further indication for the formation of a V(III) is, that in case of reaction 5 carried out on air, these signals were not observed. This may be due to oxidation of a potentially formed V(III) species to V(IV). Since expecting two proton signals for a square planar complex of ligand **44**, it is possible that a V(IV) complex with signals at 15.9 and 17.0 ppm is formed along with $V(acac)_3$ and some sort of V(V) compound, which makes an analysis very difficult. Therefore, the next approaches 8 and 9 were carried out under inert atmosphere with $V(acac)_3$ as precursor to obtain insights about the different products. First, NBu_4NOAc was used in reaction 8. The reaction was set up in a glovebox and immediately after the addition of the base, an off-white precipitate formed. After 20 minutes stirring at room temperature, the reaction mixture was filtered and the filtrate was evaporated to dryness. This residue was re-dissolved in MeCN-d_3 and analyzed by ^{1}H NMR. However, no suitable solvent was found for the precipitate formed during the reaction and thus, it was not further analyzed. In fact, the paramagnetic ^{1}H NMR of the filtrate did not show the signals at 15.92 and 17.02 ppm any more, indicating that these signals are potentially generated by a V(IV) complex of ligand **44**. Nevertheless, a new signal at 12.87 ppm appeared. At 41.50 and 47.00 ppm, it is assumed that these signals originate from $V(acac)_3$. Slight shifts are possible, because in some cases, like for this approach, the residual signal of MeCN-d_3 can hardly be assigned due to multiple signals in that region. For direct comparison, the conditions and the work-up applied in approach 7 were also applied in reaction 9, however, $V(acac)_3$ as vanadium precursor replaced $VO(acac)_2$. Both ^{1}H NMR spectra are shown in figure **44**. There, a similar peak pattern in the diamagnetic region (right zoom) can be observed. However, for approach 9, four peaks stand out.

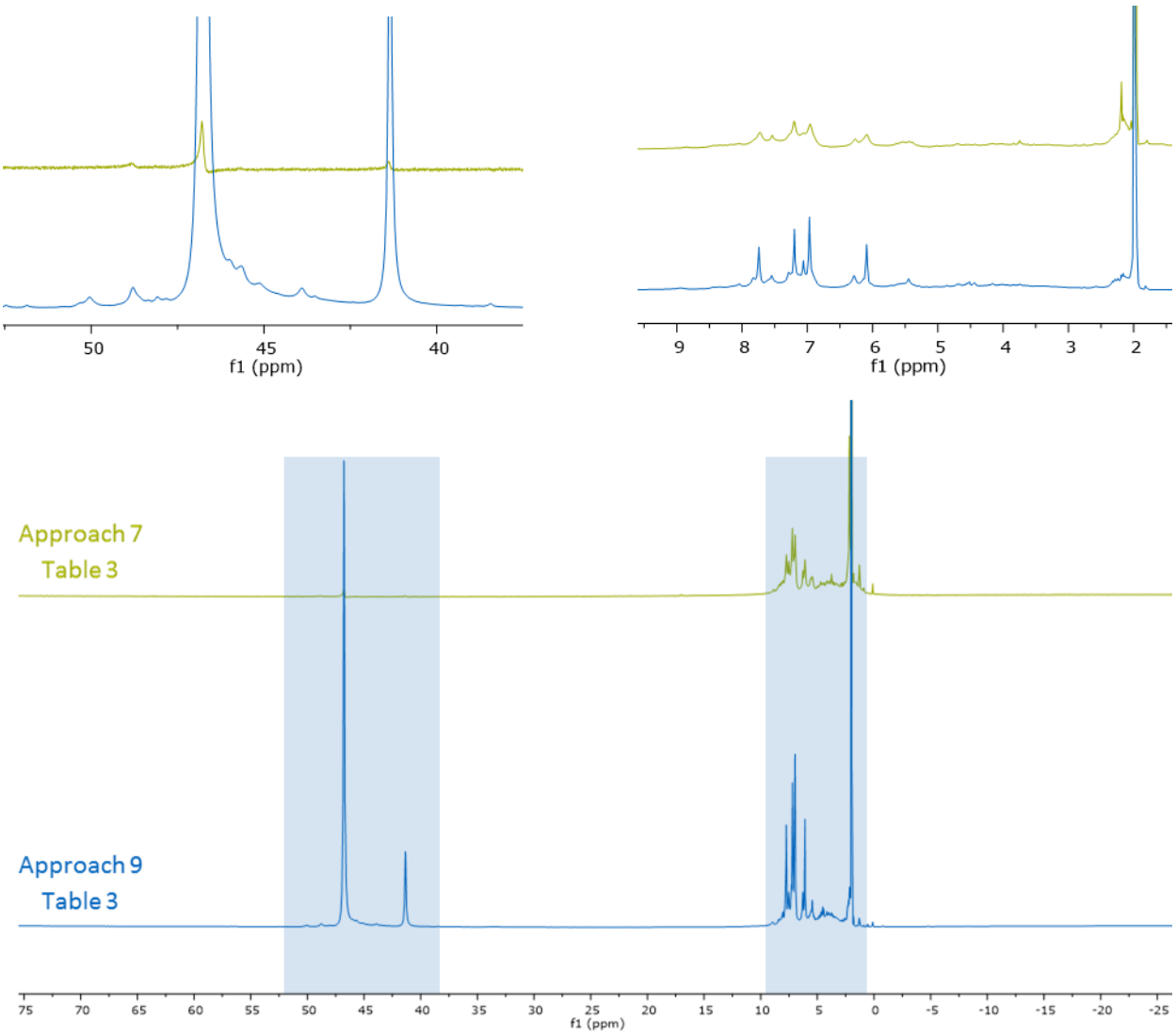

Figure **44**: Paramagnetic ^{1}H NMR spectra determined of reaction products 7 and 9 (table 3). Blue highlights indicate the regions, for which a zoom is given above the full NMR spectra.

In the paramagnetic region (zoom given on the left in figure **44**), for approach 9, $V(acac)_3$ is predominantly present together with more paramagnetic signals. An overlay of both, approach 9 and pure $V(acac)_3$, is given in the supplementary section in figure **S18**. To further analyze this approach without exposing the product to air, LIFDI MS (liquid injection field desorption ionization mass spectrometry) was performed in chloroform. Thus, different signals were observed, where not of all could be assigned. The observed signals are displayed in figure **45**.

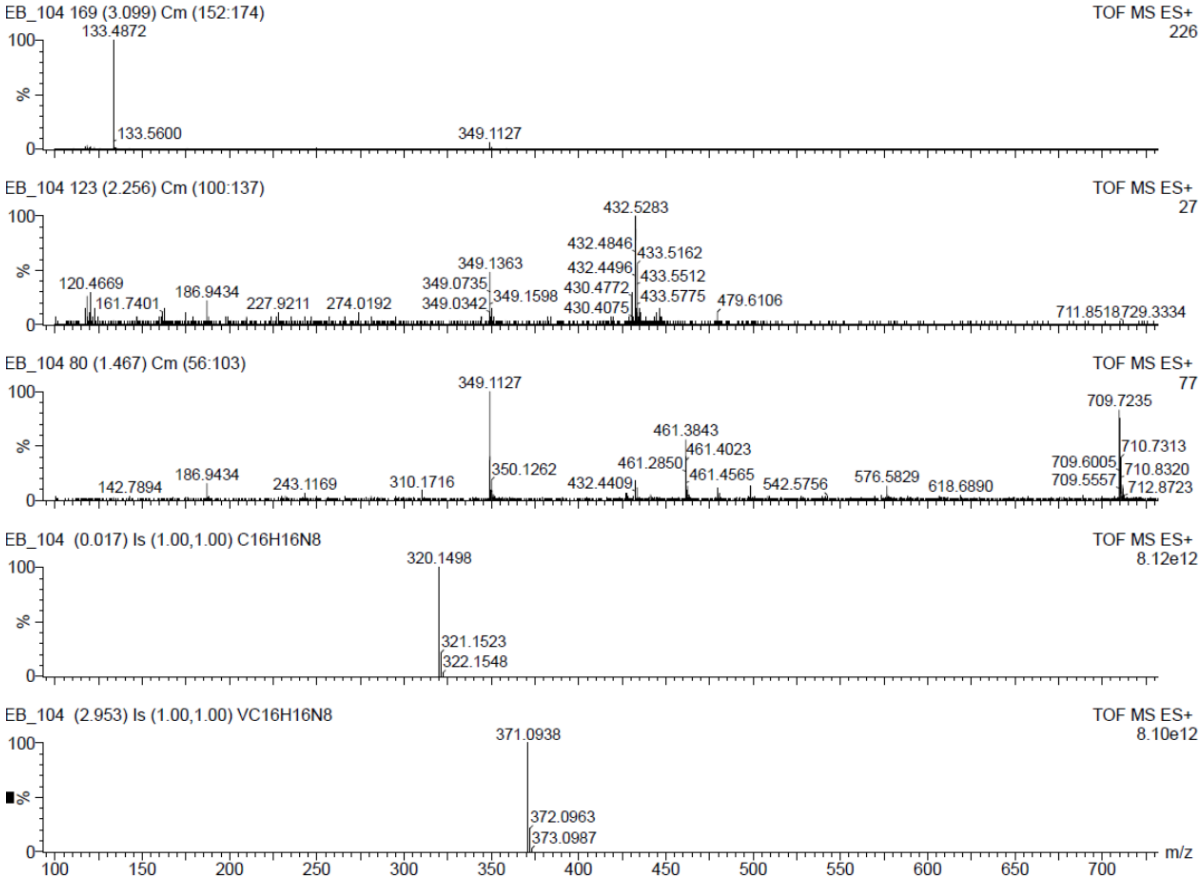

Figure **45**: LIFDI-MS spectra observed at different time points for approach 9 (table **3**). The following signals can be assigned accordingly: $[V(acac)_3+H]^+$ calcd.: 349.09, found: 349.11; free carbene ligand **44** calcd.: 320.15; found: 320.15; $[V(\mathbf{44})]^{+/0}$ calcd.: 371.09, found: 371.09. The masses are given as calculated exact masses.

The assignable signals are as follows: $[V(acac)_3+H]^+$ calcd.: 349.09, found: 349.11; free carbene ligand **44** calcd.: 320.15; found: 320.15; $[V(\mathbf{44})]^{+/0}$ calcd.: 371.09, found: 371.09. The masses were calculated as exact masses. This analysis provided strong evidence for the presence of a V(**44**) species, however, with many unassigned impurities and an unexpected charge. Unfortunately, also for this approach, no single crystals could be grown.

For the following approaches, ligand **48** (structure given in figure **46**) was used. This ligand is assumed a promising candidate for forming vanadium complexes due to the pyridyl wingtips and its chelating nature. In addition, it is less rigid than ligand **44**, which might enhance complex formation. However, the loss of symmetry may also complicate the analysis of the potential products.

For the first attempt, $VO(acac)_2$ was applied as precursor and Cs_2CO_3 was used to deprotonate the two NHC moieties.

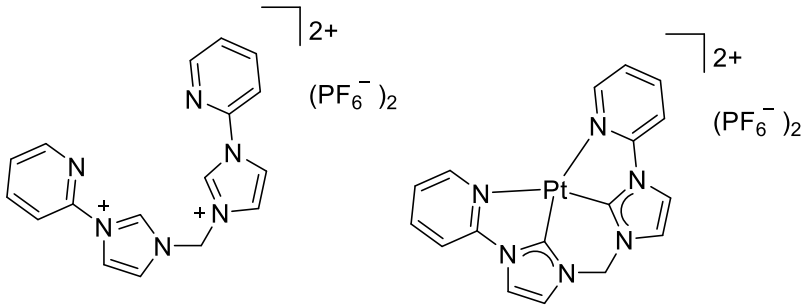

48

Figure **46**: Structures of ligand **48** and the respective Pt(II) complex published by Chen *et al*.[178]

Unfortunately, the analysis of approach 10 using ^{1}H NMR as well as ESI-MS did not reveal any reasonable reaction outcome. The determined NMR spectrum showed no signals in the paramagnetic region and in the diamagnetic area, hardly any signals were observed except for MeCN-d_3. In addition to that, the ESI-MS showed very small m/z fragments which could also not be assigned. Therefore, a repetition of this approach under inert atmosphere was carried out (reaction 11). There, surprisingly, also V(acac)$_3$ and the two signals at 15.92 and 17.02 ppm can be observed similar to approach 7. Because the applied ligand has changed, it is assumed that these signals derive from any product formed independently from the applied ligand. In addition, these signals were only observed for reactions performed under inert atmosphere. Despite these signals, numerous other signals in the diamagnetic region as well as in the paramagnetic area were visible; however, no further assignments were possible. The corresponding ^{1}H NMR is shown in the supplementary section in figure **S19**. Applying KO^{t}Bu as base (reaction 12), similar unassignable signals in the diamagnetic region can be observed in combination with small signals of V(acac)$_3$. Subsequently, KHMDS (potassium hexamethyldiasilazide) was used as base in approach 13. Thus, some very promising paramagnetic ^{1}H NMR signals were observed in combination with V(acac)$_3$, see figure **47**. The number of required signals is hard to predict because the distinct coordination of this ligand to V is not known. When a similar square planar coordination will take place as found for the corresponding iron complexes, 7 sets of signals are expected.[179] When the vanadium core would be coordinated by two ligands, as found for platinum, 8 sets of signals are expected.[178] The applied stoichiometry of 1:1 (ligand:V precursor) would not indicate the formation of a vanadium complex with two coordinating ligands, however, the presence of a huge signal of V(acac)$_3$ prevent any predictions about the available stoichiometry. Nevertheless, some of the signals observed in the diamagnetic region (see full spectrum, supplementary data figure **S20**) may be generated by some non-paramagnetic acetyl acetone-containing species. Unfortunately, attempts to grow single crystals from this promising approach failed.

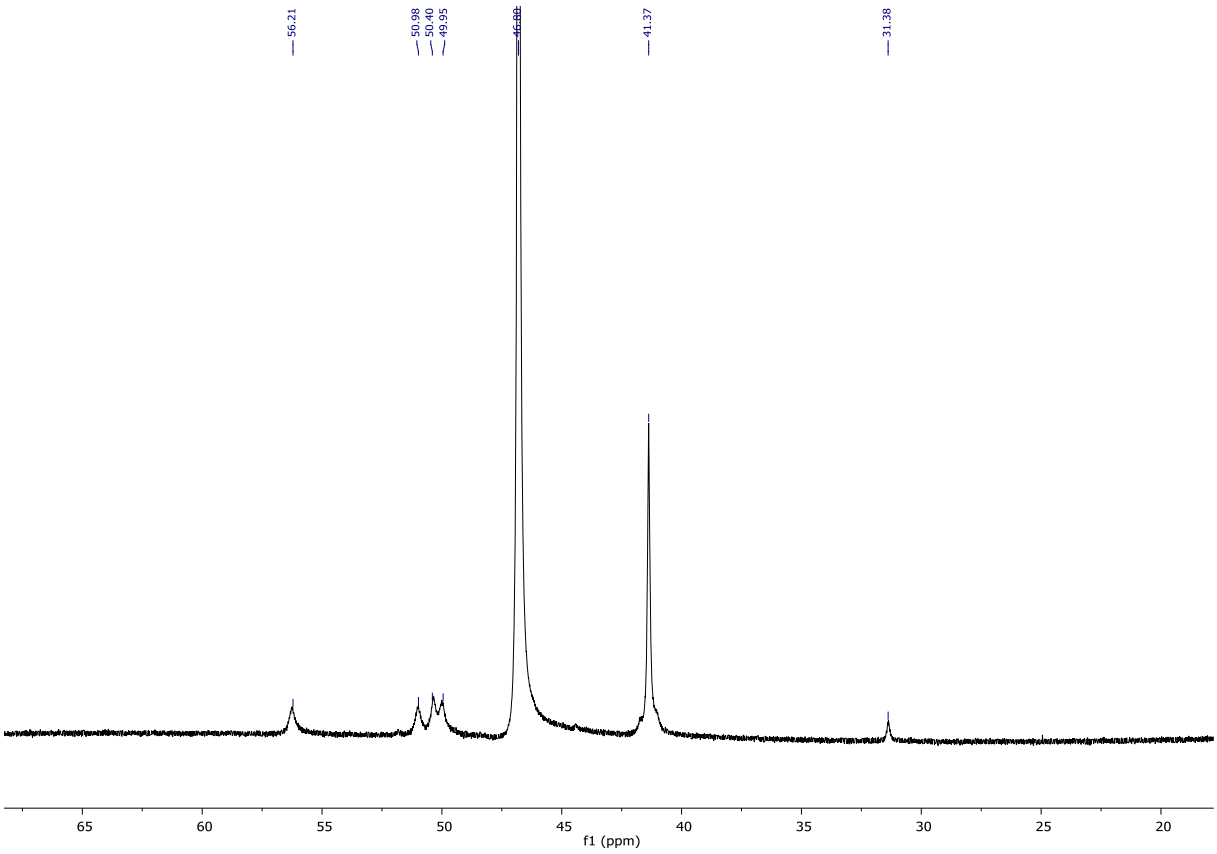

Figure **47**: Cutout of the paramagnetic region of ^{1}H NMR measured in MeCN-d_3 of reaction product 13. The full spectrum is provided in the supplementary data in figure **S20**.

Approaches 12 and 13 were repeated using V(acac)$_3$ as precursor under inert conditions. In reaction 14, KO^{t}Bu is applied as base and the reaction mixture was analyzed by paramagnetic ^{1}H NMR. This NMR showed V(acac)$_3$ and signals in the diamagnetic region, which are all located in the aromatic region from about 7 – 9 ppm. These signals do not coincide with the signals of the free ligand, however, could not be further assigned. In reaction 15, V(acac)$_3$ together with ligand **48** and KHMDS was reacted under inert atmosphere at room temperature. The resulting ^{1}H NMR showed three very small signals at 66.44, 65.35 and 63.01 ppm, which were not observed in any approach before. The diamagnetic region shows numerous signals with the same shift as observed in approach 14. The NMR spectra of both approaches are given in the supplementary data in figure **S21**. Further analysis of reaction 15 was performed by ESI-MS analysis. However, only one signal might be assigned for [V(**48**)(acac)+H]$^{3+}$. For confirmation, growth of single crystals was attempted by slow diffusion of diethyl ether, however, was not successful. Having these two promising bases (KO^{t}Bu and KHMDS) tested, two additional reactions were tested using ligand **44** (reactions 16 and 17, respectively, in table **3**). In both reactions, the formed precipitates and filtrates were isolated and attempted to analyze. In reaction 16, no V(acac)$_3$ was present, which is somewhat

surprising because it was observed in the majority of the syntheses as well as in reaction 17. Despite these signals, unassignable signals of decomposition products of the ligand are observed.

Finally, two transmetalation reactions were tested (reactions 18 and 19 in table **3**) applying silver complex **45** and VCl_4. Therefore, the silver complex was dissolved in dry and degassed DMSO-d_6 and a freshly prepared solution of VCl_4 in dry and degassed DCM was added. This mixture turned cloudy, which indicates formation of insoluble AgCl with a light blueish color. After stirring the mixtures for three days at room temperature, the mixtures were filtered over celite and DCM was removed under reduced pressure. The thus prepared DMSO-d_6 solutions were analyzed by ^{1}H NMR analysis. For both reactions, despite the residual signals of the solvents, the silver complex was still visible together with some unassignable diamagnetic signals. In conclusion, the first attempts for the synthesis of homoleptic, macrocyclic vanadium-NHC-complexes have been performed, which are a basis for future investigations.

3.2.3 Gold

Parts of this chapter were published in E.B. Bauer, M.A. Bernd, M. Schütz, J. Oberkofler, A. Pöthig, R.M. Reich and F.E. Kühn, *Dalton Transactions*, 2019, **48**, 16615-16625.

Despite the herein widely discussed small inorganic anti-cancer drug cisplatin, also Au(I) compounds are in the focus of many anti-tumor studies.[57, 58] There, one highly effective and very successful drug, [(tetra-*O*-acetyl-β-D-glucopyranosyl)thio](triethylphosphine gold(I), also known as auranofin, has to be mentioned (structure given in figure **9**). It was successfully evaluated in *in vitro* studies as well as *in vivo* leading to approval in 1985 by the Food and Drug Administration (FDA) for the treatment of rheumatoid arthritis.[72] In fact, in the same year, also the first anti-cancer studies of auranofin have been published.[180] Until today, auranofin is still part of clinical studies for different medical indications like non-small lung cancer, glioblastoma or tuberculosis. Furthermore, initially as surrogate for Pt(II) based drugs, isoelectronic (d^8) and isostructural Au(III) complexes are investigated for their biological effects.[67] Concerning the mode of action of gold based compounds, the most important discoveries are already mentioned in the introduction in chapter 1.2.2., and therefore are not further addressed here. Still, interactions and reactivity of gold compounds with thiol-containing molecules is a very important factor for the biological activity.[67] Furthermore, the stability of gold complexes and in particular Au(III) complexes is also a very important issue, because Au(III) complexes are prone to reduction by e.g. redox active enzymes, which may alter the biological effects. Therefore, the gold atoms need to be sufficiently stabilized. For instance, physiologically highly stable Au(III) porphyrin complexes were introduced in 2003 by Che *et al*.[181] These complexes were found to be very effective against different cancer cell lines as well as in cisplatin-resistant cancer cell lines and in particular in ovarian cancers A2780 and A2780cisR.

Additionally, the complexes were also shown in *in vivo* studies to effectively address these cancer cells and overcome cisplatin resistance. Noticeable, the respective Zn porphyrin complex was observed to be about 100 times less active than the corresponding Au(III) complex indicating the potency of the Au(III) center.[181] Another suitable ligand system despite porphyrins were observed to be NHCs, which have been introduced in chapter 1.2.2. The first studies on the impact of different Au(I)-NHC-complexes on isolated rat mitochondria were carried out by Berners-Price *et al.* and can be seen as milestone for the development of gold-based NHC complexes for cancer treatment.[59, 60] Since then, many different more or less active gold-NHC-complexes were introduced and studied for different medical indications, however, none of these entered clinical trials yet.[44, 57, 58, 70]

In our group, different NHC ligands have been developed and found to stabilize various transition metals in different oxidation states.[58, 80, 152-157, 182-186] As already mentioned previously, some of these complexes were investigated for their catalytic properties or in reactivity studies.[153, 155, 156, 184] In particular, ligand **44** was found to be a versatile NHC ligand able to stabilize different transition metals in high oxidation states like Fe(III) or the formal Cu(III).[154, 156] Therefore, attempts to synthesize the respective macrocyclic Au(III)-NHC-complexes were performed. Additionally, inspired by the success of the Au porphyrin complex and the fact, that an increase in lipophilicity leads in general to an increase in cytotoxicity, a new benzimidazolylidene ligand as well as the corresponding Ag(I) and Au(I) complexes were synthesized and characterized. Furthermore, the Au complexes were evaluated for their antiproliferative properties in different cancer cells of the cervix (HeLa cells), cisplatin resistant ovarian cancer (A270cisR), breast cancer (MCF-7) and prostate cancer (PC3). In these biological studies, previously published Au(I)-NHC-complexes were included to investigate the influence of the different structural features on the biological effects further. The structures are given in figure **48**, whereas green numbers indicate the novel NHC ligand as well as the novel complexes. For these compounds, the synthetic procedures and the characterization is presented in the following. In general, the complexes evaluated in this study are based on imidazolylidene or benzimidazolylidene, respectively, however, display different levels of cyclization. Additionally, different oxidation states of gold are investigated, namely Au(I) and Au(III). Together, these varying parameters result in different coordination geometries and number of coordinated gold atoms for these NHC complexes. *Tetra*-NHC ligands **44** and **49** are macrocyclic NHC ligands, ligands **50** and **46** display a linear structure. According to its structure, ligand **46** is capable of stabilizing two Au(I) atoms by two ligands resulting in complex **56**. Berners-Price already tested this complex for its effect in isolated rat mitochondria, however, no IC_{50} values are reported so far and thus, this complex is included in these studies fitting well into the series. Providing four imidazolylidene entities, linear ligand **50** coordinates four Au(I) atoms similar to ligand **46** yielding complex **55**. This complex was shown to be present in different conformers due to its flexible ligand,

which is discussed in more detail in the original publication.[186] The new benzimidazolylidene ligand **49** was shown to exhibit a box-type structure upon coordination of Ag(I) (**52**) similar to complex **45** ([Ag_4(**44**)$_2$]). Upon coordination of Au(I), a different structure is observed for **53** tough the overall composition was also found to be Au_4(**49**)$_2$ similar to the respective silver complex. Two Au(I) atoms were found to be linearly coordinated inside the ligands cavity by two NHC moieties, the other two Au(I) atoms were located between the two ligands connecting these two Au(I) NHC entities. Au(I)-NHC-complex **54** is coordinated in a box-type fashion like **52**. In case of Au(III)-NHC-complex **51**, the Au(III) center is coordinated as expected in an almost square planar fashion inside the ligand. Therefore, Au(III) complex **51** is the first one reported that is based on a macrocyclic *tetra*-NHC ligand, despite the one reported by Jenkins *et al*.[160] Additionally, it is the first evaluated in anti-cancer studies. Overall, these complexes do not contain any functionalities or targeting moieties and thus, an insight into the influence of the coordination geometry as well as the lipophilicity of these complexes is provided. Thus, a valuable basis for future investigations is presented.

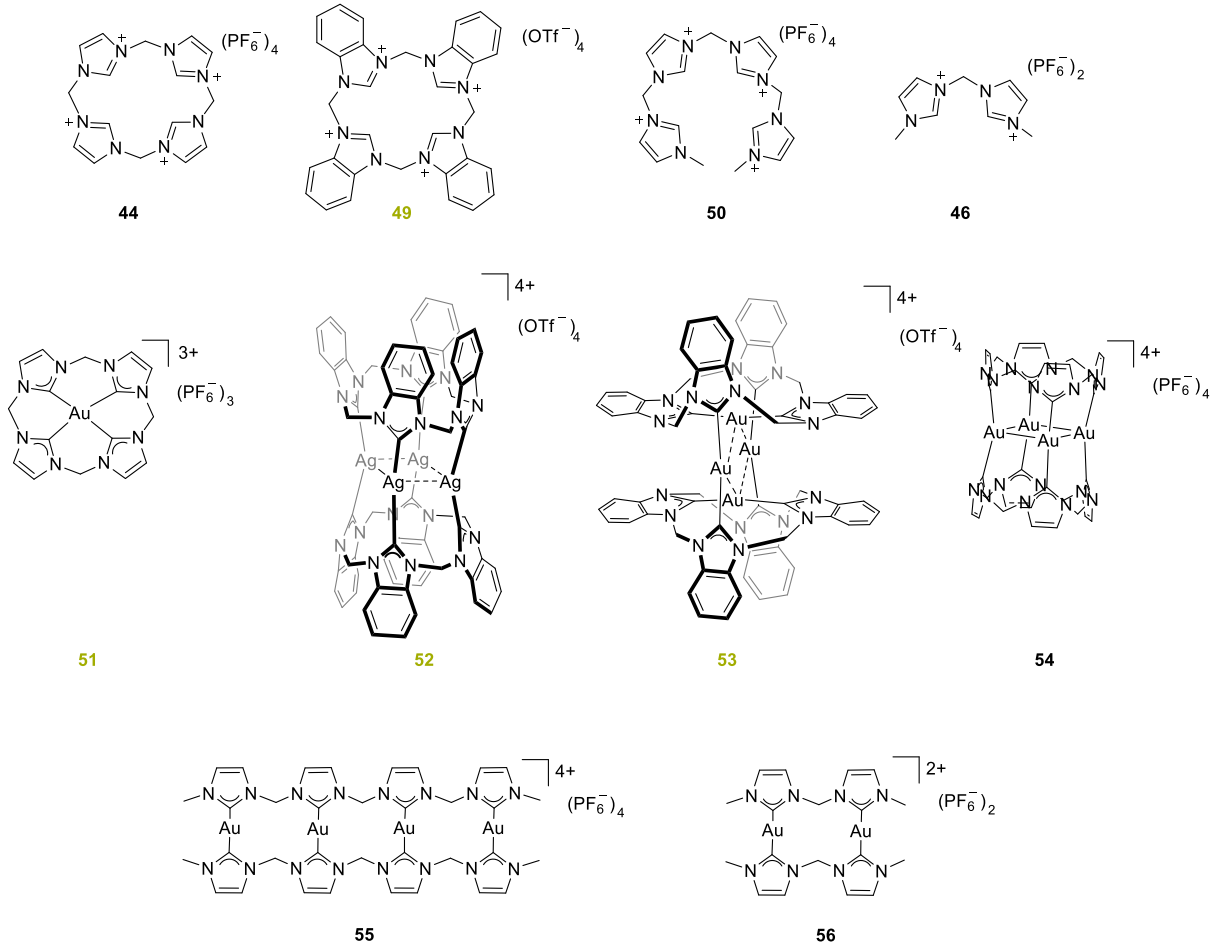

Figure **48**: Overview of the different NHC complexes and ligands evaluated for their effect in cancer cells. The green numbers indicate the newly introduced compounds for which the detailed synthetic procedures as well as the characterization is given in the following.

SYNTHESIS AND CHARACTERIZATION OF **51**

After numerous unsuccessful synthetic approaches, complex **51** was obtained by reaction of $Au(OAc)_3$ with ligand **44** in DMSO. The ^1H NMR of the pure complex in MeCN-d_3 shows two singlets, one at 6.68 ppm and the other one at 7.91 ppm (see supplementary data figure **S22**). In the ^{13}C NMR, three signals are visible with the carbene resonance at 144.33 ppm. The shift is in accordance with other Au(III)-NHC-omplexes reported in literature.[160, 187] The spectrum is given in the supplementary data in figure **S23**. A scheme of the synthesis is provided in scheme **19**.

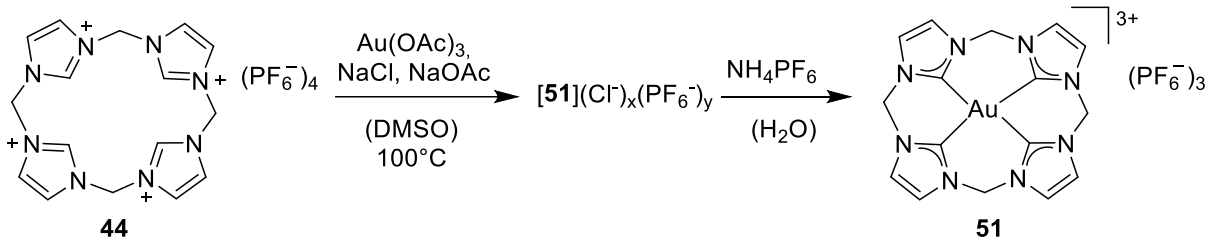

Scheme **19**: Schematic representation of the synthesis of Au(III)-NHC-complex **51**. Reprinted from Ref. [188] by permission of The Royal Society of Chemistry.[188]

As shown in scheme **19**, the successful synthesis and purification of **51** requires the addition NaOAc (1.5 equiv.) and NaCl (1.0 equiv.). Adding more equivalents of NaCl prevents purification of the complex due to formation of gold chloride adducts as well as unreacted ligand with a partial displacement of PF_6^- by Cl^-. The counterion exchange is evident from an enhanced water-solubility of the ligand resulting in non-separable product and ligand mixtures. Adding 1.0 equiv. NaCl leads to water-soluble complex **51** with at least one chloride as counterion, which also enhances crystallization of the complex. Additionally, organic impurities can be removed by washing the product with organic solvents like MeCN and DCM. Subsequent dissolution of the product in water and precipitation with NH_4PF_6 is then used to remove water-soluble impurities. However, the yield is very low (11 %) and thus, optimization of this reaction is still necessary. Single crystals of **51** suitable for X-ray diffraction were obtained by slow diffusion of diethyl ether into a DMSO/MeCN (1/1) solution containing **51**. The structure is presented in figure **49**.

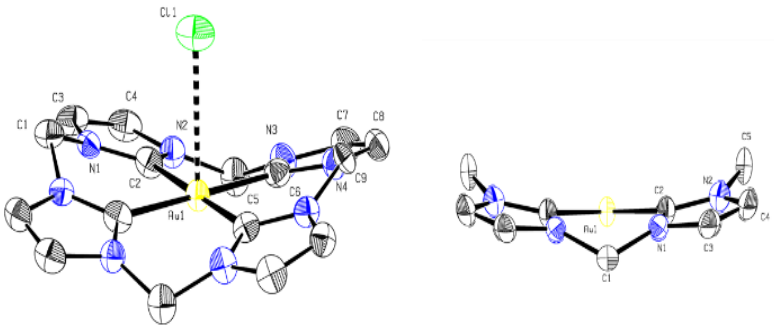

Figure **49**: ORTEP style representation of complex **51** with ellipsoids shown at a 50% probability level. Hydrogen atoms and hexafluorophosphate counterions were omitted for clarity. Selected bond lengths [Å] and angles [deg.]: Au1–C2 1.997(7), Au1–C6 1.990(7), Au–Cl 3.007(1), C2–Au1–C6a 179.6(2), C2–Au1–C6 90.0(3), C5–Au1–C5a 151.5(2), C1–Au1–C9 148.6(3). Reproduced from Ref. [188] by permissions of the Royal Society of Chemistry.

The crystal structure shows an almost square planar coordination of the Au(III) center displaying an angle of 179.62 ° of the C2–Au1–C6a axis. As shown by the perspective of **51** on the right in figure **49**, the ligand is slightly bent with angles of 148.63 ° and 151.52 ° observed for C_{bridge}–Au1–C_{bridge} leading to a slight elevation of the Au atom above the carbene carbon plane. Axially, one chloride is coordinated to the Au(III) atom with an Au–Cl distance of 3.007(1) Å. This distance is shorter than the sum of the van-der-Waals radii of both atoms (4.14 Å).[189] In literature, the reported distances for Au(III)–Cl adducts are in the same range (3.016 – 3.693 Å) or slightly shorter.[187, 190, 191] In comparison to the Au(I)–C distances found for complexes **53**, **54** and **56** (see table **4**), the Au(III)–C of **51** is slightly shorter with an average of 1.992 Å. This is in the same range as observed for further Au(III)–C distances found in literature.[160, 187] A comparison to the bond lengths of **55** was not possible, because no crystals suitable for X-ray could be obtained.

Synthesis and Characterization of Benzimidazolyl Compounds

The synthesis of ligand **49** was inspired by the synthetic procedure for ligand **44**. Therefore, methylene-1,1-bisbenzimidazole is synthesized according to previously published methods.[192] The synthesis of the macrocycle was observed to form selectively the desired *tetra*-NHC ligand without any higher cyclic analogues as by-products. The ^{1}H NMR of pure **49** shows four signals (see supplementary section figure **S24**) highlighting the high symmetry of the ligand. The singlet generated by the imidazolium protons of C1/C1a/C9/C9a is located at 10.72 ppm. In comparison to ligand **44**, this signal is downfield shifted by 1.06 ppm. The signal generated by the protons of the methylene groups bridging the benzimidazolyl entities (C8/C8a/C16/C16a) is present at 7.84 ppm. This is a downfield shift of 1.00 ppm compared to **44**. These shifts are observed due to a donation of the electron density to the aromatic ring system, which proton signals are visible as multiplets at 8.63 ppm and 7.87 ppm. In the ^{13}C NMR spectrum of **49** (presented in the supplementary data in figure **S25**), the signal of the imidazolium carbon atoms

C1/C1a/C9/C9a is located at 145.02 ppm, which is a shift of +7.26 ppm compared to **44**. The resonances of the aromatic ring can be observed at 130.10 ppm, 129.06 ppm and 114.01 ppm. The signal at 130.10 ppm can be assigned for the imidazolyl backbone carbon atoms shared with the aromatic ring whereas the other two cannot be distinguished according to 2D NMR spectroscopy (see supplementary data figures **S26** and **S27**). The resonance observed at 54.62 ppm can be assigned to the methylene groups. In addition, the signals of the triflate counterion are also present. Single crystals suitable for X-ray diffraction were grown by slow diffusion of diethyl ether into a DMF-solution of **49**. The structure is given in figure **50**.

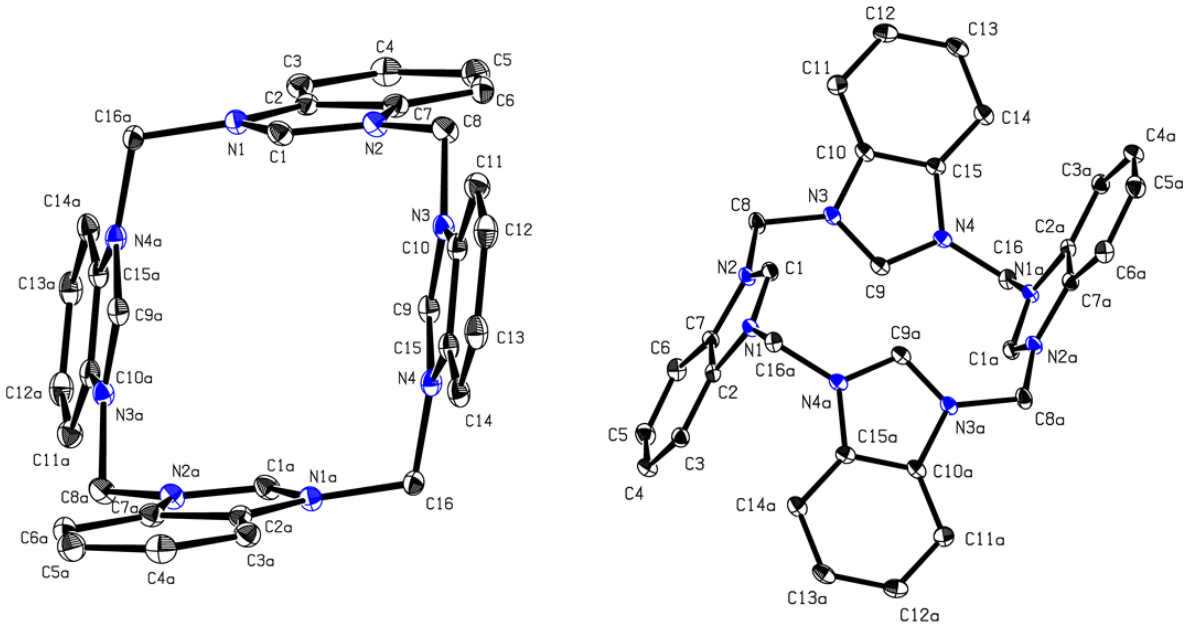

Figure **50**: ORTEP style representation of **49** with ellipsoids shown at a 50% probability level. Hydrogen atoms and triflate anions are omitted for clarity. Reprinted from Ref. [188] by permission of The Royal Society of Chemistry.

As visible in figure **50**, the ligand crystallizes in a 1,2-alterante fashion. The same conformation has been envisioned for an analogous benzimidazoline compound, yet, a 1,3-alternation may be sterically favorable.[193] The NMR data, however, do not contain information about the conformation of the ligand in solution. Moreover, the ligand was found to be air- and moisture-sensitive.

Converting **49** with Ag_2O yielded complex **52** with 38 % yield. This method is an established preparation method for Ag-NHC-complexes with Ag_2O is both, Ag(I) source and base.[157, 186] In the ^1H NMR spectrum given in the supplementary section in figure **S28**, the resonances of the protons of the bridging methylene groups were observed as doublets with coupling constants of about 15 Hz at 7.71 ppm and 7.58 ppm. Due to this splitting of the signals, a rigid, non-square planar geometry can be predicted. A similar signal pattern is observed for Ag(I) complex **45**. The proton signals of the aromatic backbone of the benzimidazole entity of **52** are located at 8.46 and 7.51 ppm, which represents a high field shift in

comparison to **49**. The determined ^{13}C NMR shows a location of the carbene resonances at about 194.27 ppm (see supplementary section figure **S29**), which are split into two doublets due to coupling with the Ag isotopes $^{107/109}Ag$.[160] Further Ag–C coupling was not observed. According to 2D NMR (HSQC and HMBC NMR, see supplementary data figures **S30** and **S31**, respectively, the signals of the carbon atoms of the imidazolyl backbones are located at 133.45 ppm, which is a shift of 3.35 ppm compared to the ligand. The signals at 125.05 and 112.56 ppm are generated by aromatic ring system, however, cannot be further assigned. The signal of the CH_2 groups is visible at 60.52 ppm as one sharp singlet. Thus, these carbon atoms are chemically equivalent. The single crystal structure determined of crystals of **52** grown by slow diffusion of diethyl ether into a solution of the complex in DMF is shown in figure **51**.

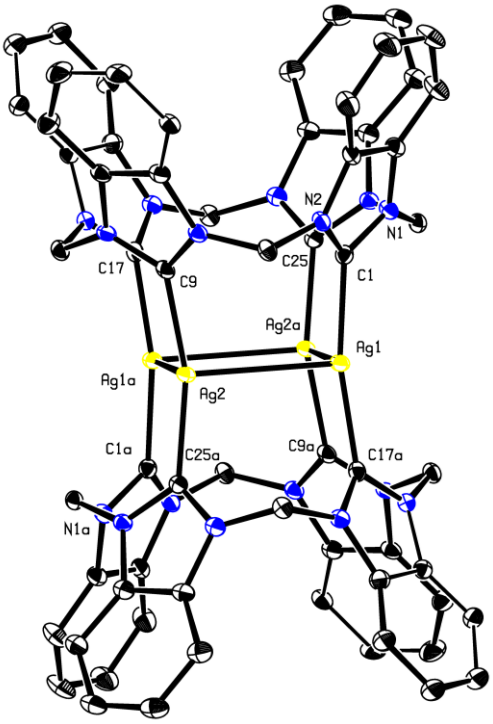

Figure **51**: ORTEP style representation of the cationic fragment of **52** with ellipsoids shown at a 50% probability level. Hydrogen atoms and triflate anions are omitted for clarity. Selected bond lengths [Å] and angles [deg.]: Ag1–Ag2 2.9645(3), Ag2–Ag1a 3.0087(4), Ag1–C1 2.100(3), Ag2–C9 2.114(3), Ag1a–C17 2.099(3), Ag2a–C25 2.110(3), C1–Ag1–C17a 166.1(2), C9–Ag2–C25a 156.1(5), Ag1–Ag2–Ag1a 96.151(10), Ag2–Ag1a–Ag2a 83.849(10). Reprinted from Ref. [188] by permission of The Royal Society of Chemistry.

Noticeable, the solid-state structure of **52** matches with the predictions made according to NMR analysis. Accordingly, a box-type coordination similar to **45** is observed with all four Ag(I) atoms located in the middle of the two coordinating ligands. The average Ag–C distance is determined as 2.11 Å, which is in the same range as determined for **45** (2.09 Å in average)[157] and reported for further Ag–C containing complexes.[183, 194] The determined Ag–Ag distances can be recognized as argentophilic interactions with a distance of 2.964(5) Å and 3.008(7) Å. These distances are shorter than the sum of the van-der-Waals

radii of both Ag atoms (3.44 Å) and are in agreement with further reported Ag–Ag distances described as argentophilic interactions.[157, 195]

Au(I) complex **53** synthesized *via* direct metalation was obtained in high purity applying chloro(tetrahydrothiophene)gold(I) as gold precursor. For deprotonation of the ligand, NaOAc was used. The ^{1}H NMR of the pure compound shows two duplets with coupling constant of about 14.6 Hz at 7.79 and 7.68 ppm (see supplementary data figure **S32**). These signals can be assigned to the protons of the methylene bridge of the ligand. The protons of the benzimidazolyl entity are located as multiplets at 8.48 ppm, 7.80 ppm, 7.10 ppm and 7.03 ppm. The number of signals indicate a loss of symmetry for these protons, whereas the methylene bridge seems to be unaffected. A similar loss of symmetry can also be observed in the ^{13}C NMR spectrum given in figure **S33**. The resonances generated by the carbene carbon atoms are located at 190.8 ppm and 180.1 ppm, which is accordance with other reported Au(I)-NHC-complexes.[157, 186, 196] These significantly deviating shifts with $\Delta\delta$ = 10.74 ppm of the carbene atoms compared to the free ligand indicate two different coordination modes for Au(I). The aromatic carbon atoms generate six signals, which are visible in the range of 133 ppm to 111 ppm. There, the imidazolyl backbone carbon atoms are located at about 132 ppm. The bridging methylene entity is present as a singlet at 58.79 ppm. These assignments are made according to 2D HSQC and HMBC spectra given in the supplementary data in figures **S34** and **S35**, respectively. Single crystals of **53** suitable for X-ray diffraction analysis were obtained by slow diffusion of diethyl ether into a solution of **53** in DMF. This analysis reveals a very interesting structure, which is represented in figure **52**.

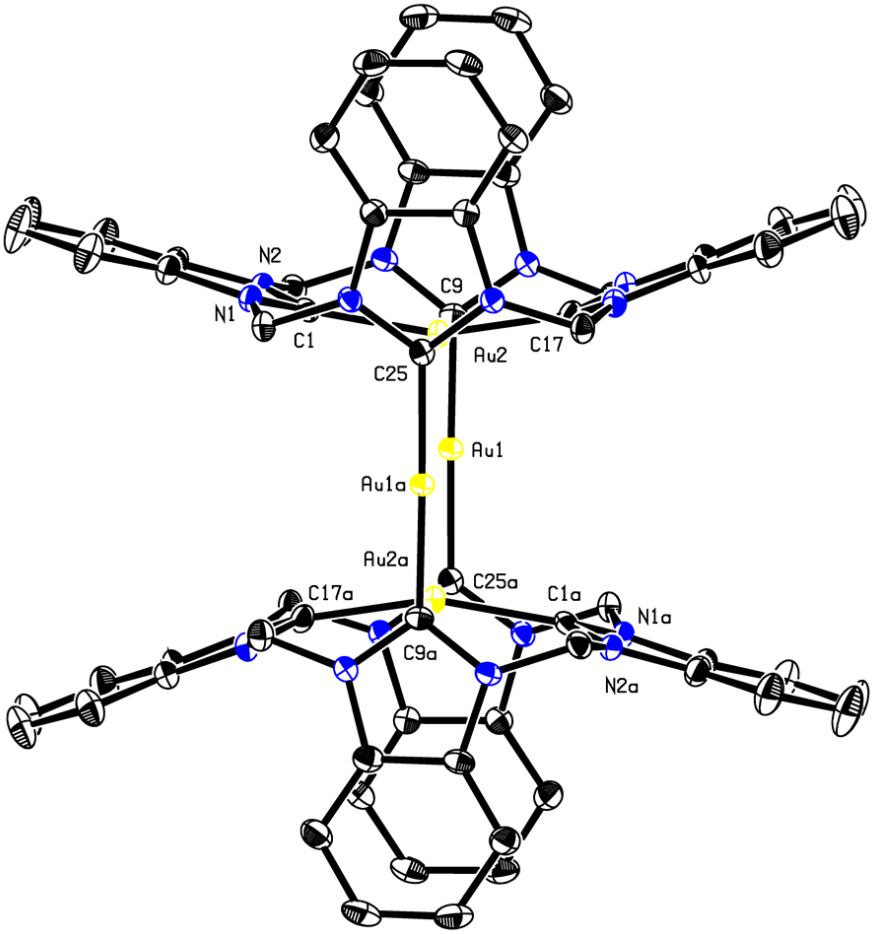

Figure **52**: ORTEP style representation of the cationic fragment of **53** with ellipsoids shown at a 50% probability level. Hydrogen atoms and triflate anions are omitted for clarity. Selected bond lengths [Å] and angles [deg.]: Au1–C25a 2.017(4), Au1–C9 2.022(3), Au2–C1 2.033(3), Au2–C17 2.032(4), Au2–C9 2.660(3), Au2–C25 2.683(3), Au1–Au2 3.1990(3), Au2–Au1a 3.3332(3), Au1–Au1a 5.139, C1–Au2–C17 161.58(15), C9–Au1–C25a 174.19(14), Au1–Au2–Au1a 103.747(5), Au2a–Au1–Au2 76.252(5). Reprinted from Ref. [188] by permission of The Royal Society of Chemistry.

The crystal structure of **53** shows the same $Au_4(L)_2$ composition as found for previously published **54**.[157] However, two of the Au(I) atoms are coordinated in an almost linear fashion inside the ligand's cavities. This coordination mode leads to a disposition of the benzimidazolyl moieties. The further two Au(I) atoms are also linearly coordinated but by each of the ligands acting as connectors between the two ligands. A similar coordination mode was found in literature for a Ag(I)-NHC-complex reported by Hahn *et al*.[197] The two Au atoms inside the ligand cavities (Au2 and Au2a, respectively) were determined to have Au–C distances of 2.033(3) Å and 2.0332(4) Å, respectively. For the other two Au(I) atoms, shorter Au–C distances were found (2.017(4) Å and 2.022(3) Å, respectively). Overall, these Au(I)–C distances are in the same range as found for other Au(I) benzimidazolyl complexes reported in literature.[198, 199] For Au1–Au2 and Au2–Au1a, distances of 3.199(0) Å and 3.333(2) Å, respectively, were determined. This is shorter than the sum of the van-der-Waals radii reported for two Au(I) atoms and can be termed an aurophilic interaction according to other reported Au–Au aurophilic interactions.[200] Nevertheless, the distance observed for Au1–Au1a is too long for any aurophilic interactions (5.139 Å). Overall, the

structural predictions made from the NMR analyses coincide with the structural features found *via* single crystal XRD indicating that the soli-state structure is maintained in solution. Noticeable, for this ligand system, a transmetalation from Ag(I) to Au(I) was not successful although numerous attempts were carried out.

An overview of some selected bond lengths and angles of complexes **51**, **52**, **53**, **54** and **56** is provided in table **4**. The details of further crystallographic data is given in the supplementary section 6.1. The data shown in table **4** show, that all Au(I)–C distances are in the same range. The Au(III)–C distances are slightly shorter and the Ag(I) distances are slightly longer, which is likewise reported in literature.[157, 197, 201] A comparison of the $C_{carbene}$–M–$C_{carbene}$ angle of **51** and **53** indicates that the Au(I) atoms of **53** are slightly less lifted out of the carbene carbon plane than the Au(III) atom of **51**.

Table **4**: Overview of selected angles and bond lengths determined for complexes **51**, **52**, **53**, **54** and **56**.

Bonds/Angles	**51**	**52**	**53**	**54**[157]	**56**[202]
M–C [Å]	1.997(7)	2.099(3)	2.017(4)	2.031(4)	2.025(8)
	1.990(7)	2.100(3)	2.022(3)	2.034(4)	2.028(8)
		2.110(3)	2.033(3)		2.032(9)
			2.032(4)		2.025(8)
		2.114(3)			
$C_{carbene}$–M–$C_{carbene}$ [deg.]	179.6(2)	166.12(1)	174.1(9)	164.8(2)	172.3(3)
		156.15(1)	161.5(8)		170.01(3)

STABILITY STUDIES

Prior to evaluation of the complexes for their antiproliferative effects in cancer cells, the stability of these complexes was assessed. Due to the light sensitivity of **52**, it was not included in the *in vitro* assays. At first, the stability of complexes **51**, **53**, **54**, **55** and **56** in RPMI1640 cell culture medium was tested, Therefore, the complexes were dissolved in a mixture of deuterated medium / deuterated DMSO (1/1 v/v) and analyzed by ^{1}H NMR spectroscopy. The thus prepared samples were analyzed right after preparation (0 h), after 24 h incubation at 37 °C and after 48 h incubation at 37 °C. After 48 h, all complexes were shown to be sufficiently stable during the 48 h period of evaluation in *in vitro* assays, because the signals of all complexes were retained and no new signals were observed in the ^{1}H NMR spectra. In case of complex **51**, however, a signal splitting of the bridging methylene groups as well as a change in integral ratio of the both signals was observed without the development of new signals. This

indicates a proton to deuterium exchange of these protons. This exchange can be reversed by replacement of D_2O by H_2O (see figure **53**).

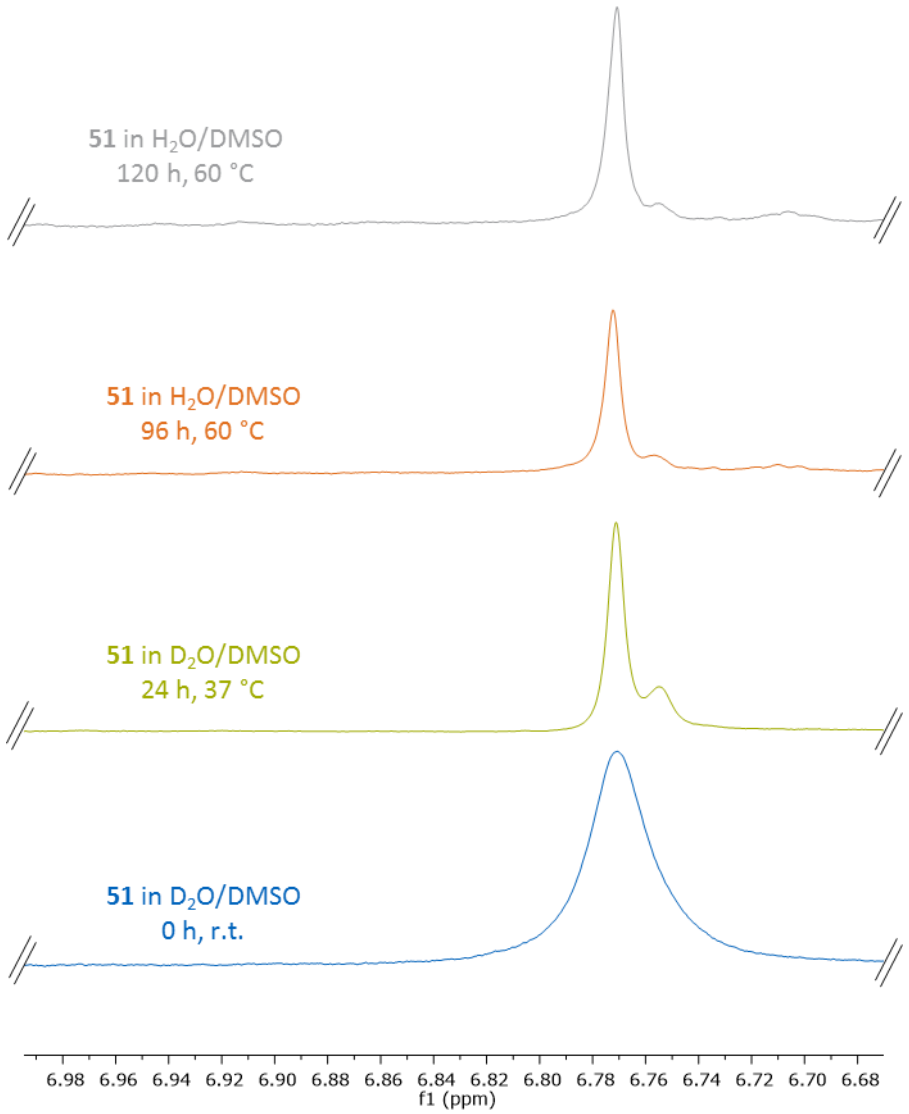

Figure **53**: Cutout of the relevant area of the ^{1}H NMR spectra of **51** in $D_2O_{PRMI\ Medium}$/DMSO-d_6 and $H_2O_{PRMI\ Medium}$/DMSO-d_6 at given temperatures and incubation times. The full spectra of this study are given in the supplementary data in figure **S36**. Reprinted from Ref. [188] by permission of The Royal Society of Chemistry.

The complete NMR spectra of the verification of the proton/deuterium exchange are given in the supplementary chapter in figure **S36**. There, it is visible that a higher temperature was needed to exchange the deuterium atoms by protons due to isotopic effects, which leads to slight decomposition of the complex. Extending the incubation time in deuterated aqueous solution at 37 °C for 5 days, the signal splitting increased and the integral ratio changed from 1:1 to about 1:0.5. The corresponding ^{1}H NMR is given in figure **54**.

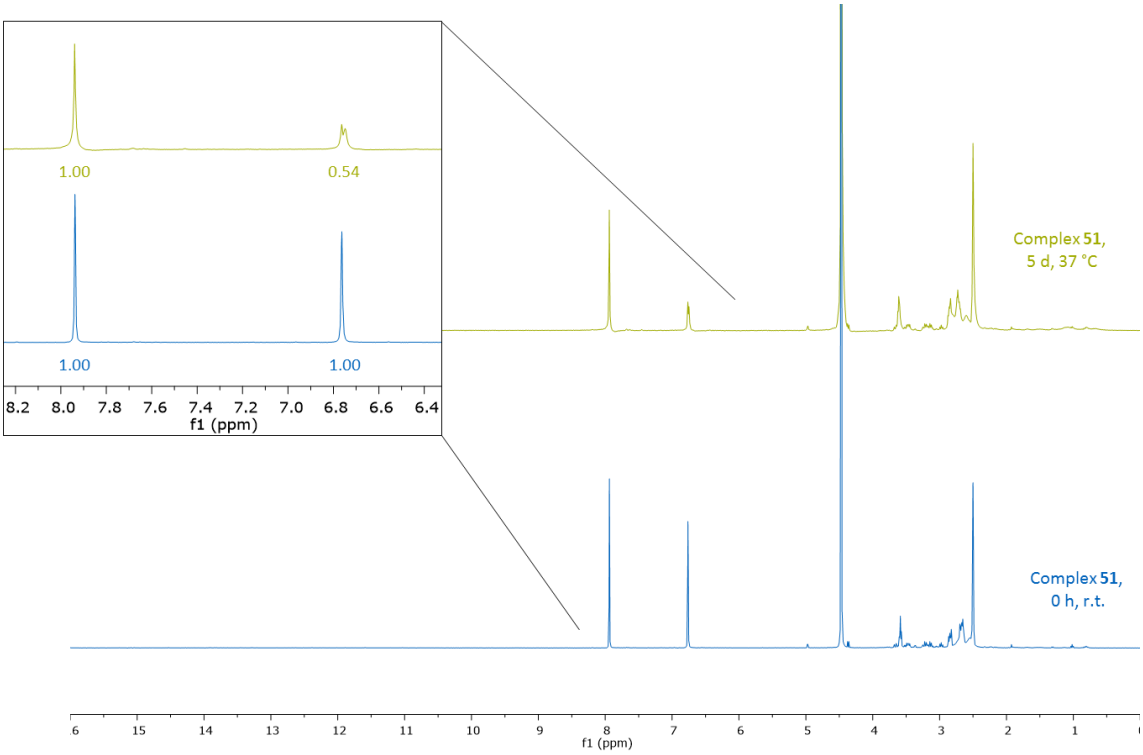

Figure **54**: ^{1}H NMR spectra of complex **51** in $D_2O_{PRMI\ Medium}$/DMSO-d_6 prior to the incubation (blue) and after five days at 37°C with the relevant area shown given in more detail on the upper left side. Reprinted from Ref. [188] by permission of The Royal Society of Chemistry.

Baker *et al.* recently reported a full deuteration of the imidazolylidene backbone of some Au(III)-NHC-complexes, which have been incubated in D_2O for 48 h at 100 °C.[187] An exchange of the backbone protons of **51** can also be observed at 37 °C by using 1,2-dichlorethane as internal standard, however, to a much smaller extend than observed for the methylene protons. Nevertheless, in principle, also a fully deuterated complex **51** is suggested to be able to obtain at higher temperature. Searching for deuterated compounds in medicinal chemistry, some recent reviews state, that deuteration is an increasingly applied method for instance for metabolite or mechanistic studies or for enhancing the pharmacokinetic properties.[203-206] Additionally, some deuterated drugs are already approved by the FDA or are part of clinical trials.[206-208] Thus, a deuteration of the methylene moieties of **51** might enhance the stability of the complex and therefore influence the biological activity. Additionally, deuteration of distinct entities of the complexes and its influence on the antiproliferative effect may provide insight into mechanistic details and/or metabolism of the complexes.

The stability of the gold complexes **51**, **53**, **54**, **55** and **56** was also assessed in the presence of glutathione. Glutathione (GSH) is a tripeptide of glutamic acid, cysteine and glycine, which is providing a thiol moiety that is able to coordinate Au atoms. Therefore, coordination to gold or even ligand exchange reactions with biological thiol containing molecules have been evaluated with this setup. Additionally, also the redox stability of the complexes is tested in this study, because GSH is readily

oxidized to GSSG upon formation of disulphide bonds between two GSH molecules. During 48 h at 37 °C, all complexes were found to be stable. Nevertheless, for complex **53**, the formation of a white precipitate was observed in course of the incubation and in the corresponding ^{1}H NMR, some sort of decomposition was visible (see supplementary data figure **S38**). A performed ESI-MS of the sample still showed the signals of complex **53**, however, no GSH or GSSG indicating a certain interaction of **53** and GSH leading to an insoluble species. In case of **51**, the NMR spectrum did not change during the incubation period (see supplementary data figure **S37**), however, the subsequent determined ESI-MS spectrum shows only small signals of **51** (see supplementary data figure **S42**). Except for the evaluation of complex **53**, GSH and GSSG were both visible in the ^{1}H NMR as well as in the ESI-MS spectra of all samples after 48 h incubation at 37 °C (see supplementary data figures **S37 – S46**).

Electrochemical studies

In order to investigate the redox stability of complexes **51** and **54**, electrochemical studies were performed. These cyclic voltammetry (CV) measurements were carried in an acetonitrile solution with the supporting electrolyte being tetra-*n*-butyl ammonium hexafluorophosphate. Both cyclic voltammograms are given below in figures **55** and **56**, respectively.

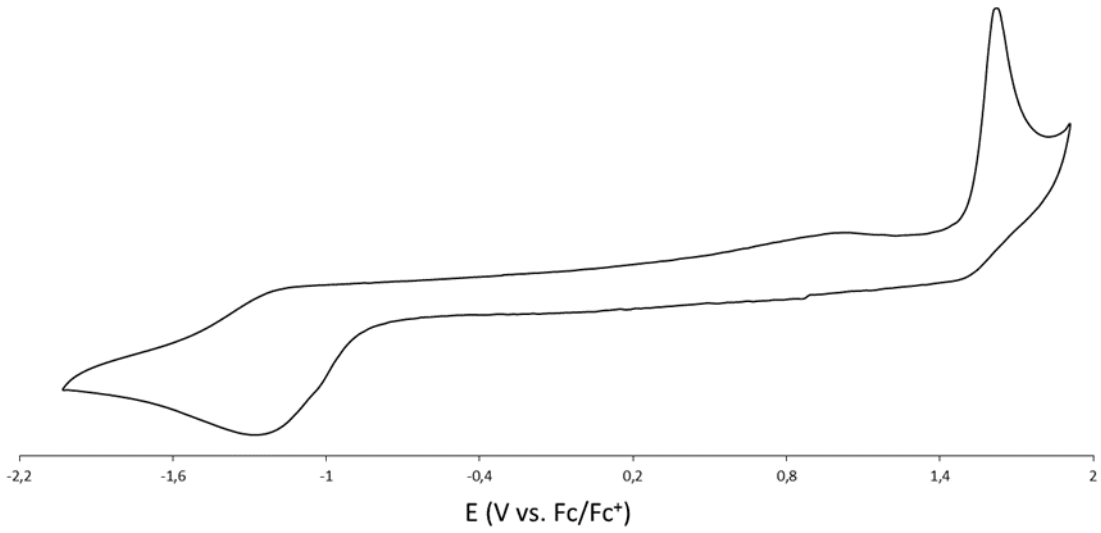

Figure **55**: Cyclic voltammogram of complex **51** relative to the half-cell potential of the Fc/Fc^{+} redox couple.

For complex **51**, an irreversible oxidation is observed at 1.63 V. Due to the irreversibility of this event, no particular oxidation/reduction product can be predicted. Furthermore, at -1.28 V, an irreversible reduction is visible, which potentially reflects the reduction from Au(III) to Au(I). However, a reduction from **51** to complex **54** would require a different stoichiometry and thus, this conversion is not likely to take place. In summary, complex **51** appears redox stable under CV conditions in a broad region. A comparable high redox stability was found for **54**. In figure **56**, two irreversible oxidation events at 1.53 V

and 1.72 V can be observed. Whether complex **51** is formed in course of these oxidation processes is not known. Still, this would demand the release of two gold atoms and no reduction process can be observed indicating the reduction to Au(0).

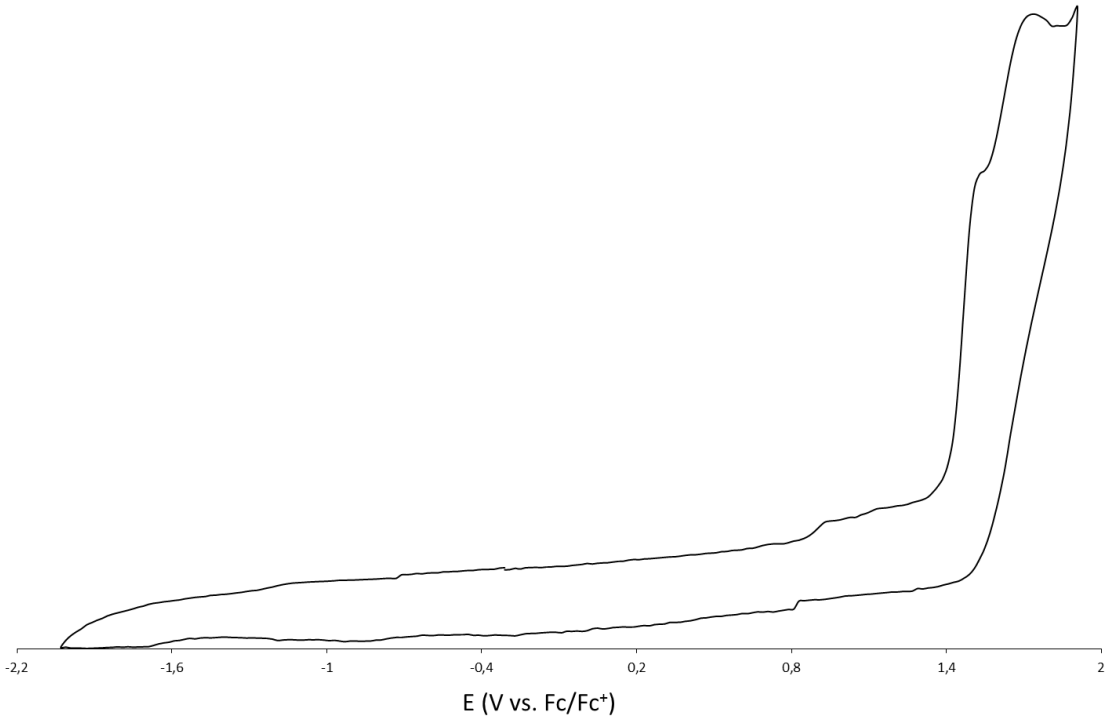

Figure **56**: Cyclic voltammogram of complex **54** relative to the half-cell potential of the Fc/Fc^+ redox couple.

IN VITRO MTT ASSAYS

Evaluation of the antiproliferative properties of Au complexes **51**, **53**, **54**, **55** and **56** and the corresponding ligands was performed in HeLa (cervix cancer), MCF-7 (breast cancer), PC3 (prostate cancer) as well as A2780cisR (cisplatin resistant ovarian cancer) cell lines by means of MTT assays. Compounds **49** and **52** were not included in the assays due to air-, water- and light-sensitivity of these compounds. Cisplatin was also evaluated as reference. The cancer cells were incubated with the compounds in different concentrations for 48 h. The thus obtained data are presented in table **5** and as well as graphically in figure **57**. The detailed graphs, which were used to determine the IC_{50} values, are given in the supplementary section in figures **S47** – **S65**. Compound **51** is observed to be not active in MCF-7 and PC3 cells and moderately active in HeLa and A2780cisR cells. This low antiproliferative effect may be due to the reactivity of the complex observed during stability studies. There, a proton to deuterium exchange was monitored representing a potential point of attack of biological nucleophiles. Complex **53** shows a certain selective antiproliferative effect on HeLa and A2780cisR cells over MCF-7 and PC3 cells.

Table **5**: IC_{50} values ± standard deviation (SD) [µM] determined for the indicated complexes and ligands in HeLa cells (cervix cancer), MCF-7 cells (breast cancer), PC3 cells (prostate cancer) and A2780cisR cells (cisplatin-resistant ovarian cancer) by MTT assays after an incubation period of 48 h. Data are adopted from Ref. [188] by permissions of The Royal Society of Chemistry.

	HeLa	MCF-7	PC3	A2780cisR
51	85.7 ± 15	n.a.	n.a.	82.1 ± 17
52	n.d.	n.d.	n.d.	n.d.
53	16.8 ± 10	n.a.	n.a.	25.7 ± 19
54	44.5 ± 20	97.7 ± 22	77.9 ± 19	78.8 ± 11
55	31.4 ± 6	4.9 ± 1.3	25.2 ± 4.2	1.7 ± 0.3
56	47.9 ± 20	43.4 ± 18	73.7 ± 20	n.a.
44	72.2 ± 19	85.5 ± 3.3	n.a.	88.8 ± 9
49	n.d.	n.d.	n.d.	n.d.
50	79 ± 22	83.9 ± 13	n.a.	n.a.
46	n.a.	n.a.	n.a.	n.a.
Cisplatin	2.8 ± 0.5	4.7 ± 0.9	3.7 ± 0.5	10.9 ± 1.7

n.a. = not active (IC_{50} > 100 µM)
n.d. = not determined

Comparison of the more lipophilic benzimidazolyl complex **53** to less lipophilic imidazolyl complex **54** shows, that **53** has a higher selectivity towards HeLa and A2780cisR cells. Complex **54** is moderately to almost not active in the entire tested cell lines, and, has higher IC_{50} values than **53**. Therefore, increasing the lipophilicity enhances the biological profile of these complexes when comparing **53** and **54**. Concerning the 4+ charge of these complexes, one can assume that this is not a major obstacle in terms of the biological activity because the same 4+ positively charges complex **55** is found to have the lowest IC_{50} values in three out of four cell lines evaluated in this study. In fact, **55** has relatively low IC_{50} values in all tested cell lines with a significant selectivity for MCF-7 (4.9 µM) and A2780cisR cells (1.7 µM). Strikingly, in A2780cisR cells, **55** has an almost 7-fold lower IC_{50} value than cisplatin. In MCF-7 cells, it has almost the same IC_{50} value as cisplatin (4.7 µM). Structurally, **55** is much more flexible than **53** and **54**, which might be a reason for the lower IC_{50} values. Complex **56** has relatively high IC_{50} values (43 – 74 µM) or no activity at all without any significant selectivity. Thus, also being reported to have strong anti-mitochondrial properties in isolated rat mitochondria, **56** was found to have quite high IC_{50} values and a high standard deviation. Therefore, it is assumed that the complex is not able to reach the mitochondria due to stability issues. However, to confirm this hypothesis, further studies need to be performed. Comparing the IC_{50} values determined for the complexes to the corresponding ligands, in general, Au coordination enhances the antiproliferative activity.

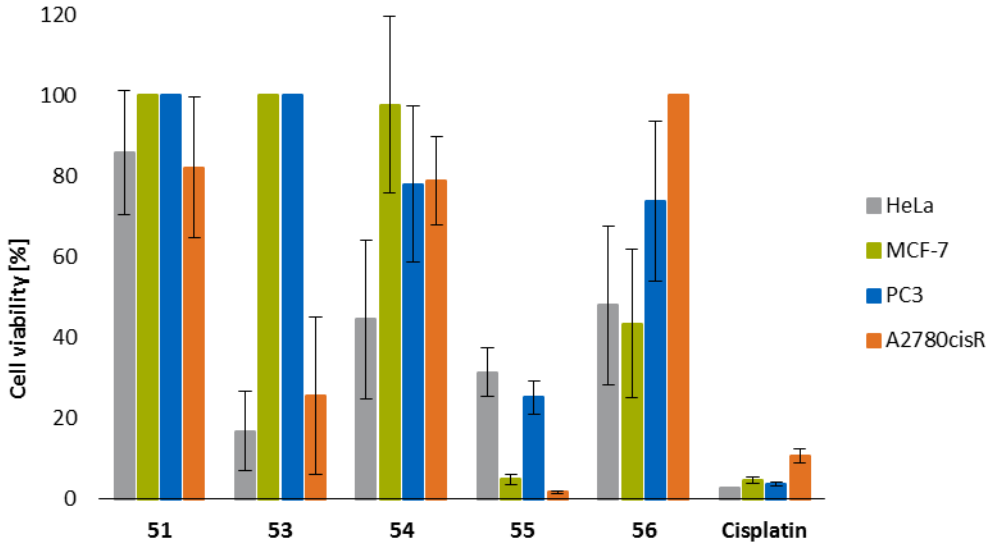

Figure **57**: Graphic representation of the IC_{50} values ± SD [µM] given in table **5** determined for the different Au(I)- and Au(III)-NHC-complexes in HeLa, MCF-7, PC3 and A2780cisR cancer cell lines by means of MTT assays with an incubation time of 48 h. This figure is taken from Ref. [188] with minor modifications by permission of The Royal Society of Chemistry.

In summary, the synthesis of a novel macrocyclic benimidazolyl ligand **49** as well as new macrocyclic gold and silver complexes **51**, **52** and **53** is presented. The compounds were characterized by multinuclear NMR spectroscopy, elemental analysis, ESI-MS, single crystal X-ray diffraction as well as cyclic voltammetry. The crystal structure of **53** reveals an interesting combination mode. Two of the Au(I) atoms are linearly coordinated by two opposing NHC moieties inside the carbene carbon atom plane of one ligand. The further two Au(I) atoms are linearly coordinated by each of the ligands connecting the both entities. These macrocyclic complexes as well as further macrocyclic and linear gold-NHC-complexes **54**, **55** and **56** were evaluated in *in vitro* for their antiproliferative effects in different cancer cell lines using the MTT assay. The thus determined IC_{50} values show, that complex **55** has the lowest IC_{50} values compared to the other complexes in three out of four cancer cell lines. Furthermore, the complex shows a significant selective cytotoxicity in MCF-7 and A2780cisR over HeLa and PC3 cells. Noticeable, in A2780cisR cells, **55** has an almost seven times lower IC_{50} value than cisplatin. Unfortunately, the complex could not be evaluated in non-cisplatin-resistance A2780 cells; however, this low value allows the assumption that **55** might be able to overcome cisplatin resistance. Complexes **51**, **54** and **56** were observed to be moderately cytotoxic with IC_{50} values ranging from 43 to 80 µM or no activity by definition of > 100 µM. One possible reason for the relatively low cytotoxicity of some of the complexes might be the instability of the complexes. In preceding stability studies, all complexes were observed to be intact at the applied conditions; however, this does not reflect the real conditions of cell studies. Thus, only assumptions about the stability are possible. In case of **51**, a proton to deuterium exchange could be monitored in D_2O solutions. Accordingly, these labile protons represent a potential point of attack for biological nucleophile, although no decomposition of reaction was

observed in the presence of GSH. Nevertheless, the deuteration opens new perspectives for e.g. mechanistic insights, metabolite studies or enhancing the pharmacokinetic properties, which is increasingly exploited in medicinal chemistry. Furthermore, as expected, an increase in lipophilicity from imidazolyl complexes to benzimidazolyl compounds leads to an increased antiproliferative effect at least in HeLa and A2780cisR cells. However, these rigid, highly positively charged complexes might hamper the effects of these complexes in cancer cells and thus, studies for synthesis and evaluation of the corresponding Pd(II) and Pt(II) are ongoing. For these complexes, a beneficial balance of charge and stability is assumed.

3.2.4 Summary of studies towards new *N*-heterocyclic carbene complexes

In summary, studies for the synthesis of various chromium, vanadium- and gold-NHC-complexes were carried out. In general, the attempts can be divided in two methods: on the one hand, the direct metalation approach and on the other hand the transmetalation. In addition, different precursor and bases were tested. In case of chromium, for both methods, different promising conditions were tested, however, the results were not reproducible and no distinct information about the reaction products could be obtained, which were attempted to characterize using paramagnetic NMR studies, ESI-MS and powder XRD. Nevertheless, according to the obtained results, transmetalation seemed to be a more promising route than a direct metalation. For synthesis of vanadium-NHC-complexes, also different vanadium sources as well as bases and ligands with different degrees of cyclization were tested. In particular when using $VO(acac)_2$ as precursor and conducting the reaction under inert atmosphere, $V(acac)_3$ could be observed as reaction product for both of the different tested NHC ligands. This was not observed when the reaction was carried out on air, underlining that this product may be $V(acac)_3$, which is air- and moisture-sensitive. However, no distinct process leading to the formation of $V(acac)_3$ could be elucidated. According to the recent publication discussing the interesting reactivity of ligand **44**, different oxidation reactions of the ligand have been identified.[156] However, for vanadium, such products could not be identified, mostly due to products mixtures and the paramagnetism of the vanadium center. Still, similar reactions possibly lead to the formation of $V(acac)_3$. Additionally, no distinct product could be isolated using different solvent mixtures or methods and the assignment of the reaction mixtures was not achieved. Nevertheless, strong hints for the formation of vanadium NHCs were observed according to paramagnetic NMR studies and ESI as well as LIFDI-MS. Further investigations are currently ongoing focusing on the isolation of the potentially formed vanadium-NHC-complexes for further analysis e.g. *via* EPR measurements. Overall, the most successful approaches were performed for the synthesis of an Au(III) complex of ligand **44**, a new benzimidazolium ligand and the corresponding Ag(I) and Au(I) complexes. These compounds were successfully synthesized and characterized by multinuclear NMR measurements, elemental analysis, ESI-MS as well as single crystal

X-ray diffraction. Together with further previously published gold-based NHC complexes, these were evaluated for their antiproliferative properties in different cancer cells revealing the lowest IC_{50} values for complex **55**. Furthermore, in preceding stability studies, a deuteration of the bridging methylene groups was observed for complex **51**. Inspired by this observation, investigations on the synthesis of a deuterated ligand **44** are part of ongoing investigations. By deuteration of the ligand, an Au(III) complex with enhanced stability may be obtained as well as e.g. deuterated iron complexes potentially providing insights into mechanism of action in biological studies and catalysis, respectively. Additionally, further ligand modifications e.g. the partial replacement of imidazole by pyrrole in **44** might be beneficial for the synthesis of a respective vanadium or chromium complexes, which is part of ongoing investigations. Such complexes might be interesting for biological applications as well as in catalysis. In summary, initial studies towards the synthesis of macrocyclic vanadium- and chromium-NHC-complexes are provided suitable for future investigations.

4 Conclusion and Outlook

In this thesis, two different ligand systems were applied and assessed for the synthesis of novel transition metal complexes. First, rigid ditopic ligands coordinating to a metal center *via* terminal pyridyl entities forming a three-dimensional cage structure were applied for the synthesis of respective molybdenum, chromium and gold-based supramolecular coordination compounds (SCCs). Second, *N*-heterocyclic carbene (NHC) ligands focusing on macrocyclic *tetra*-imidazolium ligands were evaluated for the synthesis of early transition metal complexes as well as gold and silver complexes. In conclusion, for both ligand systems, the most successfully applied metal was gold. For the synthetic approaches towards molybdenum SCCs, the dimolybdenum(II) species Mo_2^{4+} was used to study the accessibility of homoleptic pyridine complexes, which are not reported in literature so far. However, the performed studies show that this led to unidentified product mixtures due to the inherent reactivity and instability of the Mo-Mo quadruple bond and that the molybdenum core needs to be stabilized by chelating N- and O-donor ligands rather than non-chelating pyridyl ligands. As shown for quadruple bonded rhenium complexes, encapsulation of Mo_2^{4+}-containing molecules in liposomes may be a useful method to stabilize the metal center. Moreover, maybe the application of a mononuclear molybdenum center would be more suitable circumventing the issues of the reactivity of the quadruple bond. Additionally, slight modifications of the ligand structure in terms of chelation or donor atoms might also enhance SCC formation. For the synthesis of mononuclear chromium cages, some promising results were obtained according to paramagnetic NMR measurements, elemental analysis and ESI-MS, however, the analysis of the product mixtures was challenging. For further analysis, the isolation of potentially formed products is important, however, was not achieved in these studies. For chromium, $CrCl_2$ may be a suitable precursor for water-soluble complexes. Therefore, modification of the ligand structure in terms of solubility might also be an interesting approach for future investigations. Additionally, a change in solubility might be useful in terms of crystallization. Applying DMSO as solvent, DMSO was observed to coordinate preferably to chromium instead of the desired cage-ligand. All further performed crystallization attempts did not yield single crystals suitable for X-ray diffraction. Crystallization was also the major obstacle for a complete analysis of the respective gold-based cages. Different synthetic approaches for the synthesis of Au(III) SCCs were performed, where some were found to provide very promising analytical results by ESI-MS, multinuclear NMR measurements, 2D NMR and elemental analysis. However, a distinct statement about the coordination geometry and complex composition would require more accurate analytical results as well as single-crystals for the analysis *via* XRD, which was not achieved. Additionally, according to NMR studies, gold was found to interact with different parts of the ligands and thus, a modification blocking these parts will potentially enhance cage formation.

Further modifications of the ligands to P- or S-donor moieties will also be an interesting approach due to the high affinity of gold to phosphine and sulfur-containing molecules. Inspired by some recent reports by Jenkins *et al*., the synthesis of chromium-NHC-complexes was tested. In these experiments, transmetalation was found to be the most promising method. The reactions were analyzed by ESI-MS, paramagnetic NMR studies as well as powder XRD. However, besides non-reproducible results, a proper analysis of the reaction results was not possible. The synthesis of vanadium-NHC-complexes was evaluated facing similar problems. Noticeable, in these studies, reduction of $VO(acac)_2$ to $V(acac)_3$ was observed independently from the applied ligand system. Additionally, none of the products could be isolated for further analysis e.g. *via* EPR or elemental analysis. Therefore, investigations are ongoing. Finally yet importantly, the synthesis of Au(III) complex **51** was successful. Further new benzimidazolium ligand **49** as well as the respective Ag(I) and Au(I) complexes were also successfully synthesized and characterized by NMR spectroscopic methods, ESI-MS, elemental analysis, single crystal XRD as well as cyclic voltammetry. In combination with previously published gold-NHC-complexes, these compounds were tested for their antiproliferative properties in cancer cells applying the MTT assay. In these biological studies, complex **55** was found to be the most active complex in four out of three cancer cell lines with a significant selectivity for MCF-7 and A2780cisR cancer cells. Prior to these studies, the stability of these gold-NHC-complexes was assessed in cell culture medium as well as in presence of GSH. All complexes were found to be sufficiently stable for cell tests. In case of **51**, an interesting proton to deuterium exchange was observed opening new perspectives for future studies. As already reported for different compounds in medicinal chemistry, a deuteration might enhance the stability of the compounds, alter the metabolism and may provide insight into the mechanism of action. Therefore, the synthesis of deuterated NHC ligands and the corresponding transition metal complexes will be interesting for future investigations. Moreover, despite these gold-NHC-complexes, also the corresponding palladium(II)- and platinum(II)-NHC-complexes are promising for biological applications because they potentially provide an enhanced balance of stability and charge. Therefore, also studies for the synthesis as well as the biological evaluation of Pd(II)- and Pt(II)- NHC-complexes of the previously discussed ligand systems are ongoing. Furthermore, modifications of these ligands such as conjugation with biological targeting structures or coupling with e.g. sulfonyl groups or sugar-groups that are known to enhance water-solubility might be interesting for future investigations.

5 EXPERIMENTAL SECTION

5.1 General remarks

Unless otherwise states, all reagents were purchased from commercial sources and used without further purification. Air- and moisture-sensitive reaction were performed in heated glassware under argon atmosphere (Ar 5.0) with absolute solvents using either Schlenk techniques or a glovebox. The solvents as well as deuterated solvents were either dried using standard drying or distillation methods or obtained dry from a solvent purification system SPS-800 (*MBraun*). Water content was determined with a Karl-Fischer titration system. The oxygen dissolved in the thus obtained dry solvents was removed by three freeze-pump thaw cycles. Until further use, the solvents were stored under argon atmosphere over 3 Å or 4 Å molecular sieves (except for solvents known to react with molecular sieves like pyridine or acetone). Chromatographic separations were performed using silica gel (60-200 µm). NMR spectra were recorded with a BRUKER AVANCE DPX 400, a BRUKER AVANCE III 400, or a BRUKER AVANCE III 500C spectrometer at a temperature of 298 K unless otherwise stated. The spectra were referenced to the residual proton signals of ^{1}H and $^{13}C(^{1}H)$ signals of the solvents in parts per million (ppm). Abbreviations for NMR multiplicities are: singlet (s), doublet (d), triplet (t), quintet (qu.), multiplet (m), broad (b). Electrospray ionization mass spectra (ESI-MS) were measured using a THERMO SCIENTIFIC LCQ/FLEET spectrometer. UV-vis absorption spectra were acquired with an AGILENT TECHNOLOGIES CARY 60 UV-Vis spectrometer. Elemental analysis was performed by microcanalytical laboratory of the Technische Universität München and are given in mass percentages. The following compounds were synthesized according to previously published methods: **15**, **16** and $[Mo_2(OAc)_2(MeCN)_6](OTf)_2$ [115], **20**[124, 125], $Cr_2(OAc)_4$[127], **22** and **23**[126], $[Au(py)_2]BF_4$ and $[Au(py)_4](BF_4)_3$[131], **33**[132], **37** and **38**[139], **39** and **40**[140], cage ligands according to their functionalities: L-NH_2 [22], L-H[23], L-OH[22], L-Py[150]; **44** and **54**[157], **46** and **56**[202] , **50**[185] and **55**[186].

5.2 X-ray crystallographic measurements

Data were collected on a single crystal X-Ray diffractometer equipped with a CMOS detector (Photon 100), a rotating anode TXS and a Helios mirror optic using the APEX3 software package (**49**, **52** and **53**) or a single crystal x-ray diffractometer equipped with a CMOS detector (Bruker APEX III, κ-CMOS), an IMS microsource with MoKα radiation (λ = 0.71073 Å) and a Helios optic using the APEX3 software package (**17**, **18**, **19** and **51**).[209] Measurements were performed on single crystals coated with perfluorinated ether. The crystals were fixed on top of a kapton micro sampler and frozen under a stream of cold nitrogen. A matrix scan was used to determine the initial lattice parameters. Reflections were corrected for Lorentz and polarization effects, scan speed, and background using SAINT.[210]

Absorption correction, including odd and even ordered spherical harmonics was performed using SADABS or TWINABS.[211] Space group assignment was based upon systematic absences, E statistics, and successful refinement of the structure. The structures were solved using SHELXS or SHELXT with the aid of successive difference Fourier maps, and were refined against all data using SHELXL in conjunction with SHELXLE.[212, 213] Hydrogen atoms were calculated in ideal positions as follows: Methyl hydrogen atoms were refined as part of rigid rotating groups, with a C–H distance of 0.98 Å and Uiso(H) = 1.5·Ueq(C). Other H atoms were placed in calculated positions and refined using a riding model, with methylene and aromatic C–H distances of 0.99 Å and 0.95 Å, respectively, and other C–H distances of 1.00 Å, all with Uiso(H) = 1.2·Ueq(C). Non-hydrogen atoms were refined with anisotropic displacement parameters. Full-matrix least-squares refinements were carried out by minimizing Σw(Fo2 - Fc2)2 with the SHELXL weighting scheme.[212] Neutral atom scattering factors for all atoms and anomalous dispersion corrections for the non-hydrogen atoms were taken from International Tables for Crystallography.[214] A split layer refinement was used for disordered groups and additional SIMU, DELU, RIGU, ISOR and SAME restraints were used, if necessary. The unit cell of **53** contains one additional disordered molecule of dimethylformamide which was treated as a diffuse contribution to the overall scattering without specific atom positions using the PLATON/SQUEEZE procedure.[215] Images of the crystal structures were generated with Mercury and PLATON.[216, 217] The crystallographic data of **49**, **51**, **52** and **53** are provided free of charge by The Cambridge Crystallographic Data Centre.

5.3 Stability studies

The stability prior to evaluation in cancer cells was tested for complexes **51**, **53**, **54**, **55** and **56** by dissolving 6.20 µmol of the respective complex in 250 µL DMSO-d_6 and 250 µL deuterated RPMI1640 cell culture medium. The deuterated RPMI1640 medium was obtained by evaporating the aqueous solution to dryness under reduced pressure and dissolving the residual solids in D_2O. These samples were analyzed by ^{1}H NMR measurements after preparation (0 h), after 24 h incubation at 37 °C and after 48 h at 37 °C. The stability of these complexes in presence of GSH was analyzed by ^{1}H NMR as well as ESI-MS. The complexes were mixed with 4 equiv. of GSH in a solution of 100 µL DMSO-d_6 and 400 µL deuterated PBS. For complex **53**, a 1:1 mixture was used. The deuterated PBS was prepared in the same manner as the deuterated RPMI1640 medium. The thus prepared samples were evaluated by ^{1}H NMR after preparation (0 h), after 24 h at 37 °C and after 48 h at 37 °C. Afterwards, the samples were analyzed by ESI-MS.

5.4 MTT assays

HeLa, MCF-7, PC3 and A2780cisR cancer cells were cultured in RPMI1640 medium supplemented with 0.3 mg/L L-glutamine and 10 % FCS in an incubator at 37 °C, a relative humidity of 80 % and 5 % CO_2. In

order to maintain cisplatin resistance, the A2780cisR cells were incubated with medium containing 1.0 µM cisplatin every 2-3 passages. Cell medium was removed every 2-3 days and the cells were split at about 80 % confluence. HeLa, MECF-7 and PC3 cells were seeded in 96-well-plates in a concentration of 1 x 10^4 cells/mL. A2780cisR cells were seeded in a concentration of 8 x 10^4 cells/mL. All cells were seeded 24 h prior to drug exposure on 96-well-plates with two reference lanes (medium only (blank) and 100 % cells (no drugs added)) and eight lanes for different compound concentrations. For all complexes, stock solutions with an initial concentration of 10 mM (based on elemental composition) were prepared in DMSO and further diluted with cell culture medium. To prevent toxicity to cells, a final DMSO concentration of < 1 % is adjusted for each sample. 200 µL medium for reference cells and the different compound concentrations were added to the prepared cells. Then, the cells were incubated at 37 °C in the incubator for 48 h. Afterwards, 20 µL MTT (3-(4,5-dimethylthiazol-2-yl)-2,5-diphenyltetrazoliumbromide) was added to each well. After further incubation for 2-4 hours, the MTT-medium was removed and 150 µL DMSO were added. To ensure complete dissolution of the formazan crystals, the plates were shaken carefully for 10 min on a plate shaker. Then, the plates were read using a Tecan Infinite M Nano+ microplate reader at a wavelength of 570 nm. The background was subtracted at 630 nm. Cell survival was then determined as percentage by multiplying the absorbance of treated cells (minus absorbance blank) with 100 and dividing it by the absorbance of untreated cells (minus absorbance blank). Like that, a plot of the percentage of cell survival against the compound concentration was obtained which was applied calculating the IC_{50} values. All determinations were performed in independent triplicates resulting in average IC_{50} ± standard deviation values.

5.5 Electrochemical studies

Cyclic voltammograms were recorded using a Metrohm Autolab potentiostat with a gastight three-electrode cell under argon atmosphere. A glassy carbon electrode was applied as working electrode and polished prior to each measurement. A graphite stick was used as the counter electrode. The potential was measured against an Ag/AgCl (3.4 M KCl, 0.200 V vs. NHE) reference electrode and the scans were performed with a rate of 100 mV s−1. As electrolyte, a 0.1 M solution of *tetra-n*-butyl ammonium hexafluorophosphate in dried and degassed acetonitrile was applied. The concentration of the complexes were about 1 mg/mL. Ferrocene was applied as internal standard for referencing.

5.6 Synthetic procedures

5.6.1 $[Mo_2(OAc)_2(bipy)_2](OTf)_2$ (**19**)

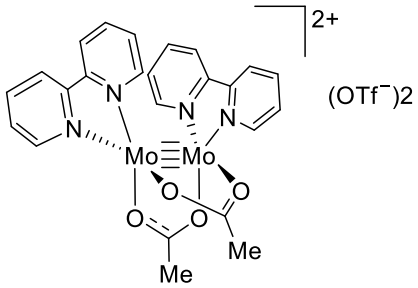

19
$C_{24}H_{22}Mo_2N_4O_4$
622.38 g/mol

$[Mo_2(OAc)_2(MeCN)_6](OTf)_2$ (50.0 mg, 0.065 mmol, 1 equiv.) was dissolved in 1.5 mL MeCN. After addition of 20.2 mg (0.13 mmol, 4 equiv.) bipyridine, the solution was stirred for one hour at room temperature. Crystals suitable for X-ray diffraction analysis were obtained by slow diffusion of diethyl ether into the acetonitrile solution.

^{1}H NMR (400 MHz, acetonitrile-d_3): δ (ppm) = 8.83 (d, 4H), 8.18 (d, 4H), 8.11 (td, 4H), 7.61 (td, 4H), 3.27 (s, 6H).

5.6.2 $[Cr(MeCN)_2](OTf)_2$ (**25**)

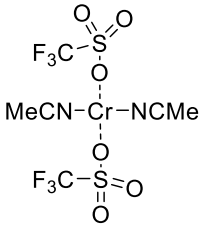

25
$C_6H_6CrF_6N_2O_6S_2$
432.23 g/mol

200 mg (5.85 mmol, 1 eqiuv.) was dissolved in a mixture of dry and degassed MeCN (1.0 mL) and DCM (2.0 mL). This is followed by addition of 0.5 mL HO_3SCF_3. The resulting blue suspension is stirred for 2 h at room temperature. The blue precipitate is isolated by filtration under argon atmosphere, washed with diethyl ether (3 x 5.0 mL), and dried *in vacuo* overnight.

Elemental analysis (%) calculated for $C_6H_6CrF_6N_2O_6S_2$: C 16.76; H 1.40; N 6.48; S 14.83; found: C 16.06, H 1.41; N 5.86; S 14.30.

5.6.3 1,3-bis(pyridin-3-ylethynyl)benzene iodine(III) benzene bistriflate (**34**)

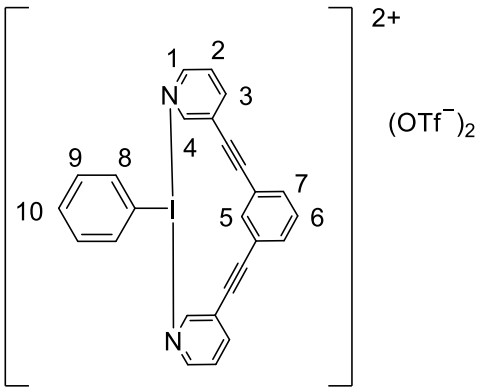

34
$C_{26}H_{17}N_2$
484.34 g/mol

The synthesis was performed according to a modified literature procedure under inert conditions.[132]

(Diacetoxy)iodobenzene (0.064 g, 0.20 mmol, 1.0 equiv.) was dissolved in 5 ml dry methylene dichloride. Trimethylsilyltriflate (0.10 ml, 0.40 mmol, 2.0 equiv.) was added dropwise at room temperature. This is followed by a dropwise addition of 1,3-bis(pyridin-3-ylethynyl)benzene (0.056 g, 0.20 mmol, 1.0 equiv.) in dry dichloromethane (5 ml) resulting in instantaneous precipitation of the product as a white solid, which was isolated by filtration and dried under reduced pressure.

^{1}H NMR (400 MHz, acetonitrile -d_3): δ (ppm) = 7.12-7.22 (m, 2H, H-9), 7.39 (dt, ^3J = 7.40 Hz, ^4J = 1.15 Hz, 1H, H-10), 7.59 (t, 1H, ^3J = 7.80 Hz, H-6), 7.73-7.80 (m, 4H, H-8, H-7), 7.89-7.92 (m, 1H, H-5), 8.08 (dd, ^3J = 8.2 Hz, ^3J = 5.9 Hz, 2H, H-2), 8.67 (dt, ^3J = 8.3 Hz, ^4J = 1.7 Hz, 2H, H-3), 8.71 (d, ^3J = 5.9 Hz, 2H, H-1), 8.89 (s, 2H, H-4);

^{13}C NMR (101 MHz, acetonitrile-d_3): δ (ppm) = 83.61, 94.66, 96.14, 120.57, 122.63, 123.17, 124.69, 128.69, 130.68, 131.42, 134.42, 135.88, 138.34, 141.87, 144.60, 149.93;

5.6.4 3,3'-(1,3-phenylenebis(ethyne-2,1-diyl))diisonicotinaldehyde (**36**)

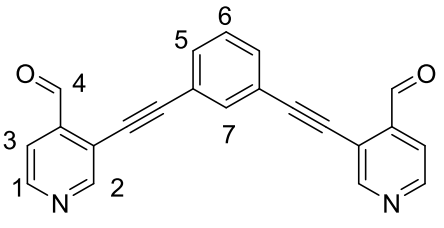

36
$C_{22}H_{12}N_2O_2$
336.35 g/mol

Diiodobenzene (0.038 g, 0.11 mmol, 1.0 equiv.), 3-ethynylisonicotinaldehyde **41** (0.061 g, 0.46 mmol, 4.0 equiv.), [PdCl2(PPh3)2] (0.008 g, 0.011 mmol, 0.10 equiv.) and CuI (0.002 g, 0.011 mmol, 0.10 equiv.) were dissolved in degassed triethylamine (10 ml) under argon atmosphere. The resulting solution was heated to 100 °C for 21 h. The solution was diluted with ethyl acetate and filtered over celite. The solvent was removed under reduced pressure and the crude product was purified using column chromatography (methylene dichloride : methanol 100:5, R_f = 0.4) to afford the product as an off-white solid (68 %).

^{1}H NMR (400 MHz, chloroform-d_1): δ (ppm) = 7.48 (t, ^3J = 7.7 Hz, 1H, H-6), 7.64 (dd, ^3J = 7.8 Hz, ^4J = 1.7 Hz, 2H, H-5), 7.75 (dd, ^3J = 5.0 Hz, ^4J = 0.9 Hz, 2H, H-3), 7.83 (t, ^4J = 1.6 Hz, 1H, H-7), 8.77 (dd, ^3J = 5.1 Hz, H-1), 9.00 (s, 2H, H-2), 10.62 Hz (d, ^4J = 0.8 Hz, 2H, H-4);

^{13}C NMR (124 MHz, chloroform-d_1): δ (ppm) = 83.31, 97.66, 119.73, 122.63, 125.46, 128.81, 132.84, 135.06, 140.79, 149.98, 154.80, 190.67;

ESI-MS (acetonitrile) m/z: [**36**+H]$^+$ calcd.: 337.10; found 337.25, [**36**+MeCN+H]$^+$ calcd.: 378.12; found: 378.34.

5.6.5 1,3-bis((4-(hept-1-en-1-yl)pyridin-3-yl)ethynyl)benzene (**37**)

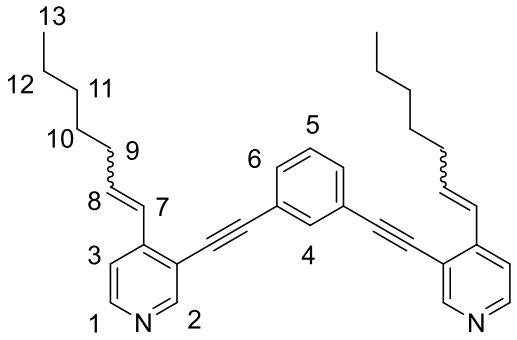

37
$C_{34}H_{36}N_2$
472.68 g/mol

Hexyltriphenylphosphonium bromide **42** (0.119 g, 0.28 mmol, 2.7 equiv.) was dissolved in dry THF in a heated Schlenk flask. *N*-butyl lithium was added dropwise at -80 °C (0.11 ml, 0.27 mmol, 2.6 equiv., 2.5 M solution in hexane) under argon atmosphere resulting in a color change to deep yellow. The solution was stirred for 2 h at -80 °C before aldehyde **36** (0.035 g, 0.10 mmol, 1.0 equiv.) was added dropwise as a solution in dry THF resulting in discoloration. The solution was allowed to warm to room temperature overnight under continuous stirring. 100 ml of water were added and the solution was extracted with diethyl ether (3 x 30 mL). The combined organic layers were washed with brine and the solvent was removed under reduced pressure. The product was isolated by column chromatography (pentane:ethyl acetate 2:1, R_f = 0.7). A separation of a 2:1 mixture of ZZ:EZ isomers was obtained as a brownish oil (33 %).

^{1}H NMR (400 MHz, methylene chloride-d_2): δ (ppm) = 0.77-0.93 (m, aliphatic region), 1.17-1.44 (m, aliphatic region), 2.14-2.20 (m, aliphatic region), 2.25-2.38 (m, aliphatic region), 5.95-6.11 (m, H-8), 6.69 (d, ^3J = 11.6 Hz, H-7, H-8), 6.83-6.91 (m, H-7), 7.29 (d, ^3J = 5.2 Hz, H-3), 7.41 (d, ^3J = 7.2 Hz, H-5), 7.55 (d, ^3J = 7.7 Hz, H-6), 7.73 (s, H-4), 8.40-8.57 (m, H-1), 8.73 (s, H-2);

^{1}H NMR (500 MHz, dimethylsulfoxide-d_6): δ (ppm) = 0.77-0.89 (m, aliphatic region), 1.10-1.37 (m, aliphatic region), 1.38-1.56 (m, aliphatic region), 2.24-2.35 (m, aliphatic region), 6.04 (dt, ^3J = 11.8 Hz, ^3J = 7.4 Hz, H-8), 6.66-6.73 (m, H-7, H-8), 6.79-6.91 (m, H-7), 7.40 (d, ^3J = 5.2 Hz, H-3), 7.50-7.58 (m, H-5), 7.62-7.75 (m, H-6), 7.78 (s, H-4), 7.81 (s, H-4), 8.47 (d, ^3J = 5.3 Hz, H-1), 8.55 (d, ^3J = 5.1 Hz, H-1), 8.71 (s, H-2), 8.76 (s, H-2);

^{13}C NMR (101 MHz, dimethylsulfoxide-d_6): δ (ppm) = 13.92, 21.99, 28.66, 30.80, 73.48, 86.00, 95.06, 109.48, 118.29, 122.99, 124.96, 129.58, 132.05, 134.02, 138.39, 146.30, 149.18, 152.64;

ESI-MS (acetonitrile) m/z: [**37**+H]+ calcd.: 473.30; found: 473.59, [**37**+H+MeCN]+ calcd.: 514.71; found: 514.35.

5.6.6 Hexyltriphenylphosphonium bromide (**42**)

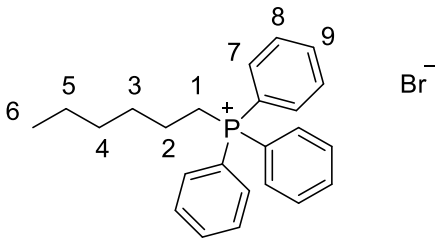

42
$C_{24}H_{28}BrP$
427.37 g/mol

The reaction was performed following a modified procedure.[141]

N-Hexylbromide (1.40 ml, 10.0 mmol, 1.0 equiv.) and triphenylphosphine (2.62 g, 10.0 mmol, 1.0 equiv.) were heated in toluene to reflux for 6 h. The solution was concentrated and diethyl ether was added. The resulting white solid was isolated by filtration and washed with diethyl ether to yield **42** (5 %).

^{1}H NMR (400 MHz, methylene chloride-d_2): δ (ppm) = 0.86 (t, ^3J = 6.9 Hz, 3H, H-6), 1.25-1.31 (m, 4H, H-5, H-4), 1.60-1.72 (m, 4H, H-3,H-2), 3.38-3.48 (m, 2H, H-1), 7.69-7.90 (m, 15H, H-7, H-8, H-9);

5.6.7 Calix[4]benzimidazolium trifluoromethanesulfonate (**49**)

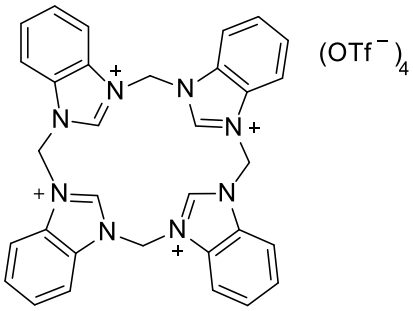

49
$C_{36}H_{28}F_{12}N_8O_{12}S_4$
1120.88 g/mol

A flask charged with methylenebisbenzimidazole (12.2 g, 49.1 mmol, 1 equiv.) dissolved in 1.6 L of dry MeCN is rigorously stirred while cooled in an ice bath. Methylene-bis(trifluoromethanesulfonate) (16.1 g, 51.6 mmol, 1.05 equiv.) is diluted in 40 mL dry MeCN , cooled to -18°C and slowly added within 2 h using a dropping funnel. After complete addition, the clear mixture is allowed to warm to room temperature and stirred overnight. The yellow solution is evaporated *in vacuo*. The crude product is washed six times with acetone yielding a white precipitate. After drying *in vacuo,* the product is obtained as white powder (6.86 g, 38 % yield).

^{1}H NMR (400 MHz, DMSO-d6): δ (ppm) = 7.84 (s, 8H, N-CH2-N), 7.85 – 7.90 (m, 8H, Carom.-H), 8.56 – 8.70 (m, 8H, Carom.-H), 10.72 (s, 4H, N-CH-N).

^{13}C NMR (101 MHz, DMSO-d6): δ (ppm) = 54.62(N-CH2-N), 114.01(Carom.), 120.63(q, JCF = 322.3 Hz, OTf), 129.06(Carom.), 130.10(Carom.), 145.02(N-CH-N).

ESI-MS (acetonitrile): m/z [1,3-bis((benzimidazol-1-yl)methyl)-benzimidazol-3-ium]$^{+}$ calcd: 379.17; found: 379.08, [**49**-4OTf·3MeCN]$^{4+}$ calcd: 161.83; found: 160.91, [**49**-4OTf]$^{4+}$ calcd: 131.06; found: 130.94;

Elemental analysis (%) calcd. for $C_{36}H_{28}F_{12}N_8O_{12}S_4$: C 38.58; H 2.52; N 10.00; S 11.44; Found: C 38.32; H 2.50; N 9.79; S 11.49.

5.6.8 Calix[4]imidazolyl-Au(III) hexafluorophosphate (**51**)

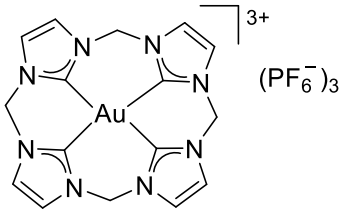

51
$C_{18}H_{20}AuF_{18}N_8P_3$
980.27 g/mol

NaCl (12.9 mg, 0.221 mmol, 1.0 eq.), NaOAc (27.2 mg, 0.332 mmol, 1.5 equiv.), $Au(OAc)_3$ (82.7 mg, 0.221 mmol, 1.0 equiv.) and 200 mg (0.221 mmol, 1.0 equiv.) **44** are suspended in 5 mL dry and degassed DMSO. The mixture is stirred at 100 °C for 4 h. Subsequently, the orange reaction mixture is centrifuged and filtered on air. MeCN is added to the DMSO solution until a volume mixture of 1:1 (MeCN:DMSO) is reached. By addition of diethyl ether, a light brown precipitate forms. The precipitate is washed with MeCN (3 x 10 mL) and DCM (2 x 10 mL). After dissolving the precipitate in water, the addition of 71.7 mg (4.0 equiv.) NH_4PF_6 gives a light brown solid, which is washed with water (3 x 10 mL) and dried under vacuum to give 1 as a light brown solid (23.0 mg, 11 %).

^{1}H NMR (400 MHz, acetonitrile-d_3): δ (ppm) = 6.68 (s, 8H, C*H*$_2$), 7.91 (s, 8H, *H*Im);

^{13}C NMR (101 MHz, acetonitrile-d_3): δ (ppm) = 66.78 (N-*C*H$_2$-N), 125.34 (CIm), 144.33 (N-$C_{carbene}$-N);

^{19}F NMR (376 MHz, acetonitrile-d_3): δ (ppm) = -70.13 (d, J_{FP} = 711.3 Hz);

^{31}P NMR (162 MHz, acetonitrile-d_3): δ (ppm) = -144.65;

ESI-MS (acetonitrile): m/z [**51**-2PF_6]$^{2+}$ calcd.: 331.04; found: 331.23, [**51**-PF_6]$^+$ calcd.: 807.04; found: 807.08;

Elemental analysis (%) calcd for $AuC_{16}H_{16}N_8P_3F_{18}$ + 0.075 DMSO: C, 20.25; H, 1.73; N, 11.70; S 0.25; Found: C, 20.46; H, 1.92; N, 11.55; S 0.25.

5.6.9 Calix[4]benzimidazolyl-Ag(I) trifluoromethanesulfonate (**52**)

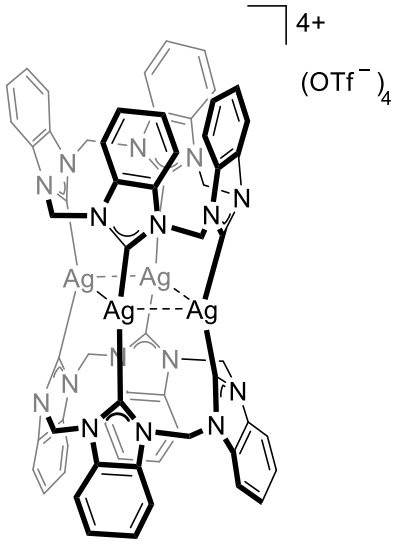

52
$C_{68}H_{48}Ag_4F_{12}N_{16}O_{12}S_4$
2068.93 g/mol

49 (100 mg, 89.0 µmol, 1.0 equiv.) is dissolved in 22 mL dry MeCN. Silver(I) oxide (207 mg, 892 µmol, 10.0 equiv.) is added and the black suspension is stirred at room temperature in the dark for 17 h. The mixture is filtered using a *Whatman* filter. The solid is discarded and the filtrate precipitated upon the addition of 40 mL diethyl ether. The suspension is filtered and the solid is washed two times with 10 mL diethyl ether. The sample is redissolved in 3 mL MeCN. A dark solid is precipitated upon fractional precipitation using diethyl ether and discarded using centrifugation. Subsequently, a tan solid is precipitated by addition of diethyl ether. After drying *in vacuo*, the product is obtained as a tan powder in a yield of 39.5 mg (19.1 µmol, 43 %).

^{1}H NMR (400 MHz, dimethylsulfoxide-d_6): δ (ppm) = 7.47 – 7.55 (m, 16 H, $C_{arom.}$-H), 7.58 (d, ^{2}J = 15.0 Hz, 8 H), 7.71 (d, ^{2}J = 15.2 Hz, 8 H), 8.38 – 8.55 (m, 16 H, $C_{arom.}$-H).

^{13}C NMR (126 MHz, dimethylsulfoxide-d_6): δ (ppm) = 60.52 (N-CH_2-N), 112.56 ($C_{arom.}$), 120.68 (q, $^{1}J_{19F13C}$ = 322.29 Hz, OTf), 125.05 ($C_{arom.}$), 133.45 ($C_{arom.}$), 194.28 ($^{1}J_{109Ag\text{-}13C}$ = 212.9 Hz, $^{1}J_{107Ag\text{-}13C}$ = 185.7 Hz, N-$C_{carbene}$-N).

ESI-MS (m/z): [**52**-4OTf]$^{4+}$ calcd: 368.01; found: 368.50;

Elemental analysis (%) calcd for $C_{68}H_{48}F_{12}N_{16}Ag_4O_{12}S_4$: C 39.48; H 2.34; N 10.89; S 6.20; Found: C 38.65; H 2.62; N 10.52; S 5.85.

5.6.10 Calix[4]benzimidazolyl-Au(I) trifluoromethanesulfonate (**53**)

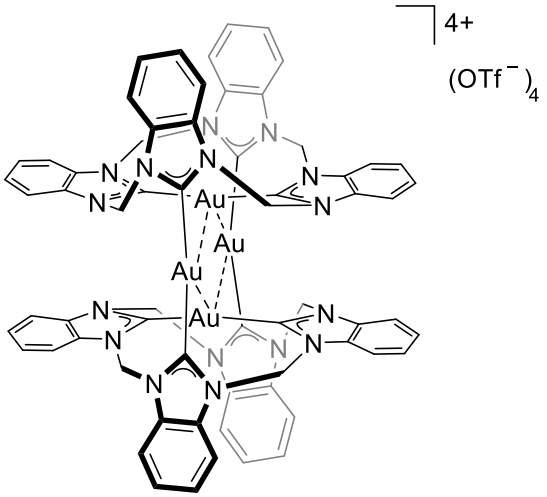

53
$C_{68}H_{48}Au_4F_{12}N_{16}O_{12}S_4$
2425.32 g/mol

49 (150 mg, 134 µmol, 2.0 eqiv.) is dissolved in 12 mL of dry DMSO with Au(THT)Cl (86.6 mg, 270 µmol, 4.04 equiv.) and NaOAc (55.0 mg, 670 µmol, 10 equiv.). The mixture is stirred for 16 h at 70 °C. The sample is reduced to a volume of 1.5 mL *in vacuo* at 70 °C. Upon addition of 40 mL MeOH, an off-white precipitate formed within 2 h of stirring. The suspension is centrifuged and the solid is washed with MeOH (2 x 3 mL). The sample is dissolved in 40 mL MeCN and filtered over celite. The solvent is reduced to approximately 3 mL and 40 mL of diethyl ether are added. The suspension is centrifuged and washed two times with 3 mL diethyl ether each. After drying *in vacuo*, the product is obtained as a white powder in a yield of 50.4 mg (21.0 µmol, 31 %).

^{1}H NMR (400 MHz, dimethylsulfoxide-d_6): δ (ppm) = 6.97 – 7.07 (m, 8 H, $C_{arom.}$-*H*), 7.07 – 7.16 (m, 8 H, $C_{arom.}$-*H*), 7.33 (d, ^2J = 14.6 Hz, 8 H, N-CH_2-N), 7.68 (d, ^2J = 14.6 Hz, 8 H, N-CH_2-N), 7.75 – 7.85 (m, 8 H, $C_{arom.}$-*H*), 8.42 – 8.56 (m, 8 H, $C_{arom.}$-*H*).

^{13}C NMR (101 MHz, dimethylsulfoxide-d_6): δ (ppm) = 58.79 (N-CH_2-N), 111.86 ($C_{arom.}$), 112.64 ($C_{arom.}$), 126.29 ($C_{arom.}$), 126.53 ($C_{arom.}$), 132.24 ($C_{arom.}$), 132.78 ($C_{arom.}$), 180.06 (N-$C_{carbene}$-N), 190.80 (N-$C_{carbene}$-N).

ESI-MS (m/z): [**53**-4OTf]$^{4+}$ calcd: 457.07; found: 457.48, [**53**-3OTf]$^{4+}$ calcd: 659.08; found: 659.37;

Elemental analysis (%) calcd for $C_{68}H_{48}F_{12}N_{16}O_{12}S_4$ + 0.5 DMSO: C 33.63; H 2.09; N 9.09; S 5.85; Found: C 33.07; H 2.14; N 8.90; S 5.64.

6 Supplementary Data

6.1 Crystallographic data

Table **6**: Crystallographic details of compounds **17**, **18**, **19**, and **49**.

	17 + 18	**19**	**49**
formula	$C_{24}H_{27}BF_6Mo_2N_6O_2$	$C_{13}H_{11}F_3NoN_2O_5S$	$C_{36}H_{28}F_{12}N_8O_{12}S_4$
CCDC number			1944345
formula weight	1496.59	460.24	1120.88
color/habit	clear dark red fragment	Clear red block	Colorless fragment
crystal dimensions [mm^3]	0.134 x 0.142 x 0.423	0.065 x 0.120 x 0.123	0.124 x 0.277 x 0.332
crystal system	monoclinic	Monoclinic	triclinic
space group	P 1 21/n 1	C 1 2/c 1	P -1
a [Å]	11.020(3)	12.790(7)	10.249(5)
b [Å]	23.585(7)	15.094(8)	11.021(6)
c [Å]	11.315(3)	16.982(8)	13.965(6)
α [°]	90	90	88.26(2)
β [°]	95.676(15)	97.85(2)	72.19(2)
γ [°]	90	90	85.185(14)
V [Å^3]	2926.4(14)	3248.(3)	1496.5(12)
Z	2	8	2
T [K]	99.99	100.05	293(2)
D_{calcd} [g/cm^{-3}]	1.698	1.883	1.568
μ [mm^{-1}]	0.928	0.996	0.273
F(000)	1488	1824	728
θ range [°]	1.73 to 29.13	2.10 to 26.43	1.85 to 26.75
index range (h, k, l)	−15 ≤ h ≤ +15 −32 ≤ k ≤ +32 −15 ≤ l ≤ +15	−15 ≤ h ≤ +15 −18 ≤ k ≤ +18 −21 ≤ l ≤ +21	-12 ≤ h ≤ +12 -13 ≤ k ≤ +13 -17 ≤ l ≤ +17
Reflections collected	91717	54141	90921
no. of indep reflns/R_{int}	7883/0.0582	3335/0.0452	6340/0.0925
No. of obsd reflns (*I*>2σ(I))	6971	2903	5243
no. of data/ restraints/params	7883/157/469	3335/0/227	6340/348/520
R1/wR2 (*I*>2σ(I))	0.0341/0.0854	0.0224/0.0482	0.0456/0.1105
R1/wR2 (*all data*)	0.0414/0.0883	0.0297/0.0509	0.0591/0.1198
GOF (on F^2)	1.229	1.024	1.074
Largest diff peak and hole [e Å^{-3}]	0.643 and -0.671	0.582 and -0.452	0.746 and -.550

Table **7**: Crystallographic details of compounds **51**, **52** and **53**.

	51	**52**	**53**
formula	$C_{16}H_{16}AuClF_{12}P_2$	$C_{68}H_{48}Ag_4F_{12}N_{16}O_{12}S_4$	$C_{68}H_{48}Au_4F_{12}N_{16}O_{12}S_4$
CCDC number	1944344	1944347	1944346
formula weight	842.72	2068.93	2425.32
color/habit	Clear pale yellow fragment	Clear orange fragment	Clear yellow fragment
crystal dimensions [mm^3]	0.194 x 0.296 x 0.419	0.084 x 0.113 x 0.472	0.039 x 0.041 x 0.103
crystal system	orthorhombic	Triclinic	Triclinic
space group	Cmcm	P -1	P -1
a [Å]	23.721(3)	11.7540(8)	12.3978(7)
b [Å]	11.1411(12)	14.5132(10)	12.7838(7)
c [Å]	12.4837(13)	15.3083(11)	16.2846(9)
α [°]	90	66.978(2)	67.459(2)
β [°]	90	88.564(2)	85.945(2)
γ [°]	90	72.316(2)	84.111(2)
V [Å^3]	3299.2(7)	2276.7(3)	2369.8(2)
Z	4	1	1
T [K]	100(2)	119(2)	100(2)
D_{calcd} [g/cm^{-3}]	1.654	1.728	1.904
μ [mm^{-1}]	4.725	1.038	6.356
F(000)	1608	1185	1312
θ range [°]	2.60 to 26.43	2.20 to 25.68	2.49 to 28.70
index range (h, k, l)	–29 ≤ h ≤ +29 –13 ≤ k ≤ +13 –15 ≤ l ≤ +15	-14 ≤ h ≤ +14 -17 ≤ k ≤ +17 -18 ≤ l ≤ +18	-16 ≤ h ≤ +16 -17 ≤ k ≤ +17 -21 ≤ l ≤ +21
Reflections collected	24519	68072	130457
no. of indep reflns/R_{int}	1822/0.1068	8642/0.0348	12237/0.0585
No. of obsd reflns (*I*>2σ(I))	1543	7693	10218
no. of data/ restraints/params	1822/0/105	8642/348/737	12237/733/811
R1/wR2 (*I*>2σ(I))	0.0666/0.1848	0.0315/0.0719	0.0266/0.0627
R1/wR2 (*all data*)	0.0854/0.1956	0.0374/0.0747	0.0373/0.0671
GOF (on F^2)	1.135	1.053	1.028
Largest diff peak and hole [e Å^{-3}]	2.891 and -1.018	1.131 and -1.138	1.857 and -1.567

6.2 NMR and ESI-MS data

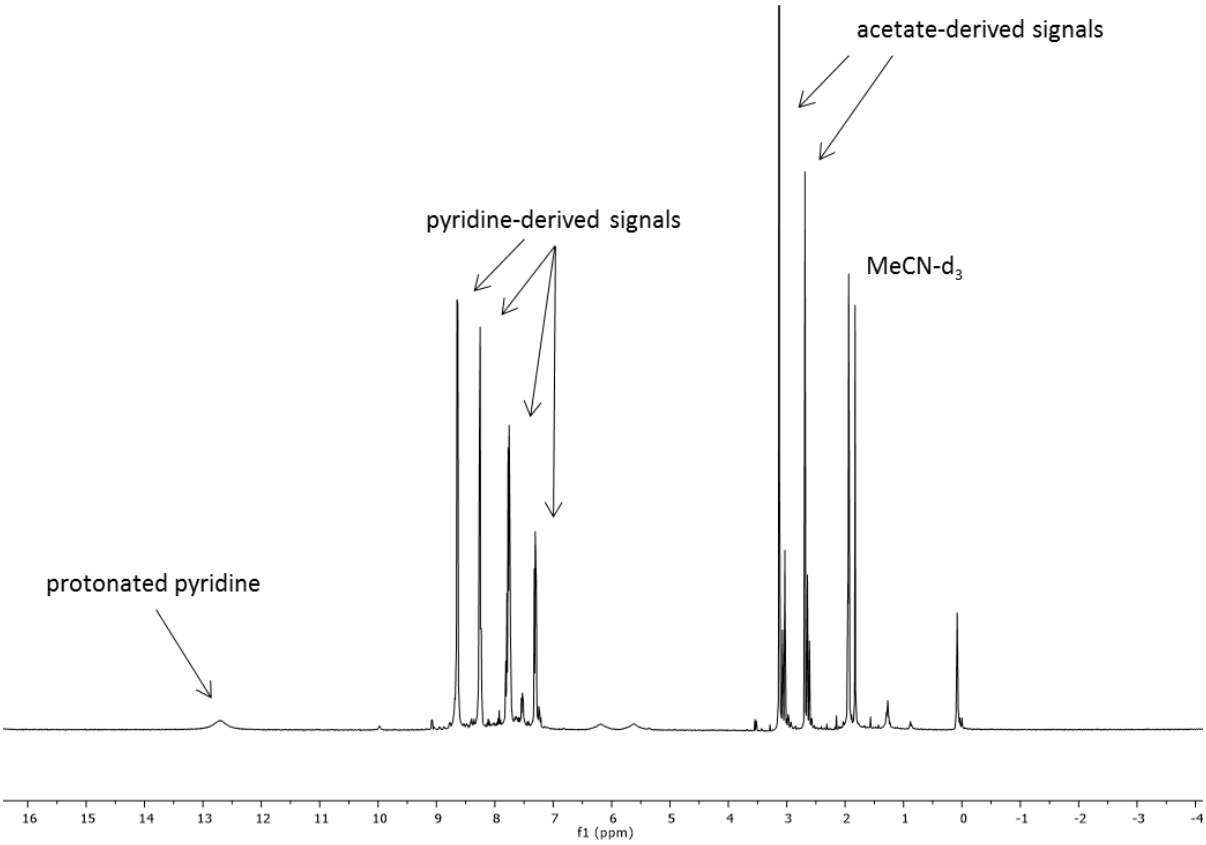

Figure **S1**: ^{1}H NMR spectrum in MeCN-d_3 of the reaction intended to yield $[Mo_2(OAc)_2(py)_6](OTf)_2$.

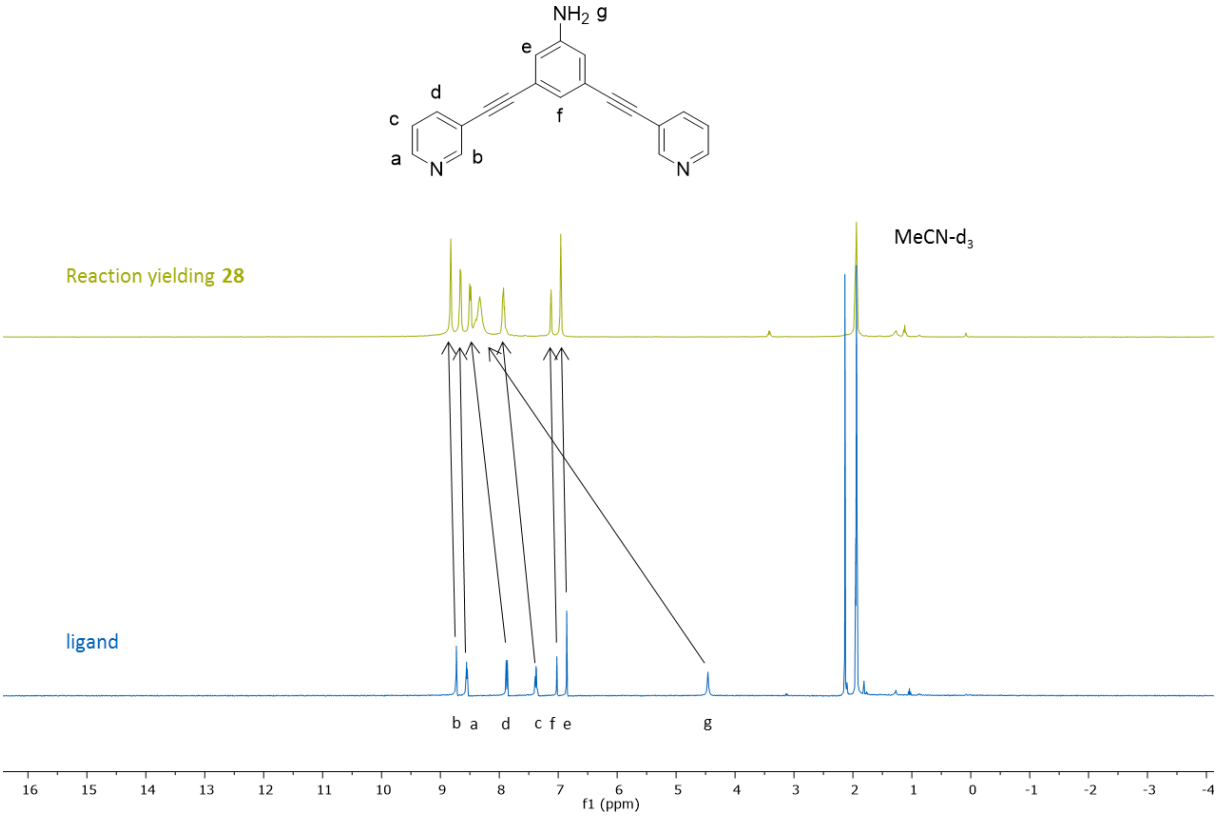

Figure **S2**: Comparison of ^{1}H NMR shifts of the free ligand and reaction yielding compound **28** determined in MeCN-d_3.

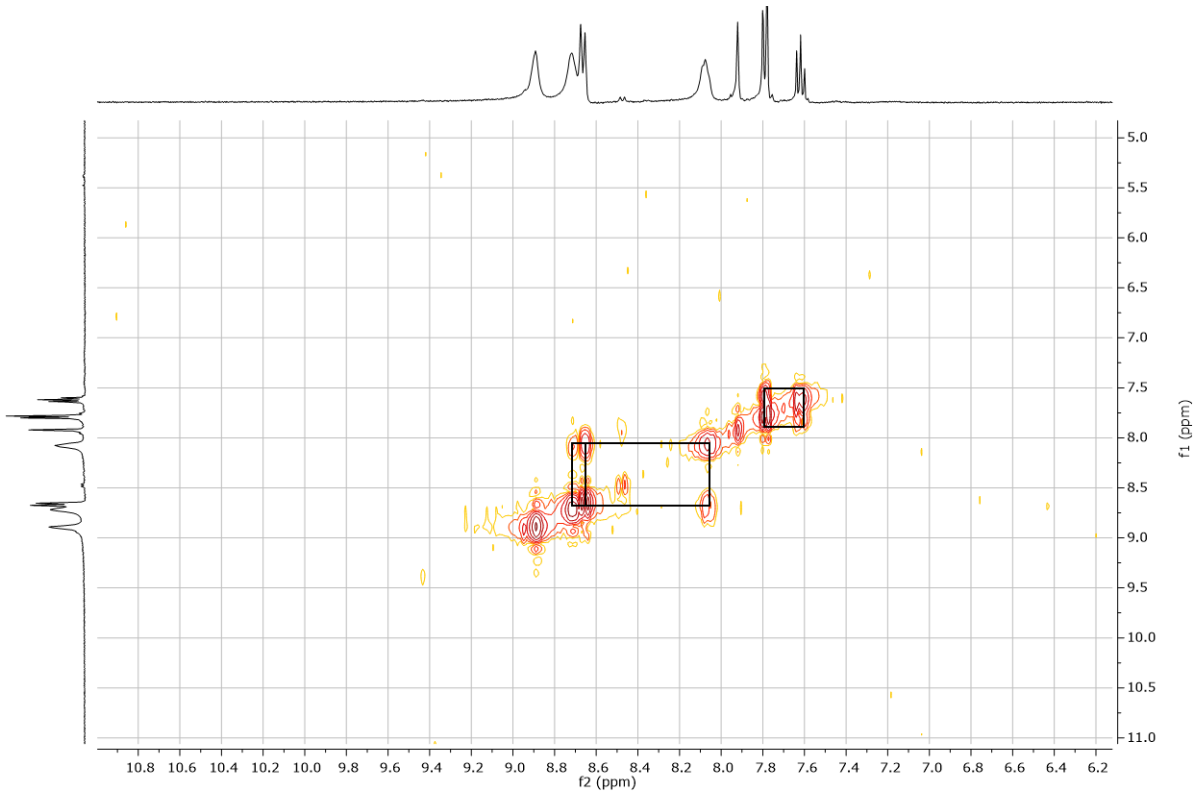

Figure **S3**: 2D COSY NMR spectrum of **30** determined in MeCN-d_3.

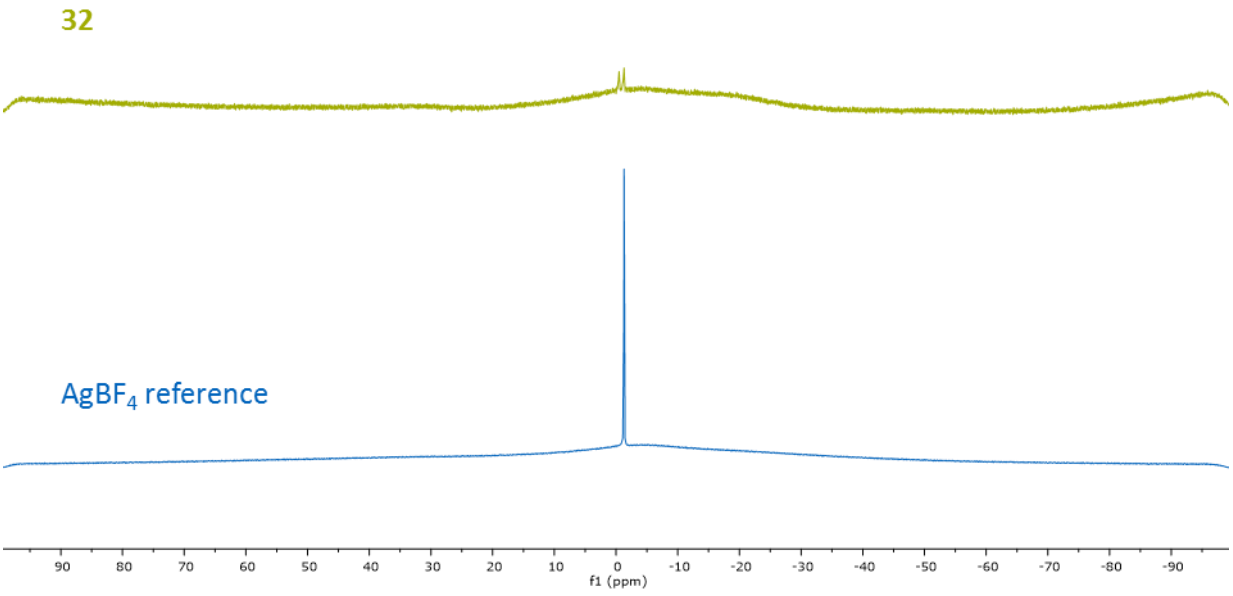

Figure **S4**: ^{11}B NMR spectra of reaction product **32** in comparison to $AgBF_4$ determined in DMSO-d_6.

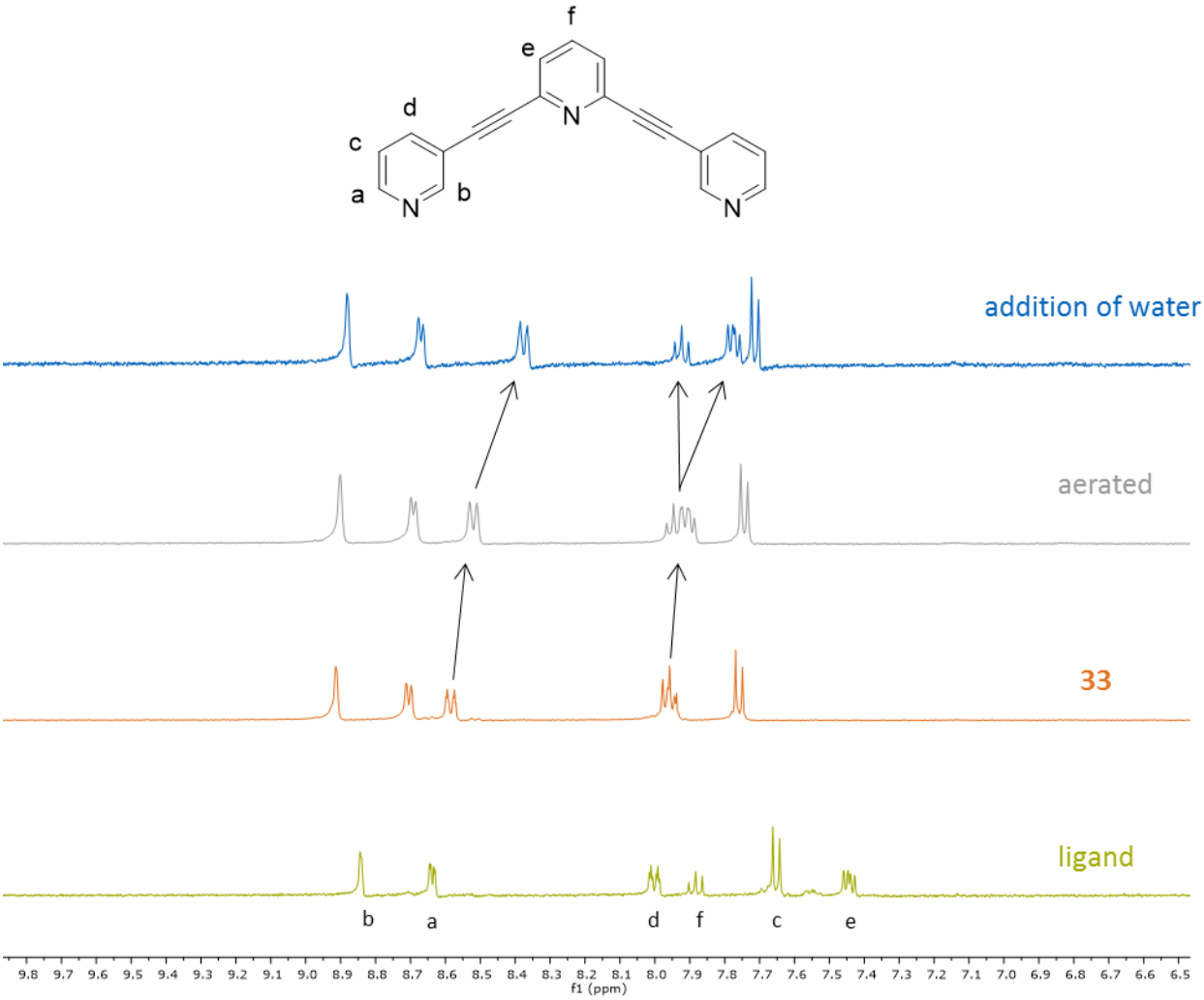

Figure **S5**: Comparison of ^{1}H NMR spectra of the respective free ligand, reaction **33**, reaction **33** in presence of air and reaction **33** exposed to water.

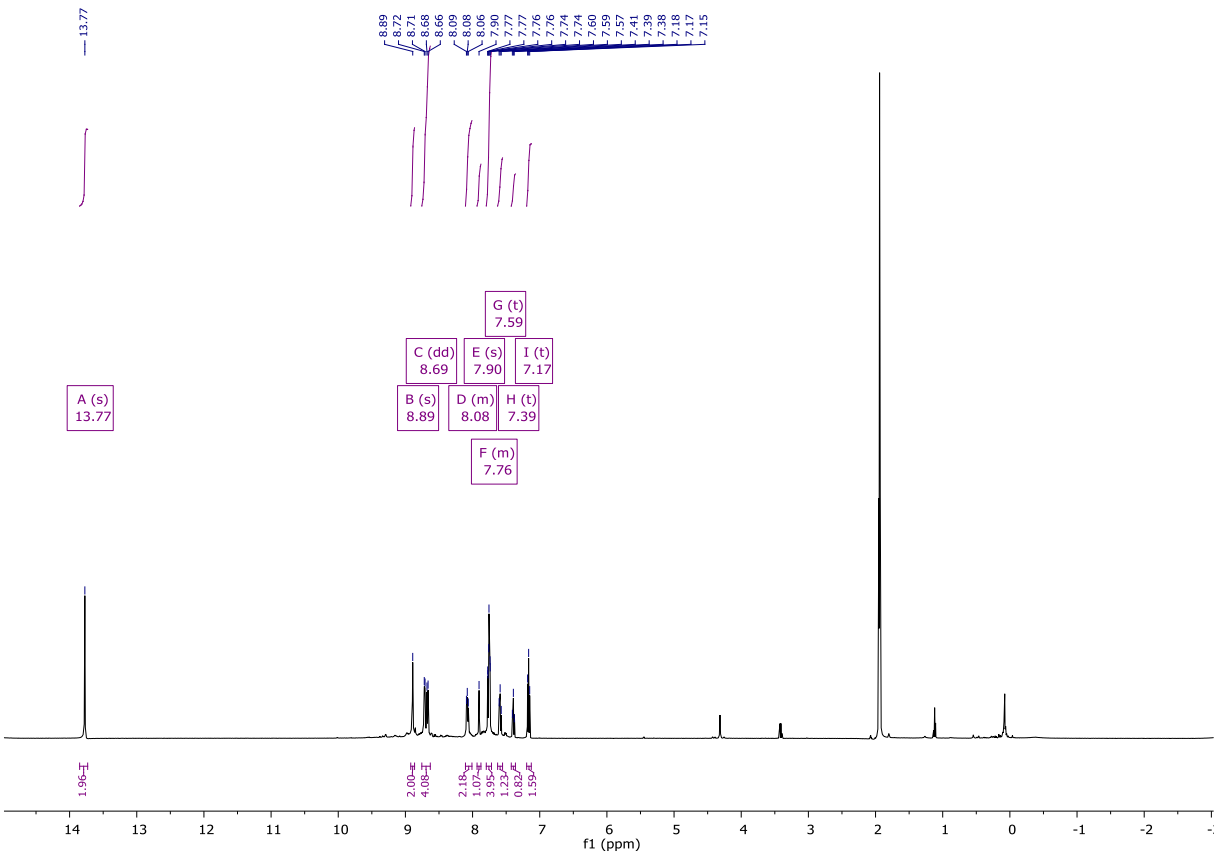

Figure **S6**: ^{1}H NMR spectrum of **34** in MeCN-d_3.

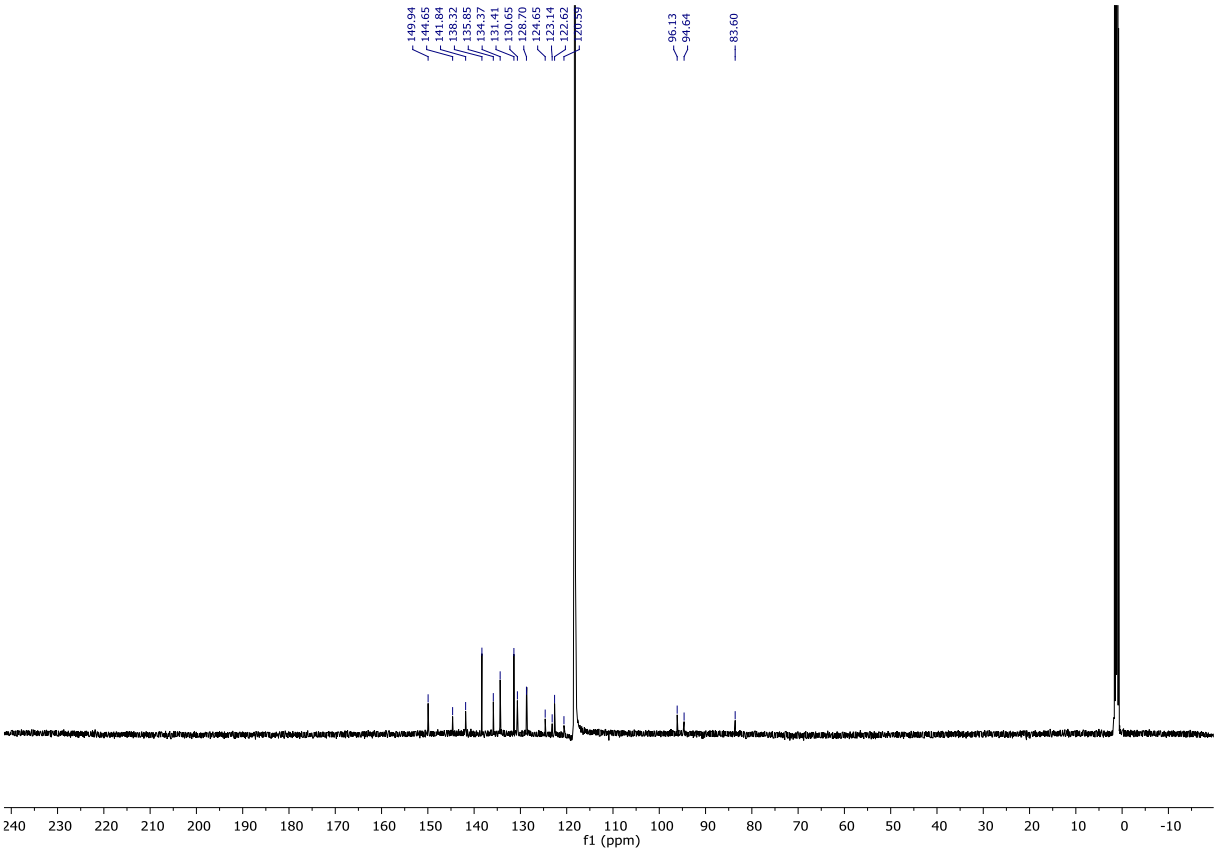

Figure **S7**: ^{13}C NMR spectrum of **34** in MeCN-d_3.

Figure **S8**: 2D COSY NMR spectrum of **34** in MeCN-d_3.

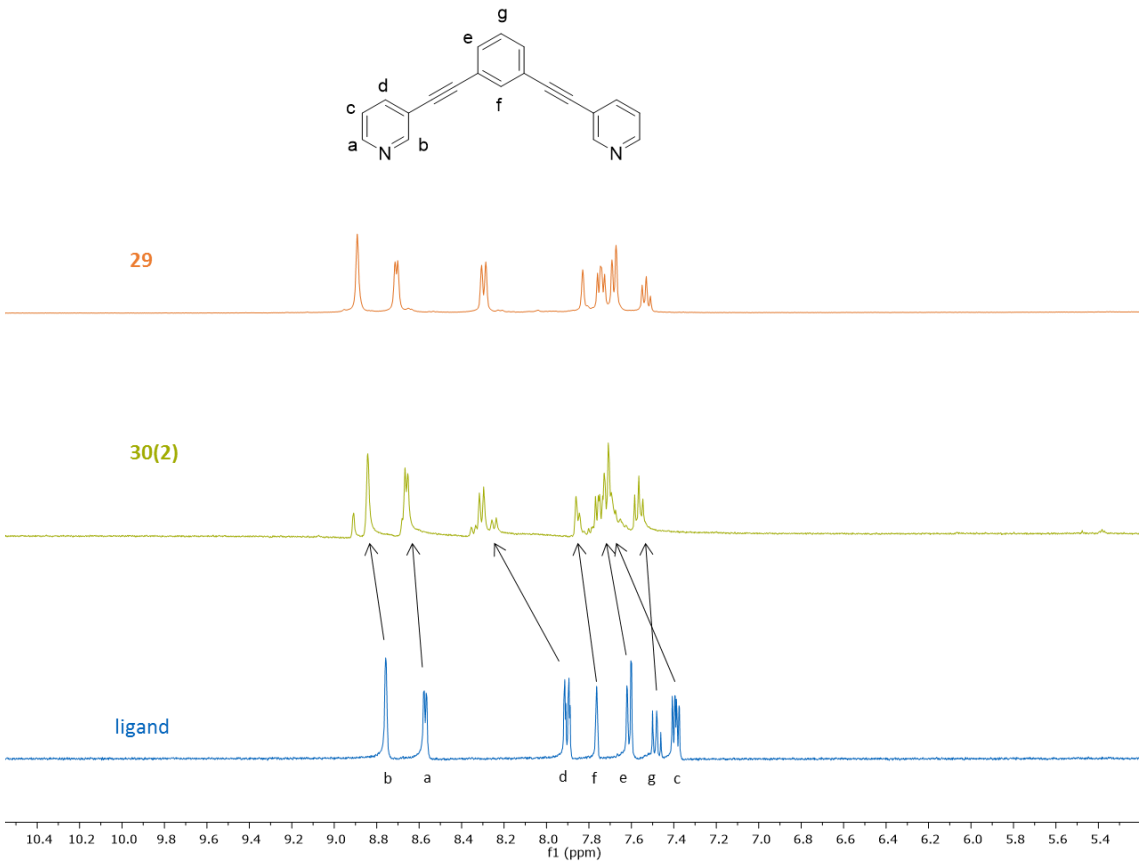

Figure **S9**: ^{1}H NMR spectra of **30(2)** in comparison to the free ligand, the reaction product and metallacycle **29** determined in MeCN-d_3.

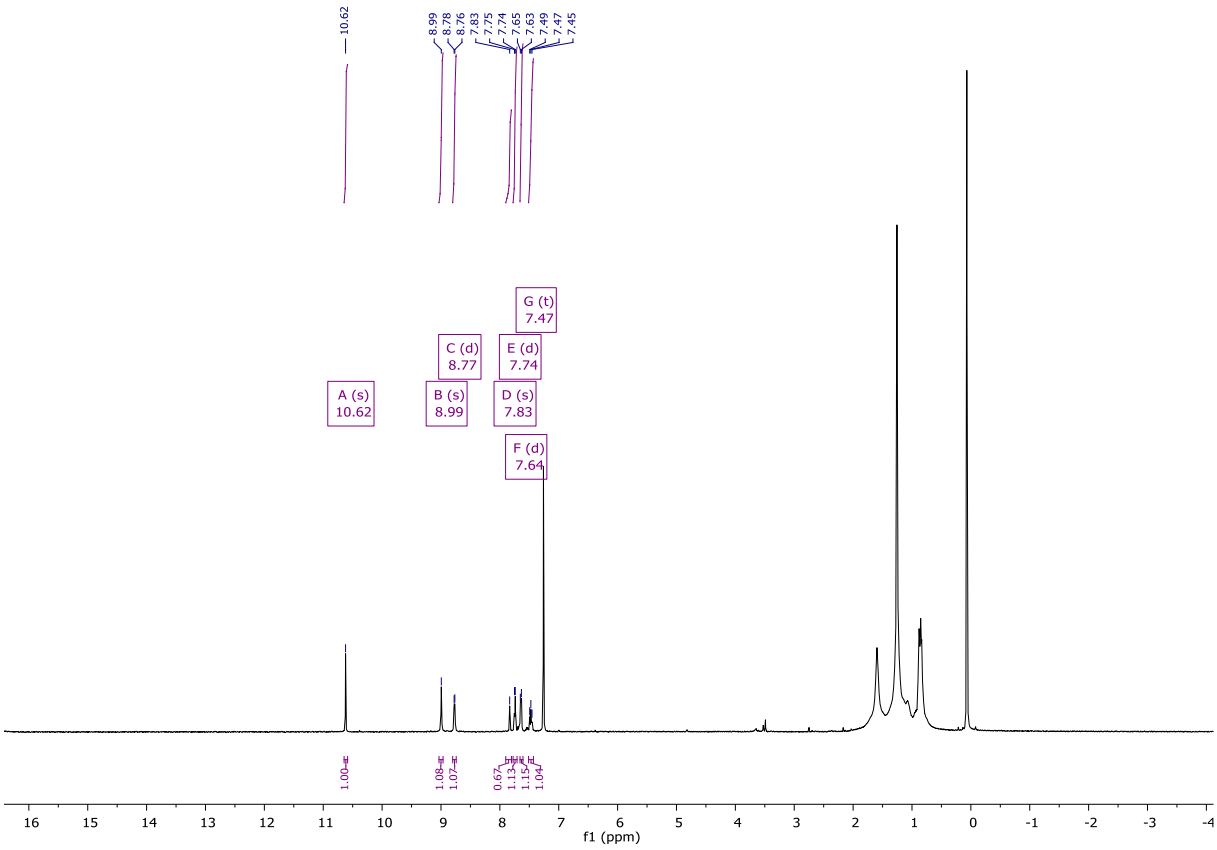

Figure **S10**: ^{1}H NMR spectrum of ligand **36** in chloroform-d_1.

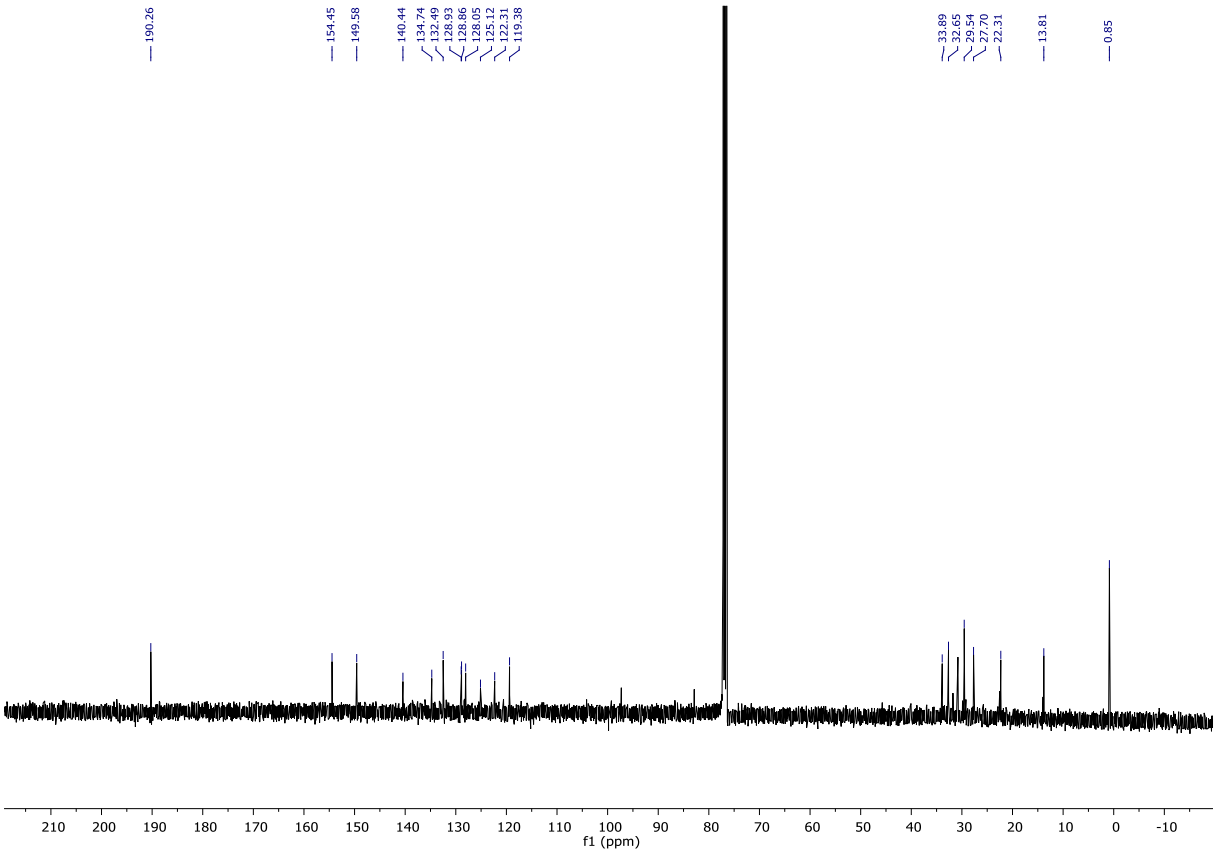

Figure **S11**: ^{13}C NMR spectrum of ligand **36** in chloroform-d_1.

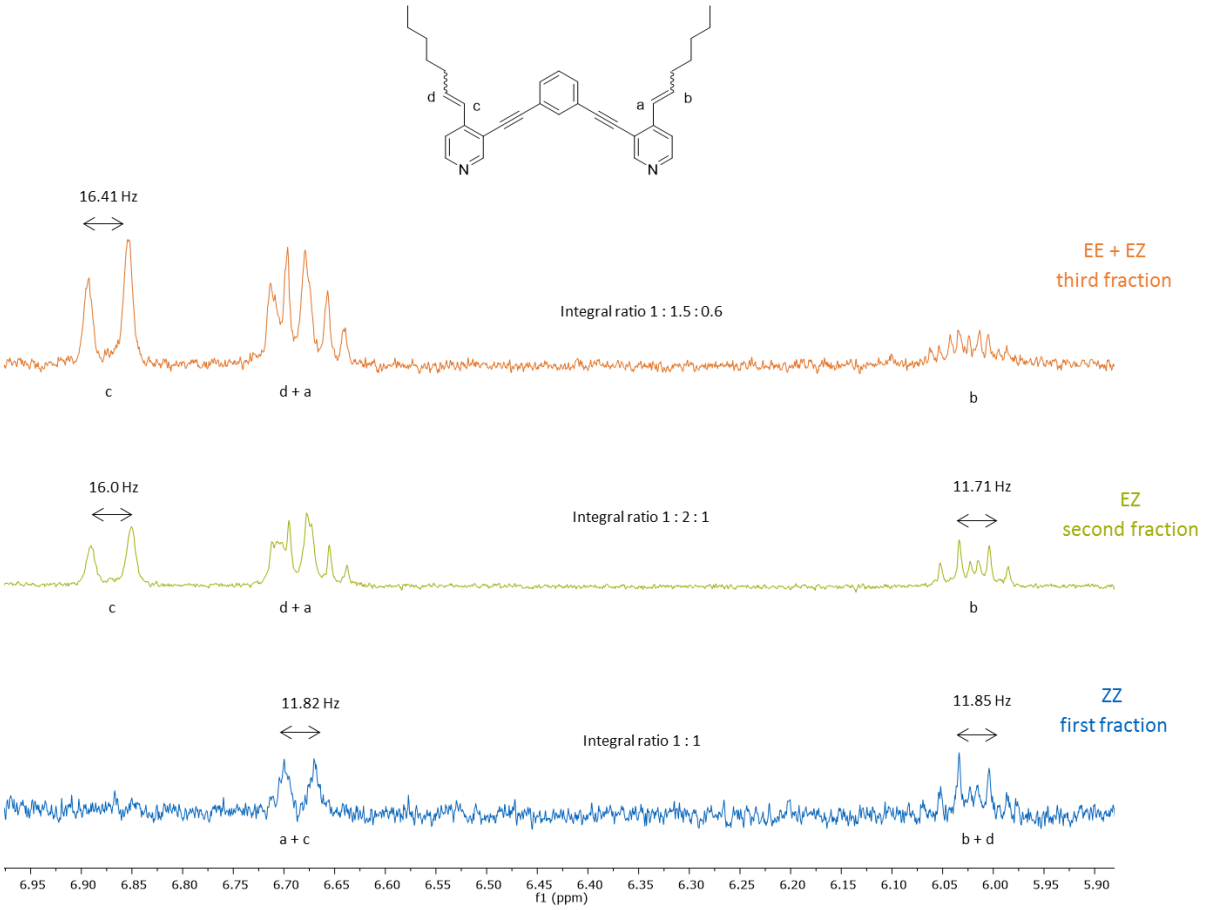

Figure **S12**: ^{1}H NMR spectra in methylene chloride-d_2 of the different eluted fractions of ligand **37** with the assignments for the different isomers and isomeric mixtures according to the determined coupling constant.

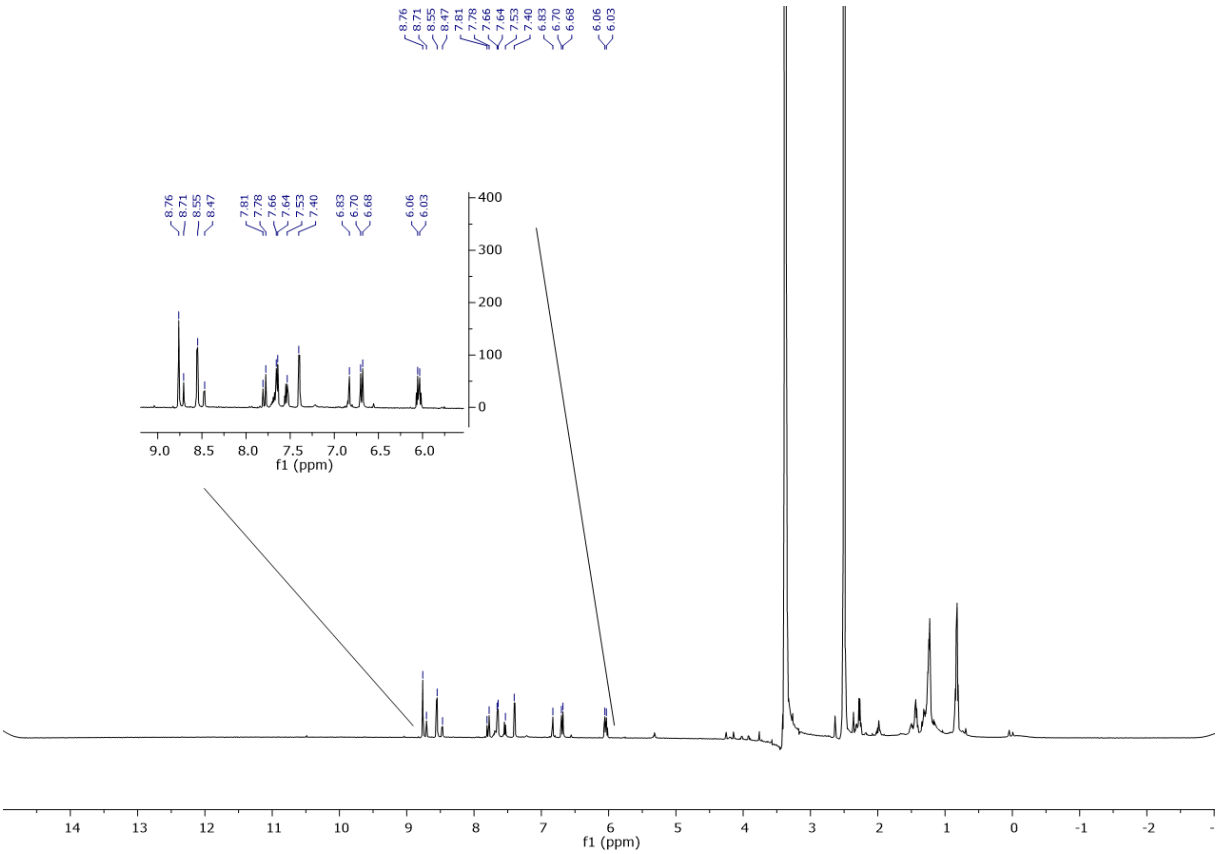

Figure **S13**: Cryo ^{1}H NMR spectrum in DMSO-d_6 of ligand **37**.

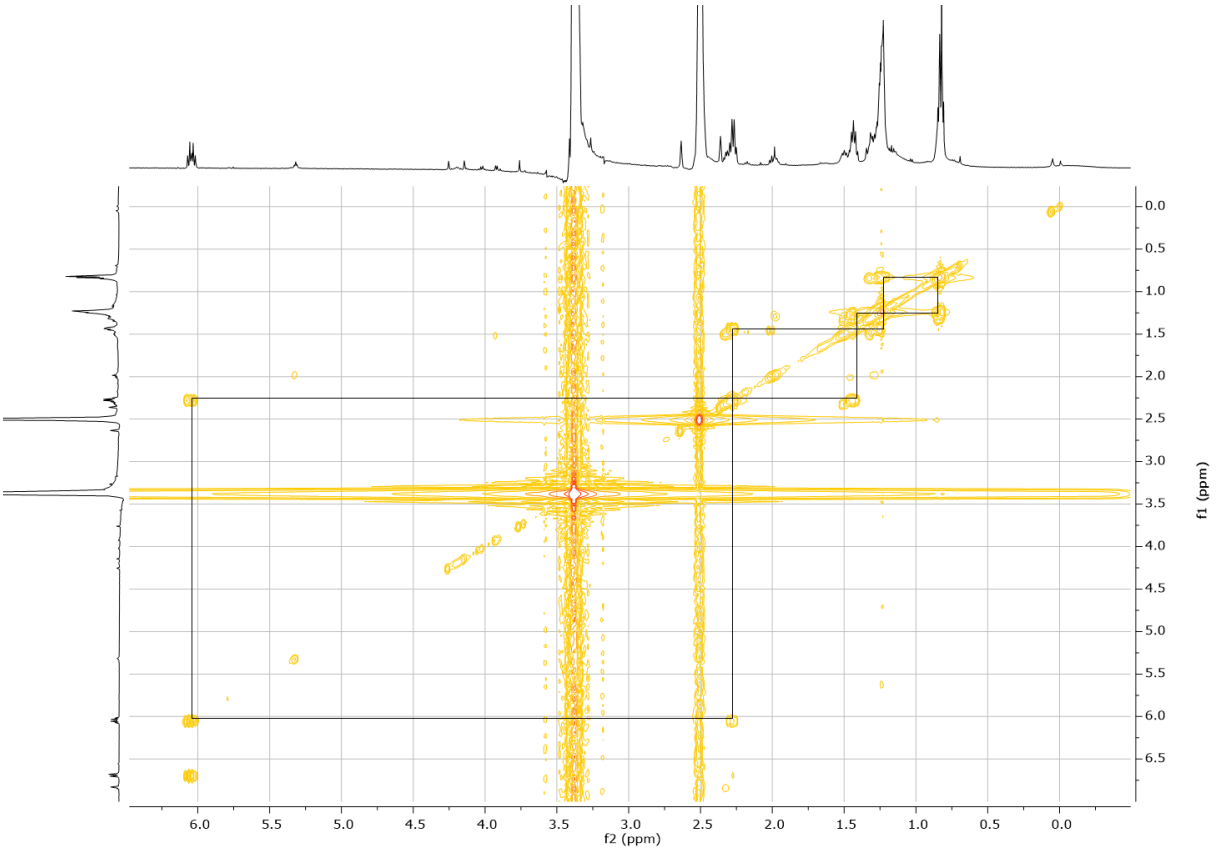

Figure **S14**: Cutout of the aliphatic region of the 2D COSY cryo NMR determined in DMSO-d_6 of ligand **37**.

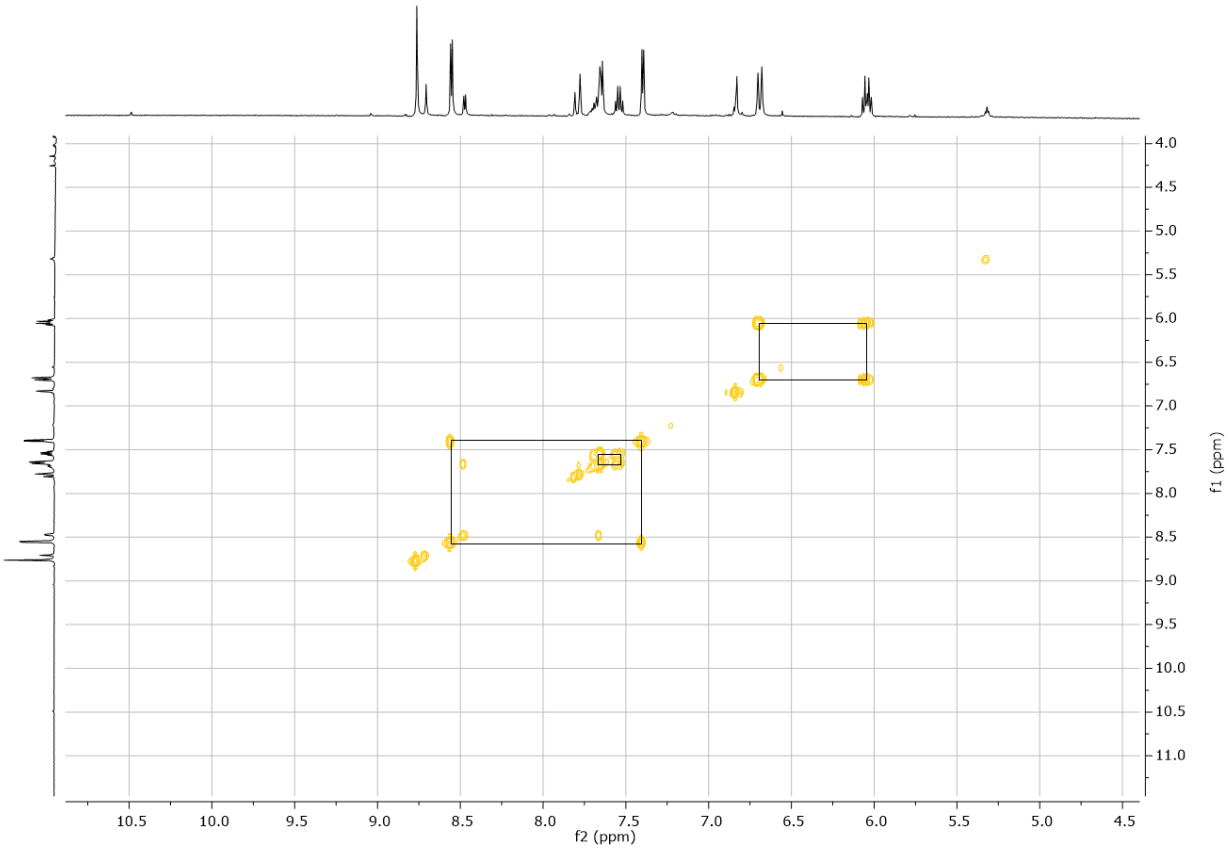

Figure **S15**: Cutout of the aromatic region of the 2D COSY cryo NMR determined in DMSO-d_6 of ligand **37**.

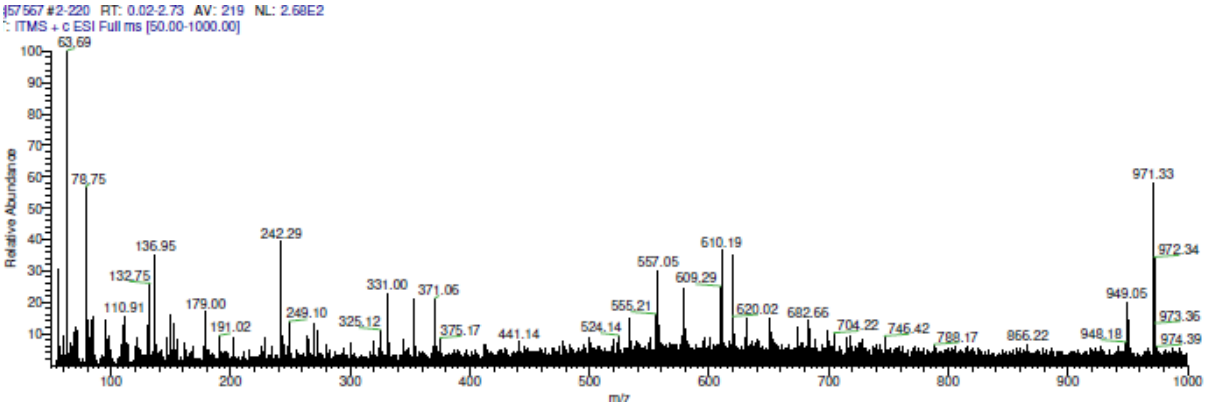

Figure **S16**: ESI-MS spectrum of reaction 5 (table **3**).

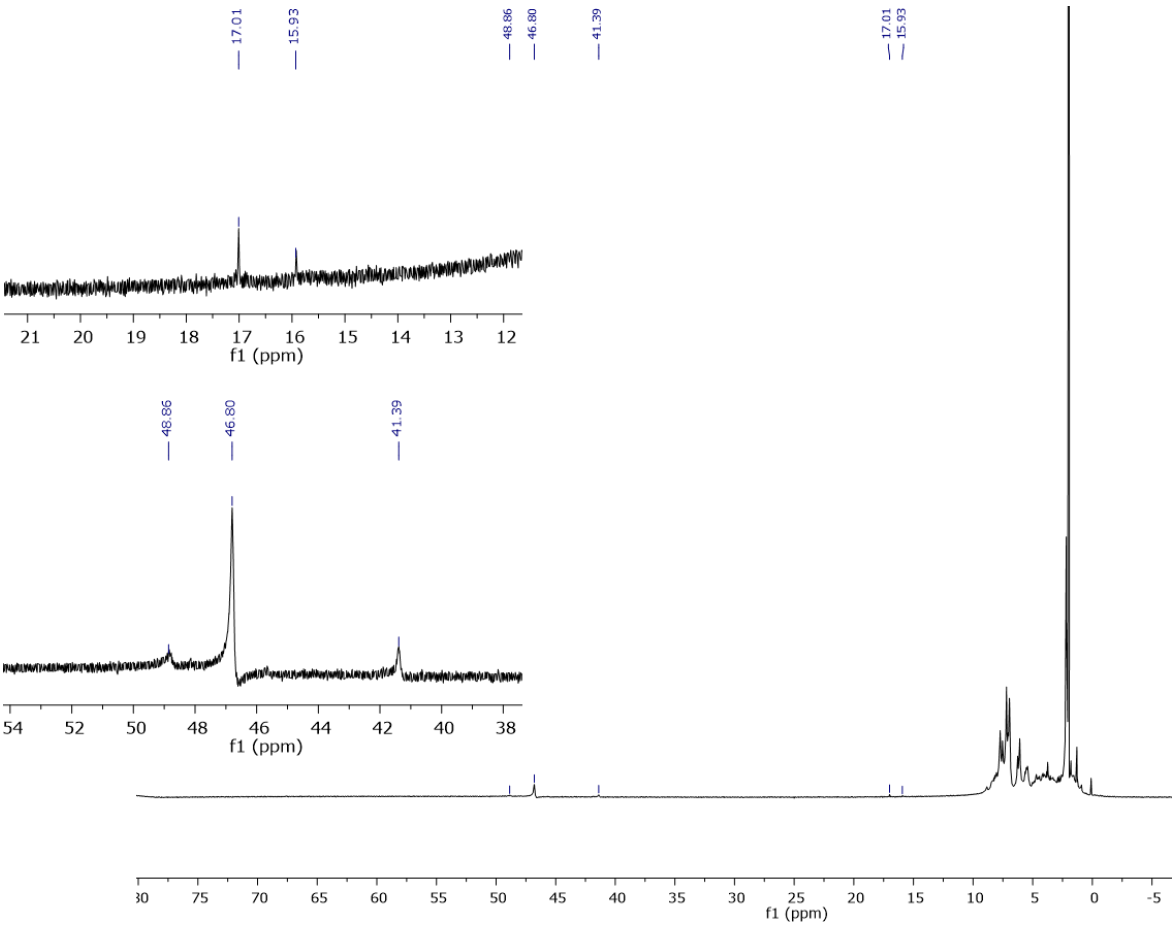

Figure **S17**: Paramagnetic ^{1}H NMR measured in CD_3CN of vanadium approach 7.

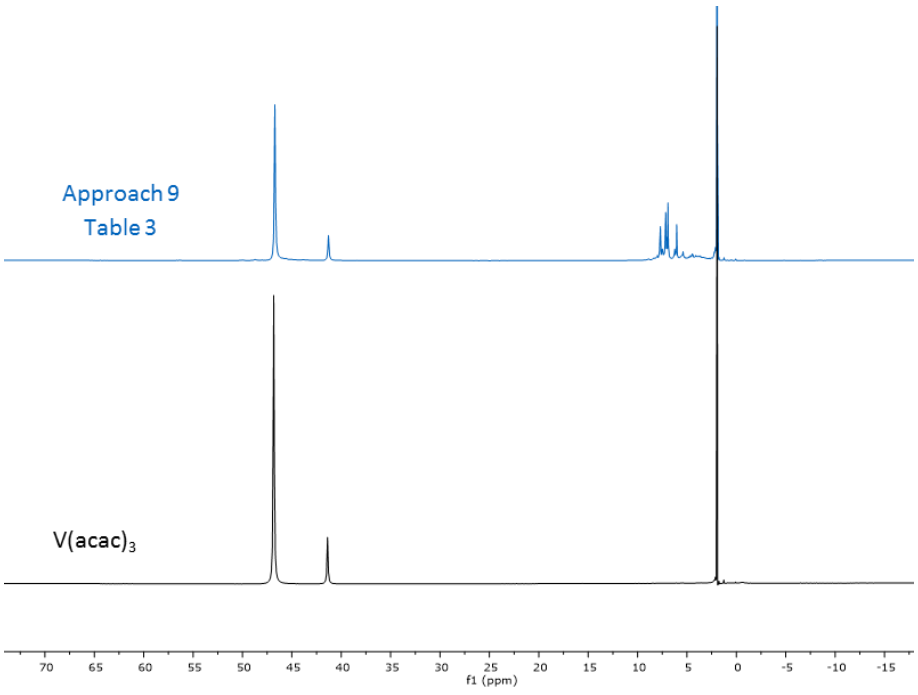

Figure **S 18**: Paramagnetic ^{1}H NMR spectra of approach 9 and $V(acac)_3$ for comparison.

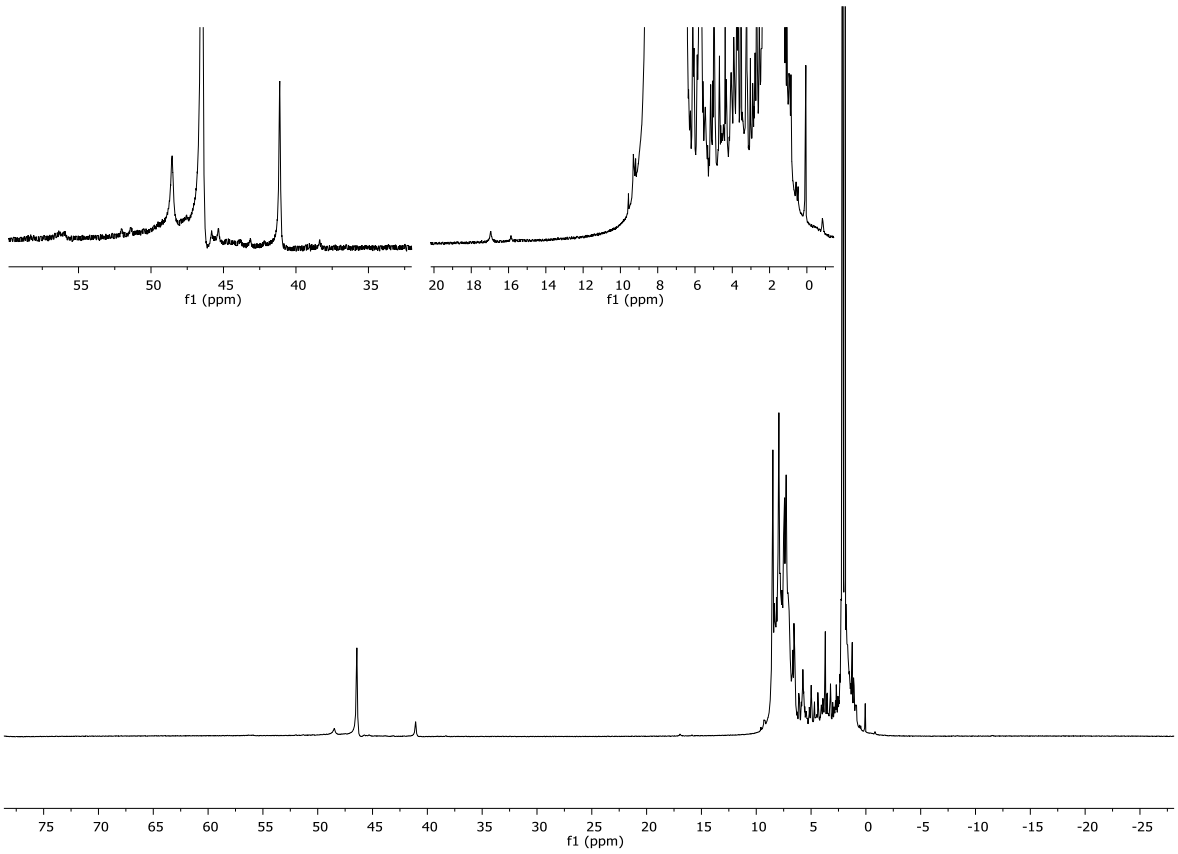

Figure **S19**: Paramagnetic ^{1}H NMR spectrum in MeCN-d_3 of reaction 11.

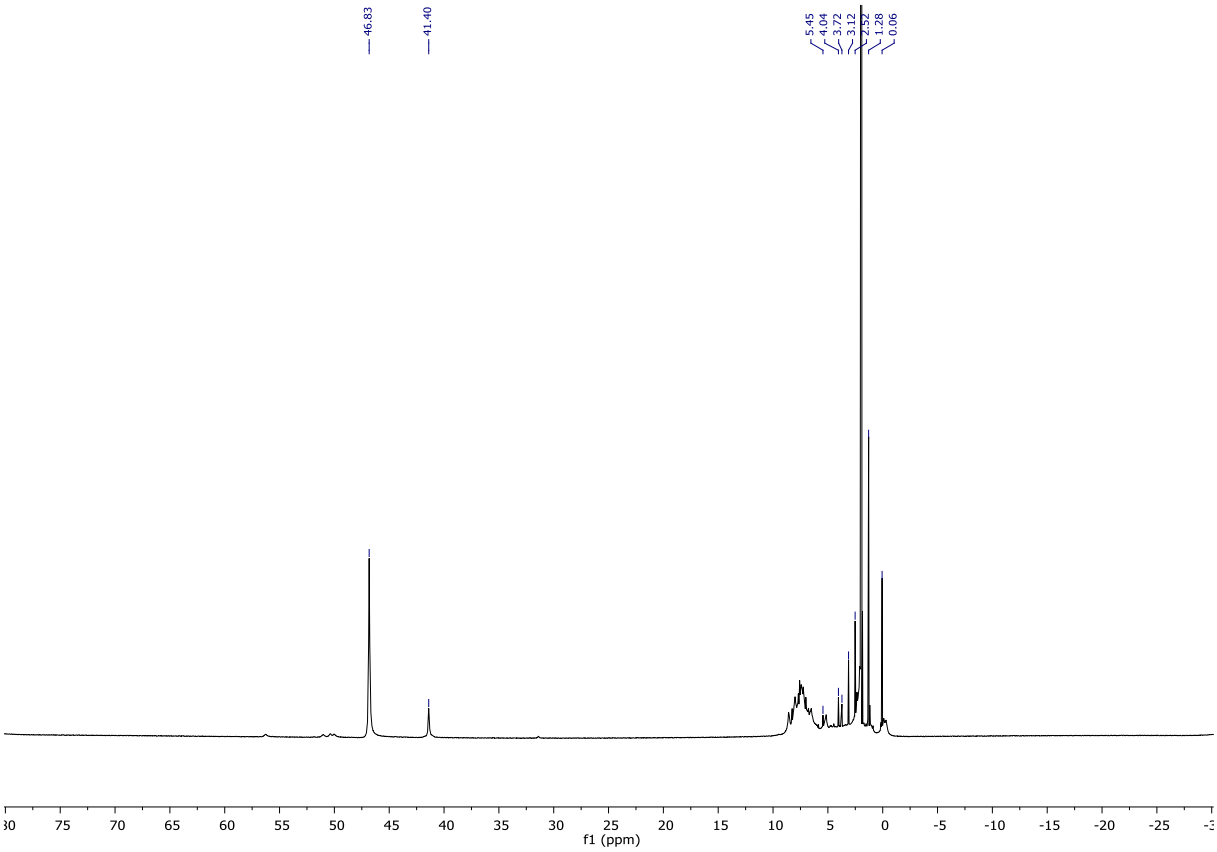

Figure **S20**: Complete ^{1}H NMR spectrum measured in MeCN-d_3 of approach 13.

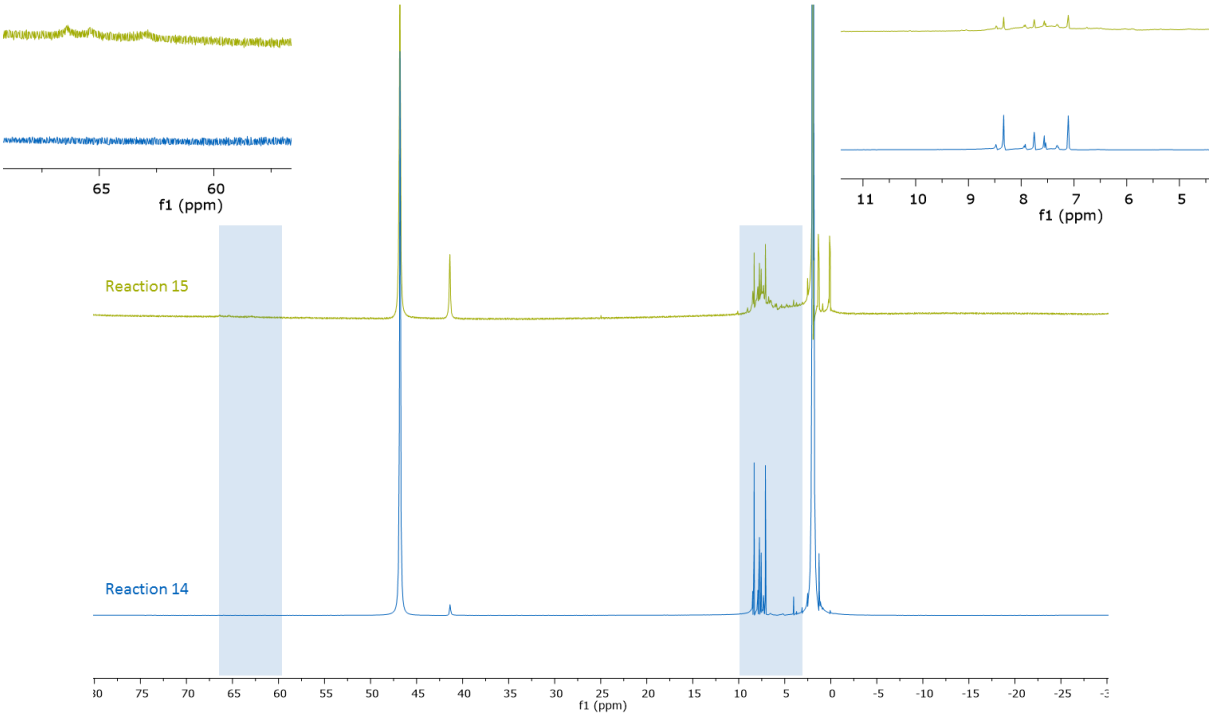

Figure **S21**: Comparison of the paramagnetic ^{1}H NMR spectra of approaches 14 and 15 with the two blue highlighted areas given in more detail.

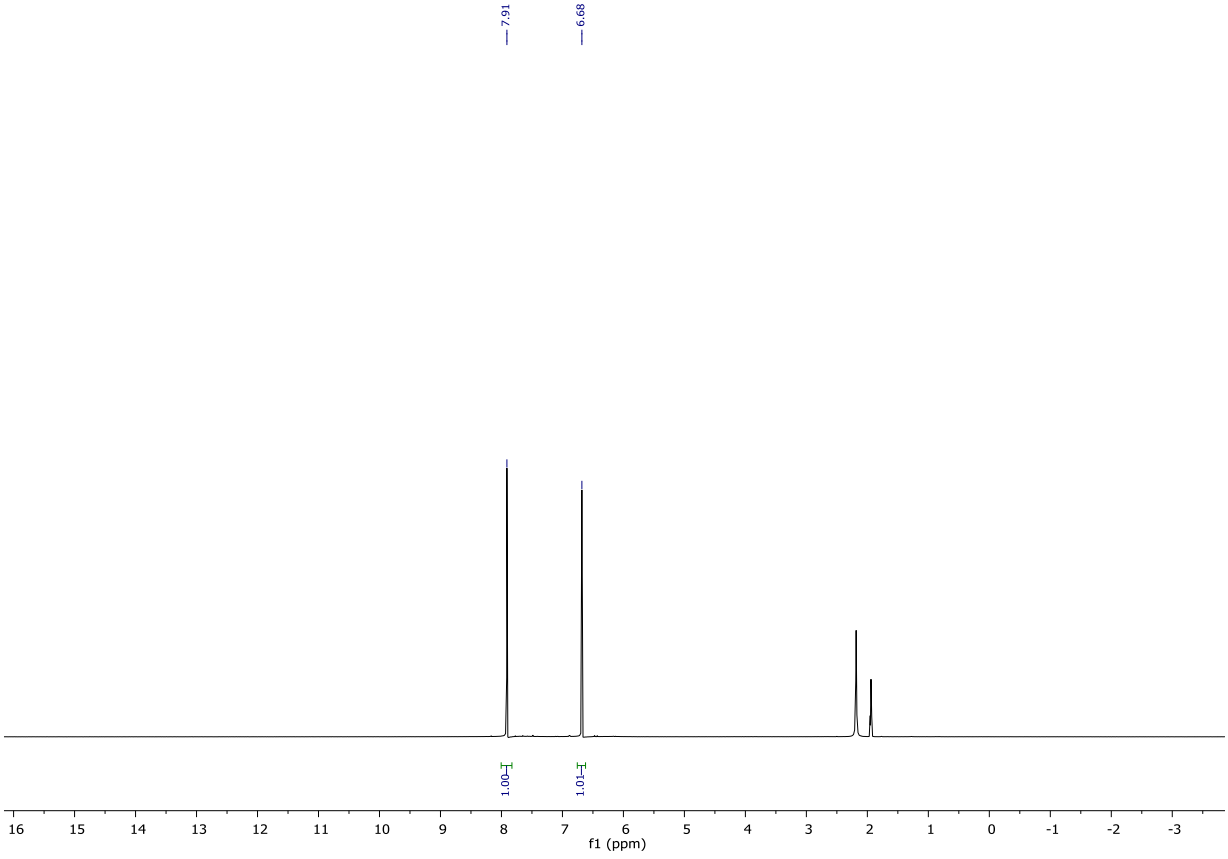

Figure **S22**: ^{1}H NMR of complex **51** measured in MeCN-d_3.

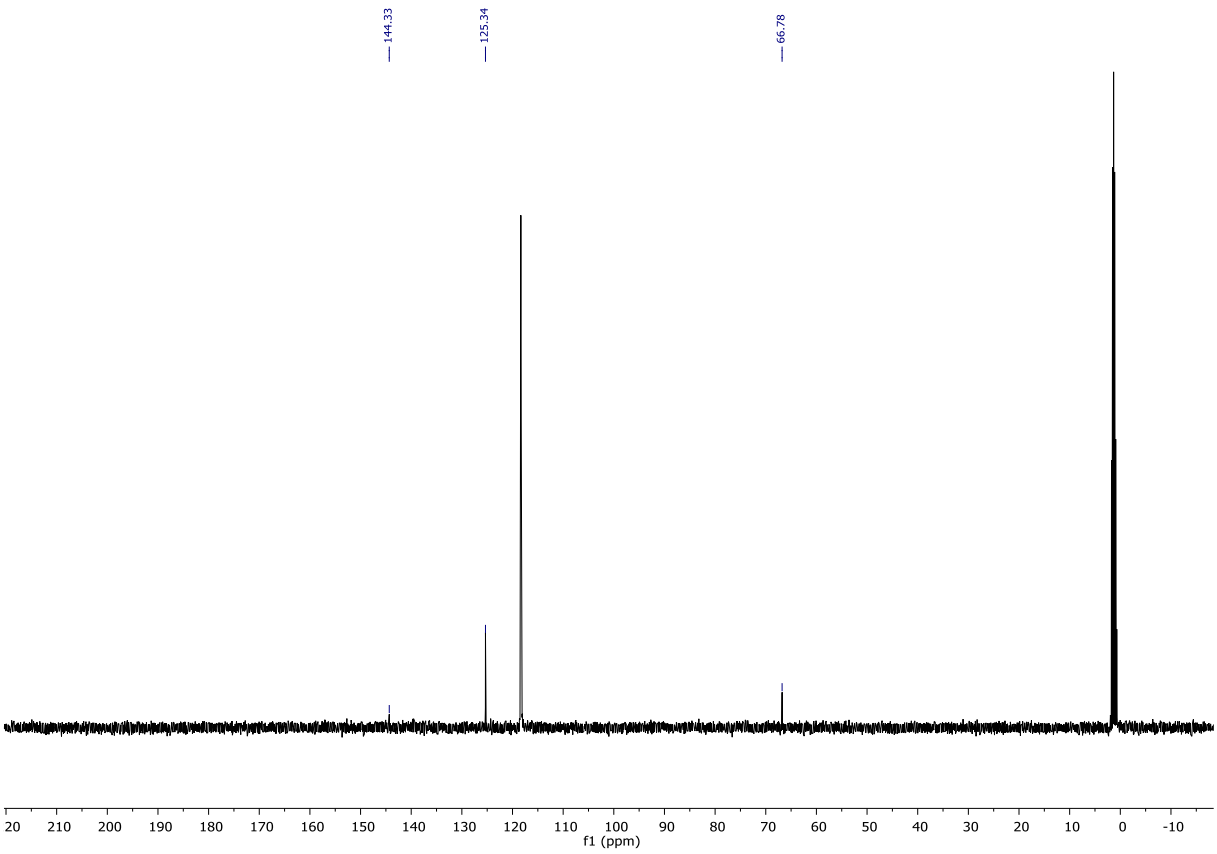

Figure **S23**: ^{13}C NMR of complex **51** determined in MeCN-d_3.

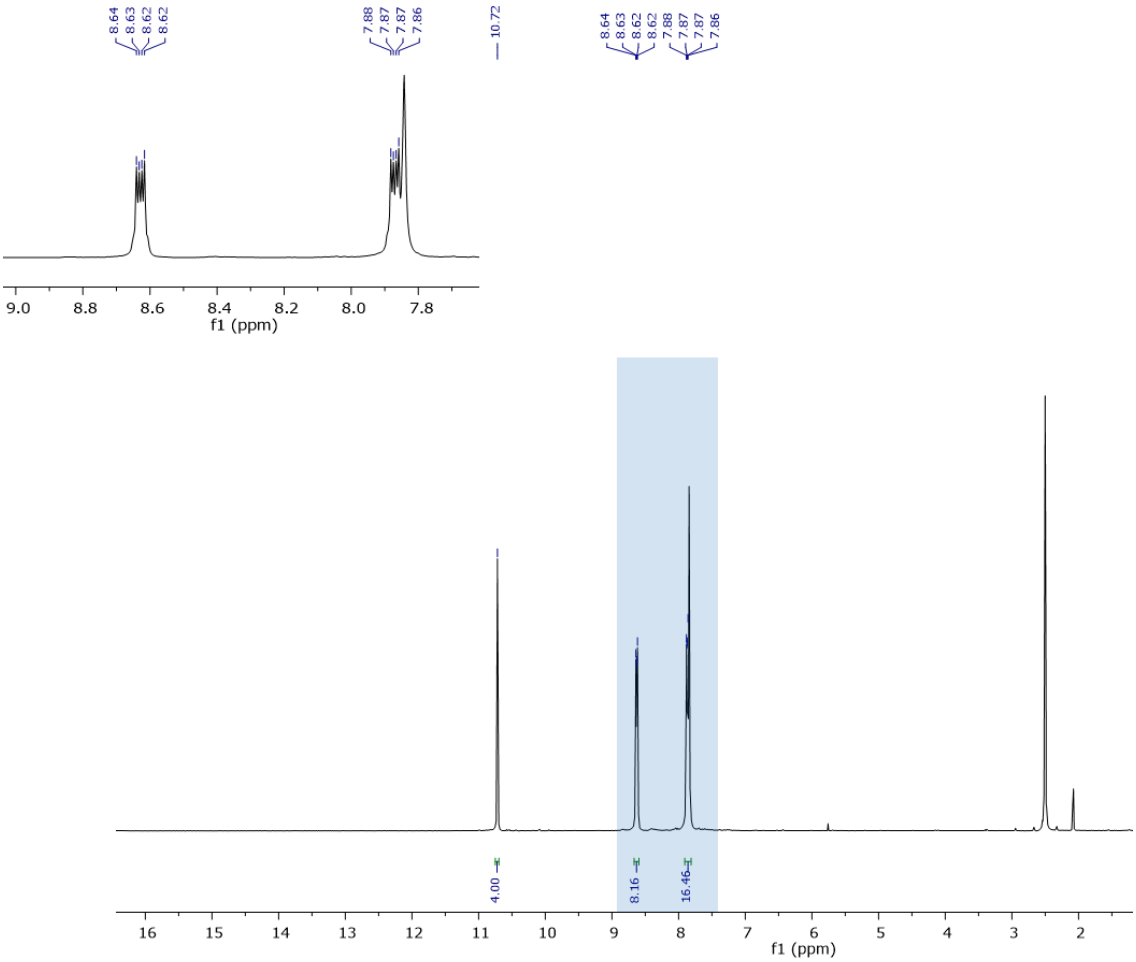

Figure **S24**: ^{1}H NMR spectrum determined in DMSO-d_6 of ligand **49**. For the blue highlighted area, a more detailed zoom is provided for better recognition of the signals.

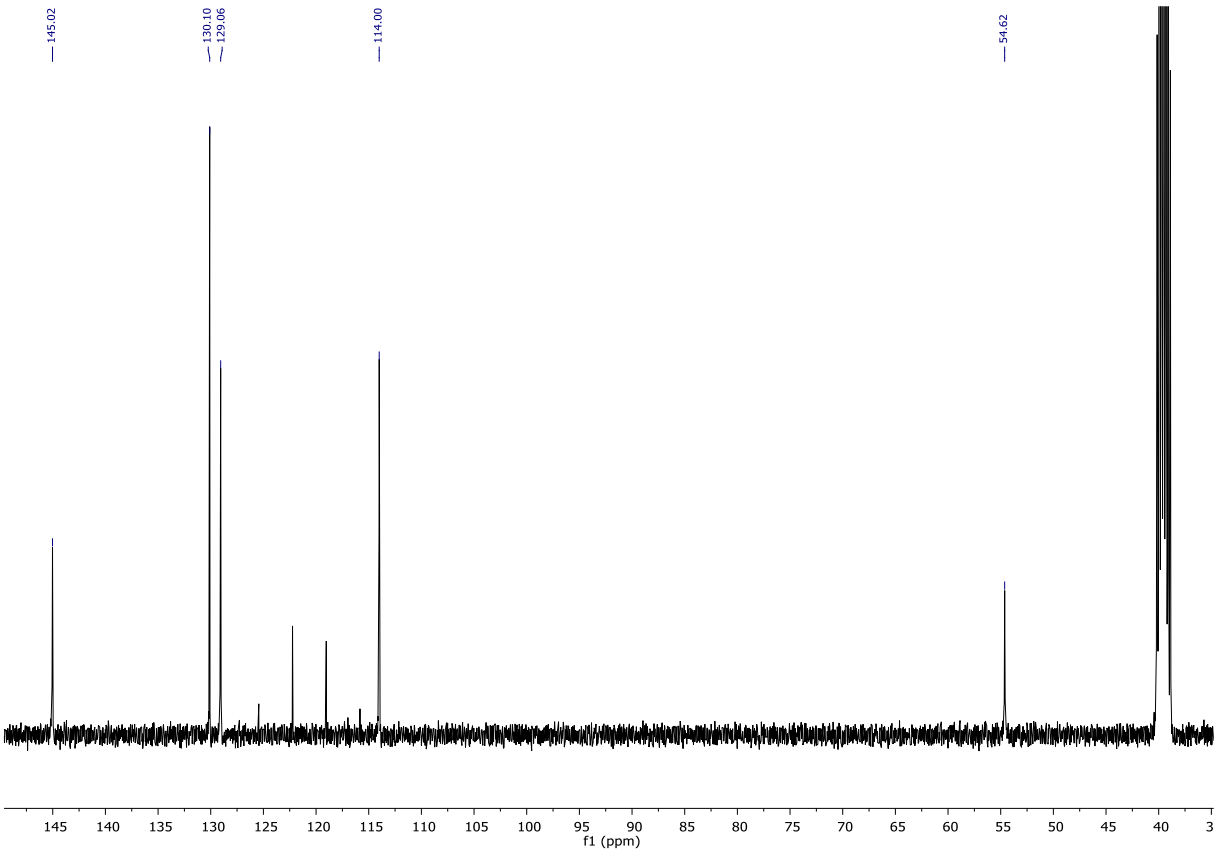

Figure **S25**: ^{13}C NMR of ligand **49** measured in DMSO-d_6.

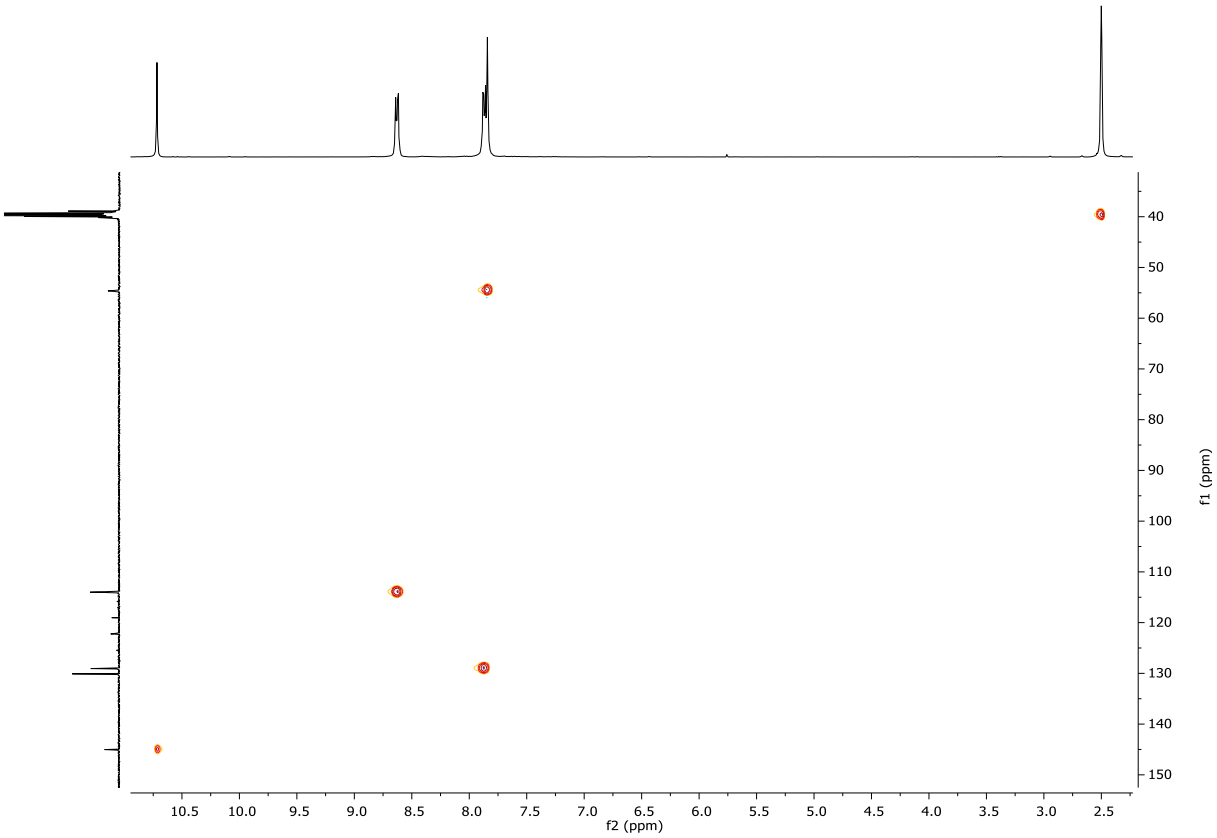

Figure **S26**: HSQC 2D NMR spectrum of **49** in DMSO-d_6.

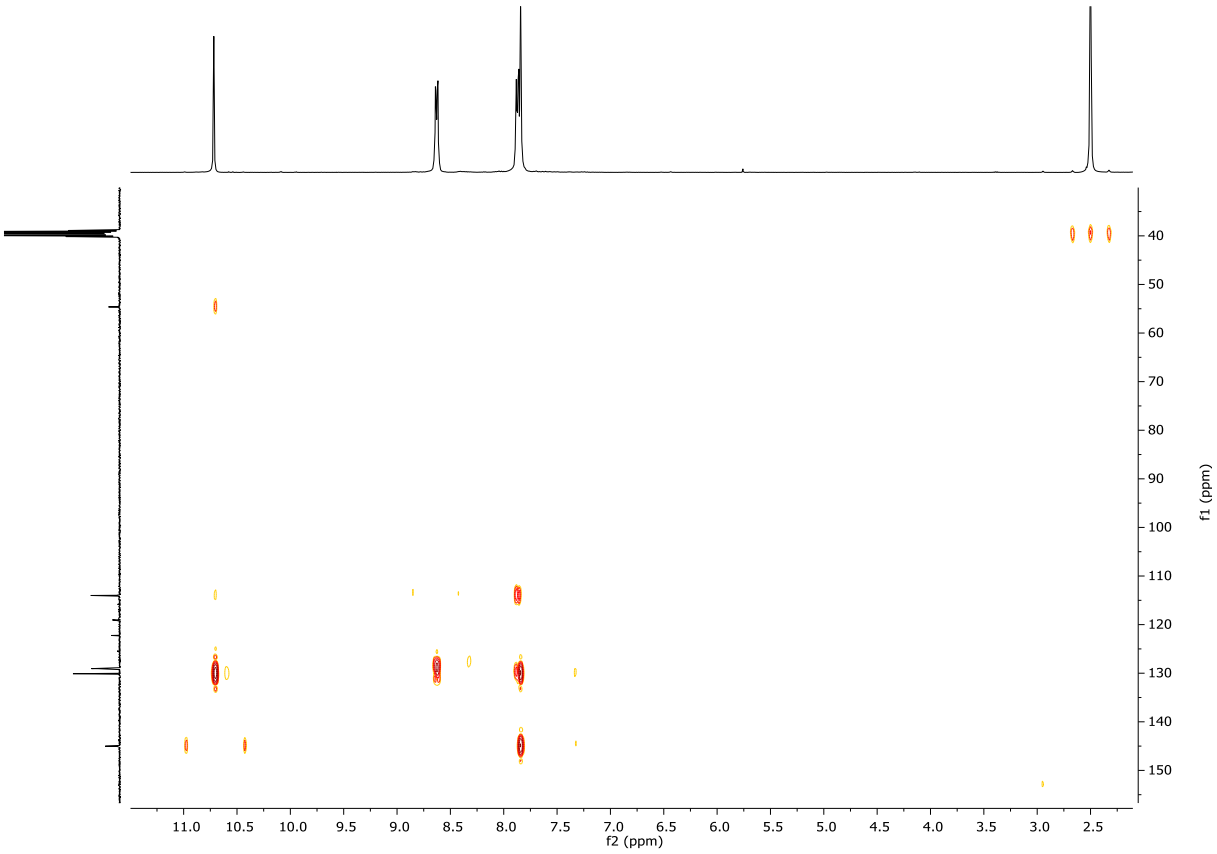

Figure **S27**: HMBC 2D NMR spectrum of **49** determined in DMSO-d_6.

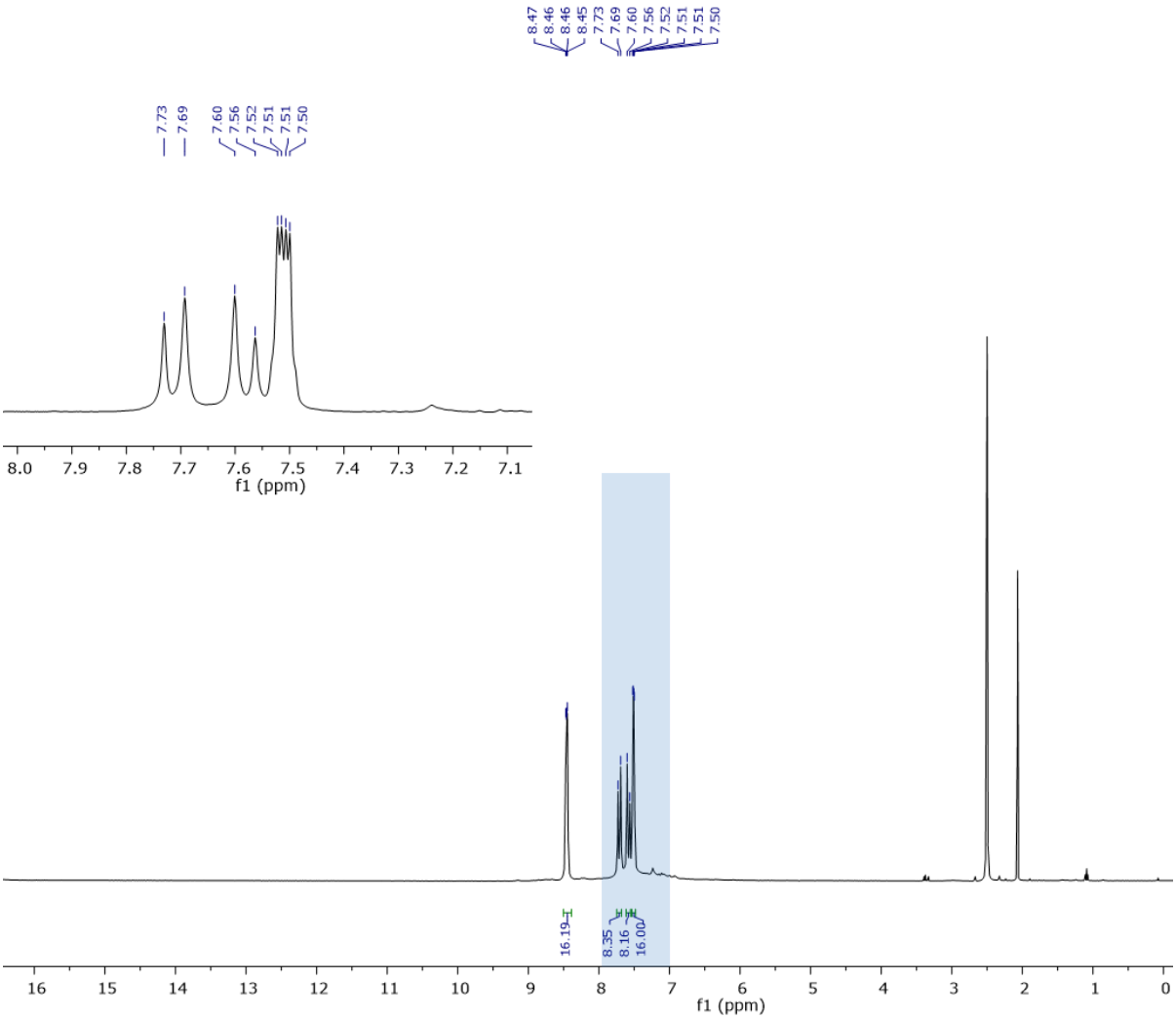

Figure **S28**: ^{1}H NMR of **52** in DMSO-d_6. Blue highlighted area is given in more detail on the left.

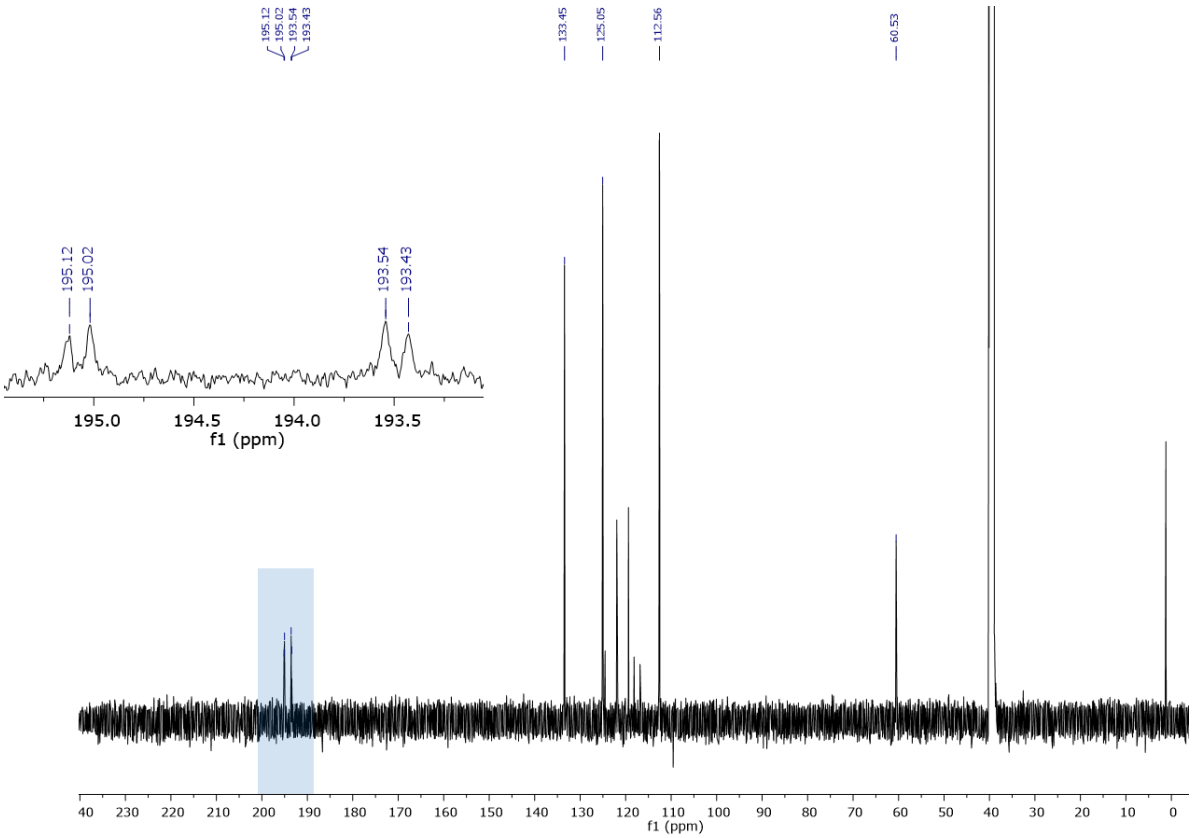

Figure **S29**: ^{13}C NMR of **52** in DMSO-d_6. The blue highlighted area is shown in more detail for better recognition of the signals. Further signals of triflate as well as remaining MeCN are visible.

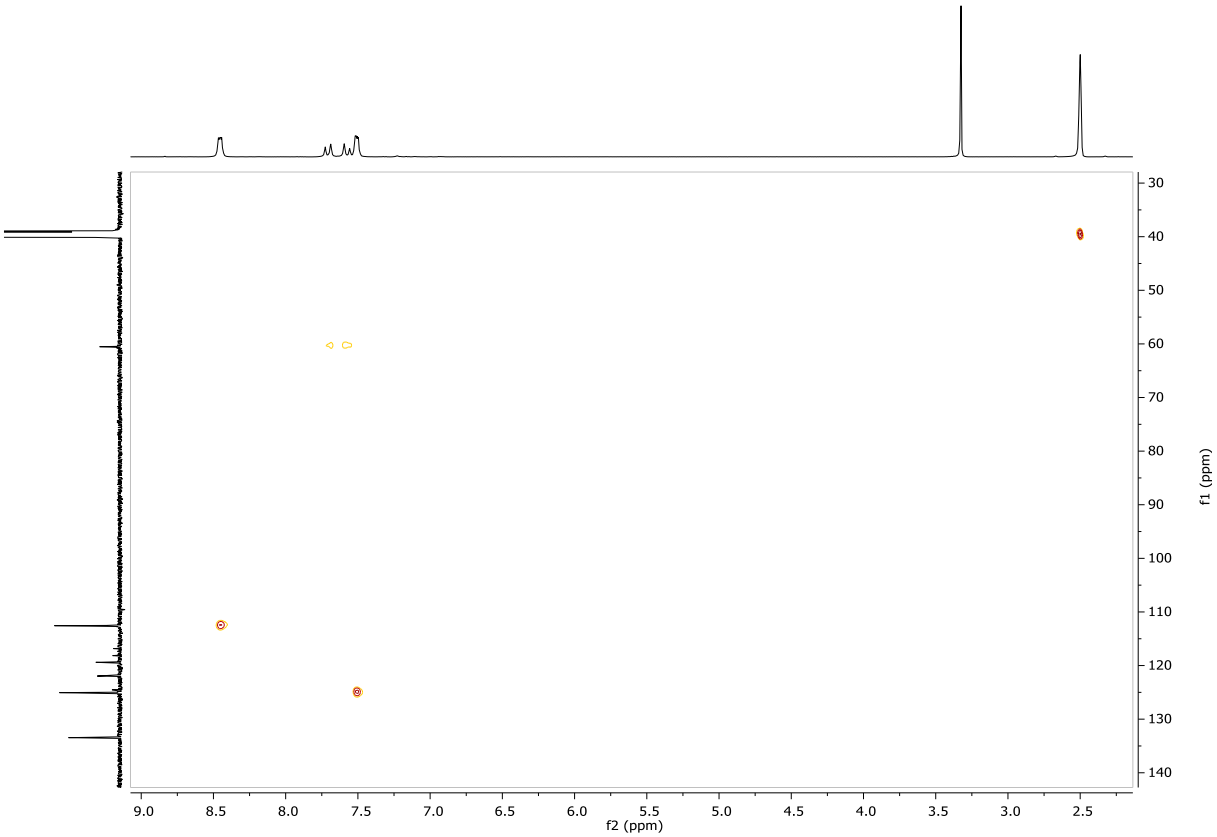

Figure **S30**: HSQC 2D NMR spectrum of complex **52** in DMSO-d_6.

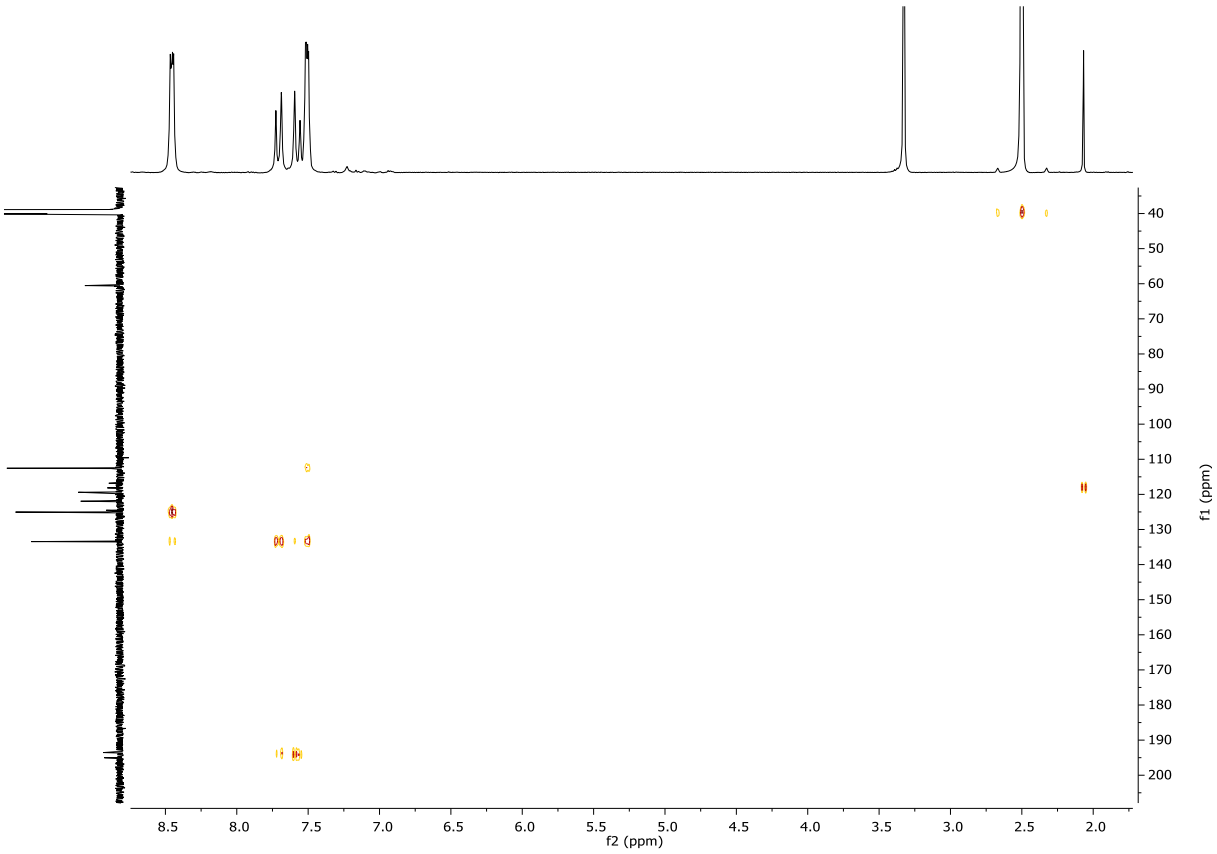

Figure **S31**: HMBC 2D NMR spectrum of **52** determined in DMSO-d_6.

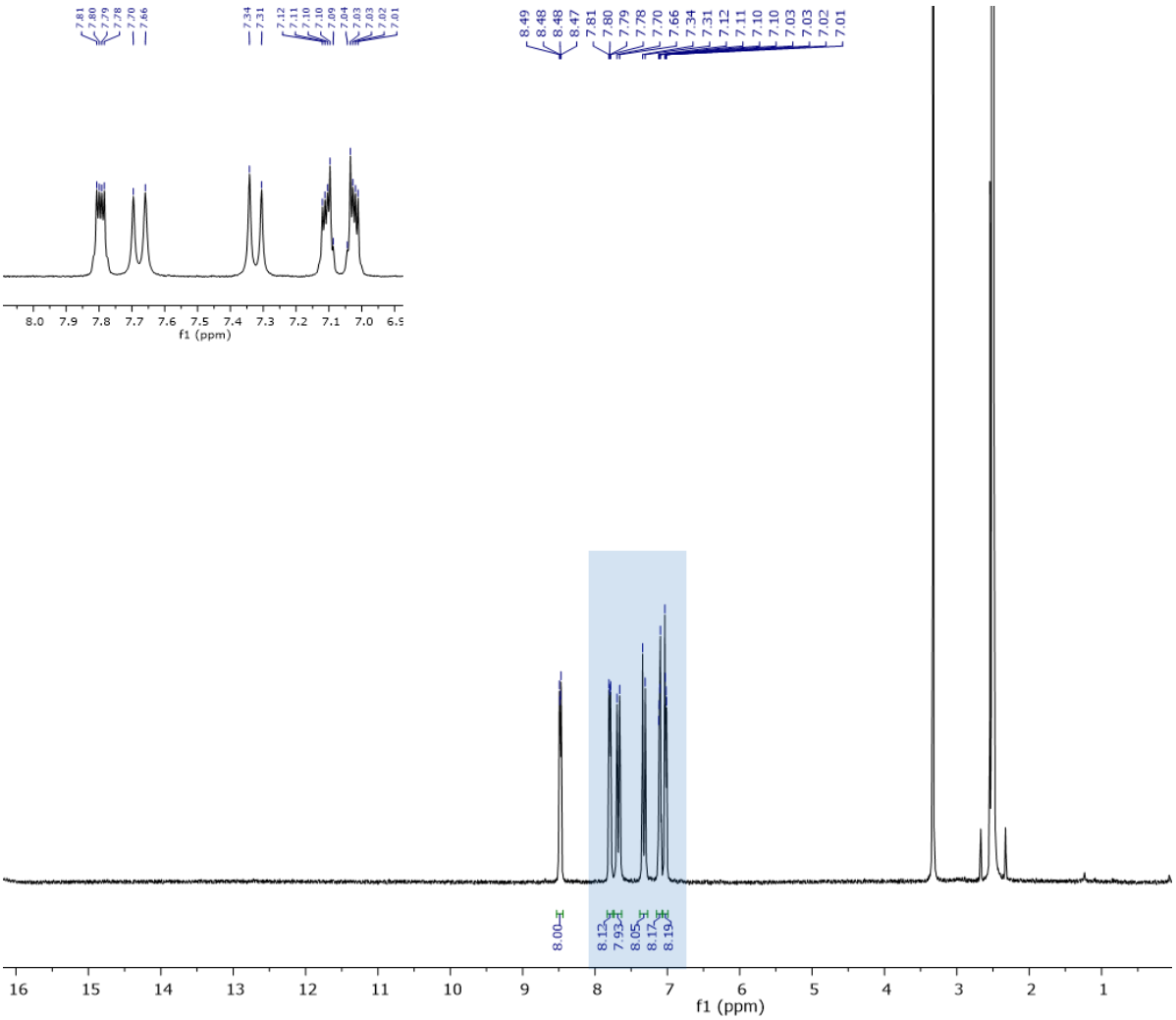

Figure **S32**: ^{1}H NMR spectrum of **53** determined in DMSO-d_6. The blue highlighted area is given in more detail on the upper left side.

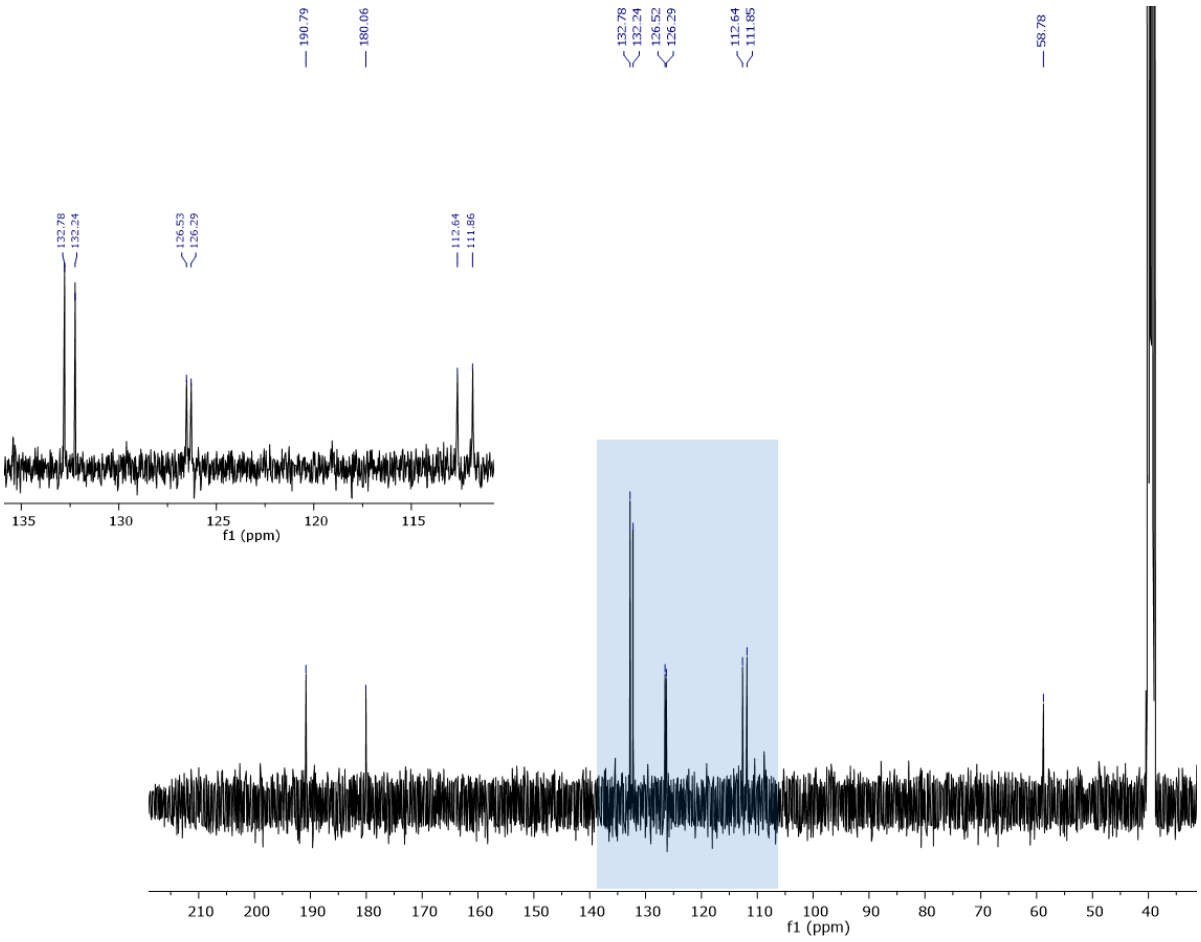

Figure **S33**: ^{13}C NMR of **53** in DMSO-d_6. The blue highlighted area is given in more detail on the upper left side.

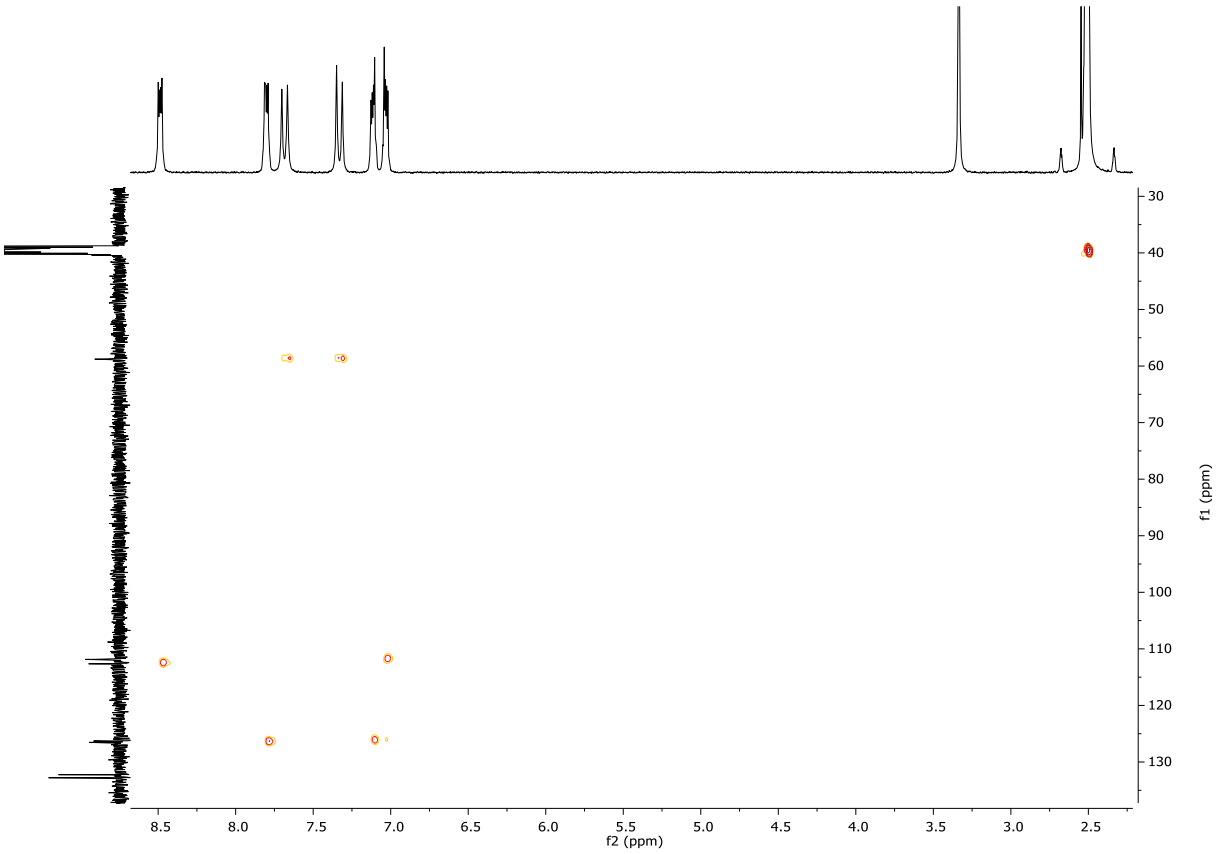

Figure **S34**: HSQC 2D NMR of **53** in DMSO-d_6.

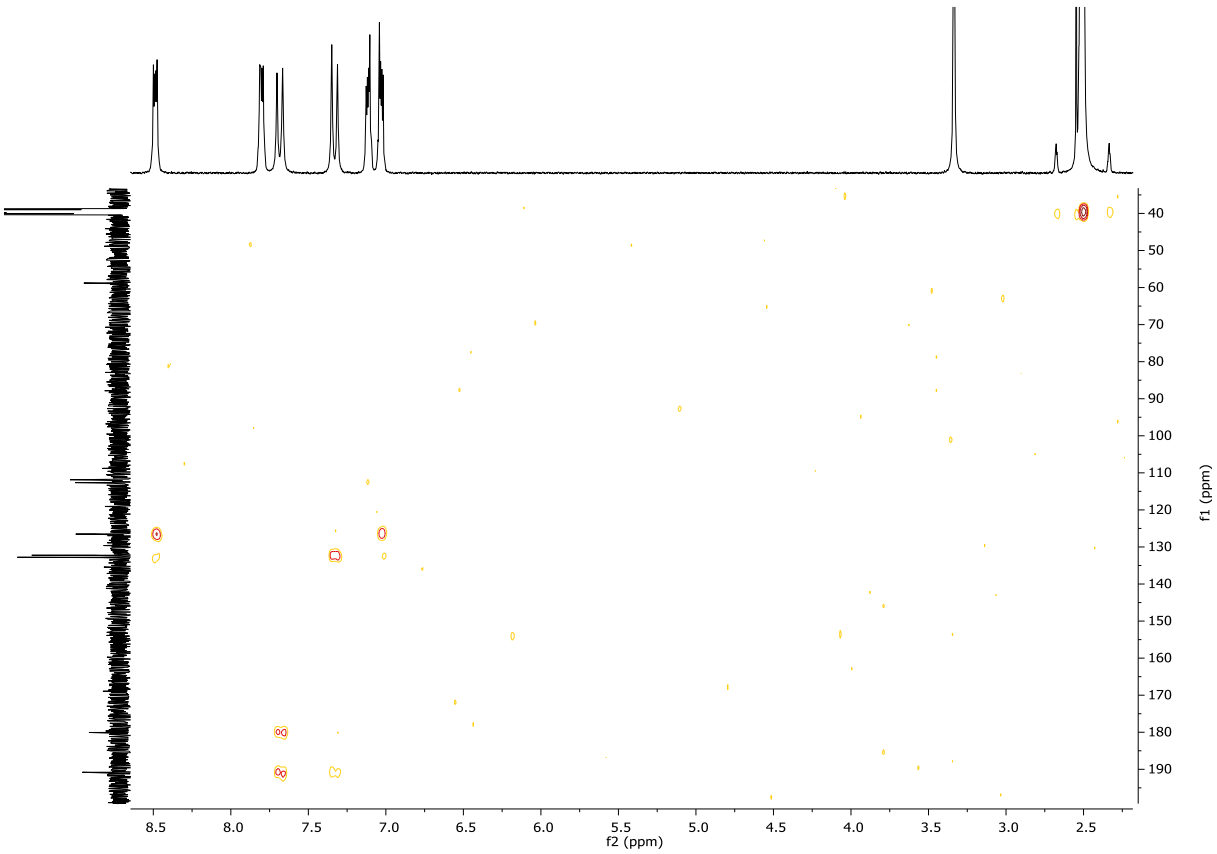

Figure **S35**: HMBC 2D NMR spectrum of **53** determined in DMSO-d_6.

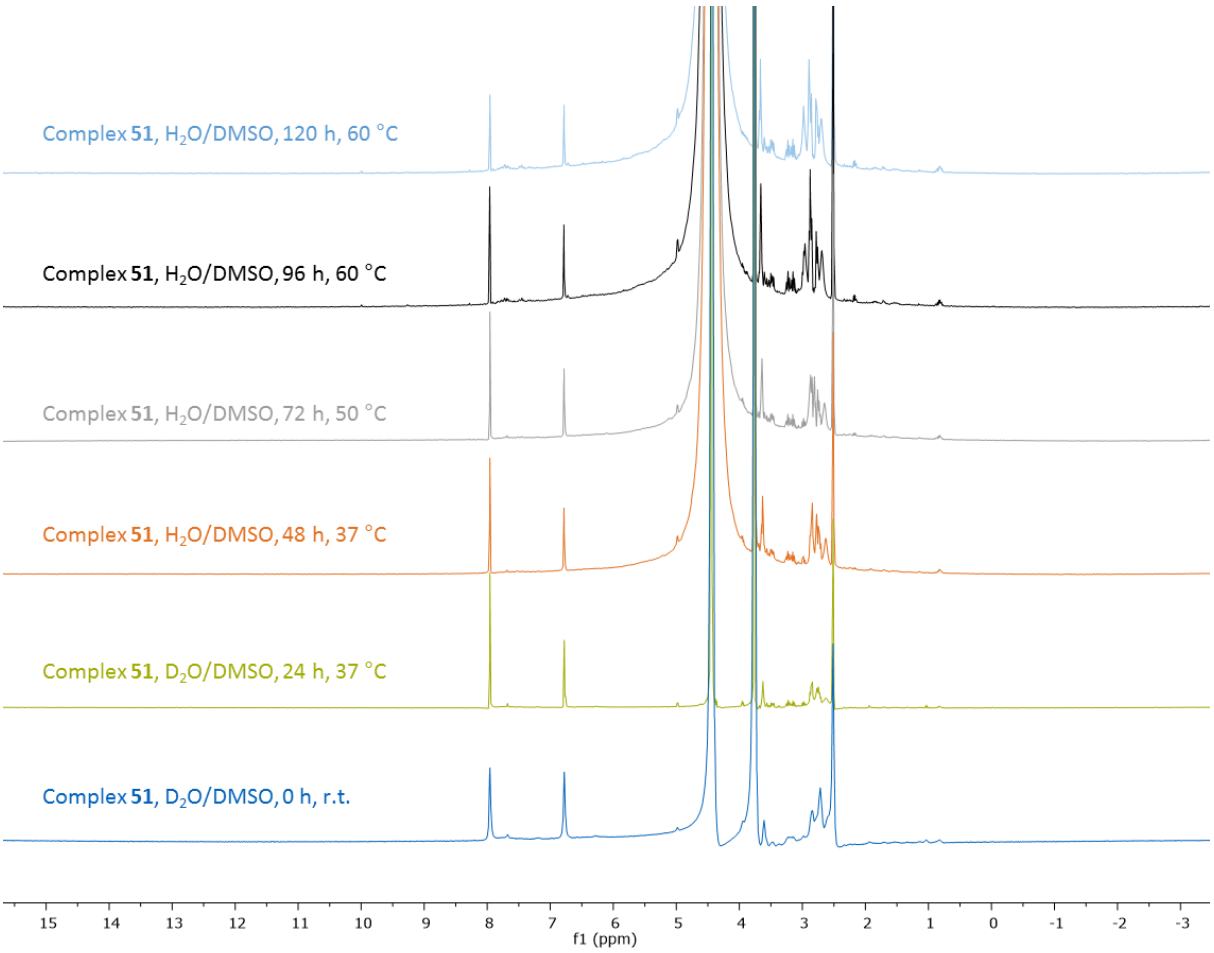

Figure **S36**: Complete ^{1}H NMR spectra of complex **51** determined in $D_2O_{RPMI\ Medium}$/DMSO-d_6 and $H_2O_{RPMI\ Medium}$/DMSO-d_6 to prove proton/deuterium exchange.

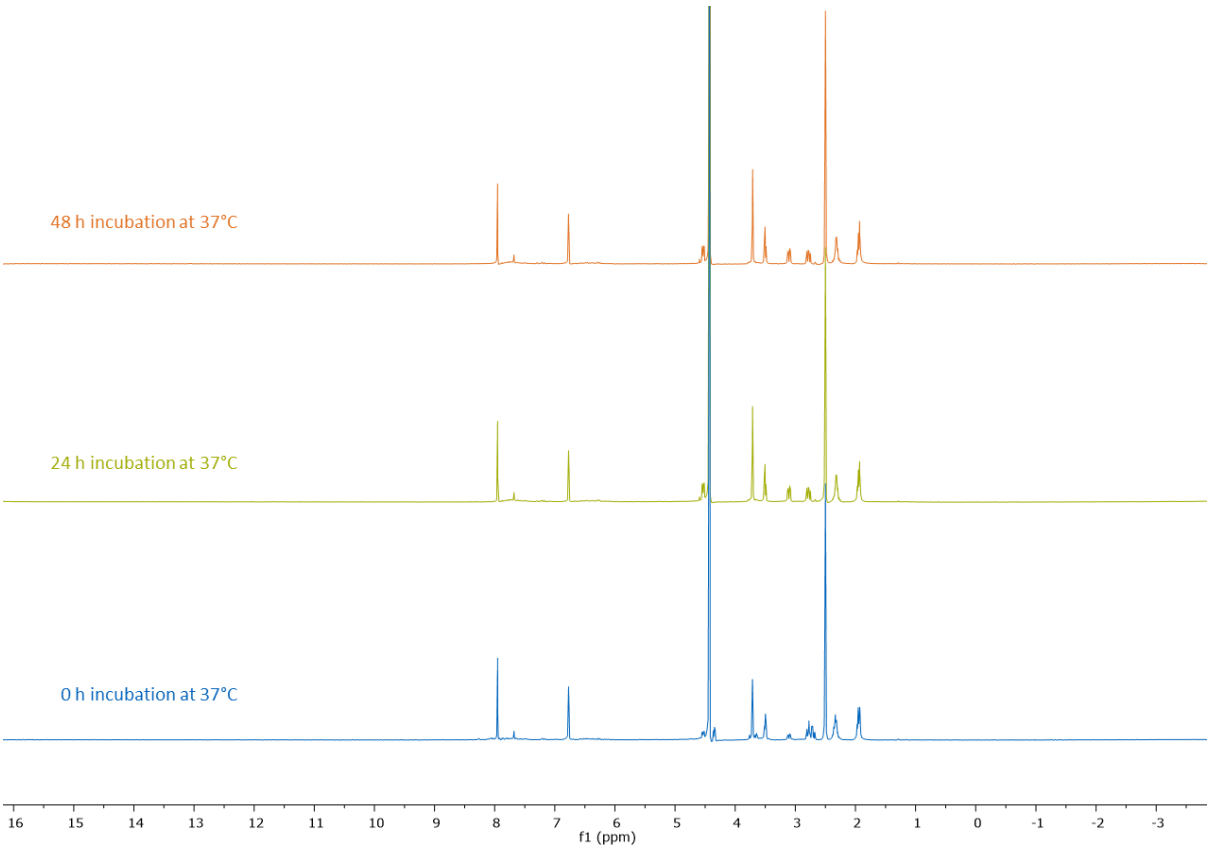

Figure **S37**: ^{1}H NMR spectra of complex **51** determined in deuterated PBS/DMSO-d_6 in the presence of GSH prior to incubation (0 h), after 24 h at 37 °C and after 48 h incubation at 37 °C.

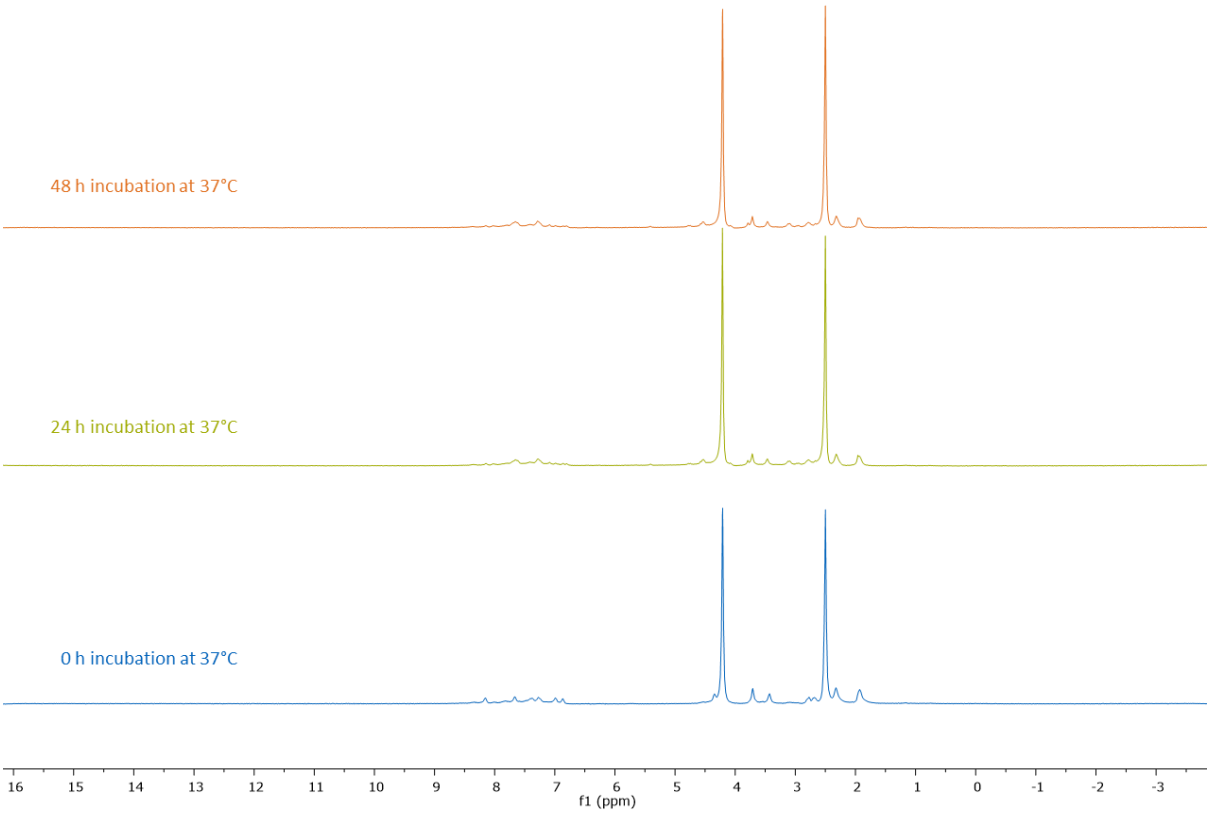

Figure **S38**: ^{1}H NMR spectra of complex **53** determined in deuterated PBS/DMSO-d_6 in the presence of GSH prior to incubation (0 h), after 24 h at 37 °C and after 48 h incubation at 37 °C.

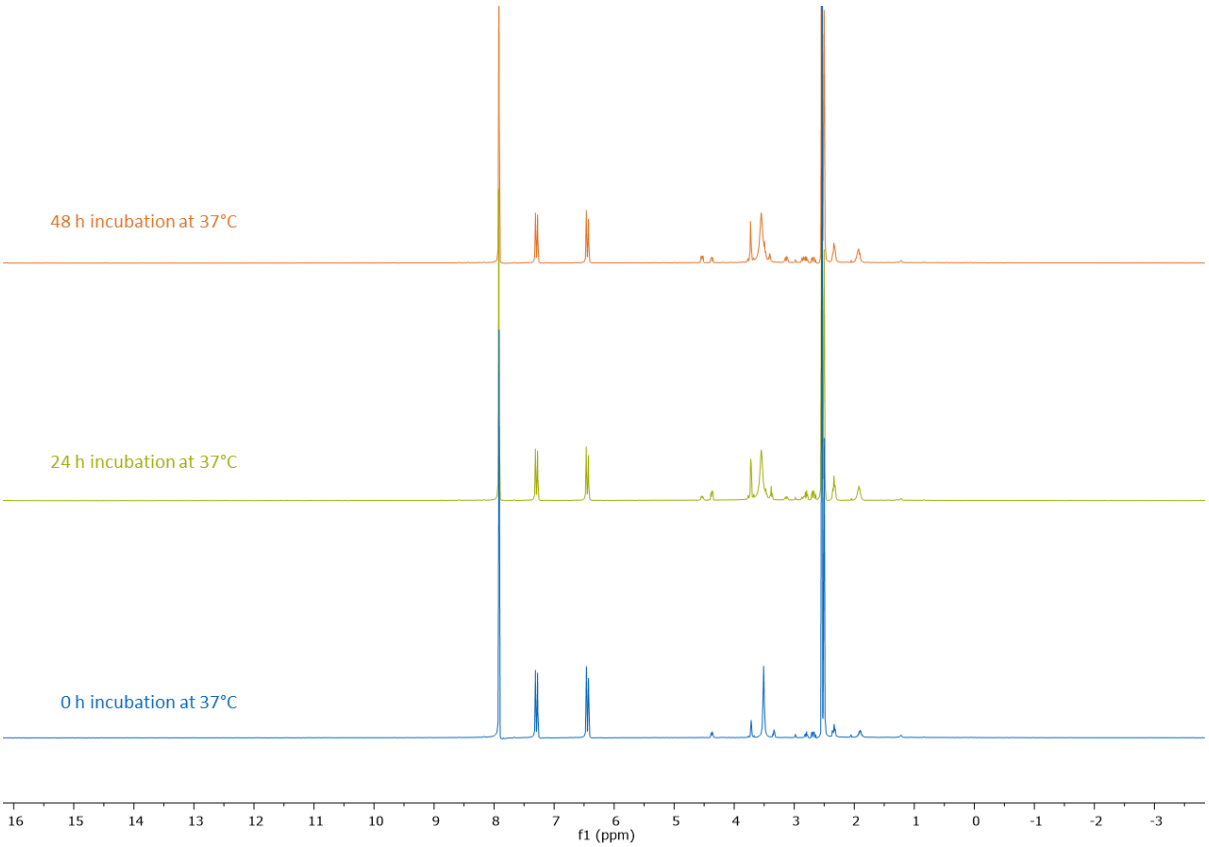

Figure **S39**: ^{1}H NMR spectra of complex **54** determined in deuterated PBS/DMSO-d_6 in the presence of GSH prior to incubation (0 h), after 24 h at 37 °C and after 48 h incubation at 37 °C.

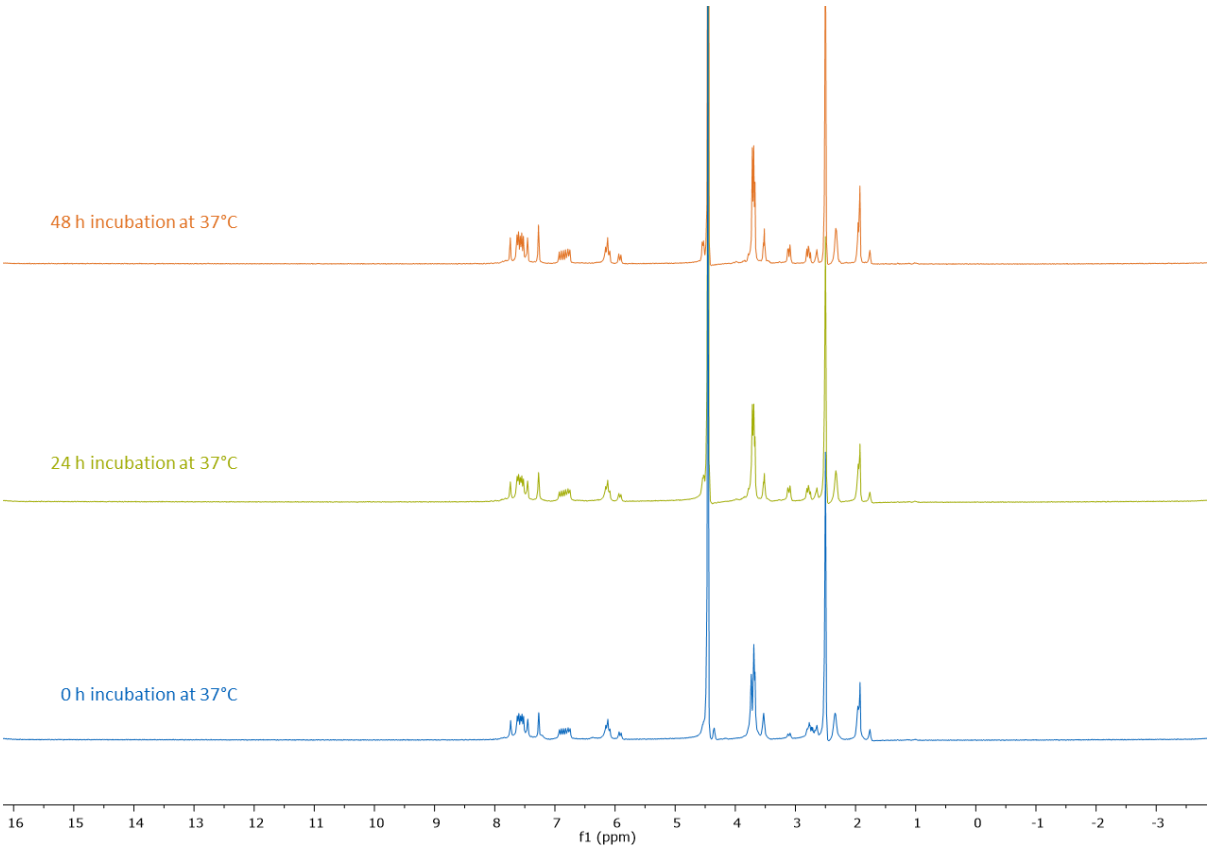

Figure **S40**: ^{1}H NMR spectra of complex **55** determined in deuterated PBS/DMSO-d_6 in the presence of GSH prior to incubation (0 h), after 24 h at 37 °C and after 48 h incubation at 37 °C.

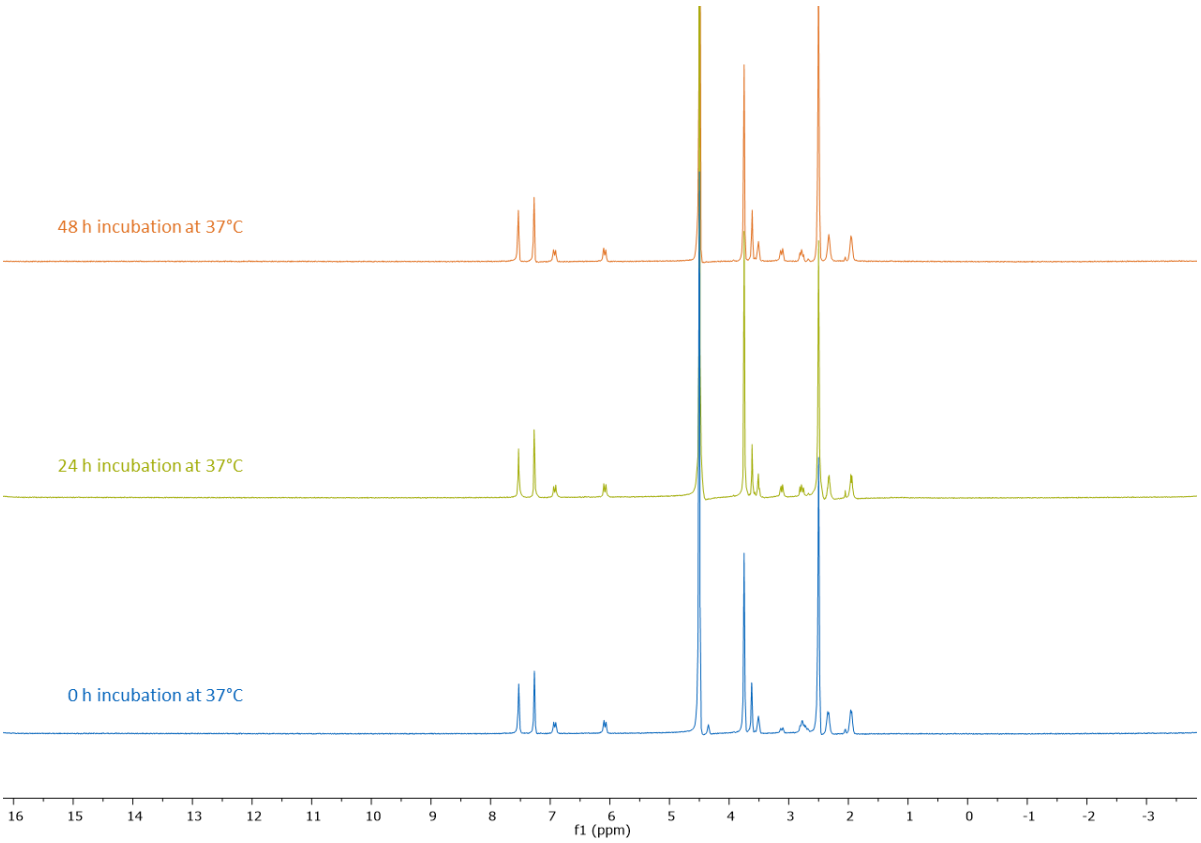

Figure **S41**: ^{1}H NMR spectra of complex **56** determined in deuterated PBS/DMSO-d_6 in the presence of GSH prior to incubation (0 h), after 24 h at 37 °C and after 48 h incubation at 37 °C.

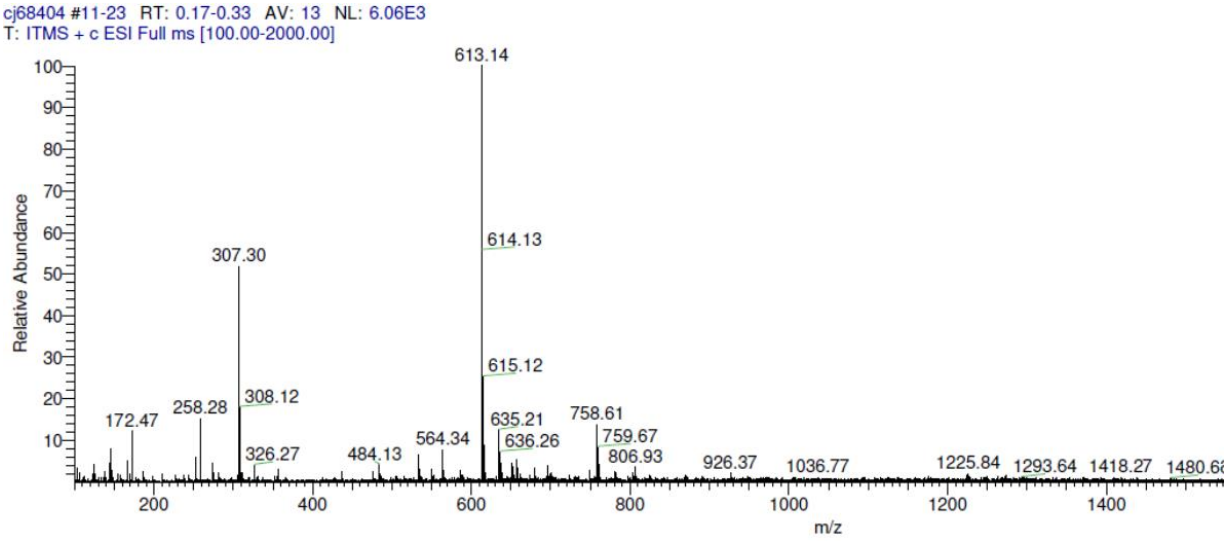

Figure **S42**: ESI-MS spectrum of complex **51** determined after 48 h of incubation at 37°C. Reprinted from Ref. [189] by permission of The Royal Society of Chemistry.

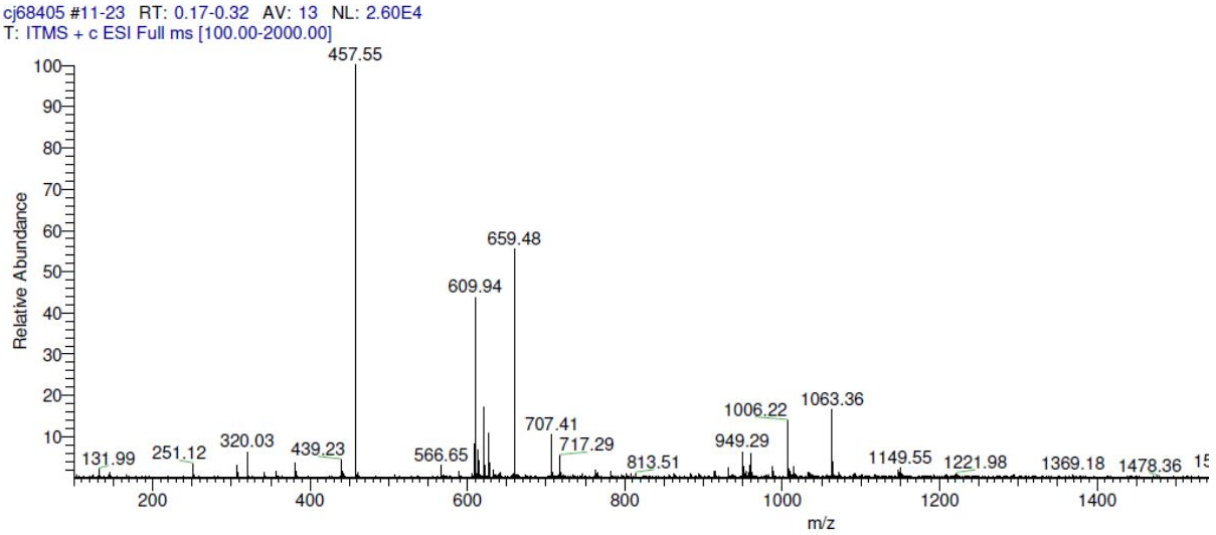

Figure **S43**: ESI-MS spectrum of complex **53** determined after 48 h of incubation at 37°C. Reprinted from Ref. [189] by permission of The Royal Society of Chemistry.

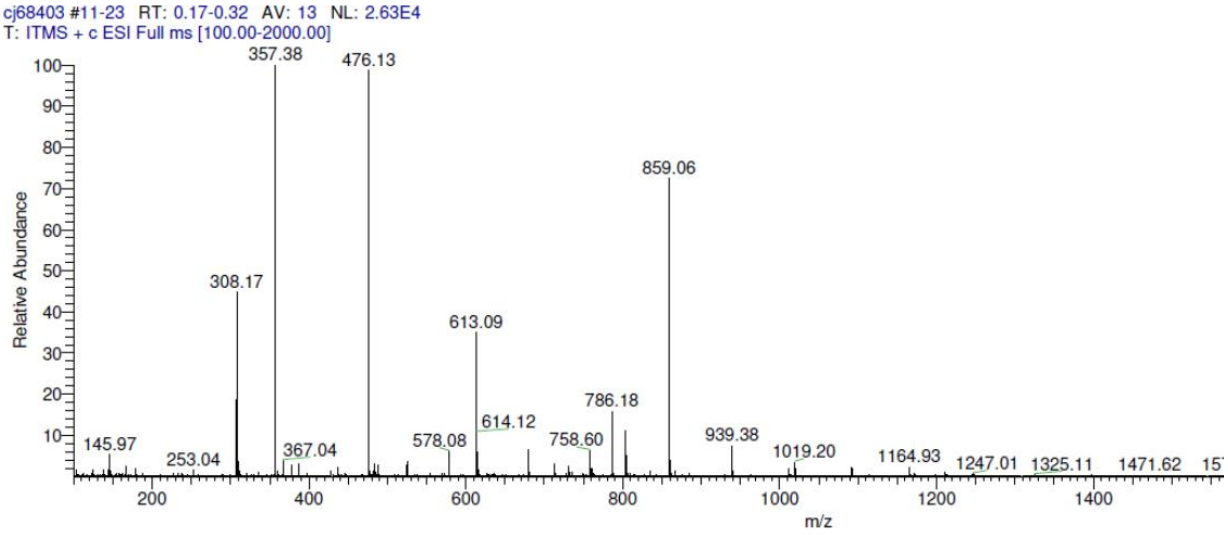

Figure **S44**: ESI-MS spectrum of complex **54** determined after 48 h of incubation at 37°C. Reprinted from Ref. [189] by permission of The Royal Society of Chemistry.

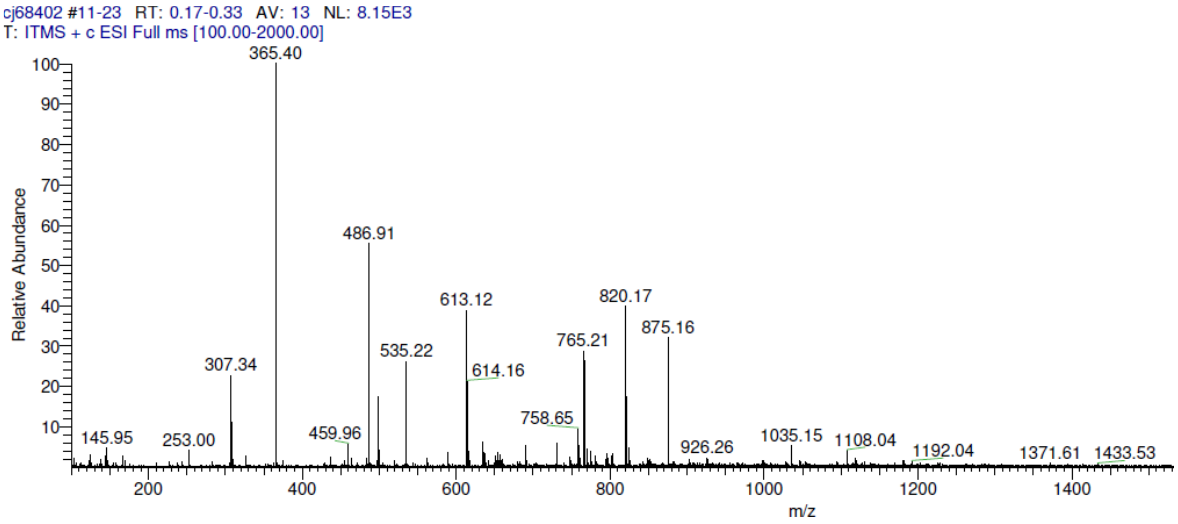

Figure S45: ESI-MS spectrum of complex 55 determined after 48 h of incubation at 37°C. Reprinted from Ref. [189] by permission of The Royal Society of Chemistry.

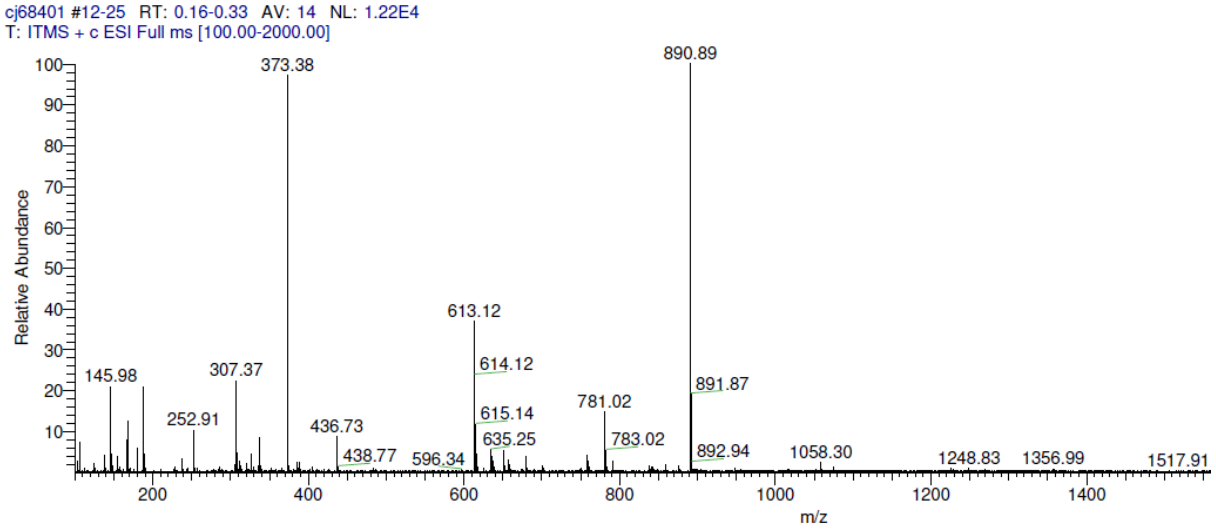

Figure S46: ESI-MS spectrum of complex 56 determined after 48 h of incubation at 37°C. Reprinted from Ref. [189] by permission of The Royal Society of Chemistry.

6.3 MTT assays

6.3.1 HeLa cells

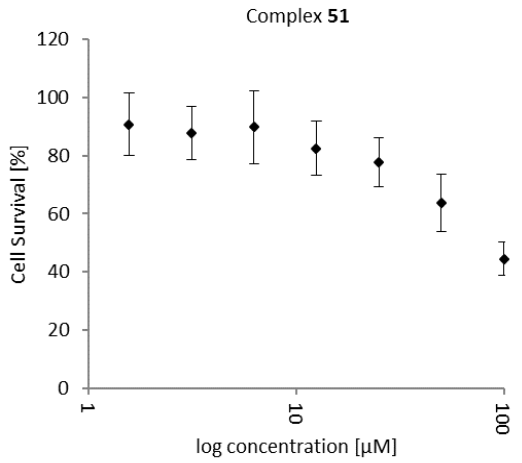

Figure S47: Cell survival [%] of HeLa cells treated with varying concentrations of complex 51 for 48 h. The standard deviation was calculated from three independent determinations. Reprinted from Ref. [188] by permission of The Royal Society of Chemistry.

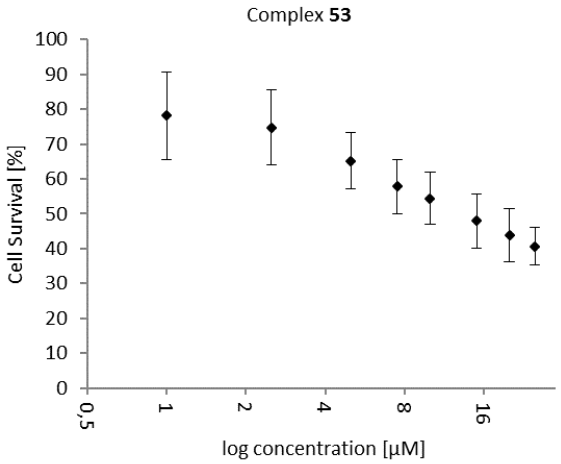

Figure S48: Cell survival [%] of HeLa cells treated with varying concentrations of complex 53 for 48 h. The standard deviation was calculated from three independent determinations. Reprinted from Ref. [188] by permission of The Royal Society of Chemistry.

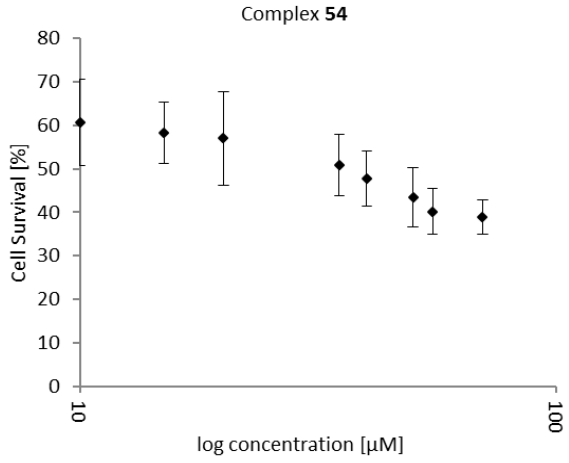

Figure S49: Cell survival [%] of HeLa cells treated with varying concentrations of complex 54 for 48 h. The standard deviation was calculated from three independent determinations. Reprinted from Ref. [188] by permission of The Royal Society of Chemistry.

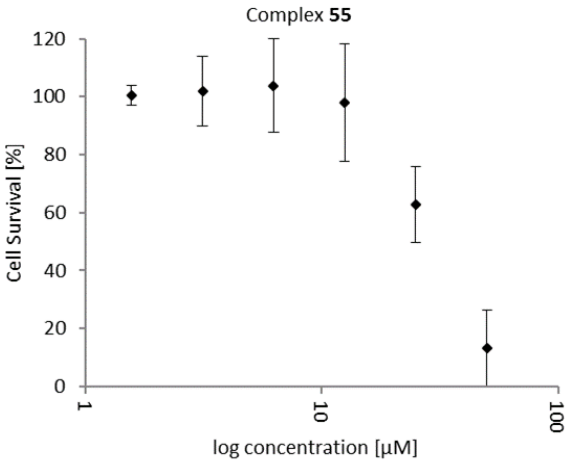

Figure S50: Cell survival [%] of HeLa cells treated with varying concentrations of complex 55 for 48 h. The standard deviation was calculated from three independent determinations. Reprinted from Ref. [188] by permission of The Royal Society of Chemistry.

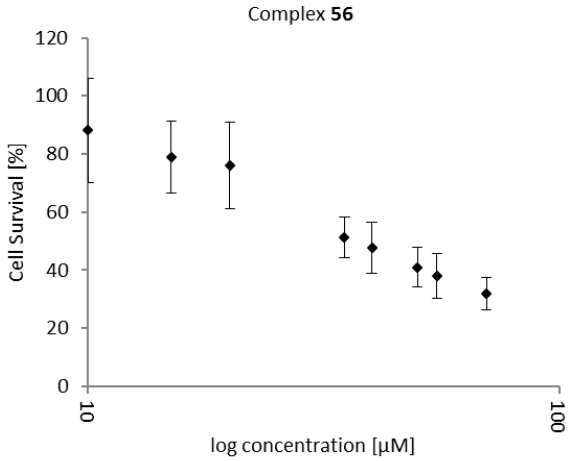

Figure S51: Cell survival [%] of HeLa cells treated with varying concentrations of complex 56 for 48 h. The standard deviation was calculated from three independent determinations. Reprinted from Ref. [188] by permission of The Royal Society of Chemistry.

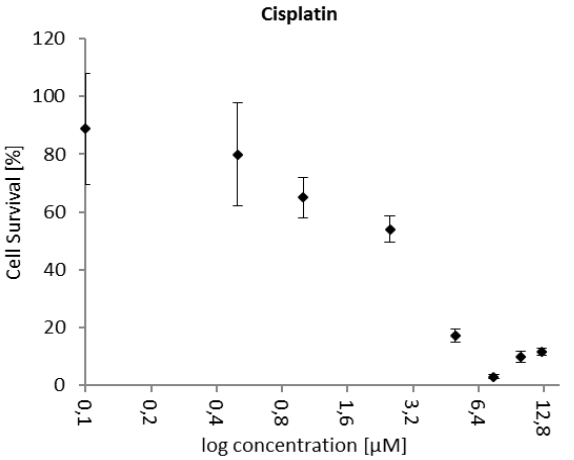

Figure S52: Cell survival [%] of HeLa cells treated with varying concentrations of cisplatin for 48 h. The standard deviation was calculated from three independent determinations. Reprinted from Ref. [188] by permission of The Royal Society of Chemistry.

6.3.2 MCF-7 cells

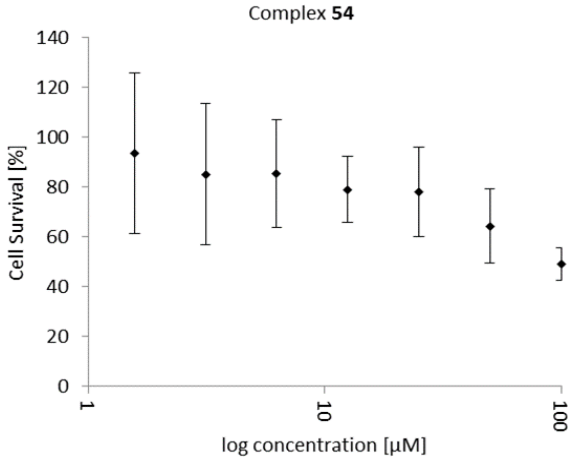

Figure S53: Cell survival [%] of MCF-7 cells treated with varying concentrations of complex 54 for 48 h. The standard deviation was calculated from three independent determinations. Reprinted from Ref. [188] by permission of The Royal Society of Chemistry.

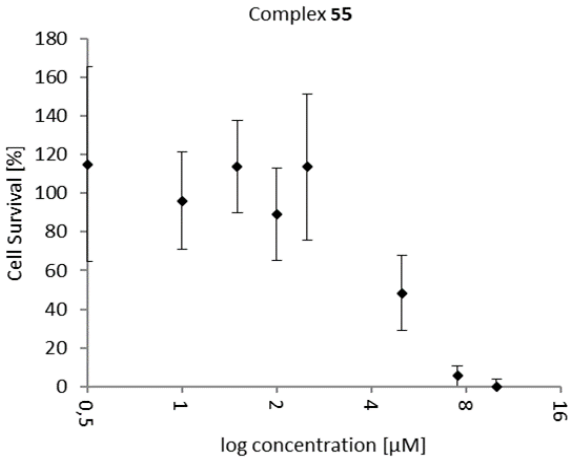

Figure S54: Cell survival [%] of MCF-7 cells treated with varying concentrations of complex 55 for 48 h. The standard deviation was calculated from three independent determinations. Reprinted from Ref. [188] by permission of The Royal Society of Chemistry.

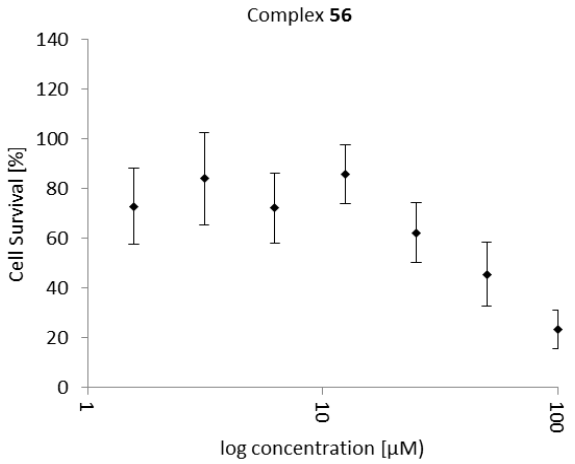

Figure S55: Cell survival [%] of MCF-7 cells treated with varying concentrations of complex 56 for 48 h. The standard deviation was calculated from three independent determinations. Reprinted from Ref. [188] by permission of The Royal Society of Chemistry.

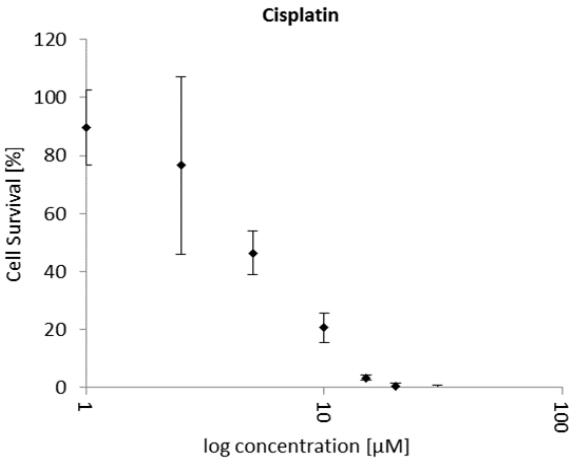

Figure S56: Cell survival [%] of MCF-7 cells treated with varying concentrations of cisplatin for 48 h. The standard deviation was calculated from three independent determinations. Reprinted from Ref. [188] by permission of The Royal Society of Chemistry.

6.3.3 PC3 cells

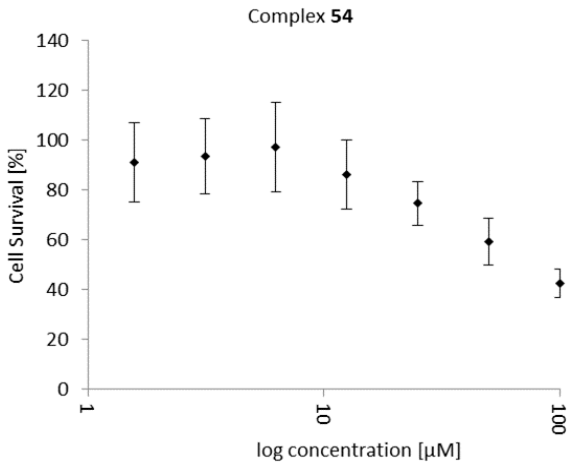

Figure S57: Cell survival [%] of PC3 cells treated with varying concentrations of complex 54 for 48 h. The standard deviation was calculated from three independent determinations. Reprinted from Ref. [188] by permission of The Royal Society of Chemistry.

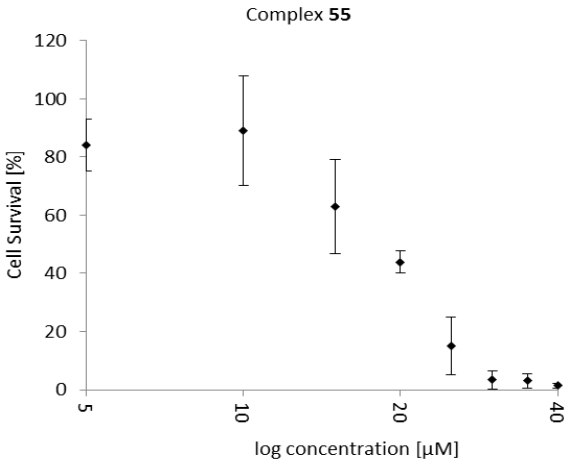

Figure S58: Cell survival [%] of PC3 cells treated with varying concentrations of complex 55 for 48 h. The standard deviation was calculated from three independent determinations. Reprinted from Ref. [188] by permission of The Royal Society of Chemistry.

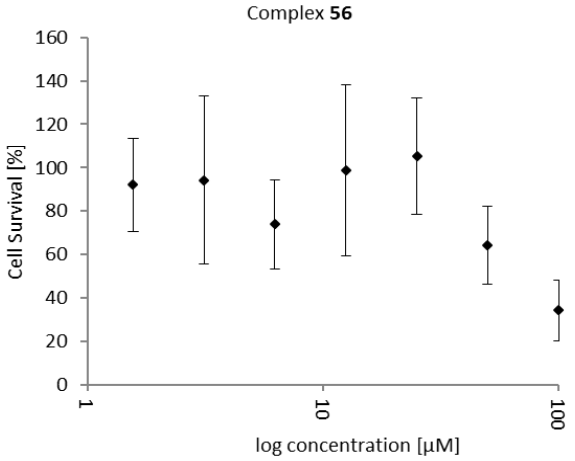

Figure S59: Cell survival [%] of PC3 cells treated with varying concentrations of complex 56 for 48 h. The standard deviation was calculated from three independent determinations. Reprinted from Ref. [188] by permission of The Royal Society of Chemistry.

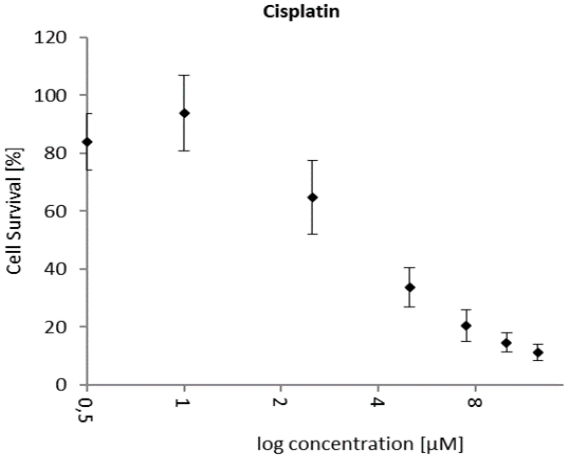

Figure S60: Cell survival [%] of PC3 cells treated with varying concentrations of cisplatin for 48 h. The standard deviation was calculated from three independent determinations. Reprinted from Ref. [188] by permission of The Royal Society of Chemistry.

6.3.4 A2780cisR cells

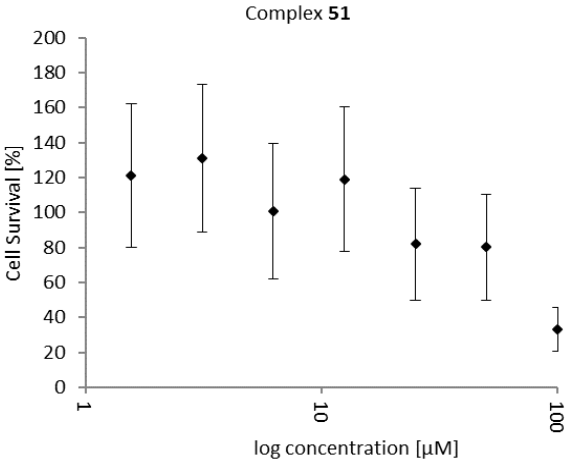

Figure S61: Cell survival [%] of A2780cisR cells treated with varying concentrations of complex 51 for 48 h. The standard deviation was calculated from three independent determinations. Reprinted from Ref. [188] by permission of The Royal Society of Chemistry.

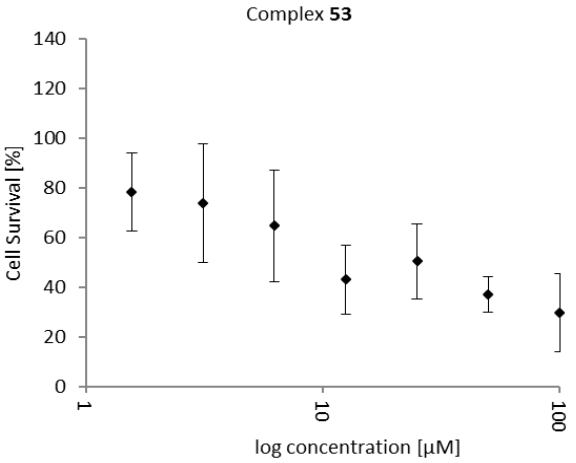

Figure S62: Cell survival [%] of A2780cisR cells treated with varying concentrations of complex 53 for 48 h. The standard deviation was calculated from three independent determinations. Reprinted from Ref. [188] by permission of The Royal Society of Chemistry.

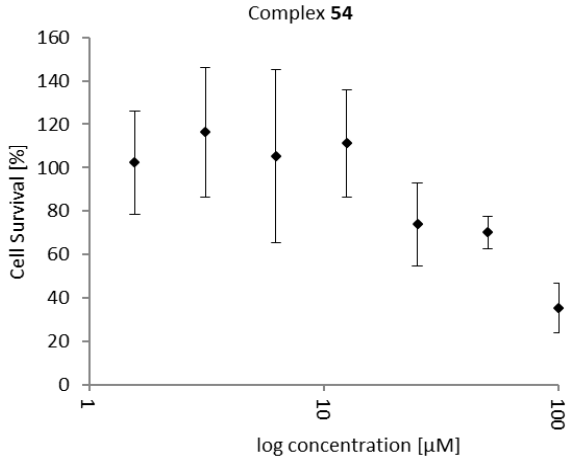

Figure S63: Cell survival [%] of A2780cisR cells treated with varying concentrations of complex 54 for 48 h. The standard deviation was calculated from three independent determinations. Reprinted from Ref. [188] by permission of The Royal Society of Chemistry.

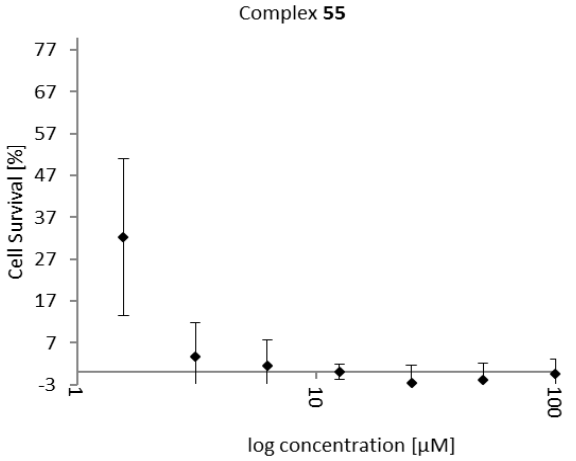

Figure S64: Cell survival [%] of A2780cisR cells treated with varying concentrations of complex 55 for 48 h. The standard deviation was calculated from three independent determinations. Reprinted from Ref. [188] by permission of The Royal Society of Chemistry.

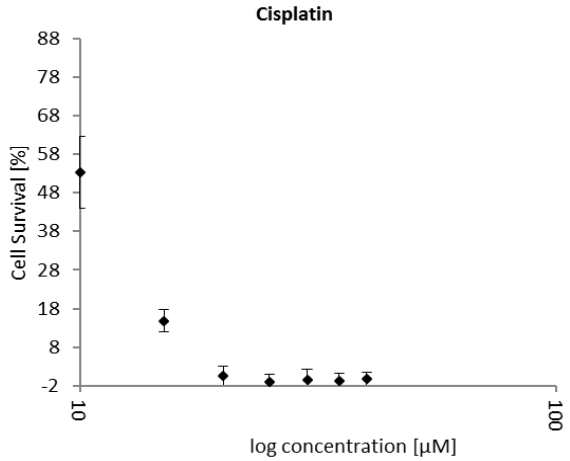

Figure S65: Cell survival [%] of A2780cisR cells treated with varying concentrations of cisplatin for 48 h. The standard deviation was calculated from three independent determinations. Reprinted from Ref. [188] by permission of The Royal Society of Chemistry.

7 Reprint Permissions

7.1 Royal Society of Chemistry

Figure 2, Reference [10]: R. Todd and S. Lippard, *Metallomics*, 2009, 1, 280-291.

Metallomics : integrated biometal science by Royal Society of Chemistry (Great Britain). Reproduced with permission of RSC Pub in the format Thesis/Dissertation via Copyright Clearance Center.

Confirmation Number: 11859966
Order Date: 10/16/2019

Customer Information

Customer: Elisabeth Bauer
Account Number: 3001528016
Organization: Technical University of Munich
Email: elisabeth.bauer@tum.de
Phone: +49 8928954112
Payment Method: Invoice

This is not an invoice

Order Details

Metallomics : integrated biometal science

Billing Status: **N/A**

Order detail ID:	72045161
ISSN:	1756-591X
Publication Type:	e-Journal
Volume:	
Issue:	
Start page:	
Publisher:	RSC Pub
Author/Editor:	Royal Society of Chemistry (Great Britain)

Permission Status: **Granted**

Permission type: Republish or display content
Type of use: Thesis/Dissertation
Order License Id: 4690870635977

Requestor type	Academic institution
Format	Print, Electronic
Portion	chart/graph/table/figure
Number of charts/graphs/tables /figures	2
The requesting person/organization	Technical University of Munich
Title or numeric reference of the portion(s)	Figure 2

Confirmation Number: 11859966

Special Rightsholder Terms & Conditions

The following terms & conditions apply to the specific publication under which they are listed

Metallomics : integrated biometal science
Permission type: Republish or display content
Type of use: Thesis/Dissertation

TERMS AND CONDITIONS

The following terms are individual to this publisher:

None

Other Terms and Conditions:

STANDARD TERMS AND CONDITIONS

1. Description of Service; Defined Terms. This Republication License enables the User to obtain licenses for republication of one or more copyrighted works as described in detail on the relevant Order Confirmation (the "Work(s)"). Copyright Clearance Center, Inc. ("CCC") grants licenses through the Service on behalf of the rightsholder identified on the Order Confirmation (the "Rightsholder"). "Republication", as used herein, generally means the inclusion of a Work, in whole or in part, in a new work or works, also as described on the Order Confirmation. "User", as used herein, means the person or entity making such republication.

2. The terms set forth in the relevant Order Confirmation, and any terms set by the Rightsholder with respect to a particular Work, govern the terms of use of Works in connection with the Service. By using the Service, the person transacting for a republication license on behalf of the User represents and warrants that he/she/it (a) has been duly authorized by the User to accept, and hereby does accept, all such terms and conditions on behalf of User, and (b) shall inform User of all such terms and conditions. In the event such person is a "freelancer" or other third party independent of User and CCC, such party shall be deemed jointly a "User" for purposes of these terms and conditions. In any event, User shall be deemed to have accepted and agreed to all such terms and conditions if User republishes the Work in any fashion.

3. Scope of License; Limitations and Obligations.

3.1 All Works and all rights therein, including copyright rights, remain the sole and exclusive property of the Rightsholder. The license created by the exchange of an Order Confirmation (and/or any invoice) and payment by User of the full amount set forth on that document includes only those rights expressly set forth in the Order Confirmation and in these terms and conditions, and conveys no other rights in the Work(s) to User. All rights not expressly granted are hereby reserved.

3.2 General Payment Terms: You may pay by credit card or through an account with us payable at the end of the month. If you and we agree that you may establish a standing account with CCC, then the following terms apply: Remit Payment to: Copyright Clearance Center, 29118 Network Place, Chicago, IL 60673-1291. Payments Due: Invoices are payable upon their delivery to you (or upon our notice to you that they are available to you for downloading). After 30 days, outstanding amounts will be subject to a service charge of 1-1/2% per month or, if less, the maximum rate allowed by applicable law. Unless otherwise specifically set forth in the Order Confirmation or in a separate written agreement signed by CCC, invoices are due and payable on "net 30" terms. While User may exercise the rights licensed immediately upon issuance of the Order Confirmation, the license is automatically revoked and is null and void, as if it had never been issued, if complete payment for the license is not received on a timely basis either from User directly or through a payment agent, such as a credit card company.

3.3 Unless otherwise provided in the Order Confirmation, any grant of rights to User (i) is "one-time" (including the editions and product family specified in the license), (ii) is non-exclusive and non-transferable and (iii) is subject to any and all limitations and restrictions (such as, but not limited to, limitations on duration of use or circulation) included in the Order Confirmation or invoice and/or in these terms and conditions. Upon completion of the licensed use, User shall either secure a new permission for further use of the Work(s) or immediately cease any new use of the Work(s) and shall render inaccessible (such as by deleting or by removing or severing links or other locators) any further copies of the Work (except for copies printed on paper in accordance with this license and still in User's stock at the end of such period).

3.4 In the event that the material for which a republication license is sought includes third party materials (such as photographs, illustrations, graphs, inserts and similar materials) which are identified in such material as having been used by permission, User is responsible for identifying, and seeking separate licenses (under this Service or otherwise) for, any of such third party materials; without a separate license, such third party materials may not be used.

3.5 Use of proper copyright notice for a Work is required as a condition of any license granted under the Service. Unless otherwise provided in the Order Confirmation, a proper copyright notice will read substantially as follows: "Republished with permission of [Rightsholder's name], from [Work's title, author, volume, edition number and year of copyright]; permission conveyed through Copyright Clearance Center, Inc. " Such notice must be provided in a reasonably legible font size and must be placed either immediately adjacent to the Work as used (for example, as part of a by-line or footnote but not as a separate electronic link) or in the place where substantially all other credits or notices for the new work containing the republished Work are located. Failure to include the required notice results in loss to the Rightsholder and CCC, and the User shall be liable to pay liquidated damages for each such failure equal to twice the use fee specified in the Order Confirmation, in addition to the use fee itself and any other fees and charges specified.

3.6 User may only make alterations to the Work if and as expressly set forth in the Order Confirmation. No Work may be used in any way that is defamatory, violates the rights of third parties (including such third parties' rights of copyright, privacy, publicity, or other tangible or intangible property), or is otherwise illegal, sexually explicit or obscene. In addition, User may not conjoin a Work with any other material that may result in damage to the reputation of the Rightsholder. User agrees to inform CCC if it becomes aware of any infringement of any rights in a Work and to cooperate with any reasonable request of CCC or the Rightsholder in connection therewith.

4. Indemnity. User hereby indemnifies and agrees to defend the Rightsholder and CCC, and their respective employees and directors, against all claims, liability, damages, costs and expenses, including legal fees and expenses, arising out of any use of a Work beyond the scope of the rights granted herein, or any use of a Work which has been altered in any unauthorized way by User, including claims of defamation or infringement of rights of copyright, publicity, privacy or other tangible or intangible property.

5. Limitation of Liability. UNDER NO CIRCUMSTANCES WILL CCC OR THE RIGHTSHOLDER BE LIABLE FOR ANY DIRECT, INDIRECT, CONSEQUENTIAL OR INCIDENTAL DAMAGES (INCLUDING WITHOUT LIMITATION DAMAGES FOR LOSS OF BUSINESS PROFITS OR INFORMATION, OR FOR BUSINESS INTERRUPTION) ARISING OUT OF THE USE OR INABILITY TO USE A WORK, EVEN IF ONE OF THEM HAS BEEN ADVISED OF THE POSSIBILITY OF SUCH DAMAGES. In any event, the total liability of the Rightsholder and CCC (including their respective employees and directors) shall not exceed the total amount actually paid by User for this license. User assumes full liability for the actions and omissions of its principals, employees, agents, affiliates, successors and assigns.

6. Limited Warranties. THE WORK(S) AND RIGHT(S) ARE PROVIDED "AS IS". CCC HAS THE RIGHT TO GRANT TO USER THE RIGHTS GRANTED IN THE ORDER CONFIRMATION DOCUMENT. CCC AND THE RIGHTSHOLDER DISCLAIM ALL OTHER WARRANTIES RELATING TO THE WORK(S) AND RIGHT(S), EITHER EXPRESS OR IMPLIED, INCLUDING WITHOUT LIMITATION IMPLIED WARRANTIES OF MERCHANTABILITY OR FITNESS FOR A PARTICULAR PURPOSE. ADDITIONAL RIGHTS MAY BE REQUIRED TO USE ILLUSTRATIONS, GRAPHS, PHOTOGRAPHS, ABSTRACTS, INSERTS OR OTHER PORTIONS OF THE WORK (AS OPPOSED TO THE ENTIRE WORK) IN A MANNER CONTEMPLATED BY USER; USER UNDERSTANDS AND AGREES THAT NEITHER CCC NOR THE RIGHTSHOLDER MAY HAVE SUCH ADDITIONAL RIGHTS TO GRANT.

7. Effect of Breach. Any failure by User to pay any amount when due, or any use by User of a Work beyond the scope of the license set forth in the Order Confirmation and/or these terms and conditions, shall be a material breach of the license created by the Order Confirmation and these terms and conditions. Any breach not cured within 30 days of written notice thereof shall result in immediate termination of such license without further notice. Any unauthorized (but licensable) use of a Work that is terminated immediately upon notice thereof may be liquidated by payment of the Rightsholder's ordinary license price therefor; any unauthorized (and unlicensable) use that is not terminated immediately for any reason (including, for example, because materials containing the Work cannot reasonably be recalled) will be subject to all remedies available at law or in equity, but in no event to a payment of less than three times the Rightsholder's ordinary license price for the most closely analogous licensable use plus Rightsholder's and/or CCC's costs and expenses incurred in collecting such payment.

8. **Miscellaneous.**

8.1 User acknowledges that CCC may, from time to time, make changes or additions to the Service or to these terms and conditions, and CCC reserves the right to send notice to the User by electronic mail or otherwise for the purposes of notifying User of such changes or additions; provided that any such changes or additions shall not apply to permissions already secured and paid for.

8.2 Use of User-related information collected through the Service is governed by CCC's privacy policy, available online here: http://www.copyright.com/content/cc3/en/tools/footer/privacypolicy.html.

8.3 The licensing transaction described in the Order Confirmation is personal to User. Therefore, User may not assign or transfer to any other person (whether a natural person or an organization of any kind) the license created by the Order Confirmation and these terms and conditions or any rights granted hereunder; provided, however, that User may assign such license in its entirety on written notice to CCC in the event of a transfer of all or substantially all of User's rights in the new material which includes the Work(s) licensed under this Service.

8.4 No amendment or waiver of any terms is binding unless set forth in writing and signed by the parties. The Rightsholder and CCC hereby object to any terms contained in any writing prepared by the User or its principals, employees, agents or affiliates and purporting to govern or otherwise relate to the licensing transaction described in the Order Confirmation, which terms are in any way inconsistent with any terms set forth in the Order Confirmation and/or in these terms and conditions or CCC's standard operating procedures, whether such writing is prepared prior to, simultaneously with or subsequent to the Order Confirmation, and whether such writing appears on a copy of the Order Confirmation or in a separate instrument.

8.5 The licensing transaction described in the Order Confirmation document shall be governed by and construed under the law of the State of New York, USA, without regard to the principles thereof of conflicts of law. Any case, controversy, suit, action, or proceeding arising out of, in connection with, or related to such licensing transaction shall be brought, at CCC's sole discretion, in any federal or state court located in the County of New York, State of New York, USA, or in any federal or state court whose geographical jurisdiction covers the location of the Rightsholder set forth in the Order Confirmation. The parties expressly submit to the personal jurisdiction and venue of each such federal or state court.If you have any comments or questions about the Service or Copyright Clearance Center, please contact us at 978-750-8400 or send an e-mail to info@copyright.com.

v 1.1

7.2 Royal Society of Chemistry

"Synthesis, characterization, and biological studies of multidentate gold(I) and gold(III) NHC complexes"

Dalton Transactions, 2019,**48**, 16615-16625. DOI: 10.1039/C9DT03183A

Reproduced with permission from The Royal Society of Chemistry.

"Authors contributing to RSC publications (journal articles, books or book chapters) do not need to formally request permission to reproduce material contained in this article provided that the correct acknowledgement is given with the reproduced material.

If you are the author of this article you do not need to formally request permission to reproduce figures, diagrams etc. contained in this article in third party publications or in a thesis or dissertation provided that the correct acknowledgement is given with the reproduced material."

8 REFERENCES

1. R. L. Siegel, K. D. Miller and A. Jemal, *CA: A Cancer Journal for Clinicians*, 2019, **69**, 7-34.
2. D. Hanahan and R. A. Weinberg, *Cell*, 2000, **100**, 57-70.
3. D. Hanahan and Robert A. Weinberg, *Cell*, 2011, **144**, 646-674.
4. X. Zhang, S. L. Marjani, Z. Hu, S. M. Weissman, X. Pan and S. Wu, *Cancer Research*, 2016, **76**, 1305-1312.
5. E. B. Bauer, A. A. Haase, R. M. Reich, D. C. Crans and F. E. Kühn, *Coordination Chemistry Reviews*, 2019, **393**, 79-117.
6. K. Strebhardt and A. Ullrich, *Nature Reviews Cancer*, 2008, **8**, 473-480.
7. B. Rosenberg, L. Van Camp and T. Krigas, *Nature*, 1965, **205**, 698-699.
8. E. Wiltshaw, *Platinum Metals Review*, 1979, **23**, 90-98.
9. L. Galluzzi, L. Senovilla, I. Vitale, J. Michels, I. Martins, O. Kepp, M. Castedo and G. Kroemer, *Oncogene*, 2011, **31**, 1869-1883.
10. R. C. Todd and S. J. Lippard, *Metallomics*, 2009, **1**, 280-291.
11. T. C. Johnstone, K. Suntharalingam and S. J. Lippard, *Chemical Reviews*, 2016, **116**, 3436-3486.
12. R. Oun, Y. E. Moussa and N. J. Wheate, *Dalton Transactions*, 2018, **47**, 6645-6653.
13. Z. H. Siddik, *Oncogene*, 2003, **22**, 7265-7279.
14. J. Zhou, G. Yu and F. Huang, *Chemical Society Reviews*, 2017, **46**, 7021-7053.
15. A. Schmidt, A. Casini and F. E. Kühn, *Coordination Chemistry Reviews*, 2014, **275**, 19-36.
16. A. Ahmedova, *Frontiers in Chemistry*, 2018, **6**, 620-620.
17. E. Puig, C. Desmarets, G. Gontard, M. N. Rager, A. L. Cooksy and H. Amouri, *Inorganic Chemistry*, 2019, **58**, 3189-3195.
18. J. Han, A. Schmidt, T. Zhang, H. Permentier, G. M. M. Groothuis, R. Bischoff, F. E. Kühn, P. Horvatovich and A. Casini, *Chemical Communications*, 2017, **53**, 1405-1408.
19. F. Kaiser, A. Schmidt, W. Heydenreuter, P. J. Altmann, A. Casini, S. A. Sieber and F. E. Kühn, *European Journal of Inorganic Chemistry*, 2016, **2016**, 5189-5196.
20. A. Schmidt, M. Hollering, M. Drees, A. Casini and F. E. Kühn, *Dalton Transactions*, 2016, **45**, 8556-8565.
21. A. Schmidt, M. Hollering, J. Han, A. Casini and F. E. Kühn, *Dalton Transactions*, 2016, **45**, 12297-12300.
22. A. Schmidt, V. Molano, M. Hollering, A. Pöthig, A. Casini and F. E. Kühn, *Chemistry – A European Journal*, 2016, **22**, 2253-2256.
23. P. Liao, B. W. Langloss, A. M. Johnson, E. R. Knudsen, F. S. Tham, R. R. Julian and R. J. Hooley, *Chemical Communications*, 2010, **46**, 4932-4934.
24. J. E. M. Lewis, E. L. Gavey, S. A. Cameron and J. D. Crowley, *Chemical Science*, 2012, **3**, 778-784.
25. J. E. Lewis, A. B. Elliott, C. J. McAdam, K. C. Gordon and J. D. Crowley, *Chemical Science*, 2014, **5**, 1833-1843.
26. D. Preston, S. M. McNeill, J. E. M. Lewis, G. I. Giles and J. D. Crowley, *Dalton Transactions*, 2016, **45**, 8050-8060.
27. Z. Li, N. Kishi, K. Yoza, M. Akita and M. Yoshizawa, *Chemistry – A European Journal*, 2012, **18**, 8358-8365.
28. N. Kishi, Z. Li, Y. Sei, M. Akita, K. Yoza, J. S. Siegel and M. Yoshizawa, *Chemistry – A European Journal*, 2013, **19**, 6313-6320.
29. A. Ahmedova, D. Momekova, M. Yamashina, P. Shestakova, G. Momekov, M. Akita and M. Yoshizawa, *Chemistry – An Asian Journal*, 2016, **11**, 474-477.
30. B. Woods, D. Döllerer, B. Aikman, M. N. Wenzel, E. J. Sayers, F. E. Kühn, A. T. Jones and A. Casini, *Journal of Inorganic Biochemistry*, 2019, **199**, 110781.
31. A. Pöthig and A. Casini, *Theranostics*, 2019, **9**, 3150-3169.

32. J. Han, A. F. B. Räder, F. Reichart, B. Aikman, M. N. Wenzel, B. Woods, M. Weinmüller, B. S. Ludwig, S. Stürup, G. M. M. Groothuis, H. P. Permentier, R. Bischoff, H. Kessler, P. Horvatovich and A. Casini, *Bioconjugate Chemistry*, 2018, **29**, 3856-3865.
33. H. Sepehrpour, W. Fu, Y. Sun and P. J. Stang, *Journal of the American Chemical Society*, 2019, **141**, 14005-14020.
34. M. N. Hopkinson, C. Richter, M. Schedler and F. Glorius, *Nature*, 2014, **510**, 485-496.
35. N. Kuhn and A. Al-Sheikh, *Coordination Chemistry Reviews*, 2005, **249**, 829-857.
36. S. Bellemin-Laponnaz and S. Dagorne, *Chemical Reviews*, 2014, **114**, 8747-8774.
37. P. L. Arnold and I. J. Casely, *Chemical Reviews*, 2009, **109**, 3599-3611.
38. W. A. Herrmann and C. Köcher, *Angewandte Chemie International Edition in English*, 1997, **36**, 2162-2187.
39. W. A. Herrmann, *Angewandte Chemie International Edition*, 2002, **41**, 1290-1309.
40. N. Marion, S. Díez-González and S. P. Nolan, *Angewandte Chemie International Edition*, 2007, **46**, 2988-3000.
41. S. Diez-Gonzalez, N. Marion and S. P. Nolan, *Chemical Reviews*, 2009, **109**, 3612-3676.
42. S. Bellemin-Laponnaz, E. Despagnet-Ayoub, S. Díez-González, L. Gade, F. Glorius, J. Louie, S. Nolan, E. Peris, T. Ritter and M. Rogers, *N-heterocyclic carbenes in transition metal catalysis*, Springer, Berlin, Heidelberg, 2004.
43. J. C. Y. Lin, R. T. W. Huang, C. S. Lee, A. Bhattacharyya, W. S. Hwang and I. J. B. Lin, *Chemical Reviews*, 2009, **109**, 3561-3598.
44. W. Liu and R. Gust, *Chemical Society Reviews*, 2013, **42**, 755-773.
45. F. Cisnetti and A. Gautier, *Angewandte Chemie International Edition*, 2013, **52**, 11976-11978.
46. K. M. Hindi, M. J. Panzner, C. A. Tessier, C. L. Cannon and W. J. Youngs, *Chemical reviews*, 2009, **109**, 3859-3884.
47. A. Kascatan-Nebioglu, M. J. Panzner, C. A. Tessier, C. L. Cannon and W. J. Youngs, *Coordination Chemistry Reviews*, 2007, **251**, 884-895.
48. E. O. Fischer and A. Maasböl, *Angewandte Chemie International Edition in English*, 1964, **3**, 580-581.
49. R. R. Schrock, *Journal of the American Chemical Society*, 1974, **96**, 6796-6797.
50. K. Öfele, *Journal of Organometallic Chemistry*, 1968, **12**, P42-P43.
51. H.-W. Wanzlick and H.-J. Schönherr, *Angewandte Chemie International Edition in English*, 1968, **7**, 141-142.
52. A. J. Arduengo, R. L. Harlow and M. Kline, *Journal of the American Chemical Society*, 1991, **113**, 361-363.
53. K. Öfele, W. A. Herrmann, D. Mihalios, M. Elison, E. Herdtweck, W. Scherer and J. Mink, *Journal of Organometallic Chemistry*, 1993, **459**, 177-184.
54. H. Jacobsen, A. Correa, A. Poater, C. Costabile and L. Cavallo, *Coordination Chemistry Reviews*, 2009, **253**, 687-703.
55. W. A. Herrmann, M. Elison, J. Fischer, C. Köcher and G. R. J. Artus, *Angewandte Chemie International Edition in English*, 1995, **34**, 2371-2374.
56. K. Riener, S. Haslinger, A. Raba, M. P. Högerl, M. Cokoja, W. A. Herrmann and F. E. Kühn, *Chemical Reviews*, 2014, **114**, 5215-5272.
57. M. Porchia, M. Pellei, M. Marinelli, F. Tisato, F. Del Bello and C. Santini, *European Journal of Medicinal Chemistry*, 2018, **146**, 709-746.
58. B. Dominelli, J. D. G. Correia and F. E. Kühn, *Journal of Organometallic Chemistry*, 2018, **866**, 153-164.
59. P. J. Barnard, M. V. Baker, S. J. Berners-Price and D. A. Day, *Journal of Inorganic Biochemistry*, 2004, **98**, 1642-1647.
60. S. J. Berners-Price and A. Filipovska, *Australian Journal of Chemistry*, 2008, **61**, 661-668.

61. R. Rubbiani, I. Kitanovic, H. Alborzinia, S. Can, A. Kitanovic, L. A. Onambele, M. Stefanopoulou, Y. Geldmacher, W. S. Sheldrick, G. Wolber, A. Prokop, S. Wölfl and I. Ott, *Journal of Medicinal Chemistry*, 2010, **53**, 8608-8618.
62. F. Hackenberg, H. Müller-Bunz, R. Smith, W. Streciwilk, X. Zhu and M. Tacke, *Organometallics*, 2013, **32**, 5551-5560.
63. B. Bertrand, M. R. M. Williams and M. Bochmann, *Chemistry – A European Journal*, 2018, **24**, 11840-11851.
64. B. Bertrand, A. de Almeida, E. P. M. van der Burgt, M. Picquet, A. Citta, A. Folda, M. P. Rigobello, P. Le Gendre, E. Bodio and A. Casini, *European Journal of Inorganic Chemistry*, 2014, **2014**, 4532-4536.
65. A. Meyer, L. Oehninger, Y. Geldmacher, H. Alborzinia, S. Wölfl, W. S. Sheldrick and I. Ott, *ChemMedChem*, 2014, **9**, 1794-1800.
66. C. Nardon, G. Boscutti and D. Fregona, *Anticancer Research*, 2014, **34**, 487-492.
67. T. Zou, C. T. Lum, C.-N. Lok, J.-J. Zhang and C.-M. Che, *Chemical Society Reviews*, 2015, **44**, 8786-8801.
68. O. Dada, G. Sánchez-Sanz, M. Tacke and X. Zhu, *Tetrahedron Letters*, 2018, **59**, 2904-2908.
69. C. Zhang, M.-L. Maddelein, R. Wai-Yin Sun, H. Gornitzka, O. Cuvillier and C. Hemmert, *European Journal of Medicinal Chemistry*, 2018, **157**, 320-332.
70. M. Mora, M. C. Gimeno and R. Visbal, *Chemical Society Reviews*, 2019, **48**, 447-462.
71. B. M. Sutton, E. McGusty, D. T. Walz and M. J. DiMartino, *Journal of Medicinal Chemistry*, 1972, **15**, 1095-1098.
72. T. Onodera, I. Momose and M. Kawada, *Chemical and Pharmaceutical Bulletin*, 2019, **67**, 186-191.
73. E. Vergara, A. Casini, F. Sorrentino, O. Zava, E. Cerrada, M. P. Rigobello, A. Bindoli, M. Laguna and P. J. Dyson, *ChemMedChem: Chemistry Enabling Drug Discovery*, 2010, **5**, 96-102.
74. A. Bindoli, M. P. Rigobello, G. Scutari, C. Gabbiani, A. Casini and L. Messori, *Coordination Chemistry Reviews*, 2009, **253**, 1692-1707.
75. L. Ortego, F. Cardoso, S. Martins, M. F. Fillat, A. Laguna, M. Meireles, M. D. Villacampa and M. C. Gimeno, *Journal of Inorganic Biochemistry*, 2014, **130**, 32-37.
76. A. Casini, R. Sun and I. Ott, *Metal Ions in Life Sciences*, 2018, **18**, 199-217.
77. C. Zhang, C. Hemmert, H. Gornitzka, O. Cuvillier, M. Zhang and R. W. Y. Sun, *ChemMedChem*, 2018, **13**, 1218-1229.
78. Q.-A. Sun, Y. Wu, F. Zappacosta, K.-T. Jeang, B. J. Lee, D. L. Hatfield and V. N. Gladyshev, *Journal of Biological Chemistry*, 1999, **274**, 24522-24530.
79. T. Zou, C.-N. Lok, P.-K. Wan, Z.-F. Zhang, S.-K. Fung and C.-M. Che, *Current Opinion in Chemical Biology*, 2018, **43**, 30-36.
80. Ö. Karaca, S. M. Meier-Menches, A. Casini and F. E. Kühn, *Chemical Communications*, 2017, **53**, 8249-8260.
81. M. J. Hannon, *Chemical Society Reviews*, 2007, **36**, 280-295.
82. C. Bazzicalupi, M. Ferraroni, F. Papi, L. Massai, B. Bertrand, L. Messori, P. Gratteri and A. Casini, *Angewandte Chemie International Edition*, 2016, **55**, 4256-4259.
83. P. Murat and S. Balasubramanian, *Current Opinion in Genetics & Development*, 2014, **25**, 22-29.
84. Z. Tan, J. Tang, Z.-Y. Kan and Y.-H. Hao, *Current Topics in Medicinal Chemistry*, 2015, **15**, 1940-1946.
85. G. W. Collie, N. H. Campbell and S. Neidle, *Nucleic Acids Research*, 2015, **43**, 4785-4799.
86. B. Bertrand, J. Fernandez-Cestau, J. Angulo, M. M. D. Cominetti, Z. A. E. Waller, M. Searcey, M. A. O'Connell and M. Bochmann, *Inorganic Chemistry*, 2017, **56**, 5728-5740.
87. L. Messori, P. Orioli, C. Tempi and G. Marcon, *Biochemical and Biophysical Research Communications*, 2001, **281**, 352-360.
88. W. M. Jarrell, A. L. Page and A. A. Elseewi, *Residue Reviews*, 1980, **74**, 1-43.
89. D. G. Barceloux and D. Barceloux, *Journal of Toxicology: Clinical Toxicology*, 1999, **37**, 231-237.

90. G. J. Brewer, R. D. Dick, D. K. Grover, V. LeClaire, M. Tseng, M. Wicha, K. Pienta, B. G. Redman, T. Jahan and V. K. Sondak, *Clinical Cancer Research*, 2000, **6**, 1-10.
91. S. Majumder, S. Pasayat, A. K. Panda, S. P. Dash, S. Roy, A. Biswas, M. E. Varma, B. N. Joshi, E. Garribba, C. Kausar, S. K. Patra, W. Kaminsky, A. Crochet and R. Dinda, *Inorganic Chemistry*, 2017, **56**, 11190-11210.
92. F. A. Cotton and D. G. Nocera, *Accounts of Chemical Research*, 2000, **33**, 483-490.
93. L. R. Falvello, B. M. Foxman and C. A. Murillo, *Inorganic Chemistry*, 2014, **53**, 9441-9456.
94. A. Shtemenko and N. Shtemenko, *The Ukrainian Biochemical Journal*, 2017, **89**, 5-30.
95. H.-J. Lunk, *ChemTexts*, 2015, **1**, 6.
96. A. Levina and P. A. Lay, *Coordination Chemistry Reviews*, 2005, **249**, 281-298.
97. D. M. Stearns, *Evaluation of chromium (III) genotoxicity with cell culture and in vitro assays*, Netherlands, 2007.
98. A. Levina, D. C. Crans and P. A. Lay, *Coordination Chemistry Reviews*, 2017, **352**, 473-498.
99. A. Levina and P. A. Lay, *Chemical Research in Toxicology*, 2008, **21**, 563-571.
100. S. M. Beladi-Mousavi, B. Khezri, L. Krejčová, Z. Heger, Z. Sofer, A. C. Fisher and M. Pumera, *ACS Applied Materials & Interfaces*, 2019, **11**, 13359-13369.
101. M. S. Amini-Fazl, R. Mohammadi and K. Kheiri, *International Journal of Biological Macromolecules*, 2019, **132**, 506-513.
102. M. K. Koley, S. U. Parsekar, N. Duraipandy, M. S. Kiran, B. Varghese, P. T. Manoharan and A. P. Koley, *Inorganica Chimica Acta*, 2018, **478**, 211-221.
103. W. Liu, R. Al-Oweini, K. Meadows, B. S. Bassil, Z. Lin, J. H. Christian, N. S. Dalal, A. M. Bossoh, I. M. Mbomekallé, P. de Oliveira, J. Iqbal and U. Kortz, *Inorganic Chemistry*, 2016, **55**, 10936-10946.
104. J. Sedlacek, L. M. D. R. S. Martins, P. Danek, A. J. L. Pombeiro and B. Cvek, *Journal of Applied Biomedicine*, 2014, **12**, 301-308.
105. M. E. Weeks, *Journal of Chemical Education*, 1932, **9**, 863-884.
106. D. Rehder, *Metallomics*, 2015, **7**, 730-742.
107. D. C. Crans, L. Yang, A. Haase and X. Yang, *Metal Ions in Life Sciences*, 2018, **18**, 251-279.
108. K. H. Thompson and C. Orvig, *Journal of Inorganic Biochemistry*, 2006, **100**, 1925-1935.
109. K. H. Thompson and C. Orvig, *Dalton Transactions*, 2006, 761-764.
110. D. C. Crans, L. Henry, G. Cardiff and B. I. Posner, *Metal Ions in Life Sciences*, 2019, **19**, 203-230.
111. E. Kioseoglou, S. Petanidis, C. Gabriel and A. Salifoglou, *Coordination Chemistry Reviews*, 2015, **301-302**, 87-105.
112. W. Legrum, *Toxicology*, 1986, **42**, 281-289.
113. T. R. Cook and P. J. Stang, *Chemical Reviews*, 2015, **115**, 7001-7045.
114. A. Casini, B. Woods and M. Wenzel, *Inorganic Chemistry*, 2017, **56**, 14715-14729.
115. F. E. Kühn, J. R. Ismeier, D. Schön, W.-M. Xue, G. Zhang and O. Nuyken, *Macromolecular Rapid Communications*, 1999, **20**, 555-559.
116. F. A. Cotton, *Journal of the Less Common Metals*, 1977, **54**, 3-12.
117. F. A. Cotton, L. M. Daniels, C. A. Murillo and X. Wang, *Polyhedron*, 1998, **17**, 2781-2793.
118. F. A. Cotton, W. H. Ilsley and W. Kaim, *Inorganic Chemistry*, 1979, **18**, 2717-2719.
119. M. H. Chisholm, *Polyhedron*, 1983, **2**, 681-722.
120. D. M. Baird, K. Y. Shih, J. H. Welch and R. D. Bereman, *Polyhedron*, 1989, **8**, 2359-2365.
121. F. A. Cotton and K. J. Wiesinger, *Inorganic Chemistry*, 1991, **30**, 871-873.
122. M. Majumdar, S. K. Patra, M. Kannan, K. R. Dunbar and J. K. Bera, *Inorganic Chemistry*, 2008, **47**, 2212-2222.
123. F. A. Cotton and J. G. Norman, *Journal of the American Chemical Society*, 1972, **94**, 5697-5702.
124. R. Ziessel, J. Suffert and M.-T. Youinou, *The Journal of Organic Chemistry*, 1996, **61**, 6535-6546.
125. P. V. James, K. Yoosaf, J. Kumar, K. G. Thomas, A. Listorti, G. Accorsi and N. Armaroli, *Photochemical & Photobiological Sciences*, 2009, **8**, 1432-1440.

126. R. T. Henriques, E. Herdtweck, F. E. Kühn, A. D. Lopes, J. Mink and C. C. Romão, *Journal of the Chemical Society, Dalton Transactions*, 1998, 1293-1298.
127. O. Levy, B. Bogoslavsky and A. Bino, *Inorganica Chimica Acta*, 2012, **391**, 179-181.
128. D. L. Reger, A. E. Pascui, P. J. Pellechia and A. Ozarowski, *Inorganic Chemistry*, 2013, **52**, 12741-12748.
129. A. J. Pell, G. Pintacuda and C. P. Grey, *Progress in Nuclear Magnetic Resonance Spectroscopy*, 2019, **111**, 1-271.
130. L. Öhrström and G. Svensson, *Inorganica Chimica Acta*, 2000, **305**, 157-162.
131. R. Corbo, G. F. Ryan, M. A. Haghighatbin, C. F. Hogan, D. J. D. Wilson, M. D. Hulett, P. J. Barnard and J. L. Dutton, *Inorganic Chemistry*, 2016, **55**, 2830-2839.
132. R. Corbo, T. P. Pell, B. D. Stringer, C. F. Hogan, D. J. D. Wilson, P. J. Barnard and J. L. Dutton, *Journal of the American Chemical Society*, 2014, **136**, 12415-12421.
133. X. Cui, A. N. Khlobystov, X. Chen, D. H. Marsh, A. J. Blake, W. Lewis, N. R. Champness, C. J. Roberts and M. Schröder, *Chemistry – A European Journal*, 2009, **15**, 8861-8873.
134. Z.-Q. Tan, J.-F. Liu, R. Liu, Y.-G. Yin and G.-B. Jiang, *Chemical Communications*, 2009, 7030-7032.
135. M. N. Hopkinson, A. D. Gee and V. Gouverneur, *Chemistry – A European Journal*, 2011, **17**, 8248-8262.
136. I. O. Koshevoy, M. Haukka, S. I. Selivanov, S. P. Tunik and T. A. Pakkanen, *Chemical Communications*, 2010, **46**, 8926-8928.
137. R. V. Honeychuck and W. H. Hersh, *Inorganic Chemistry*, 1989, **28**, 2869-2886.
138. S. M. McNeill, D. Preston, J. E. M. Lewis, A. Robert, K. Knerr-Rupp, D. O. Graham, J. R. Wright, G. I. Giles and J. D. Crowley, *Dalton Transactions*, 2015, **44**, 11129-11136.
139. M. Alam, D. J. Du Bois, R. C. Hawley, J. Kennedy-Smith, A. E. Minatti, W. S. Palmer, T. Silva and R. S. Wilhelm, 2011, **US20110071150A1**.
140. M. Li, P. Xing, Z. Huang and B. Jiang, *Chinese Journal of Chemistry*, 2013, **31**, 49-54.
141. J. Guan, Y. Zou, P. Gao, Y. Wu and Z. Yue, *Chinese Journal of Chemistry*, 2010, **28**, 1613-1617.
142. J. A. MacKay and N. R. Wetzel, *Journal of Chemical Education*, 2014, **91**, 722-725.
143. F. A. Cotton, T. S. Barnard, L. M. Daniels and C. A. Murillo, *Inorganic Chemistry Communications*, 2002, **5**, 527-532.
144. F. A. Cotton, J. P. Donahue, C. Lin and C. A. Murillo, *Inorganic Chemistry*, 2001, **40**, 1234-1244.
145. F. A. Cotton, C. Lin and C. A. Murillo, *Inorganic Chemistry*, 2001, **40**, 478-484.
146. Y. Ke, D. J. Collins and H.-C. Zhou, *Inorganic Chemistry*, 2005, **44**, 4154-4156.
147. X.-M. Cai, D. Höhne, M. Köberl, M. Cokoja, A. Pöthig, E. Herdtweck, S. Haslinger, W. A. Herrmann and F. E. Kühn, *Organometallics*, 2013, **32**, 6004-6011.
148. D. Höhne, E. Herdtweck, A. Pöthig and F. E. Kühn, *Inorganica Chimica Acta*, 2015, **424**, 210-215.
149. D. Höhne, E. Herdtweck, A. Pöthig and F. E. Kühn, *Dalton Transactions*, 2014, **43**, 15367-15374.
150. K. J. Kilpin, M. L. Gower, S. G. Telfer, G. B. Jameson and J. D. Crowley, *Inorganic Chemistry*, 2011, **50**, 1123-1134.
151. B.-C. Tzeng, M. Banik, T. Selvam and G.-H. Lee, *Crystal Growth & Design*, 2013, **13**, 4245-4251.
152. M. R. Anneser, S. Haslinger, A. Pöthig, M. Cokoja, J.-M. Basset and F. E. Kühn, *Inorganic Chemistry*, 2015, **54**, 3797-3804.
153. Ö. Karaca, M. R. Anneser, J. W. Kück, A. C. Lindhorst, M. Cokoja and F. E. Kühn, *Journal of Catalysis*, 2016, **344**, 213-220.
154. J. W. Kück, M. R. Anneser, B. Hofmann, A. Pöthig, M. Cokoja and F. E. Kühn, *ChemSusChem*, 2015, **8**, 4056-4063.
155. M. R. Anneser, S. Haslinger, A. Pöthig, M. Cokoja, V. D'Elia, M. P. Högerl, J.-M. Basset and F. E. Kühn, *Dalton Transactions*, 2016, **45**, 6449-6455.
156. Z. S. Ghavami, M. R. Anneser, F. Kaiser, P. J. Altmann, B. J. Hofmann, J. F. Schlagintweit, G. Grivani and F. E. Kühn, *Chemical Science*, 2018, **9**, 8307-8314.
157. P. J. Altmann, D. T. Weiss, C. Jandl and F. E. Kühn, *Chemistry – An Asian Journal*, 2016, **11**, 1597-1605.

158. H. M. Bass, S. A. Cramer, J. L. Price and D. M. Jenkins, *Organometallics*, 2010, **29**, 3235-3238.
159. H. M. Bass, S. A. Cramer, A. S. McCullough, K. J. Bernstein, C. R. Murdock and D. M. Jenkins, *Organometallics*, 2013, **32**, 2160-2167.
160. Z. Lu, S. A. Cramer and D. M. Jenkins, *Chemical Science*, 2012, **3**, 3081-3087.
161. G. R. Elpitiya, B. J. Malbrecht and D. M. Jenkins, *Inorganic Chemistry*, 2017, **56**, 14101-14110.
162. C. L. Keller, J. L. Kern, B. D. Terry, S. Roy and D. M. Jenkins, *Chemical Communications*, 2018, **54**, 1429-1432.
163. S. J. Hock, L.-A. Schaper, W. A. Herrmann and F. E. Kühn, *Chemical Society Reviews*, 2013, **42**, 5073-5089.
164. E. Alcalde, S. Ramos and L. Pérez-García, *Organic Letters*, 1999, **1**, 1035-1038.
165. C. D. Abernethy, G. M. Codd, M. D. Spicer and M. K. Taylor, *Journal of the American Chemical Society*, 2003, **125**, 1128-1129.
166. C. Lorber and L. Vendier, *Dalton Transactions*, 2009, 6972-6984.
167. D. Pugh, J. A. Wright, S. Freeman and A. A. Danopoulos, *Dalton Transactions*, 2006, 775-782.
168. S. Zhang, W.-C. Zhang, D.-D. Shang, Z.-Q. Zhang and Y.-X. Wu, *Dalton Transactions*, 2015, **44**, 15264-15270.
169. C. Weetman, S. Notman and P. L. Arnold, *Dalton Transactions*, 2018, **47**, 2568-2574.
170. A. Wacker, C. G. Yan, G. Kaltenpoth, A. Ginsberg, A. M. Arif, R. D. Ernst, H. Pritzkow and W. Siebert, *Journal of Organometallic Chemistry*, 2002, **641**, 195-202.
171. D. Rehder, in *Bioinorganic Vanadium Chemistry*, John Wiley & Sons, 2008, pp. 13-51.
172. A. D. Adler, F. R. Longo, F. Kampas and J. Kim, *Journal of Inorganic and Nuclear Chemistry*, 1970, **32**, 2443-2445.
173. S.-Y. Wong, R. Wai-Yin Sun, N. P. Y. Chung, C.-L. Lin and C.-M. Che, *Chemical Communications*, 2005, 3544-3546.
174. L. M. Berreau, J. A. Hays, V. G. Young Jr and L. K. Woo, *Inorganic Chemistry*, 1994, **33**, 105-108.
175. J.-L. Poncet, J.-M. Barbe, R. Guilard, H. Oumous, C. Lecomte and J. Protas, *Journal of the Chemical Society, Chemical Communications*, 1982, 1421-1422.
176. S. J. Anderson, F. J. Wells, G. Willkinson, B. Hussain and M. B. Hursthouse, *Polyhedron*, 1988, **7**, 2615-2626.
177. G. W. A. Fowles, P. T. Greene and T. E. Lester, *Journal of Inorganic and Nuclear Chemistry*, 1967, **29**, 2365-2370.
178. C. Lu, S. Gu, W. Chen and H. Qiu, *Dalton Transactions*, 2010, **39**, 4198-4204.
179. A. Raba, M. Cokoja, S. Ewald, K. Riener, E. Herdtweck, A. Pöthig, W. A. Herrmann and F. E. Kühn, *Organometallics*, 2012, **31**, 2793-2800.
180. C. K. Mirabelli, R. K. Johnson, C. M. Sung, L. Faucette, K. Muirhead and S. T. Crooke, *Cancer Research*, 1985, **45**, 32-39.
181. C.-M. Che, R. W.-Y. Sun, W.-Y. Yu, C.-B. Ko, N. Zhu and H. Sun, *Chemical Communications*, 2003, 1718-1719.
182. D. T. Weiss, M. R. Anneser, S. Haslinger, A. Pöthig, M. Cokoja, J.-M. Basset and F. E. Kühn, *Organometallics*, 2015, **34**, 5155-5166.
183. J. Rieb, B. Dominelli, D. Mayer, C. Jandl, J. Drechsel, W. Heydenreuter, S. A. Sieber and F. E. Kühn, *Dalton Transactions*, 2017, **46**, 2722-2735.
184. D. A. Hey, R. M. Reich, W. Baratta and F. E. Kühn, *Coordination Chemistry Reviews*, 2018, **374**, 114-132.
185. D. T. Weiss, S. Haslinger, C. Jandl, A. Pöthig, M. Cokoja and F. E. Kühn, *Inorganic Chemistry*, 2015, **54**, 415-417.
186. D. T. Weiss, P. J. Altmann, S. Haslinger, C. Jandl, A. Pöthig, M. Cokoja and F. E. Kühn, *Dalton Transactions*, 2015, **44**, 18329-18339.
187. A. H. Mageed, B. W. Skelton and M. V. Baker, *Dalton Transactions*, 2017, **46**, 7844-7856.
188. E. B. Bauer, M. A. Bernd, M. Schütz, J. Oberkofler, A. Pöthig, R. M. Reich and F. E. Kühn, *Dalton Transactions*, 2019, **48**, 16615-16625.

189. S. Alvarez, *Dalton Transactions*, 2013, **42**, 8617-8636.
190. P. J. Quinlivan, J.-S. Wu and R. K. Upmacis, *Acta Crystallographica Section E: Crystallographic Communications*, 2015, **71**, 810-812.
191. C. Topf, C. Hirtenlehner, M. Zabel, M. List, M. Fleck and U. Monkowius, *Organometallics*, 2011, **30**, 2755-2764.
192. N. Ahmed, B. Shirinfar, I. S. Youn, M. Yousuf and K. S. Kim, *Organic & Biomolecular Chemistry*, 2013, **11**, 6407-6413.
193. A. Rivera and M. Maldonado, *Tetrahedron Letters*, 2006, **47**, 7467-7471.
194. F. E. Hahn, C. Radloff, T. Pape and A. Hepp, *Chemistry–A European Journal*, 2008, **14**, 10900-10904.
195. H. Schmidbaur and A. Schier, *Angewandte Chemie International Edition*, 2015, **54**, 746-784.
196. T. P. Pell, B. D. Stringer, C. Tubaro, C. F. Hogan, D. J. D. Wilson and P. J. Barnard, *European Journal of Inorganic Chemistry*, 2017, **2017**, 3661-3674.
197. C. Schulte to Brinke, T. Pape and F. E. Hahn, *Dalton Transactions*, 2013, **42**, 7330-7337.
198. H. M. Wang, C. Y. Chen and I. J. Lin, *Organometallics*, 1999, **18**, 1216-1223.
199. R. Jothibasu, H. V. Huynh and L. L. Koh, *Journal of Organometallic Chemistry*, 2008, **693**, 374-380.
200. H. Schmidbaur and A. Schier, *Chemical Society Reviews*, 2012, **41**, 370-412.
201. A. Nandy, T. Samanta, S. Mallick, P. Mitra, S. K. Seth, K. D. Saha, S. S. Al-Deyab and J. Dinda, *New Journal of Chemistry*, 2016, **40**, 6289-6298.
202. P. J. Barnard, M. V. Baker, S. J. Berners-Price, B. W. Skelton and A. H. White, *Dalton Transactions*, 2004, 1038-1047.
203. S. L. Harbeson and R. D. Tung, in *Annual Reports in Medicinal Chemistry*, ed. J. E. Macor, Academic Press, 2011, vol. 46, pp. 403-417.
204. T. G. Gant, *Journal of Medicinal Chemistry*, 2014, **57**, 3595-3611.
205. J. Atzrodt, V. Derdau, W. J. Kerr and M. Reid, *Angewandte Chemie International Edition*, 2018, **57**, 1758-1784.
206. T. Pirali, M. Serafini, S. Cargnin and A. A. Genazzani, *Journal of Medicinal Chemistry*, 2019, **62**, 5276-5297.
207. C. Schmidt, *Nature Biotechnology*, 2017, **35**, 493-494.
208. A. Mullard, *Nature Reviews Drug Discovery*, 2017, **16**, 305-305.
209. *APEX suite of crystallographic software,* APEX 2, Version 2014.9-0 and APEX 3, Version 2015-5.2, Bruker AXS Inc., Madison, Wisconsin, USA, 2014/2015.
210. *SAINT,* Versions 8.32B, 8.34A and 8.38A, Bruker AXS Inc., Madison, Wisconsin, USA, 2012/2014/2017.
211. *SADABS,* Versions 2012/1, 2014/5 and 2016/2 and *TWINABS*, Version 2012/1, Bruker AXS Inc., Madison, Wisconsin, USA, 2012/2014/2016.
212. G. M. Sheldrick, *Acta Crystallographica Section C: Structural Chemistry*, 2015, **71**, 3-8.
213. C. B. Hübschle, G. M. Sheldrick and B. Dittrich, *Journal of applied crystallography*, 2011, **44**, 1281-1284.
214. *International Tables for Crystallography*, Vol. C (Ed.: A. J. Wilson), Kluwer Academic Publishers, Dordrecht, The Netherlands, 1992, Tables 6.1.1.4 (pp. 500–502), 4.2.6.8 (pp. 219–222), and 4.2.4.2 (pp. 193–199).
215. A. Spek, *Acta Crystallographica Section C*, 2015, **71**, 9-18.
216. A. Spek, *Acta Crystallographica Section D*, 2009, **65**, 148-155.
217. C. F. Macrae, I. J. Bruno, J. A. Chisholm, P. R. Edgington, P. McCabe, E. Pidcock, L. Rodriguez-Monge, R. Taylor, J. van de Streek and P. A. Wood, *Journal of Applied Crystallography*, 2008, **41**, 466-470.